Alma Mater Studiorum - Università di Bologna

DOTTORATO DI RICERCA IN

INGEGNERIA BIOMEDICA, ELETTRICA E DEI SISTEMI

Ciclo 33

Settore Concorsuale: 09/E2 - INGEGNERIA DELL'ENERGIA ELETTRICA

Settore Scientifico Disciplinare: ING-IND/33 - SISTEMI ELETTRICI PER L'ENERGIA

SCHEDULING OF RESOURCES IN RENEWABLE ENERGY COMMUNITIES

Presentata da: Camilo Orozco Corredor

Coordinatore Dottorato

Prof. Michele Monaci

Supervisore

Prof. Alberto Borghetti

Co-supervisore

Prof. Carlo Alberto Nucci

Esame finale anno 2021

"*Coming together is a beginning,*

keeping together is progress,

working together is success"

Henry Ford

Acknowledgment

I want to thank, and dedicate this thesis to, my family and loved ones. Their incredible support has been key to being able to travel this path full of effort and continuous personal growth. Regardless of the distance between us, I have always felt them by my side.

A special thanks to my supervisors. Working with them has been an honour and privilege for me. Infinite thanks to Prof. Alberto Borghetti, whose constant support and companionship have been essential to overcoming the difficulties and challenges over the course of this stage; thank you for being a great example of commitment and for your passion for excellence. Similarly, a special thanks to Prof. Carlo Alberto Nucci for his valuable discussions, suggestions and constant feedback.

I would like to thank my colleagues from the Power Systems Laboratory at the University of Bologna. They are a great team, not only with great technical skills but also personal capabilities; thank you for welcoming me kindly and always being willing to lend me a hand.

Additionally, I would like to extend a special thank you to Prof. Bart. De Schutter, who hosted me as a visiting researcher at the Delft University of Technology. The time I spent in Delft, represents a period that I will gratefully remember, full of learning, good times and great friendships.

Finally, a special recognition to my colleagues and management team at the INCITE project. Participating in this Marie Sklodowska-Curie ITN Project, funded by the European Union's HORIZON 2020 Programme, has been both an honour and an invaluable experience of professional and personal growth. I will remember, with great pleasure, the shared moments and the bonds of friendship that will surely endure.

Abstract

This work presents a detailed study of the scheduling of power and energy resources in renewable energy communities (RECs). The study has been developed starting from the analysis of a single basic unit of the community, i.e., the prosumer and its microgrid (MG), to the scheduling and expansion of the energy community concept with several prosumers through several scenarios. Both a centralized and distributed approaches have been implemented and compared to each other. Moreover, we have distinguished the optimization of the operation between two different phases: day-ahead and intra-day scheduling. A coordinated strategy has been proposed to integrate the two-aforementioned phases, considering the uncertainties associated with energy generation and demand.

In the first part, the thesis focuses on the day-ahead scheduling problem associated with the operation of a single local energy system (LES) consisting of photovoltaic (PV) units, battery energy storage (BES) units and loads. Within this context, the relevant optimization problem aimed at minimizing the electricity procurement cost has been formulated. The optimization problem is solved by both a day-ahead deterministic approach and by a multistage stochastic programming (SP) approach to consider the uncertainties of PV generation and demand. The thesis describes the generation of the scenarios, the construction of the scenario tree based on the *k*-means algorithm, and the intra-day decision-making procedure based on the solution of the multistage SP model. Moreover, the daily energy procurement costs calculated by using the SP approach are compared with those calculated by using Monte Carlo simulations. A multistage scheduling approach has been also developed to provide the optimal scheduling of an MG, in which a PV unit has been integrated with bidirectional charging stations for electric vehicles (EVs) in a parking lot.

The second part has been focused on the modelling and day-ahead scheduling of a REC. Within this context, this work deals first with the day-ahead operational planning of a grid-connected REC consisting of an internal low-voltage (LV) network and several prosumers. Each one of the participants in the community might be equipped with PV units, BES units, and local loads. The scheduling problem has been addressed by a centralized approach and by a distributed approach based on the alternating direction method of multipliers (ADMM). The ADMM-based approach is oriented to preserve, as much as possible, the confidentiality of the prosumers' equipment features, as well as the energy generation and load forecasts. Both the developed

centralized and distributed procedures provide the scheduling of the available energy resources to limit the balancing action of the external grid and allocate the internal network losses to the corresponding energy transactions. The results of the numerical tests, carried out for different case studies, including the presence of distributed storage units and of dispatchable units, confirm that the proposed approaches effectively minimize the total energy procurement cost, with an economic benefit for each one of its members (i.e., increasing revenues or reducing costs in comparison with the scenario in which the internal transactions are not allowed).

The last part of the thesis focuses on the representation of uncertainties and the intra-day operation of a REC. This work presents a coordinated day-ahead and intra-day approach to provide the optimal scheduling of the resources. In this case, the ADMM-based procedure, which is aimed at minimizing the total energy procurement costs, is adapted to cope with the impact of the fluctuation of both the local energy generation and demand during the day. To achieve this, a day-ahead multistage stochastic optimization approach is combined with an intra-day decision-making procedure, able to adjust the scheduling of the energy resources according to the current operational conditions. The day-ahead multistage stochastic model of the REC provides the set of scenario-based solutions to the intra-day approach, which includes a recursive decision-making procedure and an online optimization. The effectiveness of the coordinated day-ahead and intra-day approach is tested by means of several numerical tests considering different case studies.

Contents

List of Figures

List of Tables

Nomenclature

Acronyms

AD	Anaerobic Digestion
ADMM	Alternating Direction Method of Multipliers
BES	Battery Energy Storage
DER	Distributed Energy Resources
DSO	Distribution System Operator
EEV	Expected Value Solution
EMS	Energy Management Systems
ESS	Energy Storage System
EV	Electrical Vehicle
EVPI	Expected Value of Perfect Information
FIT	Feed-in-Tariff
G2V	Grid-to-Vehicle
KiBaM	Kinetic Battery Model
LES	Local Energy System
LHV	Lower Heating Value
LV	Low Voltage
MAE	Mean Absolute Error
MAPE	Mean Average Percentage Error
MC	Monte Carlo
MG	Microgrid
MILP	Mixed Integer Lineal Programming
MIQP	Mixed Integer Quadratic Programming
MV	Medium Voltage
MPC	Model Predictive Control
OF	Objective Function
P2P	Peer-to-Peer
PEV	Plug-In Electrical Vehicle
PV	Photovoltaic
RE	Renewable Energy
REC	Renewable Energy Community
RES	Renewable Energy Sources
RP	Recourse Problem
SME	Small or Medium Enterprise
SOCP	Second Order Cone Programming
SoE	State of Energy

SP	Stochastic Programming
SSE	Sum of the Squared Errors
TOU	Time-of-Use tariff
V2G	Vehicle-to-Grid
VSS	Value of Stochastic Solution
WS	Wait-and-See solution

List of Symbols

Model of the LES

T	set of time intervals in the optimization horizon, with $t \in T$
π^t_{buy} , π^t_{sell}	price of buying and selling energy from and to the external grid at t, respectively
P^t_{Grid}	net power exchange with the external network at t
$P^t_{\text{buy\_Grid}}$, $P^t_{\text{sell\_Grid}}$	power bought and sold from and to the external grid at t, respectively
Δt	time step
P^t_{PV}	photovoltaic power output at t
P^t_{Load}	power load at t
P^t_{BES}	battery power output at t
P^t_{ch} and P^t_{dis}	battery power output during charges and discharges at t, respectively
L^t_{BES}	losses of the battery converter at t
$P^{\text{Rated}}_{\text{Grid}}$	limit of power exchanged with the energy provider
u^t_{Grid}	binary variable to avoid simultaneous purchasing and selling processes from and to the utility grid at t, respectively
M_{Grid}	parameter for the big-M formulation associated with exchanges with the grid
$P^{\text{Rated}}_{\text{BES}}$	limit of power output of the battery
u^t_{BES}	binary variable to avoid simultaneous charging and discharging processes of the BES unit at t, respectively
M_{BES}	parameter for a big-M formulation associated with the BES
L^t_{ch} , L^t_{dis}	losses during charging and discharging of the BES unit at t
η_{ch} , η_{dis}	the converter efficiency factors for charges and discharges of the BES unit, respectively
E^t_{BES}	energy level in the battery at t
SOC^t	battery's state of charge at t
$E^{\text{max}}_{\text{BES}}$	battery's capacity
SOC^0 and SOC^{end}	initial and final value of the state of charge, respectively
SOC^{min} and SOC^{max}	minimum and maximum state of charge, respectively
Ω	set of scenarios with index ω
π^{ω}	probability of scenario ω

y_{PV}^{t} , y_{Load}^{t}	normalized time series from the forecast of PV generation and load at *t*, respectively
Φ	the one-lag autocorrelation parameter
$\varepsilon^{\omega,t}$	Gaussian white noise in scenario ω at *t*
$P_{\mathrm{PV}}^{\omega,t}$, $P_{\mathrm{Load}}^{\omega,t}$	PV generation and load in scenario ω at *t*, respectively
$\xi^{\omega,t}$	profile defined by the normalized difference between the PV production and the load in scenario ω at *t*
K	number of centroids employed by the *k*-means clustering algorithm
s	stage of the multistage stochastic model
C_k^s	centroid *k* at stage *s*
T^s	set of time periods in stage *s*

Model of the MG with EV parking lot and PV generation

C^{ω}	cost associated with scenario ω
ρ_{TOU}^{t}	TOU for purchasing energy from the grid at *t*
r	ratio between sale and purchase tariffs
$E_{\mathrm{buy\_Grid}}^{\omega,t}$, $E_{\mathrm{sell\_Grid}}^{\omega,t}$	energy bought and sold from and to the utility grid in scenario ω at *t*, respectively
$C_S^{\omega,t}$	total cost associated with the use of the V2G parking lot in scenario ω at *t*
$P_{\mathrm{V2G}}^{\omega,t}$	power exchange of the V2G parking lot in scenario ω at *t*
$E_{S+}^{\omega,t}$	total energy initially stored in the EVs that arrive in the parking lot in scenario ω at *t*
$\mu^{\omega,t}$	nonnegative utilization coefficient of $E_{S+}^{\omega,t}$ in scenario ω at *t*
$P_{\mathrm{V2G\,max}}^{\omega,t}$, $P_{\mathrm{V2G\,min}}^{\omega,t}$	maximum and minimum value of the power exchanged by the V2G parking lot in scenario ω at *t*, respectively
$E_S^{\omega,t}$	energy stored by the EV's batteries at the end of period *t* in scenario ω
$E_{S\,\max}^{\omega,t}$	maximum value of the storage capability in the EVs parking lot in scenario ω at *t*
$E_{\mathrm{EV}}^{\mathrm{Rated}}$	rated size of the EV batteries
$u(\cdot)$	step function value
$E_{\mathrm{V2G}}^{\omega,t}$	available energy for dispatching services in scenario ω at *t*
$E_{\mu}^{\omega,j,t}$	initial energy of the EVs arriving in period *j* and leaving in period *t,* in scenario ω
$l^{\omega,t}$	power losses associated with charging/discharging processes in the V2G operation in scenario ω at *t*
$P_u^{\omega,t}$	net active power provided or absorbed by unit *u* in scenario ω at *t*
$P_{u=\mathrm{V2G\,net}}^{\omega,t}$	net power of the V2G parking lot in scenario ω at *t*
c_{μ}	retrieval price for the contribution to V2G service
c_{ch} , c_{dis}	prices associated with the charging and discharging processes, respectively
N_{tot}	population of EVs willing to enter the parking lot
t_i^{+}	time of entrance of the *i*-th EV in the parking lot
E_i^0	initial charge of the *i*-th EV in the parking lot

s_i	staying time in the parking lot of the *i*-th EV
$S_+^{\omega,t}$ and $S_-^{\omega,t}$	set of EVs incoming and leaving in scenario ω at t , respectively
$E_{S+}^{\omega,t}$	increase of the energy stored in the parking lot due to arrivals in scenario ω at t
$E_{S-}^{\omega,t}$	decrease of the energy stored in the parking lot due to departures in scenario ω at t
$\psi(t)$	decreasing function of t in order to represent the increase of the incertitude with time

Model of the REC

Ω	set of participants in the REC, with i, j and $k \in \Omega$
N	total number of participants in the REC
B	set of branches of the internal network in the REC, with $b \in B$
$P^t_{\text{buy\_Grid } i}$	power bought from the utility grid by i at t
$P^t_{\text{sell\_Grid } i}$	power sold to the external utility grid by i at t
$P^t_{\text{buy } i,j}$	power bought by i from j at t
$P^t_{\text{sell } i,j}$	power sold by i to j at t
$P^t_{\text{PV } i}$	photovoltaic power output of prosumer i at t
$P^t_{\text{Load } i}$	power load of prosumer i at t
$P^t_{\text{ch } i}$, $P^t_{\text{dis } i}$	charging and discharging power of the i-th battery at t, respectively
$L^t_{b,i}$	estimated losses in branch b originated by the energy transactions of the i-th prosumer at t
R_b	resistance of branch b of the internal network
V_{n}	line-to-line rated voltage value
$F^t_{b,i}$	power flow in branch b at t, due to the energy transaction that involves the i-th prosumer
A_{Grid} , A	matrices of the configuration of the network
u^t_i	binary variable to prevent simultaneous purchases and sales by i in scenario ω at t
$P^{\max}_{\text{sell } i}$	power limit for i when selling
$P^{\max}_{\text{buy } i}$	power limit for i when buying
$P^{\max}_{\text{BES } i}$	maximum value of discharging and charging power of the i-th battery
$E^t_{\text{BES } i}$	state of energy of battery i at t
$u^t_{\text{BES } i}$	binary variable to avoid concurrent charging and discharging of the i-th battery at t
$E^{\min}_{\text{BES } i}$	minimum level of stored energy in battery i
$E^{\max}_{\text{BES } i}$	maximum storage capacity of battery i
L	set of segments employed by the piece-wise linearization of the losses, with index l
$H^t_{\text{Flow } b,l}$	breakpoint of the power flow associated with branch b and segment l at t
$H^t_{\text{Loss } b,l}$	breakpoint of the losses associated with branch b and segment l at t

$a_{b,l}^{t}$	SOS2 (Special ordered set of type 2) variables associated with the power flow/losses breakpoints in b at t

ADMM implementation

OF_i	local objective function of prosumer i
ℓ_i^t	squared norm of the imbalance of each transaction between i and j at t
λ_i^t	Lagrange multipliers of prosumer i at t
ρ	penalization parameter
m	scale factor
v	iteration of the ADMM algorithm
$\hat{P}_{\text{buy\_Grid } i}^{t}$	profile of $P_{\text{buy\_Grid } i}^{t}$ obtained at the previous iteration
$\hat{P}_{\text{sell\_Grid } i}^{t}$	profile of $P_{\text{sell\_Grid } i}^{t}$ obtained at the previous iteration
$\hat{P}_{\text{buy } i,j}^{t}$	profile of $P_{\text{buy } i,j}^{t}$ obtained at the previous iteration
$\hat{P}_{\text{sell } i,j}^{t}$	profile of $P_{\text{sell } i,j}^{t}$ obtained at the previous iteration
r_i^t	primal residual for prosumer i at t
s_i^t	dual residual for prosumer i at t
ε	convergence tolerance of the ADMM algorithm

Allocation of losses

F_b^t	power flow in branch b at t due to all the relevant transactions
$K_{\text{buy\_Grid } b,i}^{t}$, $K_{\text{sell\_Grid } b,i}^{t}$ and $K_{\text{buy } b,i,j}^{t}$	coefficients to define the proportional contribution to the losses in branch b at t
$L_{\text{buy\_Grid } b,i}^{t}$, $L_{\text{sell\_Grid } b,i}^{t}$ and $L_{\text{buy } b,j,i}^{t}$	losses in branch b at t, attributed to the transaction involving prosumer i
$T_{\text{buy\_Grid } i}^{t}$, $T_{\text{sell\_Grid } i}^{t}$ and $T_{\text{buy } i,j}^{t}$	parameters employed to identify present transactions in the first stage of the REC scheduling procedure
$\eta_{\text{buy\_Grid } i}^{t}$, $\eta_{\text{sell\_Grid } i}^{t}$ and $\eta_{\text{buy } i,j}^{t}$	efficiency parameters assigned to each buying and selling transaction involving prosumer i at t

Dispatchable generating units

$C_{\text{biogas}\,i}^{t}$	cost of using the biogas unit i at t
$P_{\text{biogas}\,i}^{t}$	power output of the dispatchable generator owned by i at t
$C_{\text{gas}\,i}$	AD gas cost of biogas unit i
U	set of segments employed by linearization with breakpoints x_u
α_u, β_u	linearization parameters of the u-th segment
$P_{\text{biogas}}^{\max}$, $P_{\text{biogas}}^{\min}$	maximum and minimum power output of the biogas unit, respectively
$C_{\text{fuel}\,i}^{\max\,\text{day}}$	maximum value of the daily fuel consumption of biogas unit i

SU_i^t	non-negative variable to indicate whether the biogas unit i starts up at t or not
w_i^t	binary variable, which indicates whether the biogas unit i is on or off during time interval t

Multistage model of the REC

Φ_i	set of scenarios of i, with $\varphi_i \in \Phi_i$
$\xi_{\varphi_i}^t$	profile obtained by the normalized difference between PV production and load in φ_i
ψ_φ	N-dimensional scenario composed of individual scenarios $\xi_{\varphi_i}^t$ of each prosumer i
Γ	set of operational scenarios of the REC, with $\psi_\varphi \in \Gamma$
$a(\psi_\varphi)$	mean intra-cluster distance of scenario ψ_φ
$b(\psi_\varphi)$	mean nearest-cluster distance of scenario ψ_φ
$s(\psi_\varphi)$	silhouette coefficient of scenario ψ_φ

Intra-day decision-making procedure in the REC

t_m	current time period for the online calculation
$\overline{P}_{\text{exc}\,i,j}^t$	average of the global variables compromising prosumers i and j at t
t_1^s , t_{end}^s	first and last time period of stage s, respectively
$E_{\text{BES}\,i}^{i\text{nitial}^s}$, $E_{\text{BES}\,i}^{\text{final}^s}$	initial and final SoE of BES unit i in stage s, respectively

Kinetic Battery Model (KiBaM)

$q1^t$	readily available charge at t
$q2^t$	bound charge a t
η_{BES}	battery's efficiency for charging and discharging
K	battery rate constant
c	battery's capacity ratio
a	battery's maximum charge rate

Scheduling model in MV with power loss reduction

Ω_0	set of branches connected to the slack bus, with $k \in \Omega_0$
v_{in}, v_{out}	square rms value of the input and output voltage, respectively
v_{min}, v_{max}	square value of the min and max voltage limits, respectively
P_{in}, P_{out}	input and output active power flows, respectively
Q_{in}, Q_{out}	input and output reactive power flows, respectively
P_{user}, Q_{user}	prosumer's net active and reactive power, respectively
P_{PV}, Q_{PV}	prosumer's active and reactive power generation, respectively
P_{LOAD}, Q_{LOAD}	prosumer's active and reactive power demand, respectively
$P_{\text{Grid\_in}}$, $P_{\text{Grid\_out}}$	input and output power flows corresponding to exchange with the external grid, respectively
P_{i+}^t , P_{i-}^t	nonnegative variables used to constrain variables $P_{\text{buy\_Grid}}$ and $P_{\text{sell\_Grid}}$, at t
u	the square rms value of the branch current
r, x	branch resistance and reactance

Chapter 1. Introduction

1.1 Introduction

One of the main challenges that our society faces today is the decarbonisation of the global energy sector. Such a transition towards a "carbon-neutral" energy paradigm has been mainly supported by the alignment of smart technologies, policy frameworks and business models to exploit the available renewable energy sources (RES). According to (IRENA 2020a), in a deeper decarbonisation perspective, renewable energy (RE) and energy efficiency measures can potentially achieve 90% of the required carbon reductions.

1.1.1 Prosumer unit as a cornerstone of the distributed paradigm

With the current energy transition pushed by social, environmental, and economic factors, the electrical system is moving towards a distributed scheme based on RES, in which customers play a new active role through self-generation of electrical energy. In the past, a central power plant was used to generate energy for everyone. Now, electricity can be produced locally using, for instance, solar panels or wind farms. In this new paradigm there is a new key player: the prosumer, who is a consumer that uses for instance solar panels to cover part of his or her energy demands, stores part of this energy in batteries for moments of scarcity and, in addition, can exchange energy with the utility grid, not only buying but selling.

The transformation toward the distributed paradigm has also been aligned with the development of smart technologies for monitoring, controlling and operating the equipment owned by the prosumers. Within this smart grid framework, the increasing amount of information and data associated with the operation of the electrical systems requires the implementation of communication technologies and optimization techniques to cope with crucial processing and decision tasks.

To achieve this, energy management systems (EMSs) have been employed to automatically, and cost-effectively, operate the local energy system (LES) that corresponds to the grid-connected prosumer during a horizon time. Through the implementation of these decision-making tools based on mathematical modelling and optimization (Williams 2013), the

prosumer is able to define the scheduling of the energy storage systems (ESSs) and other resources if any, in accordance with the local energy generation and consumption.

The obtained balancing effect of the local generation and consumption represents one of the most attractive characteristics of the prosumer's operation, opening the door to exploit the possibility of selling the excess energy to the utility grid. The deployment of these technologies, and the corresponding business models, have been supported by regulatory support policies as e.g., net-metering and feed-in-tariffs (FITs) (IRENA 2019; Masson, Briano, and Baez 2016).

As a result, in the last years, the landscape of the distribution network has drastically changed, owing to a growing penetration of distributed energy resources (DERs). In this context, the corresponding appearance of prosumers connected to the low voltage (LV) network has been consequently boosted by the increasing deployment of integrated photovoltaic-storage systems and charging services for electrical vehicles (EVs).

1.1.2 The time of prosumer-based collectives

The recent increase in the local concentration of prosumers and distributed services, based on renewables (e.g., dispatchable generating units and bidirectional charging points), has gained special interest since the implementation of adequate policies could provide an adequate environment not only to increase the self-consumption capacity of a location (Masson, Briano, and Baez 2016), but also to favour socio-economic and technical aspects at the community level.

Within this context, collective activities can provide further opportunities, adding value at several levels by bringing energy consumers and producers together and allowing them to interact actively. Governments and policy makers have understood this throughout the last years; for instance, the "Clean Energy for all Europeans" package approved by the European Union (see e.g. (EU2018/2001 2018) and (EU2019/944 2019)) determines, as a common directive for all the member states, the definition of a regulatory framework by 2021, in which fair and adequate conditions are provided for the operation and establishment of different self-consumption schemes, including direct energy transactions between different actors (e.g., producers, consumers, prosumers).

In the "Clean Energy for all Europeans" package, the following categories of collective activities have been recognized:

- **Active Customer - jointly acting final customers:** a final customer (or a group) who consumes or stores electricity generated within its premises located within confined boundaries or, where permitted by a Member State, within other premises, or who sells self-generated electricity or participates in flexibility or energy efficiency schemes, provided that those activities do not constitute its primary commercial or professional activity (EU2019/944 2019).
- **Renewables self-consumers:** a final customer operating within its premises located within confined boundaries or, where permitted by a Member State, within other premises, who generates renewable electricity for its own consumption, and who may store or sell self-generated renewable electricity, provided that, for a non-household renewables self-consumer, those activities do not constitute its primary commercial or professional activity (EU2018/2001 2018).
- **Jointly acting renewables self-consumers:** a group of at least two jointly acting renewables self-consumers in accordance who are located in the same building or multi-apartment block (EU2018/2001 2018).
- **Citizen energy community (CEC):** a legal entity, based on voluntary and open participation, controlled by members or shareholders that are natural persons, local authorities, including municipalities or small enterprises. It may engage in generation (including from RES), distribution, supply, consumption, aggregation, energy storage, energy efficiency or charging services for electric vehicles or provide other energy services to its members of shareholders (EU2019/944 2019).
- **Renewable energy community (REC):** a legal entity whose primary goal is to provide environmental, economic, or social community benefits for its shareholders/members or for the local area it operates within, instead of financial profits. It is autonomous and controlled by shareholders or members. The community shareholders may be natural persons, small or medium enterprises (SMEs) or local authorities, including municipalities (EU2018/2001 2018).

However, for practical considerations, a large diversity of alternative forms could be derived within these concepts. Figure 1.1 shows a set of criteria defined in (Delnooz, Vanschoenwinkel, and Mou 2020) in order to better identify this diversity.

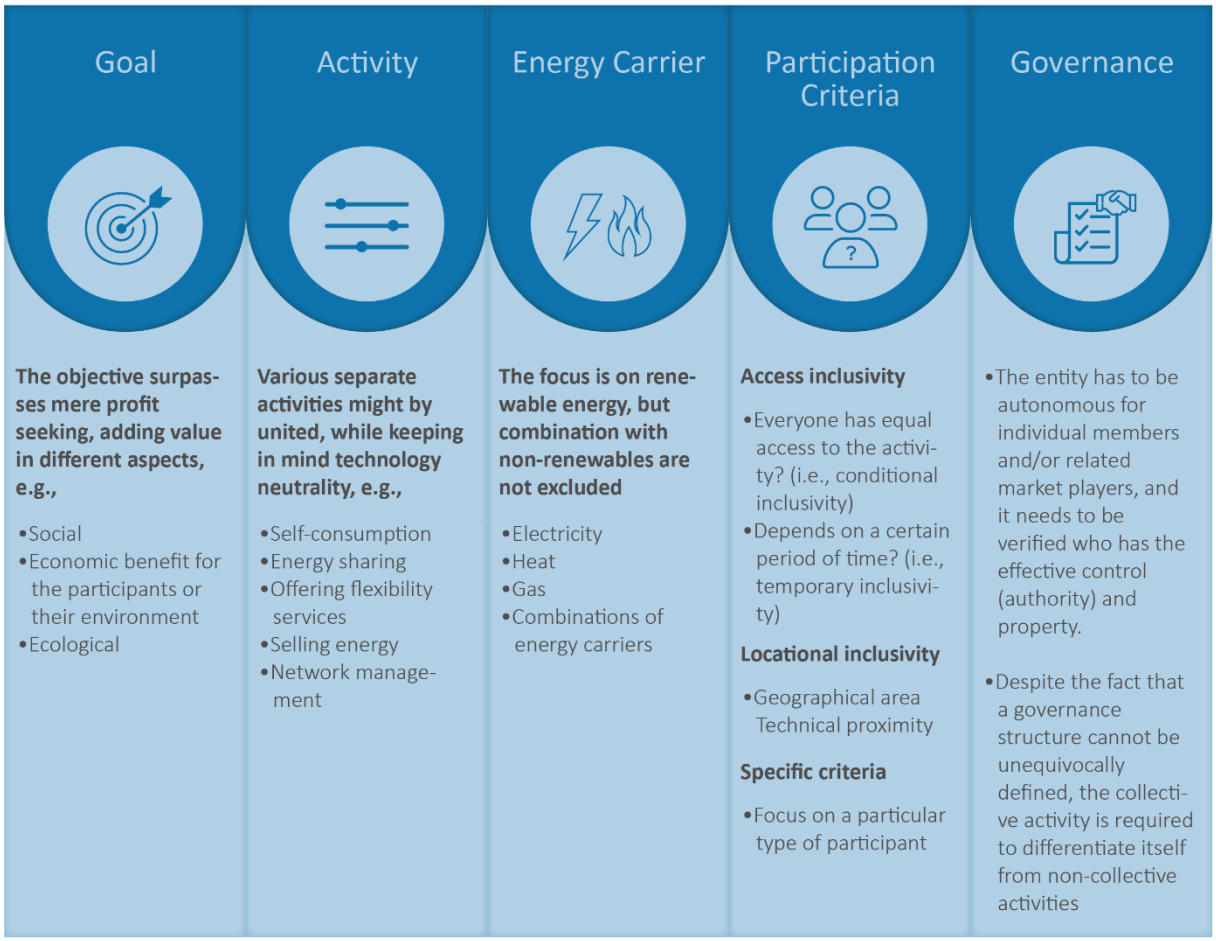

Figure 1.1 Set of criteria to categorize the collective activities; adapted from (Delnooz, Vanschoenwinkel, and Mou 2020).

Different combinations or interpretations of these criteria could lead to different definitions and concepts for collective activities. In certain cases, the current economic and technical scenario is enough to enable their adoption. However, other types of collaboration could be not sufficiently supported and, thus, require more attention in order to provide the adequate environment (Delnooz, Vanschoenwinkel, and Mou 2020).

1.1.3 Energy community: benefits and challenges

In (Frieden, Roberts, and Gubina 2019), similarities and differences between both types of energy communities have been presented. Table 1.1 shows the corresponding differences, which are of particular interest to understand the particularities in their operation and own limitations.

The economic justification for the formation of an energy community is mainly due to the difference between the price of the energy supplied by the external energy provider and the

price sold by the community to the main grid. This difference can be significant, e.g., due to the costs of the ancillary services (Lilla et al. 2020).

Table 1.1 Differences between renewable energy community and citizen energy community; adapted from (Frieden, Roberts, and Gubina 2019).

Adapted criteria	Renewable Energy Community	Citizen Energy Community
Geographical limitation	Effective control is limited to members living in proximity of the RE projects owned by the community.	No geographic limitations relating to activities, effective control or eligibility for membership in a CEC.
Membership	Based on local control and excludes large enterprises from membership	SMEs and large size enterprises can participate but are excluded from effective control.
Energy sources	All sorts of RES	All sources of electricity, not necessarily renewable.
Major purpose	Stimulating the growth of local community ownership to expand the share of RE at the national level.	CEC as a new 'non-commercial' energy market actor that can engage across the electricity market.

Energy communities can support the operation of the main grid, according to the local characteristics of the collective, while providing many socio-economic benefits for the participants. Figure 1.2 shows the main benefits presented in (IRENA 2020b).

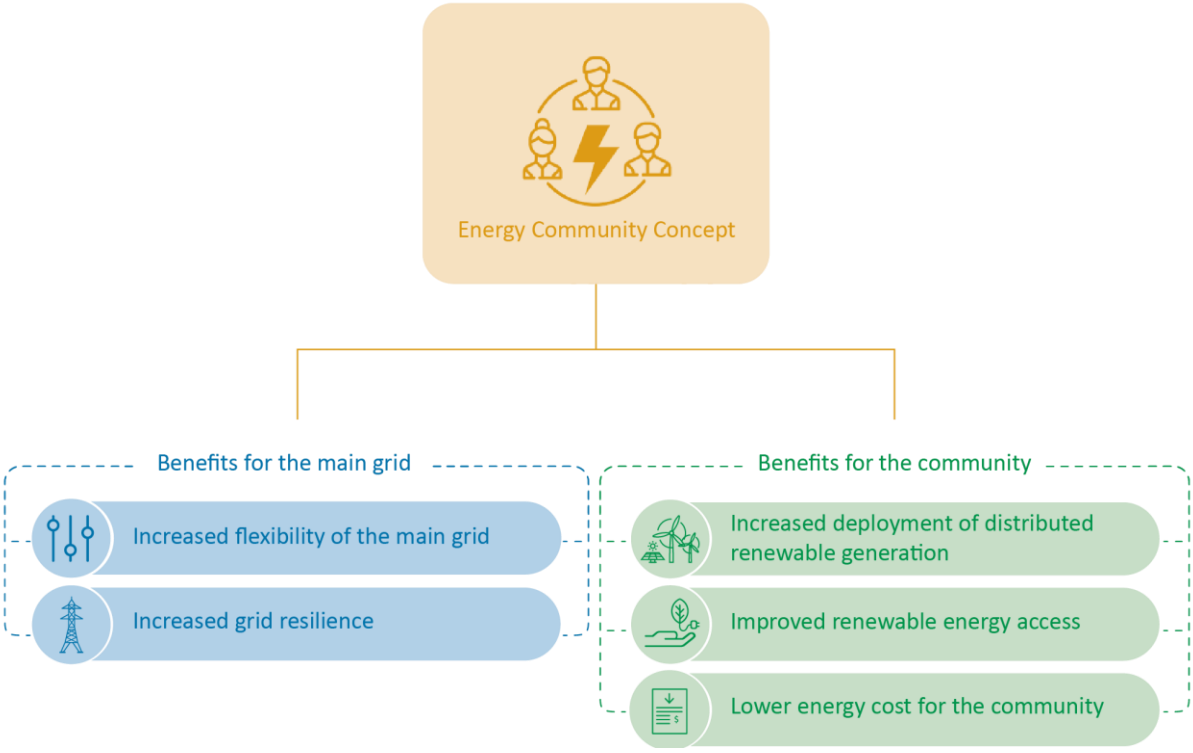

Figure 1.2 Benefits associated with energy community projects; adapted from (IRENA 2020b).

On the other hand, a detailed review of key issues and trends associated with the energy community concept, as well as the corresponding implementation, has been presented in (Koirala et al. 2016), in which technological, socio economic, environmental, and institutional aspects have been considered.

Despite the differences between different types of collectives and communities, in general, there are key technological issues, which are common at the energy community level. One of the main concerns regarding the operation of energy communities is the definition of an optimal scheduling of the resources able to align the daily operation and the proposed objectives; in other words, the effective definition and operation of a community EMS that coordinates the interaction (i.e., energy sharing and transactions) between participants, while considering the technical constraints.

Among the several issues and challenges identified in the literature, we can list those that are directly related with the daily operation of the EMS.

A. Intermittency of the renewable generation and demand

Renewable generation and energy demand are stochastic by nature. The operation of an energy community under the effect of uncertainties and the corresponding fluctuations, demands the implementation of response mechanisms to assure the balancing of renewable generation in a local community level, while reducing the impact of the uncertainties.

B. Storage system management

The flexibility provided by ESSs depends on the effective scheduling of the corresponding discharging and charging processes since the scheduling problem scales up with the number of participants. An adequate EMS is required to provide an optimal operational plan, while guaranteeing a response in an acceptable amount of time.

Moreover, the community EMS is expected to be suitable in dealing with the rising penetration of EVs. In this scenario, EVs' flexibility is expected to provide benefits such as stability and reliability to the local grid, as well as to increase the desired balancing effect to support the use of intermittent renewable generation.

C. Privacy and autonomy

In general, a common concern in energy collectives, is related to the information flow within the entity. According to the architecture and scheme adopted by the entity to accomplish the operational planning of the resources, private information might be communicated (Le Cadre and Bedo 2020).

Furthermore, the implemented mechanism for defining the operational decisions of each participant in the community could comprise his or her autonomy and independency.

This thesis deals with the scenario in which direct energy transactions between prosumers located within a REC are allowed in addition to the energy transactions with the external energy provider. In this framework, it seems crucial to study the definition and operation of the community EMS, able to achieve the goals of such an energy trading scheme.

1.2 Contribution

The main activities carried out have been focused on the study of the modelling and, more specifically, scheduling problem of RECs.

Within this context, this thesis provides a global review of the scheduling problem associated with the operation of a REC, stretching from the understanding of its basic-unit (i.e., the prosumer) and the scheduling problem of its LES or MG to the mathematical model of the day-ahead and intra-day operation of the energy community and the subsequent optimal definition of its operational planning.

In the first part of the thesis, the individual scheduling problem of the prosumer's grid-connected LES has been studied as a day-ahead deterministic problem and as a multistage stochastic problem to consider uncertainties associated with energy generation and energy consumption. The performance of these solutions has been analysed by using stochastic metrics and comparison with Monte Carlo simulations for several case studies.

The adoption of the multistage stochastic approach implied the implementation of scenario-generation techniques based on a Markov-process, and, subsequently, a tree-generation procedure, which has been addressed by *k*-means clustering method.

Furthermore, an approach is formulated to consider the integration of bidirectional charging services of EVs within a local energy system with the presence of renewable generation. The scheduling problem is adapted to a multistage scheme able to consider uncertainties associated with the operation of the different units in the system.

The second part of the thesis focuses on the mathematical model of the REC and its day-ahead scheduling problem. Two approaches have been developed to deal with the community scheduling problem, i.e., a centralized approach and a distributed optimization approach. Both approaches are aimed at minimizing the total energy procurement costs through the definition of the optimal operational plan of the available resources.

The proposed distributed approach is based on the ADMM algorithm, and is specifically oriented to better preserve the privacy and autonomy of the participants in the REC.

Since the REC is characterized by being collaborative (i.e., opposite to competitive schemes), both the centralized and distributed approaches provide the definition of fair prices associated with the exchanges of energy between participants.

The proposed approaches include a loss-allocation procedure, preserving, in the ADMM-based model, the distributed behaviour. A detailed comparison of the results obtained by both the centralized and distributed approaches has been included.

In the last part of the thesis the scheduling problem has been extended to consider the uncertainties associated with the operation of each one of the participants. To achieve this, a strategy that coordinates the day-ahead solution and the intra-day operation of the community has been proposed.

In this case, the ADMM-based approach has been adapted to a multistage stochastic scheme, providing a day-ahead scenario-based solution, which is suitable for coordinating with an intra-day decision-making procedure. The proposed approach adjusts the set values of the entire community according to the current conditions. The adoption of the multistage stochastic approach required the implementation of a routine that combines the individual stochastic situation of each prosumer in a common scenario tree. By using the obtained tree, the community can react in a coordinated way to the uncertainties, while preserving the distributed characteristics of the scheduling approach.

The intra-day decision-making procedure has been implemented as a receding horizon optimization based on the ADMM model of the REC. The intra-day procedure adjusts the set values at each time period during the day and assures that the levels of energy in the batteries at the end of each stage is equal to those defined by the day-ahead scheduling, which provide an operational framework for the online calculation. Furthermore, specific techniques are implemented in order to speed up the solution of the online ADMM procedure.

1.3 Outline

The structure of the thesis is the following:

Chapter 2 provides a description of the day-ahead scheduling problem associated with the ESS in a grid-connected local energy system with the presence of PV units and local load. The problem is studied under the assumption of a deterministic model and a multistage stochastic approach to deal with the uncertainties in the energy generation and consumption.

The second part of the chapter is devoted to the study of a multistage scheduling approach that provides the optimal scheduling of a grid-connected microgrid, in which a PV generating unit has been integrated with bidirectional charging stations for EVs in a parking lot.

Chapter 3 introduces the mathematical formulation to solve the day-ahead scheduling problem in a REC with the presence of PV-storage units and local loads. In this chapter, the problem has been addressed by means first of a centralized, and then a distributed approach based on the ADMM algorithm. Moreover, a loss-allocation procedure is presented for each one of the approaches (i.e., centralized and ADMM-based). Numerical results are presented for several operational scenarios of the community.

Furthermore, the chapter includes the study of the scenario of a community with the presence of dispatchable generating units. In this case, the corresponding centralized and distributed formulation is introduced and tested for several case studies.

In Chapter 4, a coordinated day-ahead and intra-day approach has been proposed in order to deal with the uncertainties associated with the local generation and energy consumption in the REC. The proposed approach has been tested for different case studies.

The first part of this chapter presents the implemented procedure for generating the corresponding scenario tree and the solution of the day-ahead multistage stochastic problem.

Next, the decision-making procedure employed to adjust the operation of the REC during the day is introduced. Finally, the performance of the coordinated approach is analysed by using a base case of prosumers in a LV network, and a second case, in which a transactive scheme in a medium voltage (MV) network has been adopted.

Appendix A describes the so-called kinetic battery model (KiBaM), able to better represent the batteries than the one adopted in the description of the models in the various chapters. Some calculations of the scheduling problem of the LES from Chapter 2 have been repeated considering the KiBaM representation.

Appendix B describes an additional representation of a prosumer-based community in a MV network. The model corresponds to a centralized approach, which is suitable for adapting a distributed scheme, and refers particularly to the reduction of power losses. Numerical results have been included to study the application of the approach.

Finally, Appendix C lists the published work that supported the development of this thesis.

Chapter 2. Scheduling of Local Energy Systems

Introduction

"The prosumer – key player in the energy-transition game"

The increasing participation of active prosumers in the energy-grid system has been possible thanks to challenging steps forward in regulatory, technical, and economic aspects. In this process, the alignment of enabling technologies with adequate business models has been crucial to incentivize the implementation of self-consumption schemes as the one associated with prosumers (Rodríguez-Molina et al. 2014).

This transformation of the electrical system and market conducts to the empowerment of prosumers to take more control of their operational decisions, either by implementing mechanisms for consumption regulation or by increasing their self-supply capability, while obtaining an economic compensation (Lavrijssen and Parra 2017).

In the same context, the current picture of the LV network has also been influenced by the current transition to electric mobility and the integration of DERs into microgrids (MGs). There is an increasing appearance of clusters of fast charging stations in parking lots, leading to the development of mainly two types of operation schemes regarding the interaction between plug-in electrical vehicles (PEVs) and the distribution network:

- Grid-to-Vehicle (G2V) scheme, in which the main interest of the PEVs owners is to charge the vehicles as fast as possible.
- Vehicle-to-Grid (V2G) services, in which the operation of the parking lot could be adapted based on the persistent presence of the connected EVs batteries. The V2G scheme can support the accomplishment of objectives such as load flattening and balancing of renewable generation services on site (Develder et al. 2016). In comparison with the G2V scenario, longer parking times for the EVs are expected.

In the V2G scenario, a common objective for the operator of the parking lot is to obtain an economic benefit while offering the users the option of charging their vehicles at the

lowest possible cost. To achieve these objectives, smart charging approaches are implemented to align the charging and dispatching processes of storage systems with the optimization objectives.

The definition of an adequate energy management system (EMS), able to operate the installed equipment and to cost-effectively optimize the exploitation of the available energy resources, seems crucial for the achievement of the local objectives.

This chapter is devoted to the study of the operational planning of grid-connected local energy systems (LES), which, in general, may refer either to a small industrial site, a housing unit acting as a prosumer or an MG integrating RES and fast charging stations.

In the first part of this chapter, we deal with the day-ahead optimization of the operation of a LES, in which, generating units (e.g., PV units) and battery energy storage (BES) systems have been integrated to fully exploit the available renewable resources even for the case of a limited capability of the external utility network.

Moreover, the effect of uncertainties associated with the daily local energy generation and consumption have been studied, under the adoption of a multistage stochastic scheme. To achieve this, a tree-generation technique has been proposed to model the stochastic problem associated with the operation of the considered LES.

Then, an intra-day procedure is introduced in order to adapt the day-ahead solution to the actual operational conditions. For this purpose, the stochastic optimization problem has been considered as a multistage decision problem in which the battery output set points are decided at the beginning of the day and subsequently at the end of consecutive stages during the day. The performance of the proposed approach is analysed by means of several case studies.

In the second part of the chapter, the scenario of an MG that integrates the operation of a parking lot equipped with bidirectional charging stations is studied. The considered case involves a central dispatching system that solves the optimization problem aimed at minimizing the energy procurement costs of the considered site.

Finally, a stochastic multistage approach (like the one introduced in the first part of the chapter) is adopted to deal with the additional uncertainties associated with the presence and state of EVs in the parking lot with the presence of RES.

2.1 Scheduling of a local energy system with a photovoltaic-storage system

This section is devoted to the study of a LES with the presence of RES. The considered system includes a PV unit capable of providing a significant part of the local energy consumption, and it is also equipped with a BES unit to balance the available energy and reduce the associated procurement costs during the day.

In the following, the solution of the day-ahead scheduling of a LES is introduced, which is, in general, associated with the control of the coupled PV-storage system, as dealt with in e.g., (Conte et al. 2019) and (Lilla et al. 2017), where an algorithm for a LV network, based on a mixed integer linear programming (MILP) model, has been proposed with the goal of maximizing the energy provided by the integrated system.

2.1.1 Model of the system operation

In this case, the day-ahead scheduling of the LES is represented with an optimization problem aimed at minimizing the energy procurement costs. The relevant inputs for the optimization problem are the forecast profiles of the PV generation and energy consumption and consider an optimization horizon of 24 hours.

The objective function (*OF*) considers the cost associated with the energy exchange with the external energy provider to feed the internal load for all the time horizon *T*:

$$OF = \sum_{t \in T} \left(\pi^t_{\text{buy}} P^t_{\text{buy\_Grid}} - \pi^t_{\text{sell}} P^t_{\text{sell\_Grid}} \right) \Delta t \qquad (2.1)$$

Parameters π^t_{buy} and π^t_{sell} used in (2.1) are the prices (in €/kWh) of the energy exchanged with the external grid (bought and sold, respectively); nonnegative variables $P^t_{\text{buy\_Grid}}$ and $P^t_{\text{sell\_Grid}}$ are the values of the power absorbed and injected into the external grid; parameter Δt is equal to the 15-minute time step (i.e., 0.25 h).

The power balance of the energy system is represented by (2.2), where P^t_{PV} is the active power injected into the system by the PV unit, and P^t_{Load} is the power adsorbed by the internal loads; P^t_{BES} is the battery power output (nonnegative P^t_{ch} and P^t_{dis} are the battery power outputs during charges and discharges, respectively); P^t_{Grid} is the total power exchanged with the external network at each time *t*. L^t_{BES} are the losses of the battery converter.

$$P_{\mathrm{PV}}^{t} - P_{\mathrm{BES}}^{t} + P_{\mathrm{Grid}}^{t} - P_{\mathrm{Load}}^{t} - L_{\mathrm{BES}}^{t} = 0 \tag{2.2}$$

with

$$P_{\mathrm{Grid}}^{t} = P_{\mathrm{buy\_Grid}}^{t} - P_{\mathrm{sell\_Grid}}^{t} \tag{2.3}$$

$$-P_{\mathrm{Grid}}^{\mathrm{Rated}} \le P_{\mathrm{Grid}}^{t} \le P_{\mathrm{Grid}}^{\mathrm{Rated}} \tag{2.4}$$

$$\begin{cases} P_{\mathrm{buy\_Grid}}^{t} \le (1-u_{\mathrm{Grid}}^{t}) M_{\mathrm{Grid}} \\ P_{\mathrm{sell\_Grid}}^{t} \le u_{\mathrm{Grid}}^{t} M_{\mathrm{Grid}} \end{cases} \tag{2.5}$$

$$P_{\mathrm{BES}}^{t} = P_{\mathrm{ch}}^{t} - P_{\mathrm{dis}}^{t} \tag{2.6}$$

$$-P_{\mathrm{BES}}^{\mathrm{Rated}} \le P_{\mathrm{BES}}^{t} \le P_{\mathrm{BES}}^{\mathrm{Rated}} \tag{2.7}$$

$$\begin{cases} P_{\mathrm{ch}}^{t} \le (1-u_{\mathrm{BES}}^{t}) M_{\mathrm{BES}} \\ P_{\mathrm{dis}}^{t} \le u_{\mathrm{BES}}^{t} M_{\mathrm{BES}} \end{cases} \tag{2.8}$$

$$L_{\mathrm{BES}}^{t} = L_{\mathrm{ch}}^{t} + L_{\mathrm{dis}}^{t} \tag{2.9}$$

$$\begin{cases} L_{\mathrm{ch}}^{t} = \dfrac{1-\eta_{\mathrm{ch}}}{\eta_{\mathrm{ch}}} P_{\mathrm{ch}}^{t} \\ L_{\mathrm{dis}}^{t} = \left(1-\eta_{\mathrm{dis}}\right) P_{\mathrm{dis}}^{t} \end{cases} \tag{2.10}$$

Constraint (2.4) limits the power exchanged with the grid within the maximum $P_{\mathrm{Grid}}^{\mathrm{Rated}}$. Binary variable u_{Grid}^{t} and parameter M_{Grid} (equal to $P_{\mathrm{Grid}}^{\mathrm{Rated}}$) are employed in the big-*M* formulation of constraint (2.5) to avoid simultaneous purchasing and selling processes from and to the utility grid, respectively.

In constraint (2.7), the power output of the battery is limited to the maximum value $P_{\mathrm{BES}}^{\mathrm{Rated}}$. The big-*M* formulation in (2.8) has been implemented in order to avoid concurrent charges and discharges (u_{BES}^{t} is a binary variable and parameter M_{BES} is equal to $P_{\mathrm{BES}}^{\mathrm{Rated}}$). L_{ch}^{t} and L_{dis}^{t} in (2.9) are losses during charging and discharging of the BES unit; In (2.10) η_{ch} and η_{dis} are the converter efficiency factors for charges and discharges.

The operation of the installed BES unit is represented with a simple energy balance at each time interval *t*, according to the following formulation:

$$E_{\mathrm{BES}}^{t} = E_{\mathrm{BES}}^{\max}\ SOC^{t} \tag{2.11}$$

$$SOC^{t} = SOC^{t-1} + \left(P_{\mathrm{BES}}^{t} \Delta t\right) / E_{\mathrm{BES}}^{\max} \tag{2.12}$$

$$\begin{cases} SOC^{t=0} = SOC^{0} \\ SOC^{t=|T|} = SOC^{\text{end}} \end{cases} \tag{2.13}$$

$$SOC^{\min} \leq SOC^{t} \leq SOC^{\max} \tag{2.14}$$

E_{BES}^{t} is the energy level in the battery; SOC^{t} is the battery's state of charge; $E_{\text{BES}}^{\max}$ is the battery's capacity. The energy stored in the BES unit is defined at each time period t by (2.12). SOC^{t} is constrained to the initial and final conditions in (2.13), where SOC^{0} and SOC^{end} are the initial and required final value of the state of charge, respectively. Finally, (2.14) binds SOC^{t} within the corresponding minimum and maximum state of charge (i.e., $SOC^{\min}$ and $SOC^{\max}$, respectively).

2.1.2 Deterministic day-ahead solution

Now, let us consider a test case with a LES equipped with a 1-MW PV unit, a storage system of 630 kWh, a local load with a maximum power consumption equal to 1.5 MW, and a $P_{\text{Grid}}^{\text{Rated}}$ equal to 1.5 MW. Table 2.1 shows the main parameters that characterize the operation of the BES unit.

Table 2.1 Parameters for the operation of the BES unit.

Parameter	Value
$E_{\text{BES}}^{\max}$	630 kWh
$P_{\text{BES}}^{\text{Rated}}$	630 kW
SOC^{0}	1 pu
SOC^{end}	1 pu
$SOC^{\min}$	0.1 pu
$SOC^{\max}$	1 pu

Figure 2.1 shows the day-ahead available profiles of the PV production, the load and the relevant price of buying energy from the energy provider.

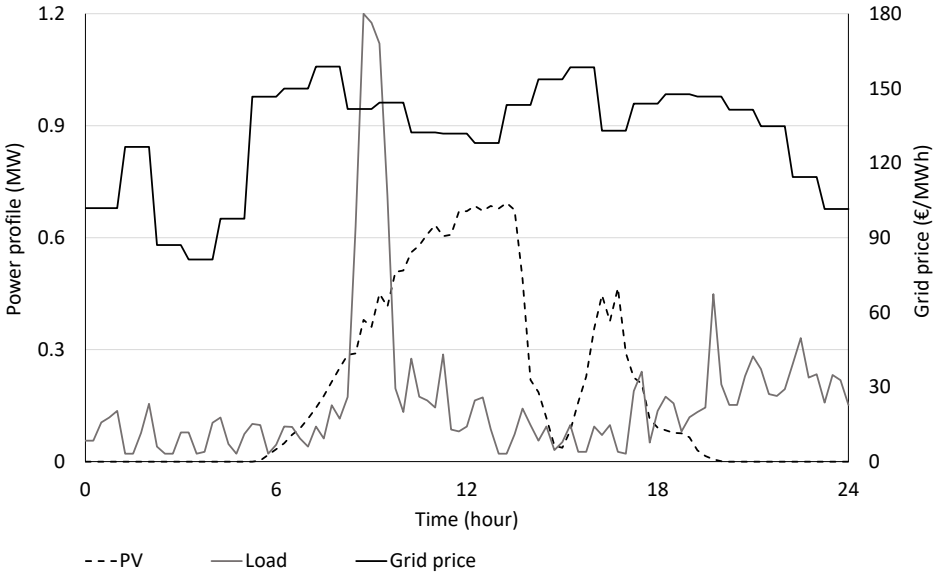

Figure 2.1 Power profile of the PV production, load and grid price.

The problem (2.1) is solved by using an MILP that considers a simple energy balance model for the battery. However, the formulation is suitable for adopting other models of the battery which could refine the calculation, e.g., the kinetic model for the battery (KiBaM) presented in Appendix A.

The model of the LES has been implemented in AIMMS Developer modelling environment (Roelofs and Bisschop 2013) and solved by using the Cplex V12.9 solver in some tens of milliseconds, with the *OF* value equal to €36.70. For the numerical tests presented in this chapter, π_{sell}^{t} is assumed to be half of π_{buy}^{t}.

Figure 2.2 shows the deterministic solution of the optimization problem (i.e., assuming a perfect forecast). Figure 2.2a shows the power flow exchanged with the utility grid (positive if consumed by the LES). In Figure 2.2b, the state of charge of the BES unit (in pu) is shown.

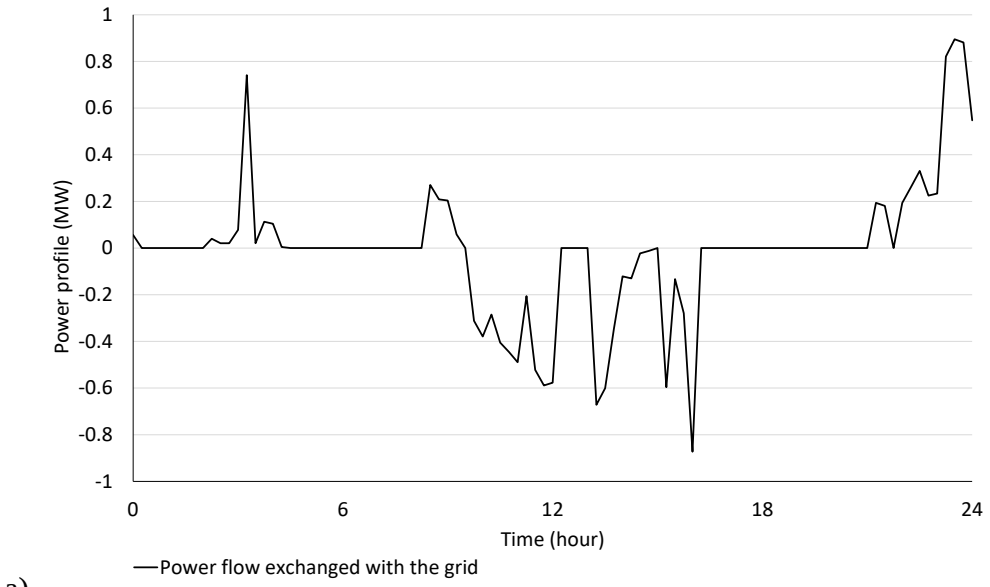

a)

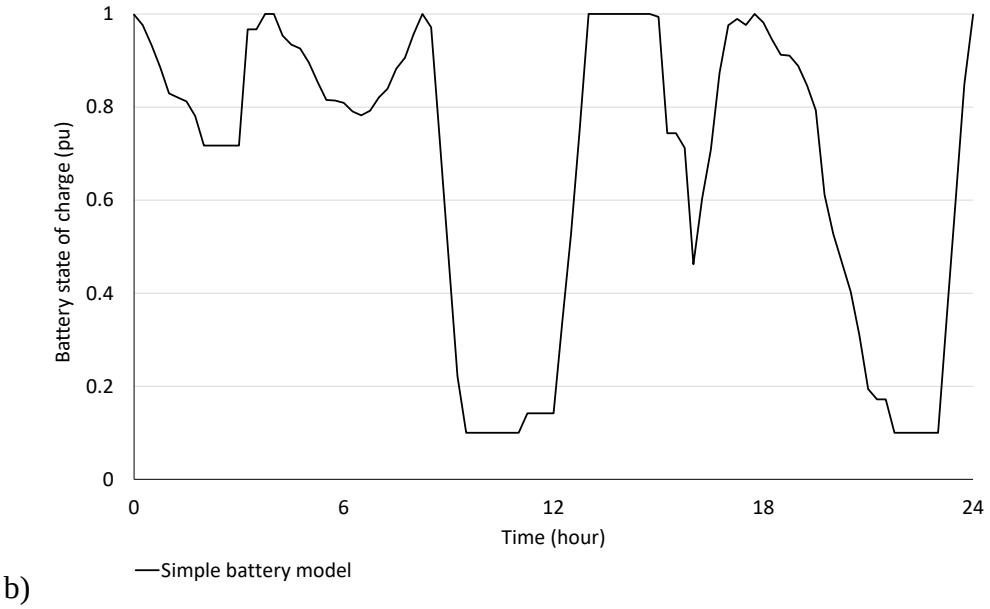

b)

Figure 2.2 Deterministic results for the LES: a) power exchanged with the grid; b) state of charge of the battery.

2.1.3 Multistage stochastic optimization to considerate uncertainties associated with the LES operation

We have seen that the problem associated with the scheduling of energy resources of a prosumer (or in a general of a LES) is suitable to be solved by means of an optimization problem. The corresponding optimization problem implements the action of an EMS that decides the operational set values for the storage units during the day, based on the day-ahead forecast profiles of the inputs and operational constraints.

However, the forecasts of both PV production and load consumption are affected by significant uncertainties; hence, either stochastic optimization approaches or Monte Carlo simulations are typically adopted to solve this kind of problems e.g., (Reddy, Sandeep, and Jung 2017) and (Lazaroiu et al. 2016).

To adapt the day-ahead solution to the intra-day operational conditions, the stochastic optimization problem can be formulated as a multistage decision problem in which the battery output setpoints are decided at the beginning of the day and, subsequently, at the end of predefined stages during the day. For such schemes, the problem needs to be modelled with a scenario tree. In this case, both the PV generation and energy consumption are uncertain, whilst, for the sake of simplicity, prices π^t_{buy} and π^t_{sell} are assumed to be known.

Denoting the set of scenarios with Ω, the scenario index with ω, and the probability of scenario ω with π^ω, the deterministic equivalent of the multistage stochastic problem is the recourse model

$$\min_{P^t_{\text{BES}}} \sum_{\omega \in \Omega} \pi^\omega \cdot OF^\omega \tag{2.15}$$

with constraints (2.2)-(2.14). The solution of the multistage stochastic programming (SP) problem implies the non-anticipativity constraints that represent the inability to anticipate the future. Therefore, scenarios sharing the same history in the scenario tree keep the coherency regarding their decisions in common past events.

Figure 2.3 shows the relevant steps to accomplish the scheduling of the BES unit present in the LES by adopting a multistage approach.

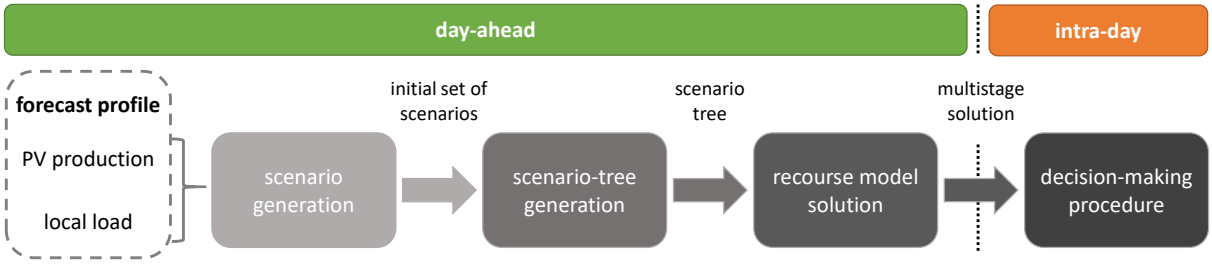

Figure 2.3 Multistage stochastic scheme for the resources scheduling of a local energy system.

In the following, we describe the procedures adopted for the generation of set Ω, the construction of the scenario tree that is used in the recourse model, and the intra-day decision-

making procedure able to adapt the solution of the multistage SP according to the current LES conditions.

A. Generation of scenarios of the PV generation and local load

For the scenario generation, we have applied the procedure described in e.g. (Osório et al. 2015), which includes a Markov-process to represent the autocorrelation that exists between consecutive observations. Starting from the forecast profiles of P_{PV}^{t} and P_{Load}^{t}, at first they are normalized by using the corresponding mean value and standard deviation; then, for each scenario ω, the normalized time series y_{PV}^{t} and y_{Load}^{t} are given by

$$\begin{aligned} z^{\omega,t} &= x^{\omega,t} + y^{t} \\ x^{\omega,t} &= \phi \cdot x^{\omega,t-1} + \varepsilon^{\omega,t} \end{aligned} \tag{2.16}$$

where ϕ is the one-lag autocorrelation parameter, assumed to be equal to 0.999, and $\varepsilon^{\omega,t}$ is a Gaussian white noise with mean zero and standard deviation $\sqrt{1-\phi^{2}}$. The PV production and load profiles for each scenario ω ($P_{\mathrm{PV}}^{\omega,t}$ and $P_{\mathrm{Load}}^{\omega,t}$, respectively) are obtained by applying the inverse transform method assuming a normal distribution, with the constraint that both profiles cannot be negative and that the difference between each profile and the corresponding forecast should not exceed 20% (in all the periods for the load and 75% of the periods for PV production). The error values employed by the scenario-generation technique are coherent with conditions reported, for instance, in (Nespoli et al. 2019), (Sangrody et al. 2017) and (Gerossier et al. 2018).

Although the study of forecasting models is out of the scope of this work, the consideration of their characteristics could be of interest to adequately set the scenario-generation technique in a specific application. To achieve this, accuracy metrics applied to forecasting models, if necessary, could be employed to define a confidence interval. For instance, in (Van der Meer, Widén, and Munkhammar 2018), metrics like the mean absolute error (MAE) and the mean average percentage error (MAPE) are employed to address the assessment of the forecasting accuracy.

In general, the number of scenarios for adequately describing this kind of stochastic process should be appropriately large. In this chapter, the multistage solution will be compared with the results of a Monte Carlo method (comparison presented in section 2.1.5); therefore, a set of 200

scenarios has been generated to limit the computational time required by the Monte Carlo method. Figure 2.4 illustrates the initial set of 200 scenarios obtained from the forecast profiles of P_{PV}^{t} and P_{Load}^{t} in Figure 2.1.

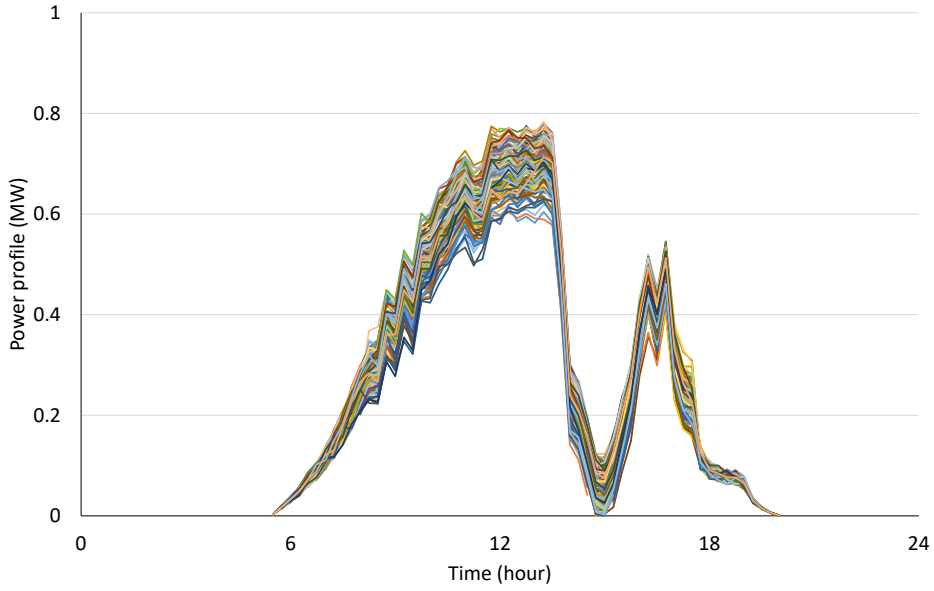

a)

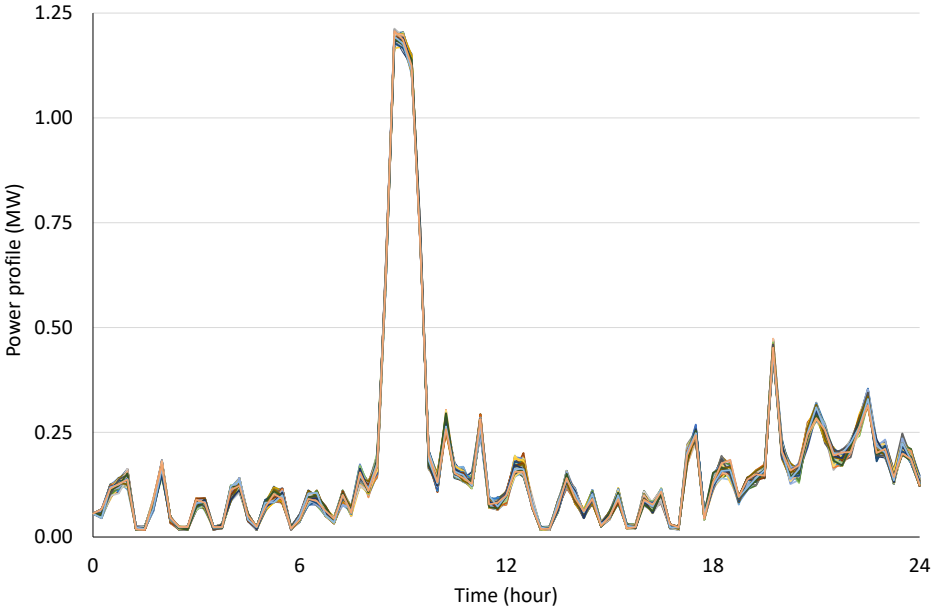

b)

Figure 2.4 Initial set of 200 scenarios: a) PV production; b) load.

B. Scenario-tree construction

In a successive step, the generated scenarios are assumed to be equiprobable and are employed to define the scenario $\xi^{\omega,t}$ which is the normalized difference between the PV production and the load:

$$\xi^{\omega,t} = \frac{P_{\mathrm{PV}}^{\omega,t} - P_{\mathrm{Load}}^{\omega,t}}{P_{\mathrm{PV}}^{t} - P_{\mathrm{Load}}^{t}} \tag{2.17}$$

In the proposed approach, the scenario tree is built by the consecutive application of the *k*-means clustering method, as described in e.g., (Pranevicius and Šutiene 2007). The main steps of this method are the following:

- At stage *s*=1 (that includes only the initial period *t*=0), all scenarios have the same value of parameter, i.e., $\xi^{\omega,t=0} = \xi^{0}$.
- At stage *s*=2 (*t*=1-6), the set of individual scenarios is divided into the predefined number *K* of desired clusters C_k^s. For this purpose, the initial *K* centres $\overline{\xi}_k^t$ are randomly selected; then each scenario $\xi^{\omega,t}$ is assigned to cluster C_k^s so to minimize the dissimilarity measure

  $$d(\xi^{\omega,t}, \overline{\xi}_k^t) = \sum_{t \in T^s} \left\| \xi^{\omega,t} - \overline{\xi}_k^t \right\|_2 \quad \forall k = 1...K \tag{2.18}$$

  where $\| \ \|_2$ indicate the Euclidean distance and T^s is the set of periods in stage *s*.
- Subsequently, the centroid of each cluster is updated as the mean of all the scenarios assigned to the cluster, and the procedure is repeated until the centres of the clusters are not modified in two consecutive iterations.

  The probability of each cluster at the considered stage π_k^s is the sum of the probabilities of the individual scenarios belonging to the cluster. All the scenarios of the same cluster are replaced by the values of the relevant centroid, i.e., $\xi^{\omega,t} = \overline{\xi}_k^t \ \ \forall t \in T^s$ if $\xi^{\omega,t} \in C_k^s$.
- At the stages following the second one, the *k*-means clustering algorithm is applied independently to each cluster defined in the previous stage.

The above-described procedure generates the scenario tree consisting, at each stage *s*, of nodes $\overline{\xi}_k^{t \in T^s}$ with the associated probabilities and the branches that connect nodes at different stages.

Figure 2.5 shows the scenario tree obtained for *K*=3, which is using three centroids. The structure of the tree is given by the defined number of centroids and the number of stages assumed for the day. In this case, we have considered five stages, with decisions every six hours for the decision variable P_{BES}^{t}.

Figure 2.5 includes the probability of each one of the branches in the tree and the total probability for each scenario from the root-node to the relevant leaf (e.g., 64 scenarios in this case).

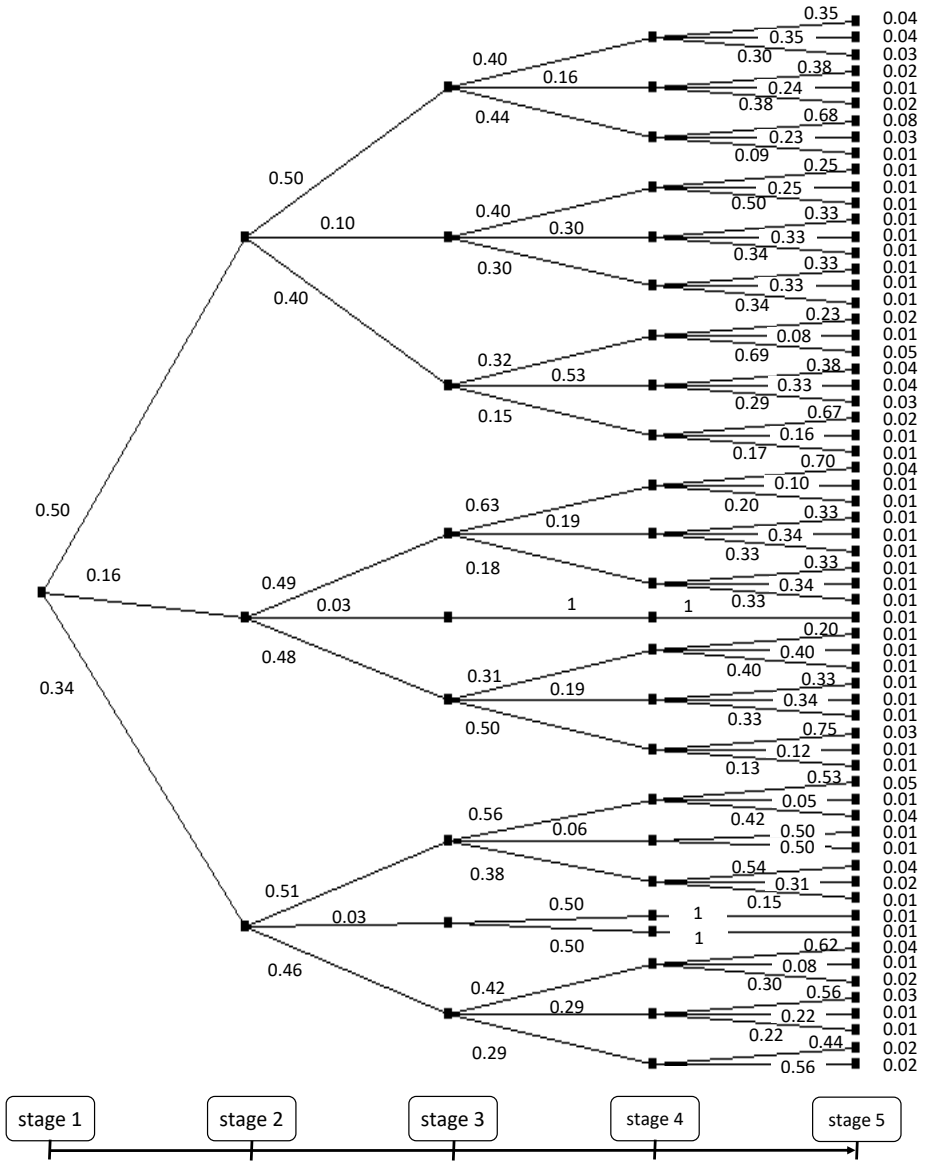

Figure 2.5 Scenario tree obtained for 200 initial scenarios and three centroids.

The first decision is made at the beginning of the day, defining the set values for all periods of the first six hours, and then they will be updated every six hours according to the successive decisions. The six-hour periods represent the stages following the first one. In the recourse solution (i.e., the stochastic solution based on the obtained tree), the values of the other variables at each period *t* are calculated at the end of the corresponding stage.

As a result, the solution of the recourse model provides the optimal values for the BES unit at each node of the tree and for the next six-hours periods (i.e., at *t*=0, *t*=6, *t*=12 and *t*=18).

2.1.4 Decision-making process for an adaptive scheduling during the day

The solution of the recourse model provides multiple possible decisions at each stage following the first one (i.e., during the day); therefore, a decision-making procedure is employed for the choice of the most appropriate decision at each stage among those indicated by the stochastic problem solution considering the current PV generation and load.

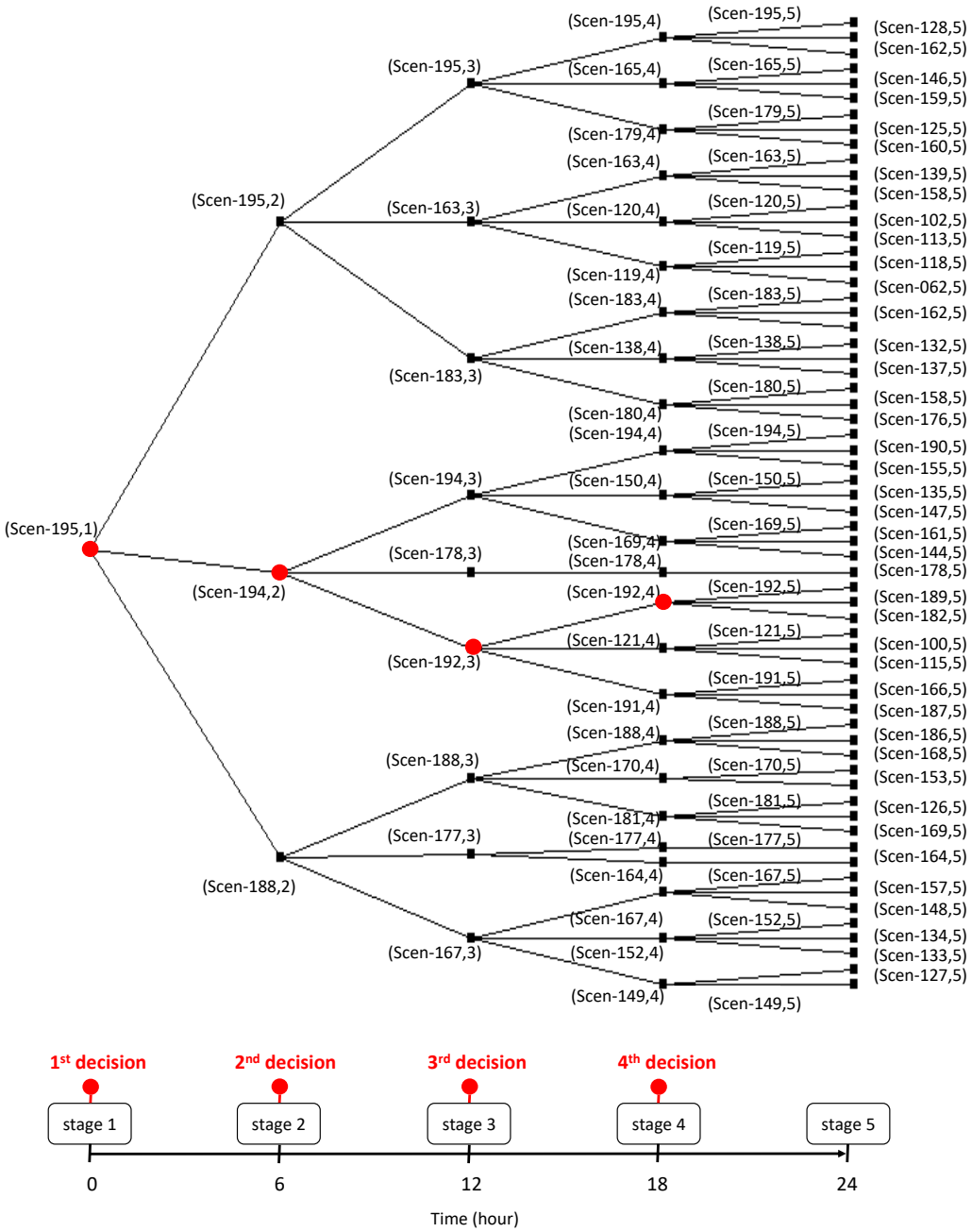

Figure 2.6 Scenario tree with the corresponding scenarios at each node. In red, an example of the solution provided by the intra-day decision-making procedure.

For instance in Figure 2.6, at the beginning of the day, the common root node dictates the set values for the first six hours (corresponding to Scen-195 in the example).

At stage *s*=2, the decision-making procedure finds the scenario of the tree that is the nearest to the profile of the difference between PV generation and load in the previous six hours, by means of the Euclidean distance. Following this decision, the set point values of the battery power output are defined for each 15-minutes time intervals (i.e., the time step Δt) for the following six hours.

At stages *s*=3 and *s*=4, the decision-making procedure finds the scenario of the tree that is the nearest to the profile of the difference between PV generation and load in the previous six hours, only among those directly connected to the node chosen in the previous stage.

2.1.5 Numerical tests for the scheduling of a LES under uncertainties

As already mentioned, the optimization procedures have been implemented in AIMMS Developer and tested by using the Cplex V12.9 MIP solver on 2-GHz processors with 8 GB of RAM, running 64-b Windows.

Table 2.2 compares the *OF* values of the stochastic solution for two different sizes of battery (630 kWh and 315 kWh) by using two different scenario trees obtained through the *k*-means clustering procedure (with the number of centroids *K* equal to three as the one in Figure 2.6 and one additional tree with *K* equal to four).

Table 2.2 SP solution, *VVS* and *EVPI* metrics for both a 630-kWh and a 315-kWh battery.

Size of the BES unit (kWh)	630		315	
Number of centroids	3	4	3	4
OF (€)	38.02	38.25	65.97	66.13
VSS (€)	2.59	2.84	1.95	2.09
EVPI (€)	0.85	1.08	0.48	0.63
Number of scenarios in the tree	64	139	64	139
Solution time (s)	1.54	2.97	1.17	3.47

Additionally, Table 2.2 also shows the Value of Stochastic Solution (*VSS*) and the Expected Value of Perfect Information (*EVPI*), which are widely used metrics in the performance of SP models. According to e.g., (Escudero et al. 2007), the *VSS* and *EVPI* can be calculated as follows:

- ***VSS*** is the difference between the expected value solution (*EEV*) and the stochastic solution, which is the *OF* from the recourse problem (*RP*) (2.15) in this case. In order to calculate *EEV*, at first, the values of the decision variables P_{BES}^{t} for each *t* are obtained

through the solution of the deterministic model in which all random variables are replaced by their expected values; then, *EEV* is the solution of the stochastic problem in which the decision variables are fixed parameters.

- ***EVPI*** is the difference between the stochastic solution and the wait-and-see (*WS*) solution. The *WS* solution is given by the calculation of the expected value of the set of deterministic solutions, each relevant to one of the tree scenarios.

As expected, the higher the number of centroids, the longer the computational effort due to the enlargement of the tree, as shown by the comparison of the solution times and the number of scenarios in the trees reported in Table 2.2 for K=3 and K=4. However, in this instance a more detailed clustering increases the *VSS*, even with an initial set of scenarios not very large with respect to the final dimensions of the tree.

Furthermore, the results in Table 2.2 show a significant increase in the *OF* values for the case with a 315kWh-sized battery, since the balancing effect of using the BES unit is less evident, and, additionally, we can see a decrease of both metrics, namely *VSS* and *EVPI*.

In the following, the performance of the SP approach is compared with the Monte Carlo simulation technique, in which the deterministic model is solved for each initial scenario, and then the P_{BES}^{t} values are set to equal to the average of the corresponding values obtained by the deterministic solutions. For this purpose, the daily energy procurement costs calculated by the SP approach are compared with those calculated by the Monte Carlo method.

Figure 2.7 shows, for each scenario in the tree obtained with three centroids, the comparison of the *OF* values calculated by using the Monte Carlo method and those given by the intra-day decision-making procedure based on the SP solution. The figure also includes the *OF* values of the deterministic solutions that are assuming a perfect forecast for each intra-day scenario.

In general, the SP approach provides better results with respect to Monte Carlo, and this is confirmed also by Figure 2.8 that shows the same comparison for 50 different scenarios from those included in the initial set Ω. In the case of the 3-centroids tree, the adoption of the SP approach also employs a shorter solution time with respect to the Monte Carlo simulations that require around five seconds (without parallel computing).

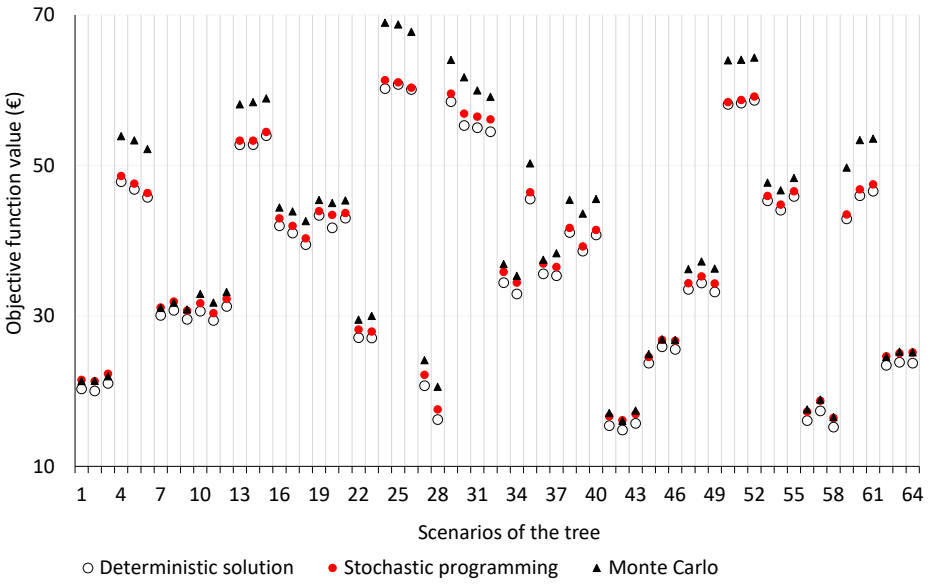

Figure 2.7 Comparison of the *OF* values for each scenario of the tree obtained by applying the *k*-means clustering with three centroids (630-kWh battery).

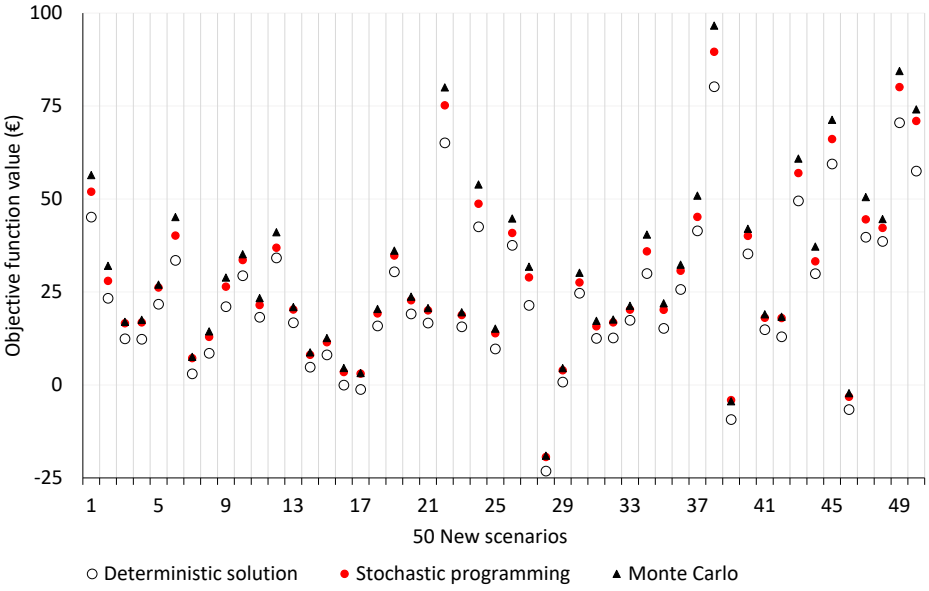

Figure 2.8 Comparison of the *OF* values for 50 new scenarios (630-kWh battery).

Table 2.3 shows the average values of the following differences for three different set of scenarios, namely the scenarios of the tree, the initial set of 200 scenarios, and 50 scenarios different from those of the previous sets:

- ***SP-MC*:** Difference between the *OF* values given by the intra-day decision-making procedure and the Monte Carlo solution.
- ***SP-WS*:** Difference between the *OF* values given by the intra-day decision-making procedure and the deterministic solution.

The results in Table 2.3 show the advantage of using the SP approach and the benefit of a more accurate clustering procedure. For the case of the 315-kWh battery, the results confirm, in general, the advantages of using four centroids, although the average differences are smaller than for the 630-kWh battery.

Table 2.3 Comparison between SP solutions and Monte Carlo simulations and between SP and deterministic solutions for both a 630-kWh and a 315-kWh battery.

Size of the BES unit (kWh)		630		315	
Number of centroids		3	4	3	4
Scenarios of the tree	*SP – MC*	-2.51	-2.55	-1.61	-1.58
	SP – WS	0.97	1.13	0.56	0.66
Set of initial scenarios	*SP – MC*	-2.05	-2.47	-1.13	-1.44
	SP – WS	5.17	2.70	2.21	1.91
Set of new scenarios	*SP – MC*	-2.28	-2.29	-1.12	-1.14
	SP – WS	4.85	4.84	2.81	2.79

Finally, to test the performance of the SP approach under different conditions, the profile of the local load has been replaced by a new one, obtaining a new set of load scenarios that replace those of Figure 2.4b. Table 2.4 shows the corresponding results regarding *OF* values and metrics and Table 2.5 presents the performance comparison of the SP solution and Monte Carlo simulations and of the SP and deterministic solutions for a battery of 630 kWh.

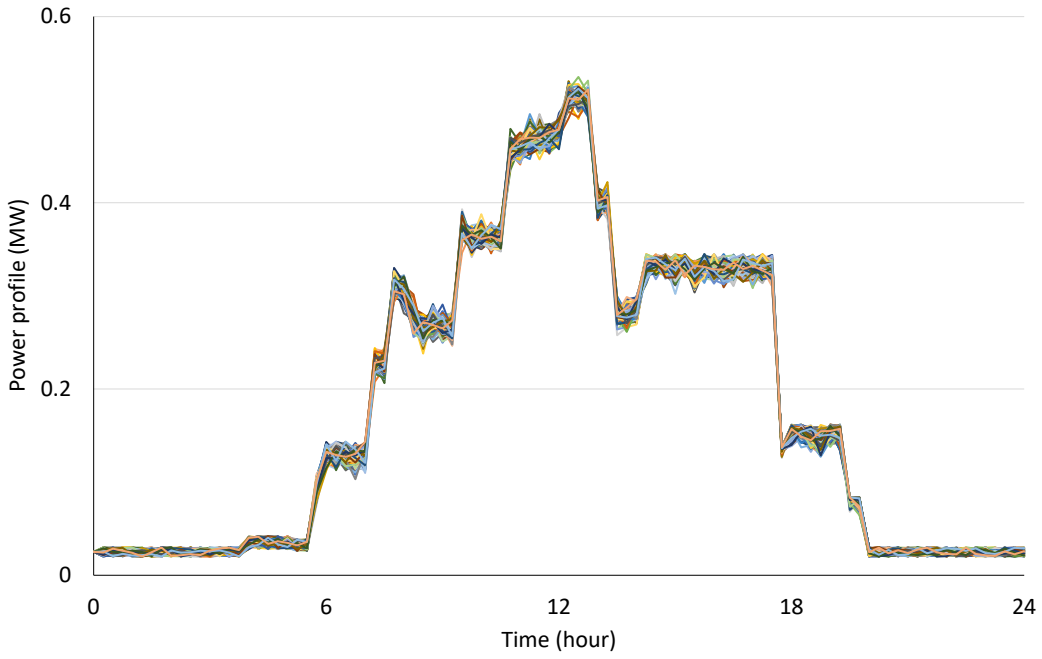

Figure 2.9 Scenarios obtained for a different forecast of load profile.

The results confirm the advantages of the SP. Only in the case of the 50 new scenarios, and using three centroids, the average performance for the stochastic solution is higher than the one obtained by using the Monte Carlo simulations. The use of four centroids increases the *VSS* and allows for reaching improved results with respect to the Monte Carlo technique.

Table 2.4 SP Solution, *VVS* and *EVPI* metrics (630-kWh battery and load scenarios of Figure 2.9).

Number of Centroids	3	4
OF (€)	-2.94	-2.33
VSS (€)	1.75	2.52
EVPI (€)	2.66	3.19
Number of scenarios in the tree	74	169
Solution time (s)	1.53	4.45

Table 2.5 Performance comparison between SP solution and Monte Carlo simulations and between SP and deterministic solutions (630-kWh battery and load scenarios of Figure 2.9).

Number of centroids		3	4
Scenarios of the tree	*SP – MC*	-1.37	-1.84
	SP – WS	3.71	3.37
Set of initial scenarios	*SP – MC*	-0.28	-1.06
	SP – WS	7.19	6.41
Set of new scenarios	*SP – MC*	0.64	-0.39
	SP – WS	9.35	8.33

2.2 Scheduling of microgrids with the presence of renewables and EV charging stations

This second part of the chapter is focused on the study of the operation of an MG including a parking lot equipped with bidirectional charging stations for PEVs. The considered MG might include an integrated system of renewable generation (e.g., PV panels) and stationary BES units, as the one illustrated in Figure 2.10. The energy procurement cost associated with the operation of the considered site is minimized by a central dispatching system.

The literature on charging load modelling is becoming quite large, as shown in the recent survey presented in (Xiang et al. 2019). An analysis of the advantages and drawbacks of different approaches to the integration of EVs is presented in (García-Villalobos et al. 2014). Additionally, a study of the state-of-the-art of fast-charging stations including experimental test has been introduced in (Sbordone et al. 2015).

The integrated operation of parking facilities with RES as the one considered in this chapter has been extensively studied, as shown in, e.g., (Mwasilu et al. 2014). An evaluation of the integration of PEVs with PV systems, in order to cope with the fluctuation of solar irradiance, has been performed in (Traube et al. 2013). An additional approach that takes into account the uncertainties of PEVs arrival and grid power price has been presented in (T. Zhang et al. 2014). Furthermore, a generation scheduling method for the coordinated operation of an industrial microgrid, which considers electricity and heat generation, electrical loads, PV units and PEVs is presented in (Derakhshandeh et al. 2013).

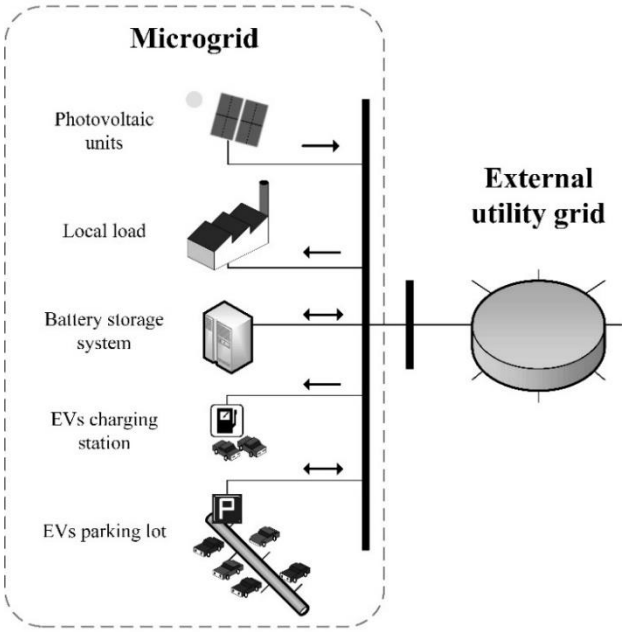

Figure 2.10 Scheme of a microgrid with both local generation and EV charging stations.

An optimization model for the assessment of the contribution of V2G systems has been proposed in (Battistelli, Baringo, and Conejo 2012). The method in (Zakariazadeh, Jadid, and Siano 2015) contemplates the presence of an aggregator acting as an intermediate agent between end-users and the distribution system operators (DSOs). Moreover, a study of the feasibility of premium tariffs rates for V2G services similar to feed-in-tariff (FIT) programs for RES, has been presented in (Richardson 2013).

To cost-effectively operate such an electric system, it is crucial to consider the uncertainties associated with the presence and state of the vehicles in the parking lot, the PV generation, and the local load.

Therefore, in this chapter, an approach based on a multistage stochastic optimization as the one introduced in section 2.1.3, has been adopted. For this purpose, we make reference to the linear programming model presented in (Dabbagh, Sheikh-El-Eslami, and Borghetti 2016), although

the procedure can be suitably adapted to be used with different stochastic models for the optimal operation of EV parking lots in MGs (e.g., those presented in (Battistelli, Baringo, and Conejo 2012) and (Honarmand, Zakariazadeh, and Jadid 2014)) and in power distribution systems (e.g., (Khodayar, Wu, and Shahidehpour 2012) and (Shafie-Khah et al. 2016)).

A scenario tree obtained by means of the scenario reduction technique is employed by the EMS to model and solve the day-ahead scheduling of the energy resources in the site. The use of the initial energy in the EVs entering the parking is limited. The model considers other typical constraints (such as maximum number of available charging stations, size of the EV batteries, and the power ratings of charging stations). Moreover, a procedure aimed at guaranteeing a feasible solution for the operation of the site is introduced.

2.2.1 Multistage stochastic model for the day-ahead scheduling problem

The model described in this section is aimed at defining the day-ahead scheduling of the global charging and discharging of the EV batteries connected to the charging stations in order to minimize the energy procurement cost. The considered site is connected to the external utility grid and includes a PV unit and local loads.

The linear programming model presented in (Dabbagh, Sheikh-El-Eslami, and Borghetti 2016) is characterized by the introduction of specific operating rules relevant to the initial energy available in the EVs entering the parking lot. In the following, the two-stage stochastic model proposed in (Dabbagh, Sheikh-El-Eslami, and Borghetti 2016) will be extended into a multistage stochastic programming model, following the approach of (Borghetti et al. 2017).

The stochastic optimization problem considered by the dispatching centre is represented by (2.19) with an optimization horizon corresponding to the next day (divided into one-hour periods):

$$\min \sum_{\omega} \pi^{\omega} C^{\omega} \tag{2.19}$$

with

$$C^{\omega} = \sum_{t} \left[\rho_{\mathrm{TOU}}^{t} \left(E_{\mathrm{buy\_Grid}}^{\omega,t} - rE_{\mathrm{sell\_Grid}}^{\omega,t} \right) + C_{S}^{\omega,t} \right] \tag{2.20}$$

the cost associated with scenario ω is represented by C^{ω} and ρ_{TOU}^{t} corresponds to the Time-of-Use (TOU) tariff for purchasing energy from the grid in period *t*. Value *r* is the ratio between sale and purchase tariffs. $E_{\mathrm{buy\_Grid}}^{\omega,t}$ and $E_{\mathrm{sell\_Grid}}^{\omega,t}$ correspond to the energy bought and sold from

and to the utility grid, respectively. $C_S^{\omega,t}$ is the total cost associated with the use of the V2G parking lot.

For the V2G parking lot, the decision variables $P_{\mathrm{V2G}}^{\omega,t}$ represents the power exchange of the V2G parking lot calculated for each node of the scenario tree (positive when selling to the grid), and $\mu^{\omega,t}$ is the nonnegative utilization coefficient of the total energy initially stored in the EVs that arrive in the parking lot at time *t* ($E_{S+}^{\omega,t}$).

The constraints that represent the behaviour of the V2G parking lot are:

$$P_{\mathrm{V2G\,min}}^{\omega,t} \le P_{\mathrm{V2G}}^{\omega,t} \le P_{\mathrm{V2G\,max}}^{\omega,t} \tag{2.21}$$

$$E_S^{\omega,t} = (1-\delta)E_S^{\omega,(t-1)} - P_{\mathrm{V2G}}^{\omega,t}\Delta t + E_{S+}^{\omega,t} - E_{S-}^{\omega,t} \tag{2.22}$$

$$E_S^{\omega,t} \le E_{S\,\max}^{\omega,t} \tag{2.23}$$

$$0 \le \mu^{\omega,t} \le \frac{\left(E_{S+}^{\omega,t} - e_{\min} N_{\mathrm{in}}^{\omega,t} E_{\mathrm{EV}}^{\mathrm{Rated}}\right)}{E_{S+}^{\omega,t}} \cdot u\left(E_{S+}^{\omega,t} - e_{\min} N_{\mathrm{in}}^{\omega,t} E_{\mathrm{EV}}^{\mathrm{Rated}}\right) \tag{2.24}$$

$$E_{\mathrm{V2G}}^{\omega,t} = (1-\delta)E_{\mathrm{V2G}}^{\omega,(t-1)} - P_{\mathrm{V2G}}^{\omega,t}\Delta t + \mu^{\omega,t}E_{S+}^{\omega,t} + \sum_{j=0}^{t}(1-\mu^{\omega,t})E_{\mu}^{\omega,j,t} - E_{S-}^{\omega,t} \tag{2.25}$$

$$l^{\omega,t} \ge \begin{cases} (1-\eta_{\mathrm{dis}})P_{\mathrm{V2G}}^{\omega,t} \\ \left(1-\dfrac{1}{1-\eta_{\mathrm{ch}}}\right)P_{\mathrm{V2G}}^{\omega,t} \end{cases} \tag{2.26}$$

$$C_S^{\omega,t} \ge \begin{cases} c_{\mathrm{dis}}P_{\mathrm{V2G}}^{\omega,t}\Delta t + c_{\mu}\mu^{\omega,t}E_{S+}^{\omega,t} \\ -c_{\mathrm{ch}}P_{\mathrm{V2G}}^{\omega,t}\Delta t + c_{\mu}\mu^{\omega,t}E_{S+}^{\omega,t} \end{cases} \tag{2.27}$$

Constraint (2.21) binds the power exchange of the V2G parking lot within its maximum and minimum value, represented with $P_{\mathrm{V2G\,max}}^{\omega,t}$ and $P_{\mathrm{V2G\,min}}^{\omega,t}$, respectively. The energy stored by the EV's batteries at the end of period *t*, i.e., $E_S^{\omega,t}$, is determined by (2.22). Constraint (2.23) limits the maximum value of the storage capability, where $E_{S\,\max}^{\omega,t}$ represents the corresponding maximum.

When EVs reach the parking lot, their energy adds to the total energy of the V2G parking lot $E_S^{\omega,t}$. Constraint (2.24) limits the maximum value of $\mu^{\omega,t}$ so that initial charge of the battery

may be used only for the amount exceeding a predefined minimum fraction $e_{\min}$ of the rated energy size $E_{\mathrm{EV}}^{\mathrm{Rated}}$. Additionally, this constraint avoids deep discharge conditions. Function $u(\cdot)$ in (2.24) represents the step function with value 0 for negative arguments and 1 for positive arguments.

Constraint (2.25) is introduced to calculate the available energy for dispatching services $E_{\mathrm{V2G}}^{\omega,t}$. To achieve this, the dispatching centre determines the exploitation factor $\mu^{\omega,t}$ of the total energy $E_S^{\omega,t}$. $E_\mu^{\omega,j,t}$ corresponds to the initial energy of the EVs arriving in period *j* and leaving in time period *t* (*j*=0 indicates the EVs already parked when the optimization horizon begins).

This scheme permits the implementation of the battery-to-battery charging strategy in a V2G system. The total cost $C_S^{\omega,t}$ considers the cost of this retrieval according to price c_μ. Such a cost is considered at the arriving time of the EVs, whilst the associated energy can be retrieved in all the period during the parking time.

Variable $l^{\omega,t}$, in (2.26), corresponds to the power losses associated with charging/discharging processes, with η_{ch} and η_{dis} equal to the average efficiency of the EV's batteries and charging stations during charging and discharging, respectively. In (2.27), the prices associated with the charging and discharging processes (i.e., c_{ch} and c_{dis}, respectively) are also considered for the calculation of $C_S^{\omega,t}$.

Disregarding network power losses, the energy balance in each period of the microgrid is

$$\sum_u P_u^{\omega,t}\Delta t = E_{\mathrm{sell\_Grid}}^{\omega,t} - E_{\mathrm{buy\_Grid}}^{\omega,t} \tag{2.28}$$

where $P_u^{\omega,t}$ indicates the net active power provided or absorbed by unit *u* (positive if provided to the MG), which corresponds, in the considered case, to the parking lot, the PV unit and the local load in the MG. Both $l_{t\omega}$ and $C_S^{\omega,t}$ (nonnegative variables according to (2.26) and (2.27) , respectively) are minimized as a result of the minimization of the objective function in (2.19) . The net power of the V2G parking lot $P_{u=\mathrm{V2G\ net}}^{\omega,t}$ is given by

$$P_{u=\mathrm{V2G\ net}}^{\omega,t} = P_{\mathrm{V2G}}^{\omega,t} - l^{\omega,t} \tag{2.29}$$

In this model, the power values associated with the PV unit and the local loads cannot be dispatched.

2.2.2 Scenarios and tree generation procedures

Following the scheme introduced in section 2.1.3, a set of equiprobable scenarios is obtained and used as input for the scenario-tree generation. This section includes the considerations for the scenario generation of the V2G parking lot and the scenario generation for the power profile associated with the PV unit and the local loads.

A. Conditions for the scenarios associated with the V2G parking lot

For each scenario ω of the V2G parking lot, a population of N_{tot} EVs willing to enter the parking lot is generated according to chosen statistical distributions (e.g., a normal distribution with the mean value equal to the forecasted number of potential users of the parking lot).

In this approach, the number of available charging stations is limited. Hence, the amount of EVs from the total N_{tot} that can be connected to a charging station will depend on the available parking-spots. Each *i*-th EV is characterized by the parameters: time of entrance (t_i^+), initial charge (E_i^0) and staying time in the parking lot (s_i). For illustrative purposes in this chapter, these parameters are also generated according to a normal distribution with mean value equal to the forecasted value. Although the rated capacity of the batteries is considered constant and equal for all the EVs, it could also be assumed as a variable.

The energy stored E_i^- is equal to 1 pu if the time of stay s_i is long enough to get a full recharge, otherwise is set to ratio between s_i and the time needed for a full recharge. For scenario ω, the procedure builds two sets: $S_+^{\omega,t}$, which considers the EVs incoming at time *t*, and $S_-^{\omega,t}$, which consider the EVs leaving at time *t*.

On the basis of these sets, the procedure calculates the parameters needed in (2.21)-(2.27):

- the increase of the energy stored in the parking lot due to arrivals at time *t* $\left(E_{S+}^{\omega,t} = \sum_{i \in S_+^{\omega,t}} E_i^0\right)$
- the decrease of the energy stored in the parking lot due to departures at time *t* $\left(E_{S-}^{\omega,t} = \sum_{i \in S_-^{\omega,t}} E_i^-\right)$
- the decrease of the energy stored in the parking lot at time *t* due to the initial charge of the EVs entered at time *j* and leaving at *t* $\left(E_{\mu}^{\omega,j,t} = \sum_{i \in \left\{S_+^{\omega,j} \cap S_-^{\omega,t}\right\}} E_i^0\right)$.

B. Conditions for the scenarios associated with the PV unit and local loads

The scenario generation for the PV unit and of the local loads are generated by using the day-ahead forecasts and the probability distributions that characterize the expected deviations with respect to the forecasts following the scheme in section 2.1.3A.

To avoid unrealistic scenarios for the PV unit power output, all the $P_{\mathrm{PV}}^{\omega,t}$ profiles do not differ by more than 10% from the forecasted profile for at least 90% of the time. In the case of local loads and the amount of EVs at the charging stations (i.e., added load associated with G2V service), the profiles are obtained by multiplying the forecasted profile by $1+k(t)$, where $k(t)$ is generated by using a normal distribution with mean value equal to 0 and standard deviation $\sigma=\sqrt{1-\psi(t)^2}$, and $\psi(t)$ is a decreasing function of *t* in order to represent the increase of the incertitude with time.

C. Tree generation by using k-means

Following the procedure adopted in (Orozco et al. 2018), after the generation of the set of initial scenarios, a *k*-means clustering method is employed in order to aggregate the set of initial scenarios and build the corresponding scenario tree.

In the studied case, and for illustrative purposes, the 24-hour optimization horizon is divided into four decision stages (with decisions every six hours). The relevant parameters considered by the clustering procedure are the number of parked EVs, PV generation and the non-dispatchable load in the MG. Figure 2.11 shows the main steps of the implemented method based on the *k*-means clustering procedure and described in detail in section 2.1.3.

Each scenario $\xi^{\omega,t}$ corresponds to a realization of the stochastic parameters of number of EVs in the parking lot, PV generation, and total load (i.e., considering local load and charge of EVs at the charge station G2V) in the form:

$$\xi^{\omega,t}=\left[N_{\mathrm{EV}}^{\omega,t},P_{\mathrm{PV}}^{\omega,t},P_{\mathrm{Load}}^{\omega,t}\right] \tag{2.30}$$

At each defined stage, each scenario is grouped to one of the centroids of the algorithm based on the average value of the number of parked EVs, PV output and total local load in the six-hour.

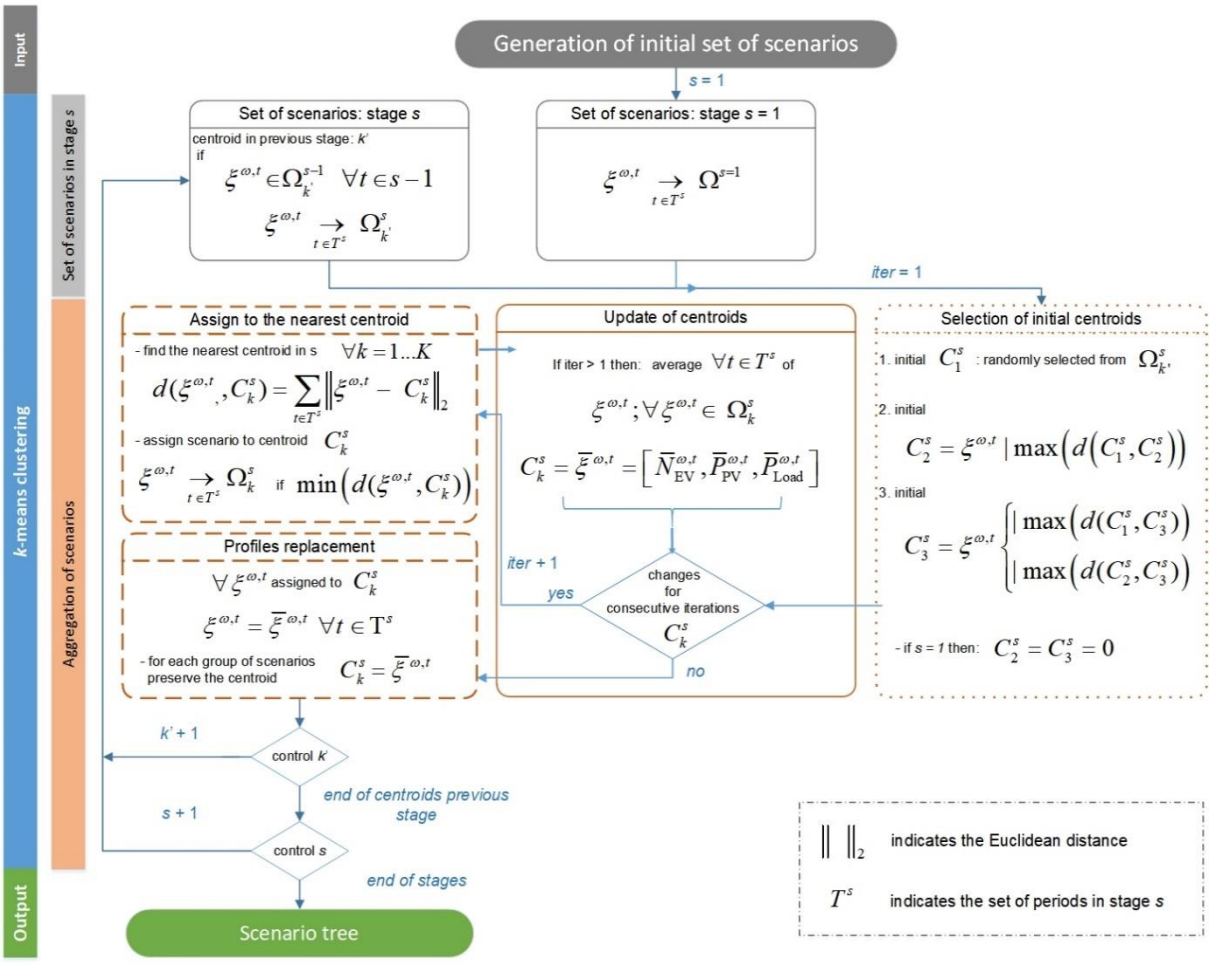

Figure 2.11 Implemented *k*-means algorithm.

All the values of the parameters of the scenarios grouped together are averaged in order to assign a unique value to each of them for each hour of the stage. At each period *j*, the values of $E_{\mu}^{\omega,j,t}$ for all the scenarios in the same group are averaged for all $t > j$.

Moreover, a matrix that contains the number of EVs that arrive in period *j* and leave in period *t* is defined and averaged as done for $E_{\mu}^{\omega,j,t}$. In order to guarantee the existence of a feasible solution of the optimization problem of the V2G parking lot, this matrix is used to define the averaged values of the number of parked EVs, and therefore of $E_{S\max}^{\omega,t}$, whilst $E_{\mu}^{\omega,j,t}$ is used to define the average values of $E_{S+}^{\omega,t}$ and of $E_{S-}^{\omega,t}$.

2.2.3 Case study of a microgrid with the presence of renewable and EV charging stations

For illustrative purposes, let us consider a grid-connected MG composed of a parking lot with 100 charging points, each with 7 kW rated power, a 3.5-MWp photovoltaic system, and local loads up to 3 MW. For the considered case study, the parking lot is assumed empty at time *t*=0,

the energy capacity of the EVs batteries is 24 kWh, efficiencies η_{ch} and η_{dis} are equal to 0.96, c_{μ} is 1.8 €/MWh, minimum energy value e_{min} is equal to 0.2 pu, price ρ^{t}_{TOU} is equal to 72.39 €/MWh from 7am to 11pm and is equal to 51.62 €/MWh in the other hours, ratio r between selling and buying price of electric energy is equal to 0.5, and δ is neglected.

An initial set with 60 scenarios has been generated for all the stochastic variables that model the operation of the site. Table 2.6 shows the parameters that characterize the normal distributions (i.e., mean value and standard deviation) employed by the scenario generation of N_{Tot}, t_i^+, E_i^0 and s_i.

Table 2.6 Parameters of the normal distribution functions for the V2G scenario generation.

Population parameters	Mean value	Standard deviation
Time of entrance t_i^+	9	2
Initial charge (pu) E_i^0	0.3	0.3
Time of stay s_i	8	2
Number of entrances N_{Tot}	100	10

Figure 2.12 shows the resulting profiles for EVs in the parking lot $N_{EV}^{\omega,t}$.

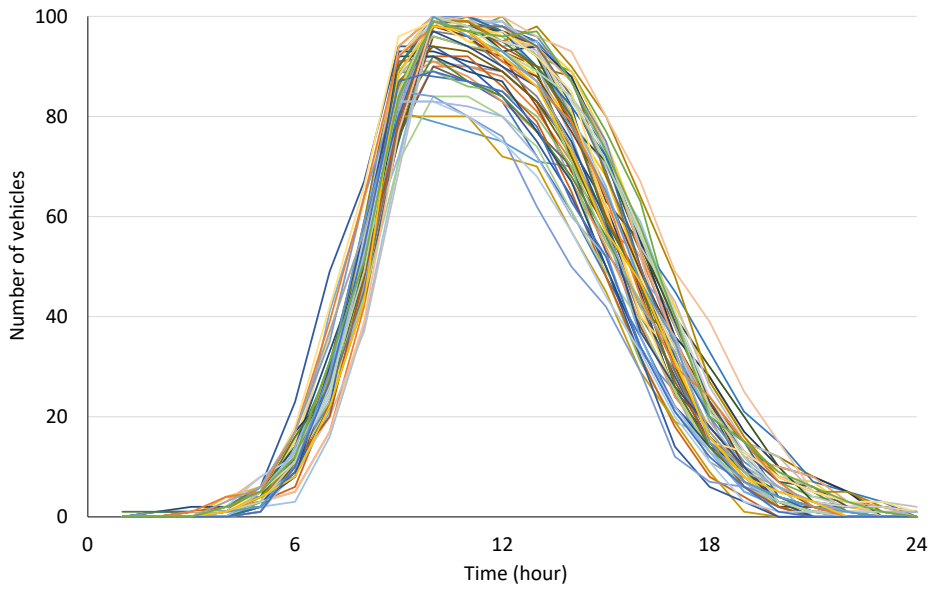

Figure 2.12 Number of parked EVs in the parking lot $N_{EV}^{\omega,t}$.

Figure 2.13 shows the profiles of the PV obtained by assuming ϕ = 0.999. Figure 2.14 shows the profiles of the total load in the MG by assuming ψ linearly, decreasing from one at t =1 to 0.99 at t = 24.

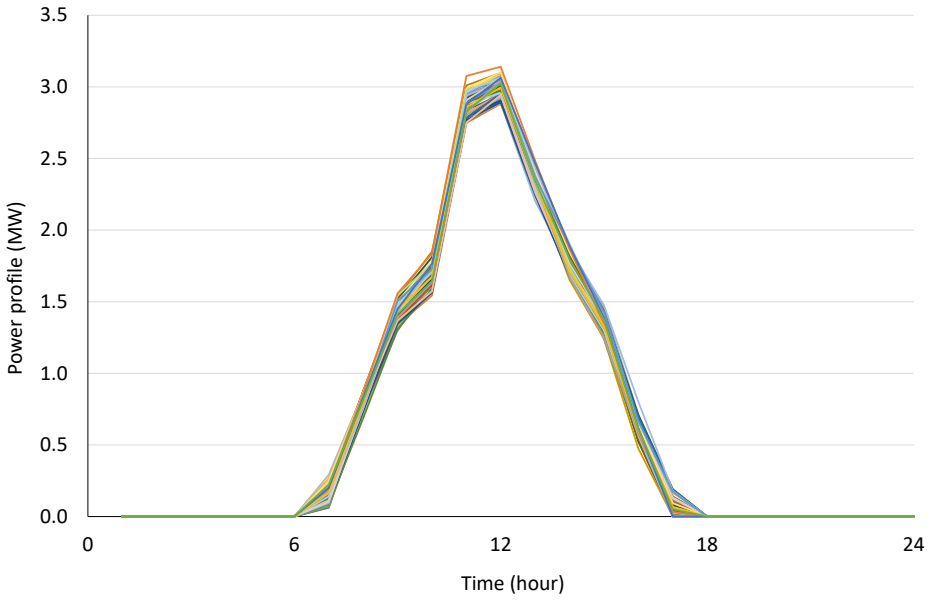

Figure 2.13 PV output profiles.

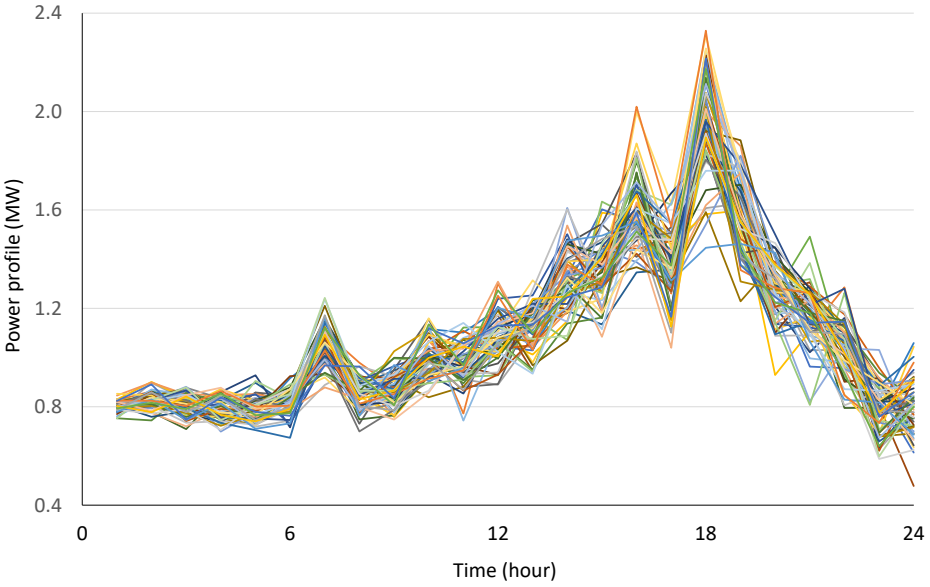

Figure 2.14 Total load profiles.

Figure 2.15 shows the structure of the scenario tree obtained by the implemented *k*-means procedure.

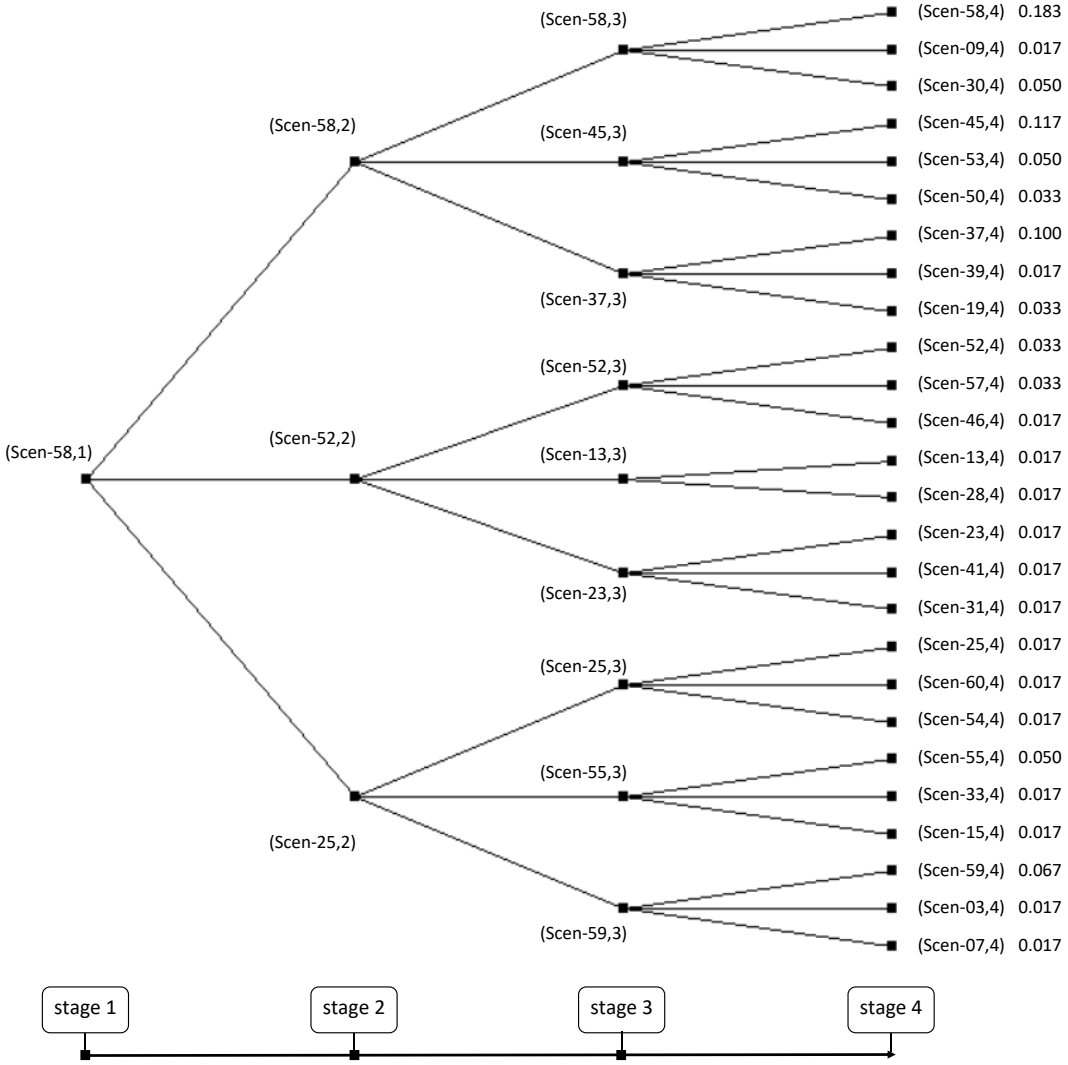

Figure 2.15 Multistage scenario tree for the microgrid with the presence of bidirectional charging stations.

Figure 2.16 - Figure 2.20 show the profiles obtained after the clustering procedure (i.e., 26 aggregated scenarios in the scenario tree of Figure 2.15). Figure 2.16 shows the number of parked EVs $N_{\mathrm{EV}}^{\omega,t}$ and Figure 2.17 shows the total energy entering the parking lot associated with EV arrivals at each time period t $E_{S+}^{\omega,t}$.

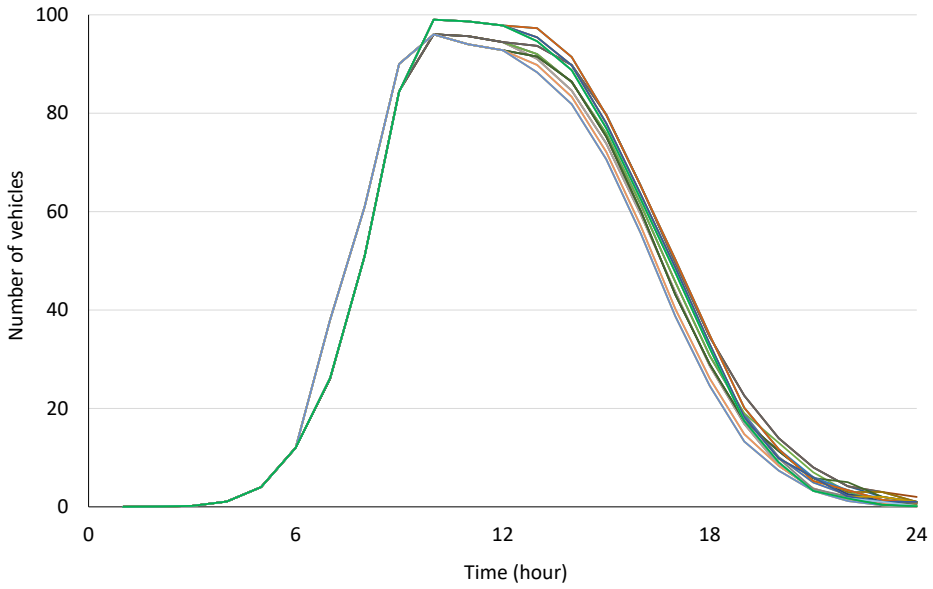

Figure 2.16 Selected scenarios of number of parked EVs $N_{\mathrm{EV}}^{\omega,t}$.

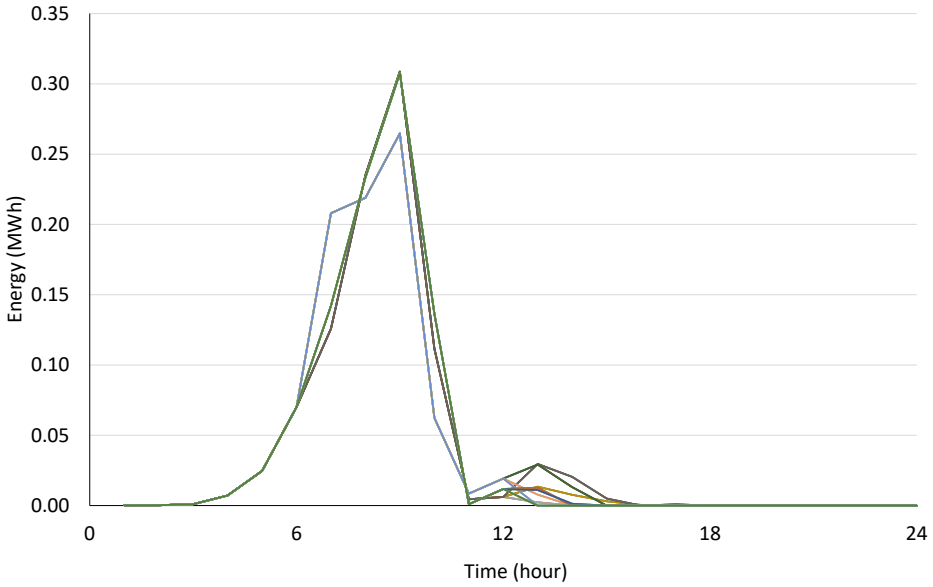

Figure 2.17 Selected scenarios of total energy $E_{S+}^{\omega,t}$ entering the parking lot due to EVs arrivals.

Figure 2.18 shows the total energy leaving the parking lot due to EV departures at each time period *t* that is $E_{S-}^{\omega,t}$, Figure 2.19 shows the PV power outputs and Figure 2.20 shows the local load profiles.

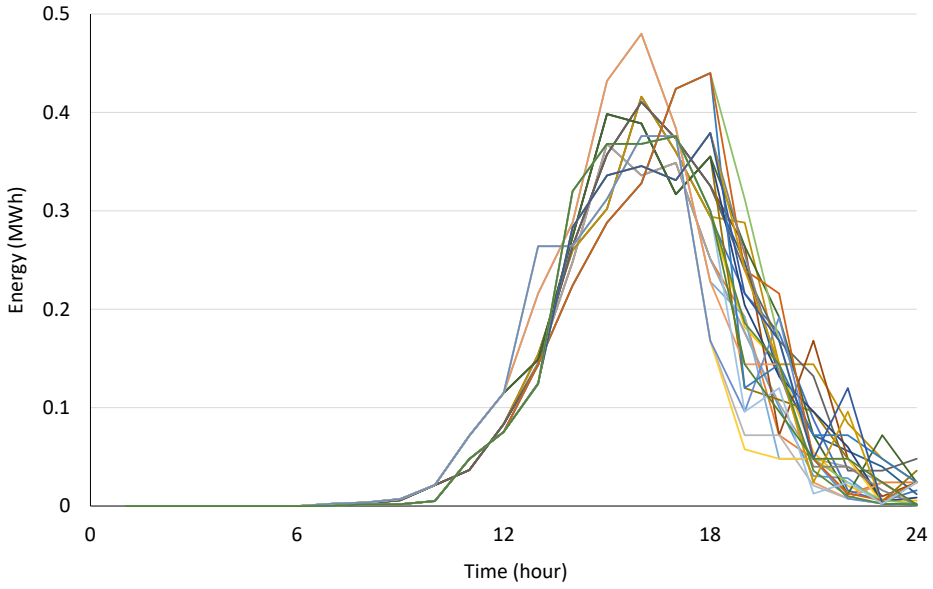

Figure 2.18 Selected scenarios for the total energy $E_{S-}^{\omega,t}$ leaving the parking lot due to EVs departures.

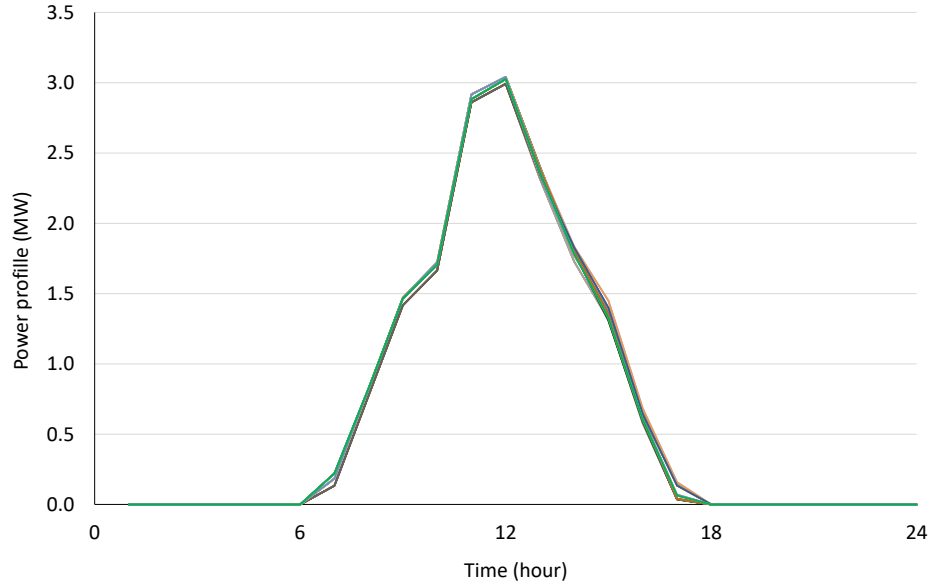

Figure 2.19 Selected scenarios for the power delivered by the photovoltaic system.

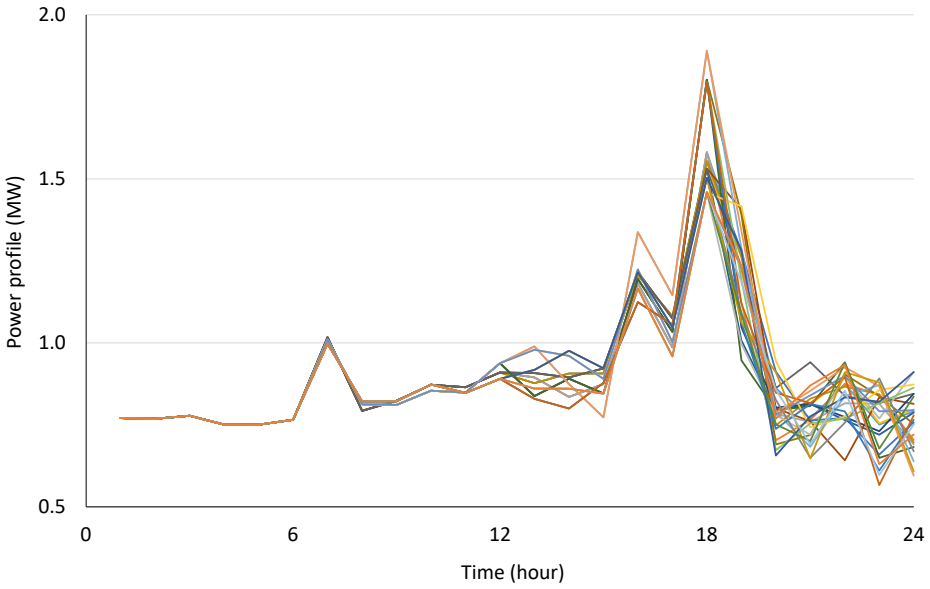

Figure 2.20 Selected scenarios for the power consumptions of the local loads of the microgrid.

2.2.4 Solution of the multistage stochastic model

The optimization procedures have been implemented in AIMMS Developer modelling environment and solved in around 15 s by using the Cplex V12.9 MIP solver.

Figure 2.21 shows the dispatched power of the V2G parking lot.

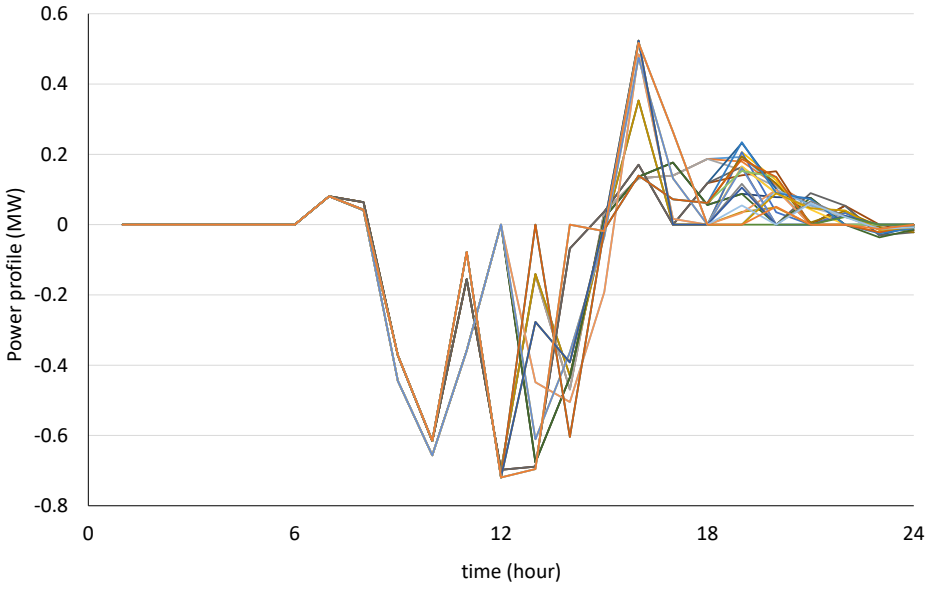

Figure 2.21 Power delivered by the parking lot calculated by the stochastic optimization model in the selected scenarios.

The results of Figure 2.21 can be compared with the power profiles at the EV charging station shown in Figure 2.22, which correspond to an uncontrolled charge of the EVs for each of the

60 scenarios before grouping. In particular, Figure 2.21 illustrates the effect of the energy stored during the hours of maximum production of the PV unit and the power contribution of the parking lot during the evening load-peak hours.

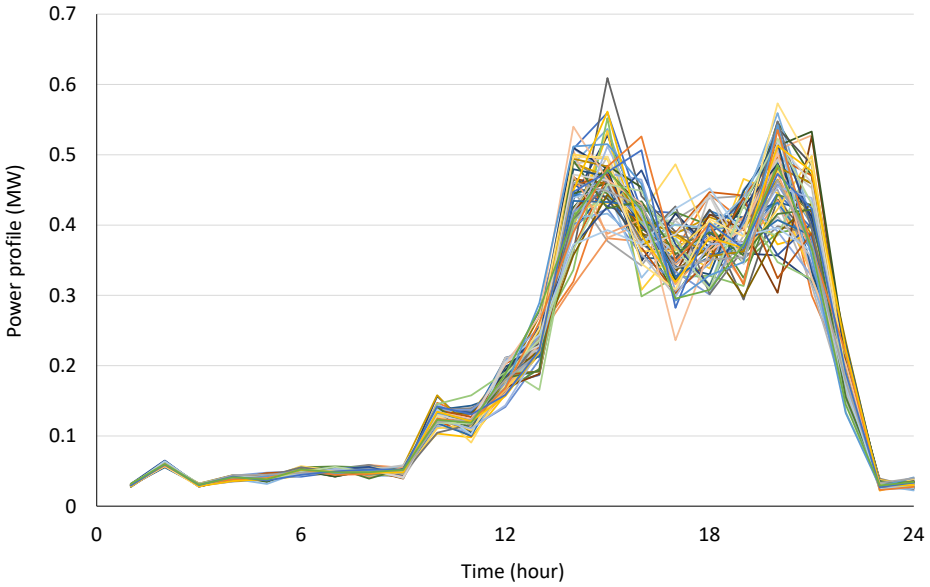

Figure 2.22 Uncontrolled charge at the EV charging station for the 60 initial scenarios.

Figure 2.23 shows the profile of $\mu^{\omega,t}$ for the scenario tree in Figure 2.15.

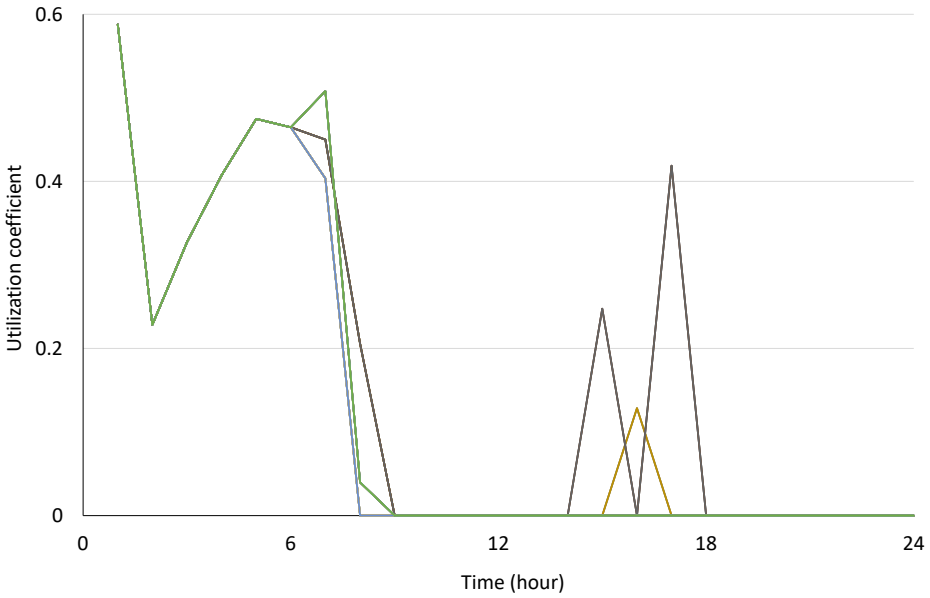

Figure 2.23 Utilization coefficient calculated by the stochastic optimization model in the selected scenarios (e_{min}=0.2 pu).

The initial energy of the incoming EVs is used in the early morning in order to increase the storage of the PV output in the parking lot during the following hours (taking into account the

low value of the ratio between sale and purchase utility tariffs) and in late afternoon although the effect is limited due to the few EVs entering in those hours.

Figure 2.24 shows the total energy stored in the parking lot, and Figure 2.25 shows the power exchange between the microgrid and the external utility grid.

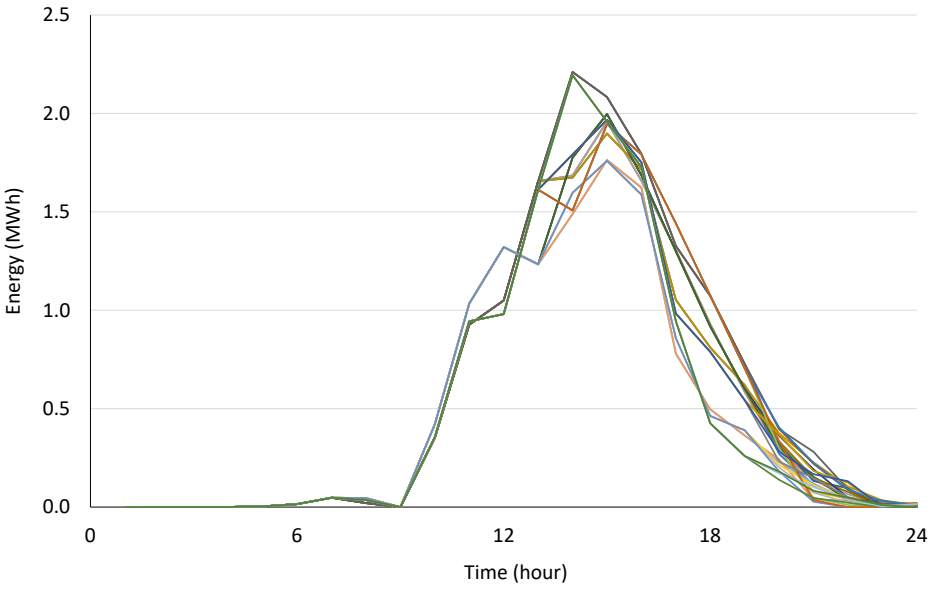

Figure 2.24 Energy stored in the parking lot.

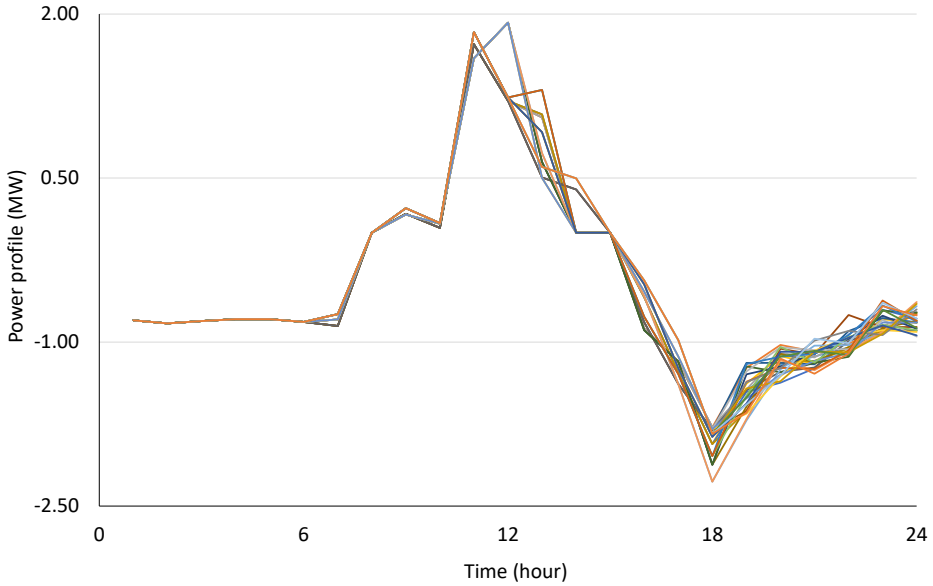

Figure 2.25 Power exchanged between the microgrid and the external grid (positive if exported from the microgrid).

We compare now the *RP* cost values obtained for different values of the minimum energy value $e_{\min}$, which is used in (2.24) in order to limit utilization coefficient $\mu^{\omega,t}$ of the initial charge of

the vehicle arriving in the parking lot. As expected, Table 2.7 shows that larger values of e_{min} cause the increase of the objective function values. Furthermore, Figure 2.26 shows the effect of the different e_{min} values on the profile of utilization coefficient $\mu^{\omega,t}$. For e_{min} values equal and exceeding 0.5 pu, the resulting $\mu^{\omega,t}$ is always 0.

Table 2.7 Objective function of the recourse problem for different values of e_{min}

e_{min} (pu)	0.1	0.15	0.2	0.3	0.4	0.5
RP (€)	864.38	864.52	864.74	865.46	867.29	867.30

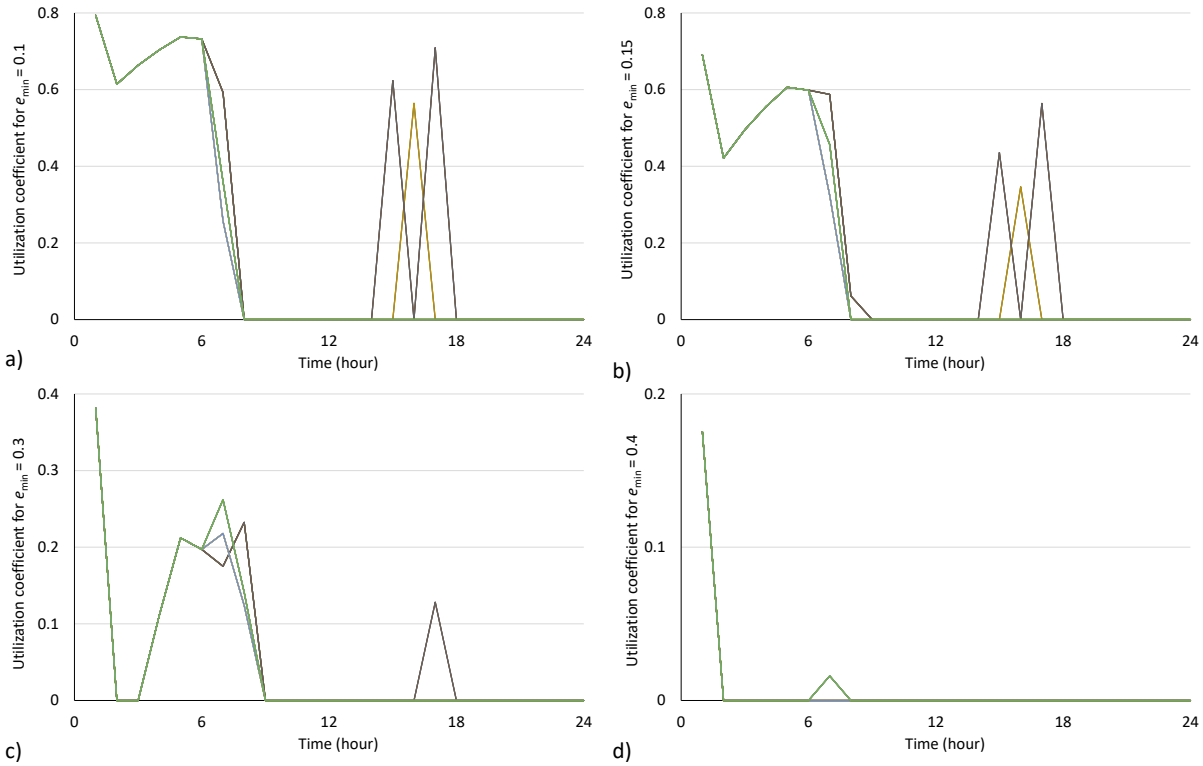

Figure 2.26 Profiles of utilization coefficient $\mu^{\omega,t}$ calculated by the stochastic optimization model for different values of e_{min}: a) 0.1 pu; b) 0.15 pu; c) 0.3 pu; d) 0.4 pu.

Table 2.8 shows the resulting *OF* from the stochastic problem (2.19), namely: *EEV*, recourse problem *RP*, and *WS*, according to the definition introduced in section 2.1.5. Additionally, it includes the resulting metrics *VSS* and *EVPI*.

Table 2.8 Performance evaluation for the multistage stochastic solution.

Solution	Cost value (€)	*VSS* (€)	*EVPI* (€)
EEV	870.79		
RP	864.74	6.04	0.05
WS	864.69		

For a further comparison, the value of the objective function obtained from the deterministic problem, which uses, as input, the average values of the stochastic parameters $N_{\mathrm{EV}}^{\omega,t}$, $P_{\mathrm{PV}}^{\omega,t}$ and $P_{\mathrm{Load}}^{\omega,t}$ is € 907.55. The average value of the deterministic solution for an initial set of 60 scenarios, which does not provide a unique profile of charges, discharges, and utilization coefficient $\mu^{\omega,t}$, is € 851.62.

In view of these results, the adoption of the multistage stochastic model is expected to allow a significant improved flexibility and cost reduction for many scenarios with respect to the adoption of the solution provided by the forecast-based deterministic model.

2.3 Conclusions of the chapter

With the current energy transition towards a distributed scheme, the increasing appearance of prosumers in the electrical system will be expected. The establishment of such a prosumer-based paradigm demands the alignment of technologies that will allow the operation of the installed equipment, coupling the effective exploitation of the available energy resources and the economic benefit.

Consequently, the cost-effective operation of such systems requires the implementation of an energy management system that optimize the scheduling of the resources during the day.

The first part of this chapter deals with the scheduling of a local energy system equipped with an integrated PV-storage system in order to cover the local energy demand and minimize the daily energy procurement cost.

For the considered case, a deterministic solution has been proposed and subsequently extended to a multistage stochastic approach in order to consider the uncertainties associated with the energy generation and consumption.

The multistage stochastic approach represents an attractive method for the day-ahead scheduling in local energy systems and provides improved results with respect to the application of the Monte Carlo method, which is another widely used method to deal with uncertainties.

The adoption of a multistage approach requires the proper construction of a scenario tree to represent the outcome of the stochastic events. To that end, a clustering procedure based on the *k*-means algorithm has been adopted for the corresponding scenario tree generation. The *k*-

means clustering procedure provides appropriate results even with a limited number of centroids, in addition to a reasonable computational effort for the considered multistage stochastic programming problem.

To adapt the day-ahead multistage stochastic solution to the current operational conditions, an intra-day decision making procedure has been introduced. Such a procedure adapts the set values of the power output of the battery choosing at the end of each stage during the day the most similar scenario among those defined in the tree.

The numerical results have confirmed the economic benefit by using the intra-day decision-making procedure in comparison with a day-ahead deterministic model based only on the forecast of the stochastic parameters. Additionally, to evaluate the performance of the multistage stochastic optimization, the value of the stochastic solution (*VSS*) and the expected valued of perfect information (*EVPI*) have been calculated, confirming the advantage of the multistage stochastic approach over the solution given by the mentioned forecast-based model.

Next, the second part of the chapter dealt with the operation of a microgrid with a parking lot that allows bidirectional charging services. The optimization problem minimizes the daily cost of the microgrid by means of a multistage stochastic problem. To that end, the uncertainties associated with the number of parked EVs, the PV generation and the non-dispatchable loads in the microgrid are represented by the relevant scenario tree.

The proposed formulation for the dispatchable problem of the parking lot is suitable to be modelled by means of a scenario tree. The one described in this chapter is obtained by means of the *k*-means clustering procedure. The implemented clustering procedure allows the solution of the scenario-based multistage optimization model with a reasonable computational effort.

As expected, in this case, the calculation of the *VVS* and *EVPI* metrics confirms the advantage of the multistage scenario-based approach over the solution given by a deterministic model based only on the forecast of the stochastic parameters.

This chapter shows that the appropriate scheduling of the parking lot, especially if it is provided with bidirectional charging stations, facilitates the integration of renewable generation inside the microgrid and reduces the need of dedicated stationary storage units.

Chapter 3. Day-Ahead Scheduling of a Renewable Energy Community

Introduction

"When mathematical optimization meets cooperation"

In recent years, the regulation of several countries has been shaping the conditions for allowing direct energy transactions between electricity end-users and their neighbours, within a so-called energy community.

In this context, renewable energy communities equipped with both distributed generation units based on renewable resources, and storage units will favour the local balance between production and consumption during the day, while reducing congestion and efficiency issues for the network. Moreover, from the participants point of view, an economic justification for the establishment of a REC is the expected gap between the prices of buying and selling energy from and to the external electricity provider, respectively, which can further be increased by various factors, e.g., due to costs of the ancillary services.

Regulatory challenges and opportunities for such collectives are analysed in e.g., (Inês et al. 2020) and (Sokoøowski 2018), which also refers to the recent legal framework called "Clean Energy for all Europeans" approved by the European Union (see e.g., (EU2018/2001 2018) and (EU2019/944 2019)).

In the literature, there are several studies dedicated to practical case studies of local energy market (LEM) schemes between end-users, e.g., (C. Zhang et al. 2017) and references therein. One of the main references, among real implementations, is the Brooklyn microgrid project (Mengelkamp et al. 2018).

This chapter deals with the scenario in which energy transactions are allowed not only with the external energy provider, but also between participants in a REC. The members of the community can be residential or small commercial/industrial sites connected to the same distribution network. Each participant can, in general, consume or produce

electricity during different time periods, i.e., can act as a prosumer. Furthermore, each prosumer may be equipped with local generation units (PV panels in this chapter) and BES units to cover the local demand.

The community scheme considered in this chapter is characterized by being local and cooperative that is all the prosumers are connected to the same LV distribution network and collaborate, without any competitive behaviour, for the common goal of minimizing the costs related to the exchanges with the utility grid.

The peer-to-peer (P2P) transactive scenario, such as in, e.g., (Le Cadre et al. 2020), (Paudel et al. 2019) and references therein, is aligned with different characteristics as the ones considered in this chapter. Since, in those schemes the self-interested users exploit their own resources in a noncooperative scheme. (Guerrero, Chapman, and Verbič 2019) presents a properties comparison between a P2P and a community-based approach, which implement LEMs in LV networks.

In general, the energy community concept implies the implementation of an EMS to achieve the prosumers' common goals and the optimal operation of the installed energy resources (Belli et al. 2017). According to several approaches presented in the literature (e.g., (Yan et al. 2018), (Liu et al. 2019) and references therein), a day-ahead scheduling procedure is convenient for minimizing the energy procurement costs of the community.

Typically, such scheduling problem of resources can effectively be addressed by centralized models. Nevertheless, distributed approaches have gained special interest: e.g., (Lee et al. 2015) proposes a distributed mechanism based on game theory to define a competitive trading scheme among several microgrids, in (Zhao et al. 2018) a primal Benders decomposition approach has been used, whilst (Moret and Pinson 2019) and (Kargarian et al. 2018) employ the alternating direction method of multipliers (ADMM).

Indeed, ADMM is one of the most frequently adopted consensus algorithms (see, e.g., (Boyd et al. 2010; H. Wang and Huang 2018; Dvorkin et al. 2018), and references therein), and it has been recently investigated for the solution of scheduling problems in MGs, as well as for the more general problem of the optimal operation of multi-microgrids and active distribution networks.

With respect to a centralized approach, a distributed approach appears more suitable to define the scheduling of the community, in which the participants will collaborate to a

common goal while preserving their privacy and independence, and it can exploit the implementation of blockchain or, in general, distributed ledger technologies (e.g., (Vangulick, Cornelusse, and Ernst 2018),(Di Silvestre et al. 2018),(van Leeuwen et al. 2020)).

In its first part, this chapter focuses on the day-ahead centralized model to deal with the scheduling problem of a REC. Then, the distributed approach is introduced, in which the centralized problem is decomposed by means of the ADMM.

Moreover, in a subsequent section, a procedure that seeks an allocation of the losses associated with the energy transactions in the REC is introduced, for both a centralized and ADMM-based approach. The results of such procedures are compared considering different scenarios.

Several publications in the field have pointed out a lack in the consideration of network constraints for the modelling of local energy markets specifically in low-voltage networks (e.g., (Guerrero, Chapman, and Verbic 2018)). The approaches presented in this chapter are also oriented to contribute to close the gap by providing optimization and modelling insights of the renewable energy community network, specifically in the losses-allocation field.

Finally, to close the chapter, the scheduling of communities that integrate dispatchable generating units is studied. In such a scheme, an additional increase in the energy self-consumption rate and a peak-demand reduction will be expected. Furthermore, the exploitation of renewable resources represents an attractive aspect of the integration of dispatchable generators; for instance, by using anaerobic digestion (AD) technologies, which allows the electricity generation from waste generated by e.g., agriculture activity (Thimsen 2004).

3.1 Centralized approach for the day-ahead scheduling of the community

The scheduling function of the community can be formulated as a centralized optimization problem, in which the set values for the operation of all the participants are defined by a central control unit. In this scenario, the central unit collects all the characteristics of the available equipment in the community, as well as the data regarding forecast profiles of the local energy generation and consumption and keeps all of the information updated.

The scheme shown in Figure 3.1 corresponds to a community with an internal LV distribution network, which is connected to a point of common coupling, through an MV/LV transformer, to the external utility grid. In the considered scenario, each prosumer uses the available energy resources in cooperation with the other participants to minimize the energy procurement cost of the entire REC. Since the considered collective of prosumers has been characterized for a collaborative behaviour, the participants cannot act as producer and as consumer simultaneously.

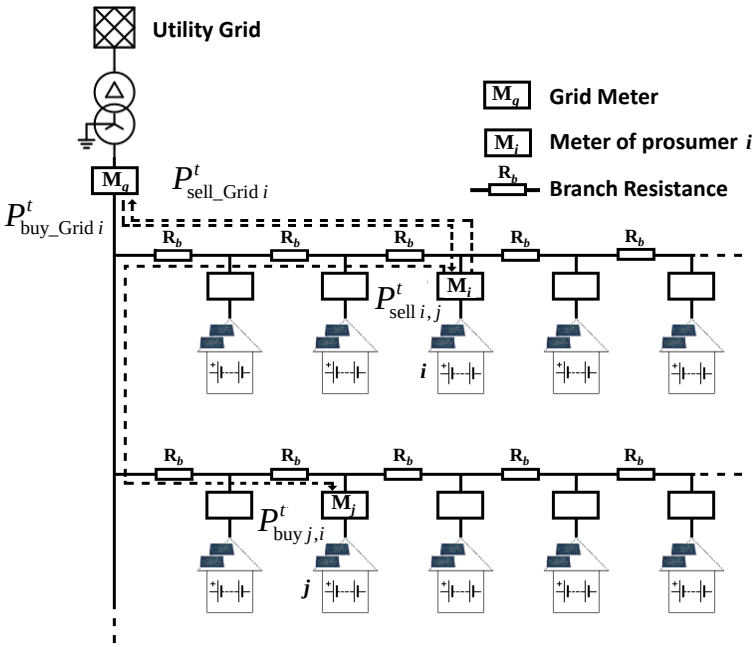

Figure 3.1 Scheme of the renewable energy community; adapted from (Lilla et al. 2020).

The grid meter M_g in Figure 3.1, positioned at the point of common coupling with the external utility grid, is bidirectional and measures the energy exchanged during each time interval. In section 3.2 a distributed alternative will be introduced, in which the presence of the bidirectional meter M_i owned by each prosumer i will be relevant for measuring the energy that the specific prosumer exchanges with the internal network during each time interval.

As already mentioned, the operation of such a collective of prosumers requires the implementation of an EMS for the optimal exploitation of the available resources; hence, this chapter deals with the day-ahead scheduling of the community to define the optimal scheduling during the following day. The resulting operational plan is especially oriented to provide set values for the BES units and energy transactions between participants in the community. For illustrative purposes, in this chapter the prices associated with energy transactions with the external energy provider are assumed predefined, although they vary according to the time of day.

The electricity billing procedure can be described according to the following steps.

I. During each time interval, if the community buys energy from the utility grid (measured by M_g), the relevant cost is allocated to each consumer *i* (i.e., to each prosumer who consumes energy more than the local generation during that time interval) proportionally to the ratio between its consumption measured by M_i and the total consumption in the community (i.e., the sum of the measured energies by all the prosumers acting as consumers).

II. If the community sells energy to the utility grid (measured by M_g), the corresponding revenue is allocated to each producer *j* (i.e., to each prosumer that produces energy more than the local load during that time interval) proportionally to the contribution of *j* to the total REC production (i.e., to the ratio between the energy measured by M_j and the sum of the measurements of all the prosumers acting as producers).

III. Each consumer *i* is also charged for the energy bought from the producers of the community (i.e., for the difference between the measurement of M_i and the energy allocated to consumer *i* in step I). The corresponding revenue of producer *j* is estimated proportionally to the contribution of *j* to the total community production as in step II. The day-ahead scheduling procedure calculates the energy prices for each producer *j* during each time interval.

3.1.1 Mathematical model of the centralized scheduling

Now, let us introduce the formulation of the optimization problem, which minimizes the total energy procurement cost by defining the optimal scheduling of the energy resources for the following day. For this purpose, the set of participants in the community has been denoted as $\Omega = \{1, 2, \ldots, N\}$, the set of time intervals *t* in the 24-hour horizon as $T = \{1, 2, \ldots, t_{end}\}$, and $B = \{1, 2, \ldots, b_{end}\}$ corresponds to the set of branches *b* in the internal network of the community.

The objective function (3.1) corresponds to a typical minimization of the total energy procurement cost given by the costs associated with the exchanges of electricity with the external electricity provider during the day

$$OF = \sum_{\substack{t\in T \\ i\in\Omega}} \left(\pi^t_{\text{buy}} P^t_{\text{buy\_Grid}\,i} - \pi^t_{\text{sell}} P^t_{\text{sell\_Grid}\,i} \right) \Delta t \tag{3.1}$$

where $P^t_{\text{buy\_Grid}\,i}$ represents the power bought from the utility grid by prosumer *i* at time period *t* and $P^t_{\text{sell\_Grid}\,i}$ corresponds to the power sold to the external utility grid by prosumer *i* at time period *t*. The power profiles included in this chapter are expressed in kW.

The prices when buying and selling energy from and to the external utility grid (in €/kWh), i.e., π^t_{buy} and π^t_{sell}, respectively, are assumed deterministic for the next day. Time step Δt is equal to 0.25 h within an optimization horizon of 24 hours (i.e., divided into 96 periods).

The constraints considered by the community model are the following:

$$P^t_{\text{sell}\,i,j} - P^t_{\text{buy}\,j,i} = 0 \qquad i \text{ and } j \in \Omega \tag{3.2}$$

$$P^t_{\text{PV}\,i} + P^t_{\text{dis}\,i} + P^t_{\text{buy\_Grid}\,i} + \sum_{\substack{j\in\Omega \\ j\neq i}} P^t_{\text{buy}\,i,j} = P^t_{\text{Load}\,i} + P^t_{\text{ch}\,i} + P^t_{\text{sell\_Grid}\,i} + \sum_{\substack{j\in\Omega \\ j\neq i}} P^t_{\text{sell}\,i,j} + \tfrac{1}{2}\sum_{b\in B} L^t_{b,i} \quad i \text{ and } j \in \Omega \tag{3.3}$$

$$\begin{cases} P^t_{\text{buy\_Grid}\,i} = 0 \text{ and } P^t_{\text{buy}\,i,j} = 0 \text{ if } u^t_i = 0 \\ P^t_{\text{sell\_Grid}\,i} = 0 \text{ and } P^t_{\text{sell}\,i,j} = 0 \text{ if } u^t_i = 1 \end{cases} \qquad \begin{matrix} u^t_i \in \{1,0\} \\ i \text{ and } j \in \Omega \end{matrix} \tag{3.4}$$

$$0 \le P^t_{\text{buy\_Grid}\,i} \le P^{\max}_{\text{buy}\,i} \quad 0 \le P^t_{\text{sell\_Grid}\,i} \le P^{\max}_{\text{sell}\,i} \qquad i \in \Omega \tag{3.5}$$

$$0 \le P^t_{\text{buy}\,i,j} \le P^{\max}_{\text{buy}\,i} \qquad 0 \le P^t_{\text{sell}\,i,j} \le P^{\max}_{\text{sell}\,i} \qquad i \text{ and } j \in \Omega \tag{3.6}$$

$$E^t_{\text{BES}\,i} = E^{t-1}_{\text{BES}\,i} + (P^t_{\text{ch}\,i}\eta_{\text{ch}\,i} - P^t_{\text{dis}\,i}/\eta_{\text{dis}\,i})\Delta t \qquad \begin{matrix} i \in \Omega \\ t > 1 \end{matrix} \tag{3.7}$$

$$\begin{cases} E^{t=1}_{\text{BES}\,i} = E^{\max}_{\text{BES}\,i} + (P^{t=1}_{\text{ch}\,i}\,\eta_{\text{ch}\,i} - P^{t=1}_{\text{dis}\,i}/\eta_{\text{dis}\,i})\Delta t \\ E^{t_{\text{end}}}_{\text{BES}\,i} = E^{\max}_{\text{BES}\,i} \end{cases} \qquad i \in \Omega \tag{3.8}$$

$$\begin{cases} P^t_{\text{ch}\,i} = 0 \;\text{ if }\; u^t_{\text{BES}\,i} = 0 \quad u^t_{\text{BES}\,i} \in \{1,0\} \\ P^t_{\text{dis}\,i} = 0 \;\text{ if }\; u^t_{\text{BES}\,i} = 1 \quad i \in \Omega \end{cases} \qquad i \in \Omega \tag{3.9}$$

$$0 \le P^t_{\text{dis}\,i} \le P^{\max}_{\text{BES}\,i} \qquad 0 \le P^t_{\text{ch}\,i} \le P^{\max}_{\text{BES}\,i} \qquad i \in \Omega \qquad (3.10)$$

$$E^{\min}_{\text{BES}\,i} \le E^t_{\text{BES}\,i} \le E^{\max}_{\text{BES}\,i} \qquad i \in \Omega \qquad (3.11)$$

Constraint (3.2) represents the equilibrium between non-negative variable $P^t_{\text{buy}\,j,i}$, which is the power bought by prosumer *j* from *i* at time period *t*, and non-negative variable $P^t_{\text{sell}\,i,j}$, which is the power sold by prosumer *i* to *j*. Constraint (3.2) couples all the selling transactions between prosumer *i* and the other participants in the community, so that the price is the same for all the selling transaction of the participants during time interval *t*.

Constraint (3.3) corresponds to the power balance for prosumer *i* in time interval *t*: where the forecast profiles of PV generation and load are given by parameters $P^t_{\text{PV}\,i}$ and $P^t_{\text{Load}\,i}$; the charging and discharging power of the battery owned by prosumer *i* are represented with the non-negative variables $P^t_{\text{ch}\,i}$ and $P^t_{\text{dis}\,i}$, respectively; $L^t_{b,i}$ represents an estimation of the losses in branch *b* originated from the energy transactions concerning the *i*-th prosumer. Since each transaction is between two prosumers, only half of the power loss is attributed to each prosumer. The omission of the concurrent presence of the transactions of all the prosumers is an approximation justified by the lack of counter-flows due to the assumed non-competitive behaviour of the participants in the community.

$L^t_{b,i}$ in (3.3) is defined by the following constraints

$$L^t_{b,i} = \frac{R_b}{3V_n^2}\left(F^t_{b,i}\right)^2 \qquad i \in \Omega \qquad (3.12)$$

$$F^t_{b,i} = A_{\text{Grid}\,b,i}P^t_{\text{buy\_Grid}\,i} - A_{\text{Grid}\,b,i}P^t_{\text{sell\_Grid}\,i} + \sum_{j\in\Omega} A_{b,i,j}P^t_{\text{buy}\,i,j} - \sum_{j\in\Omega} A_{b,i,j}P^t_{\text{sell}\,i,j} \qquad i \text{ and } j \in \Omega \qquad (3.13)$$

In (3.12), R_b corresponds to the resistance of branch *b*, V_n is the line-to-line rated voltage value, and $F^t_{b,i}$ is the three-phase power flow in branch *b* due to the transaction that involves *i*-th prosumer. The relative transactions are assumed positive when directed from the substation to the end of the feeder, and negative in the opposite direction. Constraint (3.12) assumes rms bus voltage values equal to the rated value; the same constraint considers a balanced LV network and neglects reactive power flows.

In (3.13), the position of each branch with respect to the buses where the prosumers are connected are described by 2-D matrix A_{Grid} and 3-D array A, assuming a radial configuration:

- $A_{\text{Grid } b,i}$ is the b,i element of matrix A_{Grid}. When the power flow due to the energy transaction between the i-th prosumer and the external energy provider crosses the branch b, it takes the value 1; in any other case, it takes the value 0.
- $A_{b.i,j}$ is the b,i,j element of array A. If the power flow created when i buys from j, crosses the branch b in the assumed positive direction, then the value of the element is equal to 1. If the corresponding power flow crosses in the negative direction, the value of the element is -1. The value is 0 if the branch b is not crossed by the power flow created by the corresponding energy transaction between prosumers i and j.

Indicator constraints (3.4) employ the binary variable u_i^t, to prevent simultaneous purchases and sales by the prosumer i.

Constraints (3.5) and (3.6) limit the energy bought and sold by prosumer i at each period t. If $P_{\text{PV}\,i}^t - P_{\text{Load}\,i}^t + P_{\text{BES}\,i}^{\max}$ is above 0, then $P_{\text{sell}\,i}^{\max}$ takes that value; if it is lower or equal to 0, $P_{\text{sell}\,i}^{\max}$ is equal to 0. If $P_{\text{Load}\,i}^t - P_{\text{PV}\,i}^t + P_{\text{BES}\,i}^{\max}$ is above 0, then $P_{\text{buy}\,i}^{\max}$ takes that value; if it is lower or equal to 0, $P_{\text{buy}\,i}^{\max}$ is equal to 0. $P_{\text{BES}\,i}^{\max}$ is the maximum power output of the BES unit owned by prosumer i.

The state of energy (SoE) of the battery of prosumer i is given by (3.7) and (3.8), which represent a simple energy balance model, where $E_{\text{BES}\,i}^t$ is the SoE at time t (in kWh) and $E_{\text{BES}\,i}^{\max}$ is the maximum storage capacity. The non-negative parameters $\eta_{\text{ch}\ i}$ and $\eta_{\text{dis}\,i}$ are values lower than 1 and represent the charging and discharging efficiencies, respectively. In (3.8) the BES units are assumed fully charged at the beginning and at the end of the day. The binary variable $u_{\text{BES}\,i}^t$ in indicator constraints (3.9) prevents the concurrent charging and discharging processes of the batteries. In (3.10), the discharging and charging power of the BES units are bound within the maximum value $P_{\text{BES}\,i}^{\max}$. Constraint (3.11) limits the value of the SoE between minimum level $E_{\text{BES}\,i}^{\min}$ and maximum $E_{\text{BES}\,i}^{\max}$.

In the proposed MILP model for the centralized scheduling of the REC, constraint (3.12) is replaced by its piecewise linear approximation described in, e.g., (Williams 2013). For such linearization, a set L of segments has been created. Each segment is defined by breakpoints

$H^t_{\text{Flow}\,b,l}$, obtained by dividing the allowed range of F^t_b into $|L|$ intervals. Each breakpoint $H^t_{\text{Flow}\,b,l}$ defines a breakpoint $H^t_{\text{Loss}\,b,l}$ of the piecewise representation of L^t_b, which is given by

$$F^t_b = \sum_{l \in L} a^t_{b,l}\ H^t_{\text{Flow}\,b,l} \tag{3.14}$$

$$L^t_b = \sum_{l \in L} a^t_{b,l}\ H^t_{\text{Loss}\,b,l} \tag{3.15}$$

$$\sum_{l \in L} a^t_{b,l} = 1 \quad l \in L \tag{3.16}$$

where $a^t_{b,l}$ are SOS2 variables, i.e., they are linked with a special ordered set of type 2 constraints, so that, at most two and consecutive variables can be non-zero. Since the losses are calculated separately for each transaction, the model (3.14)-(3.16) is applied for each prosumer *i* by using the power flow defined by (3.13).

3.1.2 Case study of a renewable energy community with centralized scheduling

Now, let us consider a REC composed of two LV feeders, like the one illustrated in Figure 3.1. Each feeder consists of five lines, each with resistance R_b = 189 mΩ. Five prosumers are connected to each feeder (numbered from the beginning of the feeder to the end): prosumers 1-5 to a feeder and prosumers 6-10 to the other. Each prosumer may be equipped with a PV-storage system and a load.

The load profiles adopted for each prosumer are shown in Figure 3.2. For all the PV units we assumed the same profile of the ratio between power output and panel surface, shown in Figure 3.3. The area of the PV unit of each prosumer is given in Table 3.1. Figure 3.3 also shows the price profile of the energy bought from the utility grid (i.e., π^t_{buy}). We assume that the price of the energy sold by the community to the utility grid (i.e., π^t_{sell}) is half of π^t_{buy}. The total daily consumption of the community is 313 kWh and the corresponding PV production is 231 kWh (73.8% of the load).

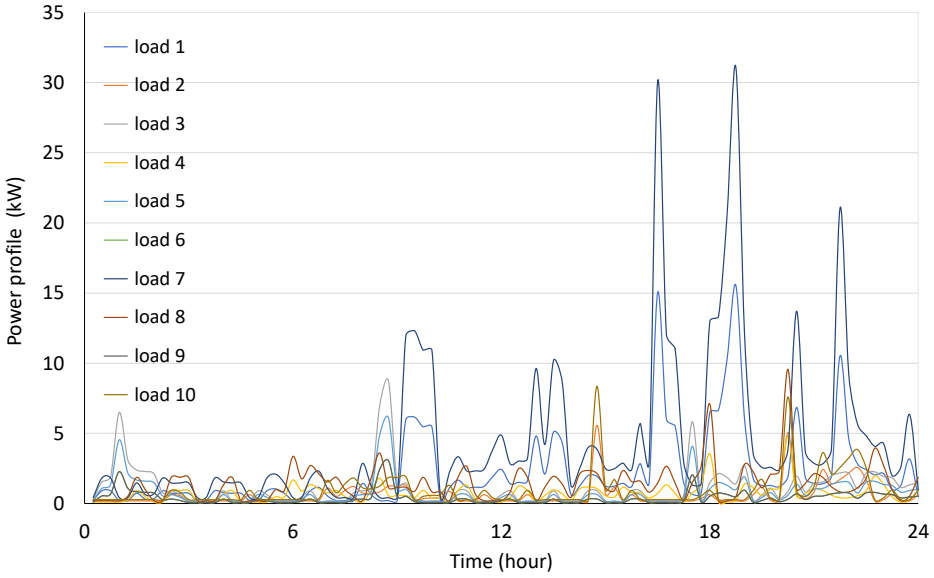

Figure 3.2 Load profile of each prosumer.

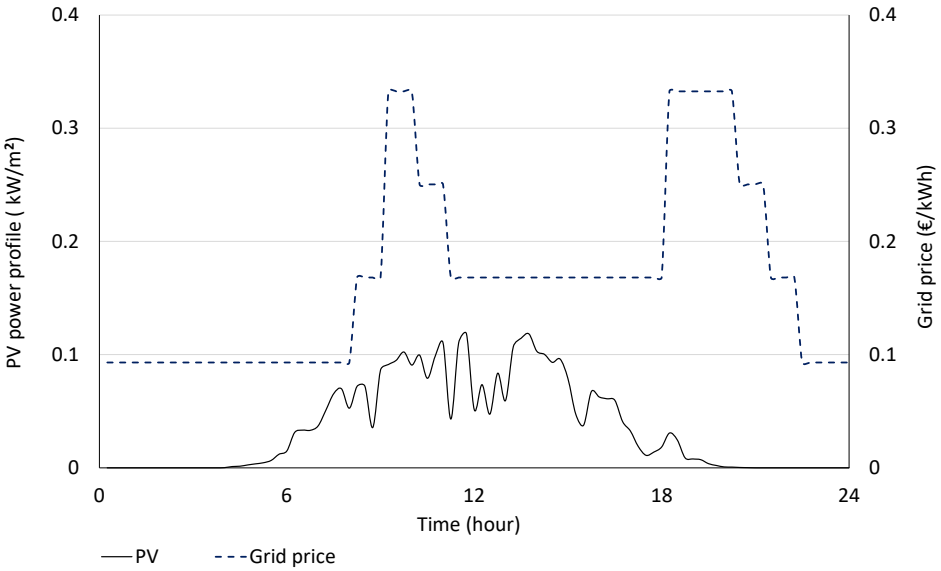

Figure 3.3 Profile of the PV production and Grid purchase price.

Table 3.1 PV panel surface for each prosumer.

Prosumer	1	2	3	4	5	6	7	8	9	10
Area (m^2)	32	14	21	32	28	14	42	32	14	42

Sizes $E_{\mathrm{BES}}^{\max}$ of the BES units are shown in Table 3.2 and the corresponding $P_{\mathrm{BES}}^{\max}$ values are assumed to be equal to the ratio $E_{\mathrm{BES}}^{\max} / \Delta t$. The total capacity of the BES units is 30 kWh (13% of the daily PV production).

Table 3.2 Sizes of the BES units in the community.

Prosumer	1	2	3	4	5	6	7	8	9	10
Size (kWh)	5	3	4	2	3	1	2	2	2	6

To test the proposed centralized formulation, the MILP model of the community has been implemented in the AIMMS Developer modelling environment and solved by using the Cplex V12.9 solver. As already mentioned, all the calculations refer to a time window of one day, divided into 96 periods of 15 minutes each.

Figure 3.4 shows the total power flow at the connection of the community with the external energy provider. The total *OF* value of (3.1) obtained by means of the centralized scheduling of the resources in the community, is €18.06. The solution of the centralized model requires around 10 s.

The power profiles from each prosumer when it exchanges energy with the others i.e., when selling and buying, are presented in Figure 3.5 and Figure 3.6, respectively.

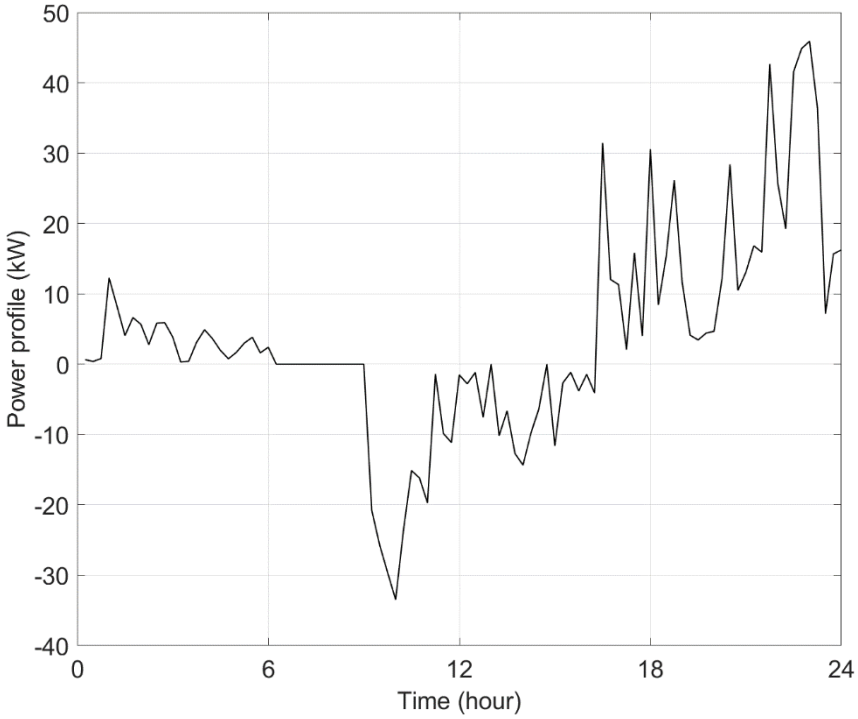

Figure 3.4 Power flow exchanged with the external energy provider (positive if consumed by the community), obtained using the centralized approach.

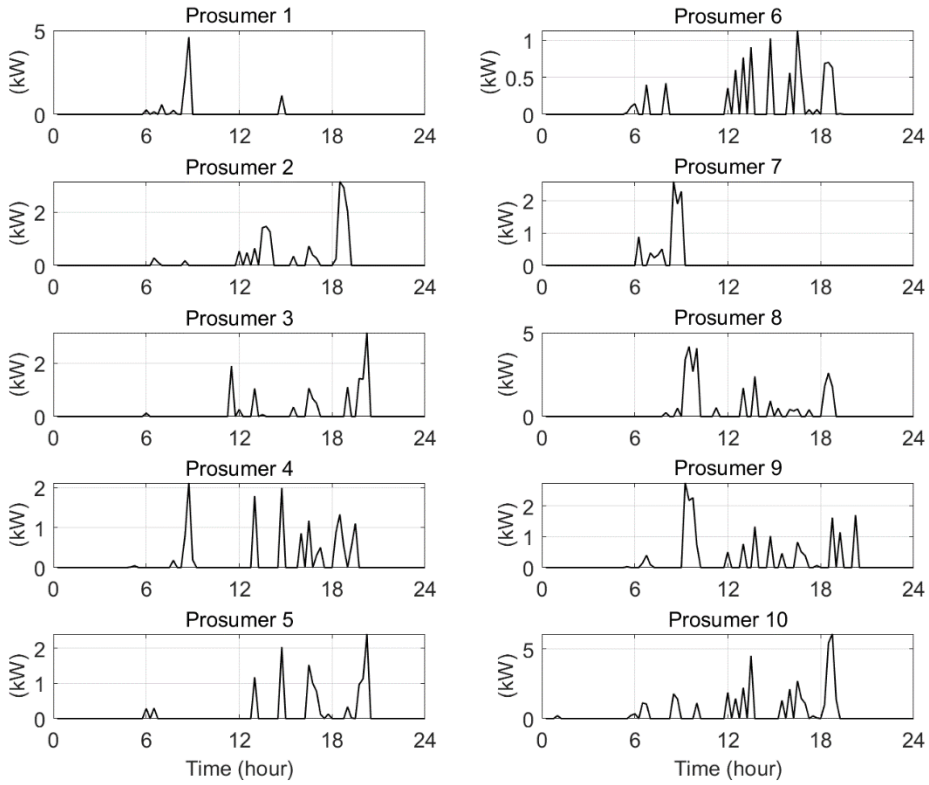

Figure 3.5 Power flows from every prosumer when it sells to the others (excluding the utility grid), obtained using the centralized approach.

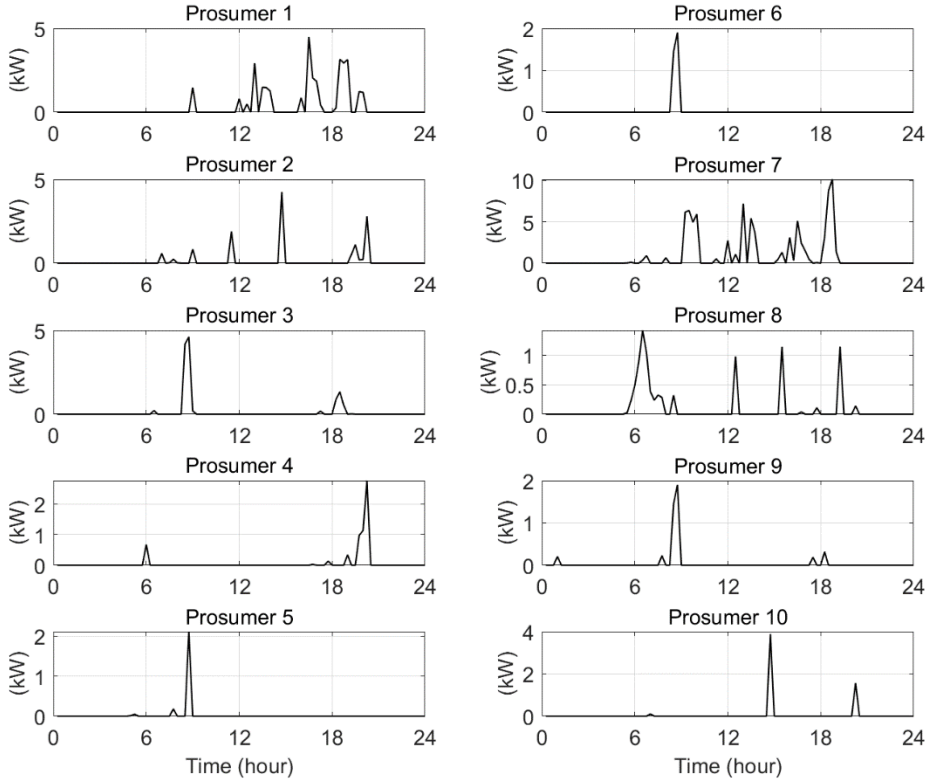

Figure 3.6 Power flows from every prosumer when it buys from the others (excluding the utility grid), obtained using the centralized approach.

Figure 3.7 shows the detail of the SoE profiles of each BES unit, whilst Figure 3.8 provides the profiles of the total energy contained in the BES units of the community.

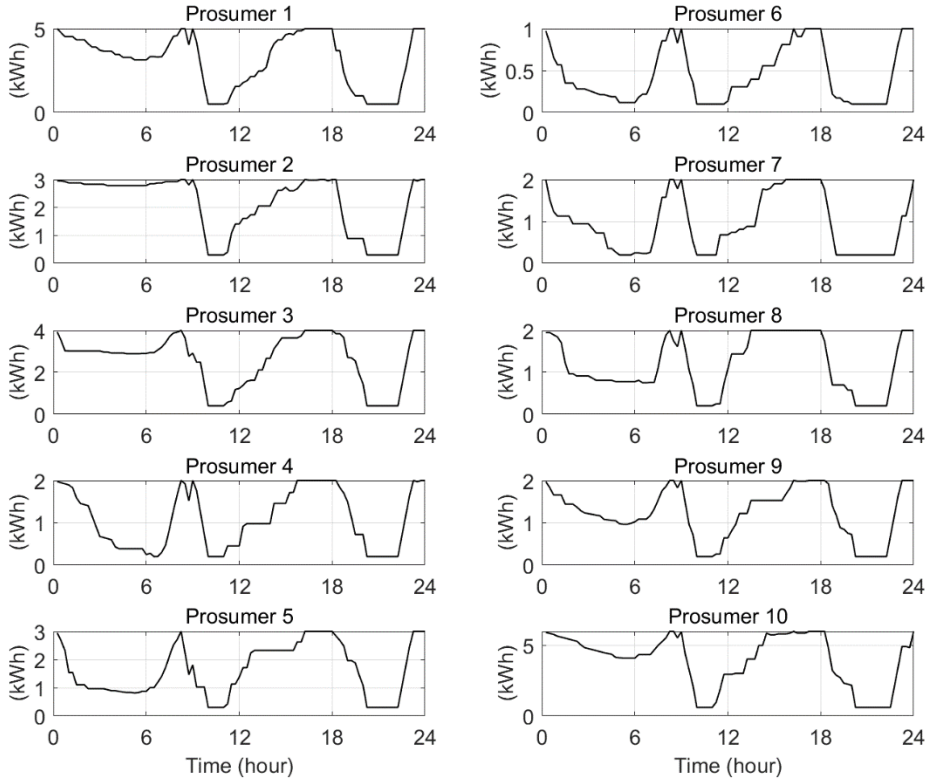

Figure 3.7 Battery SoE for each prosumer, obtained using the centralized approach.

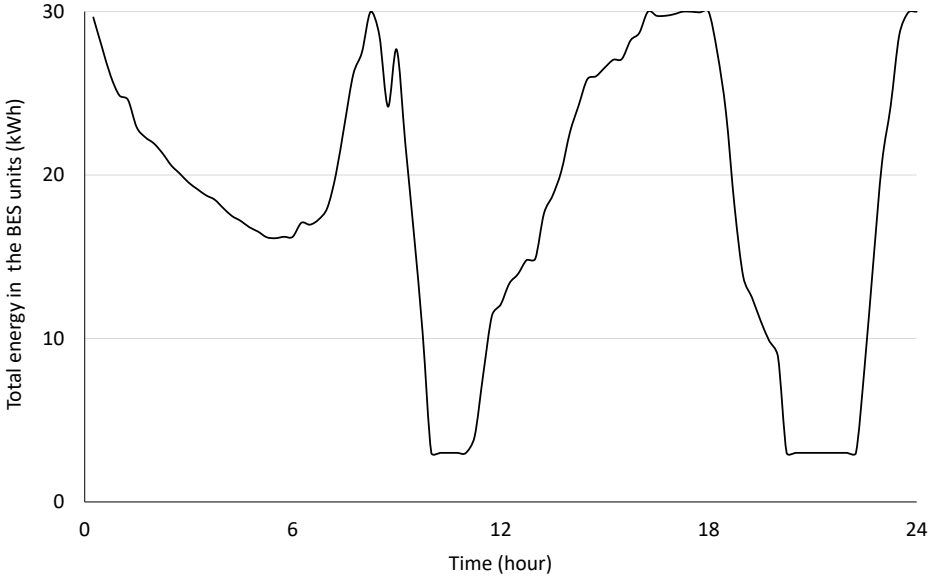

Figure 3.8 Total energy in the batteries of the community, obtained using the centralized approach.

Figure 3.9 shows the energy prices for the participants in the community at time period *t*. For the case of the centralized model, the prices correspond to the Lagrangian multiplier associated

to constraint (3.2). In Figure 3.9, the dotted lines correspond to the prices of the energy purchased from and sold to the utility grid (i.e., π^t_{buy} and π^t_{sell}, respectively), whilst the solid round markers represent the prices of prosumers when acting as producers and selling energy to any other participant in the community. The comparison of Figure 3.9 and Figure 3.4 shows that the prices of the energy transactions in the community are not equal to π^t_{buy} or π^t_{sell} when there is no power exchange with the utility grid, that is during the time interval starting just after 6 am.

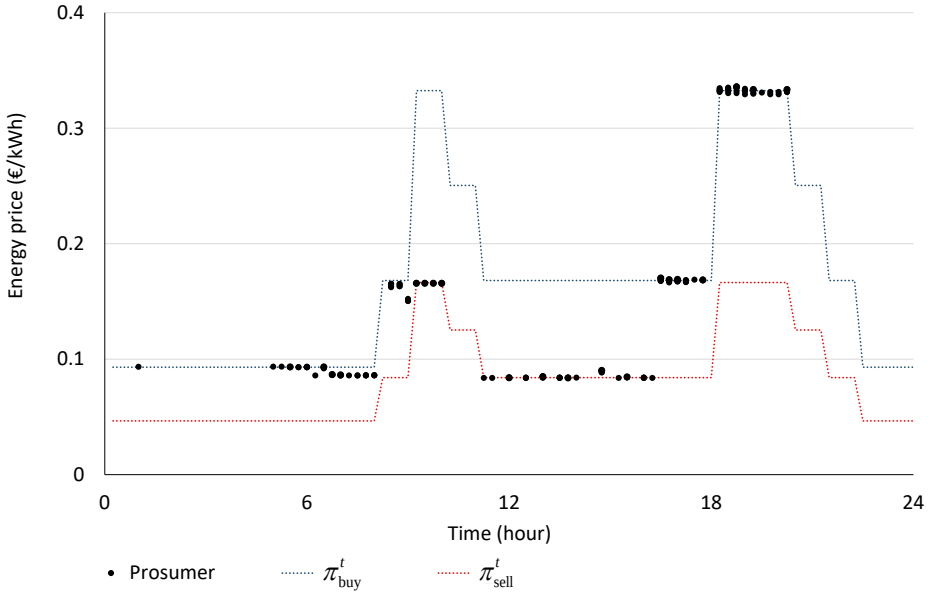

Figure 3.9 Energy prices of selling prosumers, obtained using the centralized approach.

Table 3.3 and Table 3.4 compare the individual energy procurement costs of each member of the REC, taking into account: the exchanges with the external energy provider; the exchanges with other prosumers; and the prices of Figure 3.9. Furthermore, the tables show the corresponding values obtained by preventing the transactions between prosumers. The total energy procurement cost of the community is around 16% less than the corresponding cost without energy transactions between prosumers.

Table 3.3 Energy procurement cost in € (negative values indicate revenues) for each prosumer in feeder 1, obtained using the centralized solution.

Prosumer	1	2	3	4	5
Cooperative – Centralized	5.23	0.08	0.96	-0.99	-0.65
Without internal exchanges	5.46	0.28	1.10	-0.82	-0.46

Table 3.4 Energy procurement cost in € (negative values indicate revenues) for each prosumer in feeder 2, obtained using the centralized solution.

Prosumer	6	7	8	9	10
Cooperative – Centralized	-0.21	14.79	1.63	-0.47	-2.30
Without internal exchanges	-0.15	16.38	1.71	-0.30	-1.67

3.2 Distributed approach for the day-ahead scheduling of the community

In this section, we consider the scheduling function for the community structured as a distributed optimization algorithm, which is aimed at minimizing the energy procurement cost. Compared to a centralized approach, the use of a distributed approach, limits the information that every prosumer needs to communicate.

In the following, we introduce a distributed procedure based on the ADMM algorithm to solve the scheduling problem associated with the operation of the community. The formulation follows the proposed approach of (Orozco et al. 2019) and (Lilla et al. 2020). The main inputs of the decisions of each participant in the community are the forecast of his or her own PV production and local load.

In the ADMM algorithm, *OF* (3.1) is decomposed into local subproblems, one for each prosumer *i*, by means of the Lagrangian decomposition. The objective function of each subproblem is given by

$$OF_i = \min_{\substack{P^t_{\text{buy\_Grid}\,i},\, P^t_{\text{sell\_Grid}\,i} \\ P^t_{\text{buy}\,i,j},\, P^t_{\text{sell}\,i,j}}} \sum_{t\in T} \left[\begin{array}{l} \pi^t_{\text{buy}} P^t_{\text{buy\_Grid}\,i} \Delta t - \pi^t_{\text{sell}} P^t_{\text{sell\_Grid}\,i} \Delta t + \\ \sum_{\substack{j\in\Omega \\ j\neq i}} \lambda^t_j P^t_{\text{buy}\,i,j} \Delta t - \lambda^t_i \sum_{\substack{j\in\Omega \\ j\neq i}} P^t_{\text{sell}\,i,j} \Delta t + \ell^t_i \end{array} \right] \tag{3.17}$$

where

$$\ell^t_i = m \cdot \rho \cdot [\sum_{\substack{j\in\Omega \\ j\neq i}} (\hat{P}^t_{\text{buy}\,j,i} - P^t_{\text{sell}\,i,j})^2 + \sum_{\substack{j\in\Omega \\ j\neq i}} (P^t_{\text{buy}\,i,j} - \hat{P}^t_{\text{sell}\,j,i})^2] \tag{3.18}$$

Equation (3.17) represents the summation of three terms:

i. costs and revenues associated with exchanges of energy with the external energy provider, considering the respective prices;

ii. costs and revenues for the energy transactions of prosumer *i* with the other prosumers, where λ_i^t and λ_j^t are the Lagrangian multipliers of the equilibrium between power sold and bought in each internal transaction;

iii. the squared norm of the imbalance of each energy transaction between prosumer *i* and every other prosumer *j*.

In this scenario, the prosumers' decisions are coordinated by means of a distributed procedure that iteratively updates the multipliers. This procedure only requires the information regarding energy exchanges between prosumers, as shown in (Lilla et al. 2020). Furthermore, a distributed procedure is more appropriate when the implementation of new transaction methods based, e.g., on blockchain (Munsing, Mather, and Moura 2017; Di Silvestre et al. 2018), or, more generally, on distributed ledger technologies is required.

At the beginning of the procedure, Lagrange multipliers λ_i^t, penalization parameter ρ, and scale factor *m* are initialized. Then, at each iteration *v*, the local subproblem (3.17) is solved by each one of the prosumers considering the set of constraints (3.3)-(3.11) and (3.14)-(3.16) for each prosumer *i* (i.e., the set introduced for the operation model of the community in section 3.1). As we can see, constraint (3.2) (from the centralized model) is not present, since the problem has been decoupled by means of the augmented Lagrangian function in (3.17).

Subsequently, the prosumers communicate to each other values $P^t_{\text{buy}\,i,j}$ and $P^t_{\text{sell}\,i,j}$ obtained at the end of their own optimization problem. Then, each prosumer *i* updates the Lagrangian multipliers λ_i^t (i.e., the prices associated with the internal energy exchanges in the community) based on the imbalance between their local variables and the values communicated by the others prosumers, and denoted by a hat in (3.18), such that: parameters $\hat{P}^t_{\text{buy\_Grid}\,i}$ and $\hat{P}^t_{\text{sell\_Grid}\,i}$ are the values in the previous iteration of power bought and sold by prosumer *i* from and to the utility grid, respectively; parameters $\hat{P}^t_{\text{buy}\,i,j}$ and $\hat{P}^t_{\text{sell}\,i,j}$ are the values in the previous iteration of power exchange between prosumers *i* and *j* (i.e., bought and sold respectively). At each iteration, the corresponding imbalances will be reflected in the primal residual r_i^t.

Furthermore, the convergence of the ADMM procedure is improved by adding the following constraints, starting from the second iteration, as they provide a coordination between the selling and purchasing decisions of prosumer *i* with respect to those of the other prosumers:

$$P^t_{\text{sell}\,i,j} \le \hat{P}^t_{\text{buy\_Grid}\,j} + \sum_{\substack{i\in\Omega \\ k\neq j}} \hat{P}^t_{\text{buy}\,j,k} \qquad j \text{ and } k \in \Omega \qquad (3.19)$$

$$P^t_{\text{buy}\,i,j} \le \hat{P}^t_{\text{sell\_Grid}\,j} + \sum_{\substack{i\in\Omega \\ k\neq j}} \hat{P}^t_{\text{sell}\,j,k} \qquad j \text{ and } k \in \Omega \qquad (3.20)$$

In order to speed up the convergence of the distributed procedure, the value of penalization parameter ρ and scale factor m are adjusted at each iteration according to Figure 3.10, which shows the iterative procedure that implements the ADMM procedure, where $\| \ \|_2$ is the Euclidian norm and s_i^ν is the $|T|$-dimensional vector of the dual residual elements.

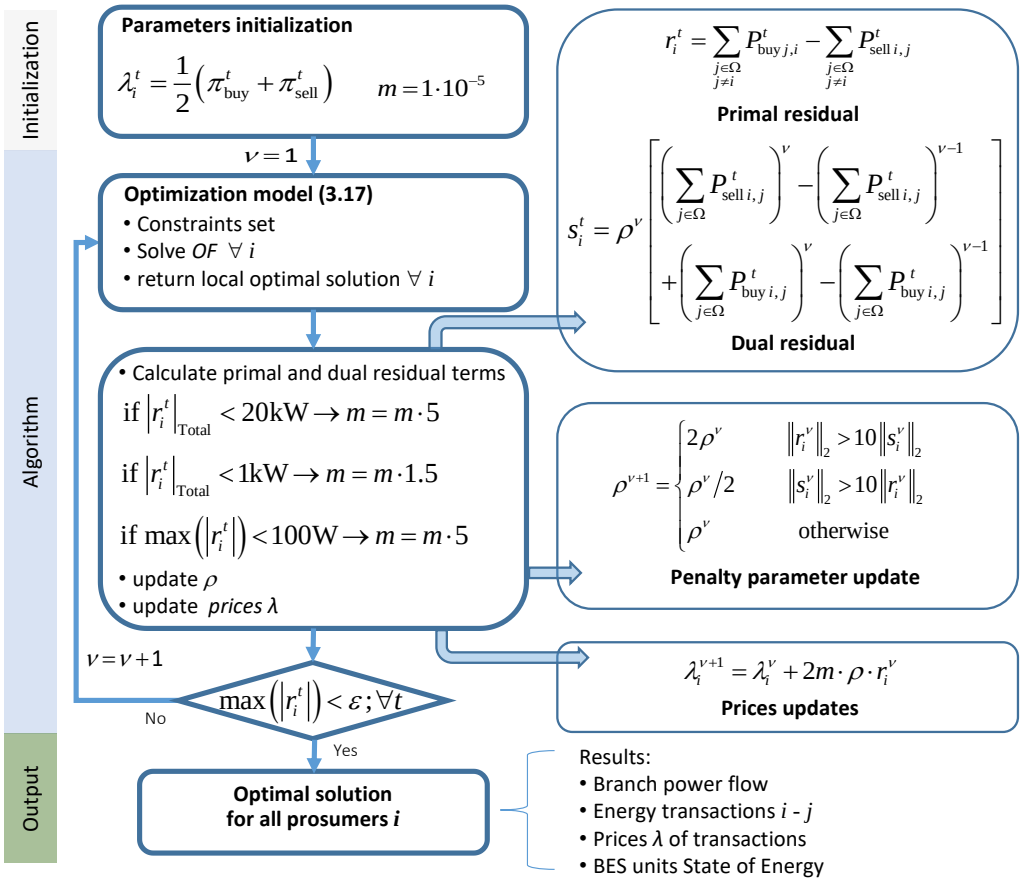

Figure 3.10 Implemented ADMM algorithm with parameter update scheme.

In the case study included in this chapter, the scale factor m is multiplied by 5 and 1.5 when the maximum value of the total mismatch $r^t = \sum_i \left|r_i^t\right|$ becomes less than 20 kW and 1 kW, respectively, and further by 5 when $\max\left(\left|r_i^t\right|\right) < 100$ W. These values are suitable to be adapted

according to the case and the characteristics of the REC to accelerate the convergence of the algorithm.

Then, the distributed procedure is iteratively repeated until the absolute values of all residuals r_i^t are less than a small tolerance ε.

Once the procedure converges, ℓ_i^t tends to zero, and the value *OF* for the community is equal to the summations of the prosumer's objectives:

$$OF = \sum_{i \in \Omega} OF_i \tag{3.21}$$

As described in (Boyd et al. 2010), the convergence of ADMM to a global optimal point is not guaranteed when it is applied to nonconvex problems. However, it will possibly have better convergence than other local optimization methods, and it has been successfully applied to large-scale mixed integer problems as shown in, e.g.,(Zheng et al. 2018).

In the models considered in this chapter, the binary variables are used only in indicator constraints (3.4) and (3.9). These constraints do not affect the optimal value of the *OF* but are useful for finding the solution among those with the optimal value of *OF*, which can be more easily applied, i.e., avoiding the occurrence of prosumers who buy and sell energy without benefit (i.e., at the same price). Furthermore, these constraints, together with (3.19) and (3.20) make the ADMM convergence significantly faster.

In literature, there is a wide range of studies that examine the convergence of the ADMM algorithm e.g., (Moret and Pinson 2019) and (Crespo-Vazquez et al. 2020).

3.2.1 Implementation and numerical tests for the day-ahead ADMM approach

The distributed approach has been implemented and tested in the AIMMS Developer modelling. For this purpose, the MIQP (mixed integer quadratic programming) solver has been used for the ADMM model by using the Cplex V12.9 solver. For the test cases considered in this chapter, the tolerance parameter ε is assumed to be equal to 15 W.

For the same case study introduced in the previous section, the total *OF* value of (3.21) is, €18.12. Figure 3.11 shows the total power flow at the connection of the community with the utility grid obtained, by means of the distributed procedure.

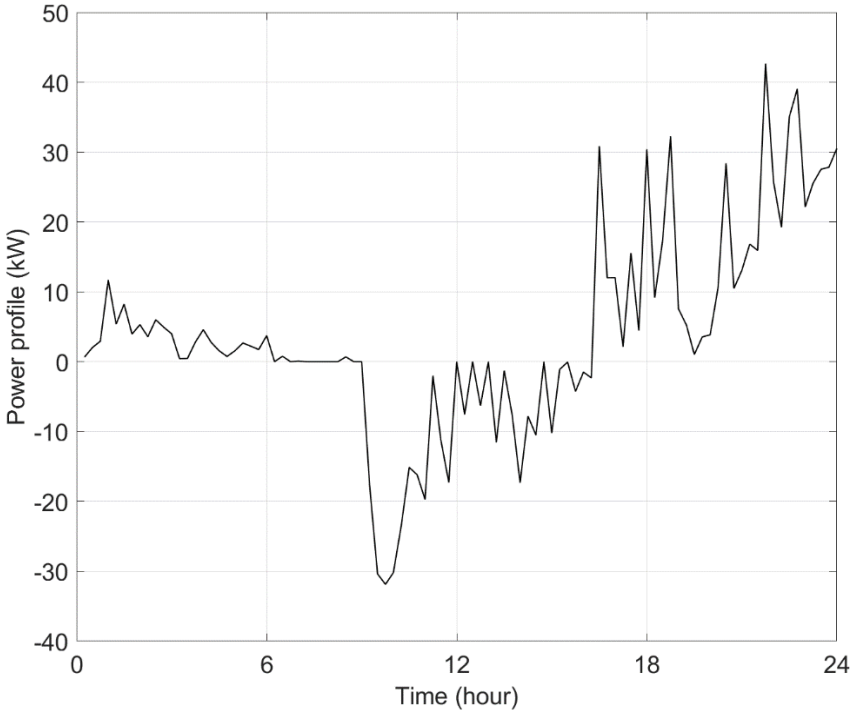

Figure 3.11 Power flow exchanged with the utility grid (positive if consumed by the community): obtained using the ADMM approach.

The power profiles from each prosumer when it exchanges energy with the others i.e., when selling and buying, are shown in Figure 3.12 and Figure 3.13, respectively.

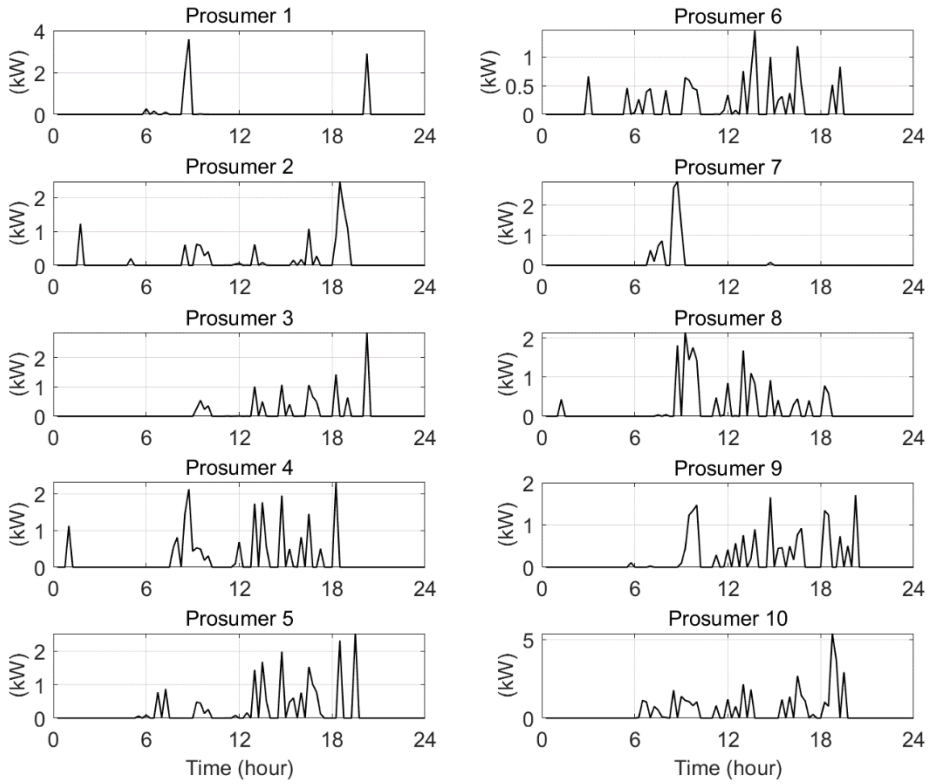

Figure 3.12 Power flows from every prosumer when it sells to the others (excluding the utility grid), obtained using the ADMM approach.

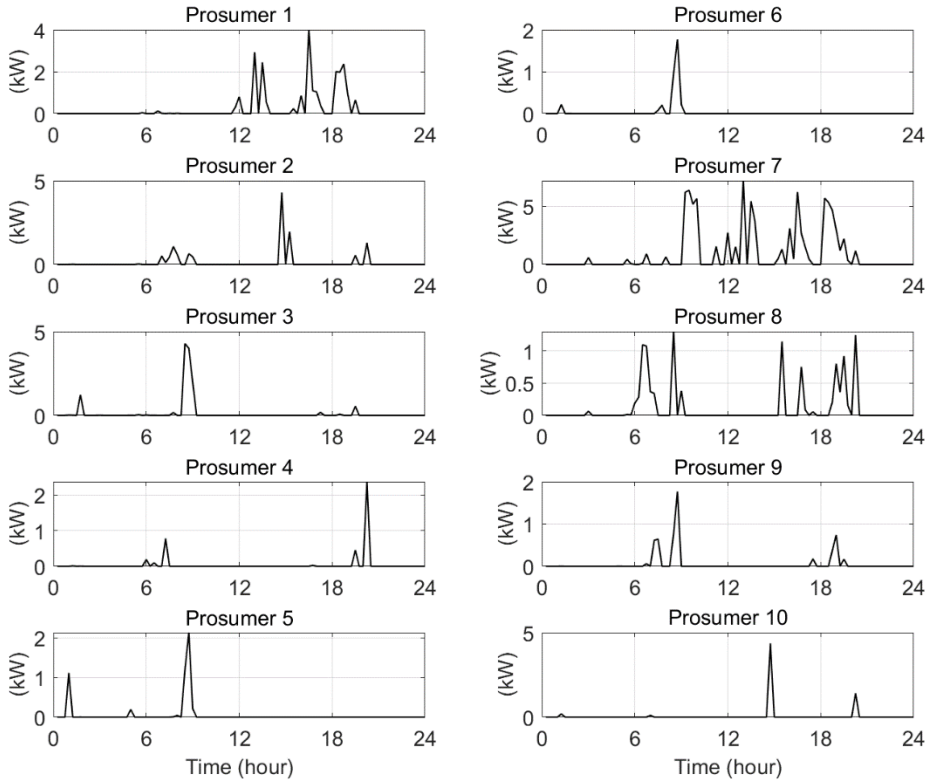

Figure 3.13 Power flows from every prosumer when it buys from the others (excluding the utility grid), obtained using the ADMM approach

Figure 3.14 shows the detail of the SoE profiles of each BES unit in the community and Figure 3.15 provides the profile of the total energy stored in the BES units of the REC.

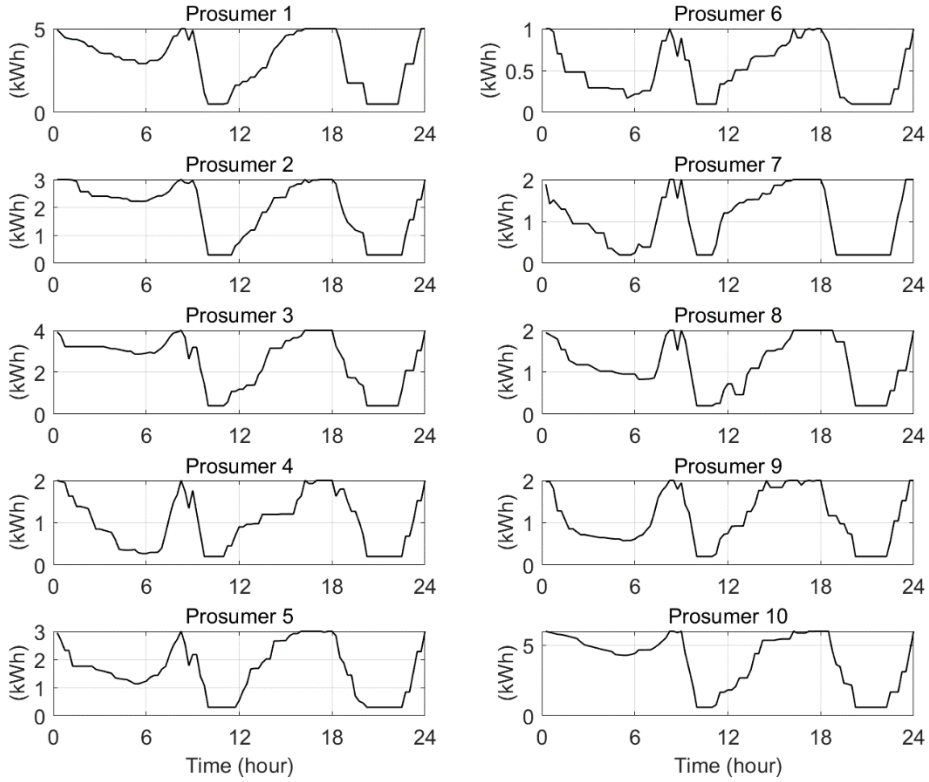

Figure 3.14 Battery SoE for each prosumer in the community, obtained using the ADMM approach.

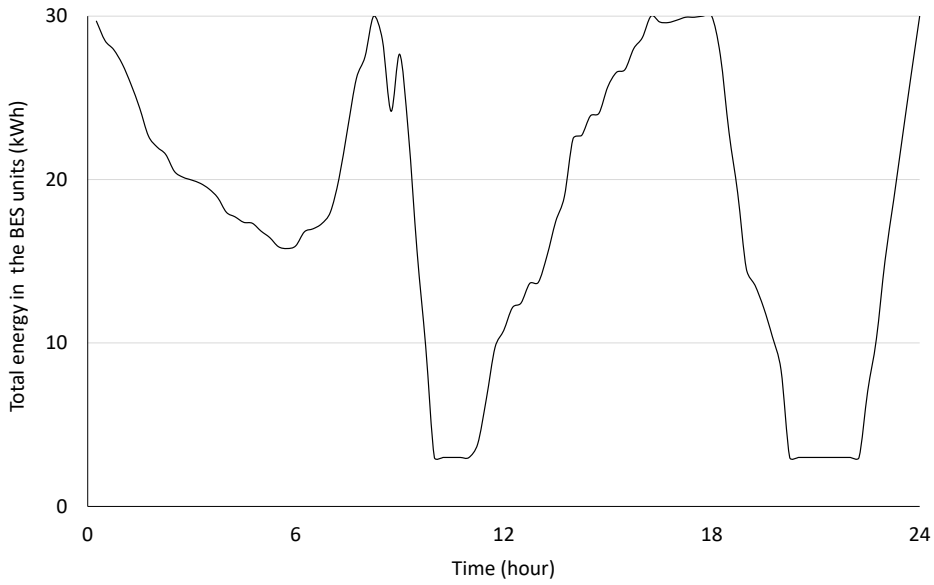

Figure 3.15 Total energy in the batteries of the community, obtained using the ADMM approach.

Figure 3.16 shows the energy prices λ_i^t of each prosumer *i*. The dotted lines correspond to the prices associated with energy transactions with the external provider (i.e., π_{buy}^t and π_{sell}^t), while the black solid marks represent the transaction prices of the various prosumers when they sell energy to any other member of the community. Again, the comparison of Figure 3.16 and Figure 3.11 also confirm for the distributed approach that the prices of the internal transactions tend to be different from π_{buy}^t and π_{sell}^t only if there is no power exchange with the utility grid.

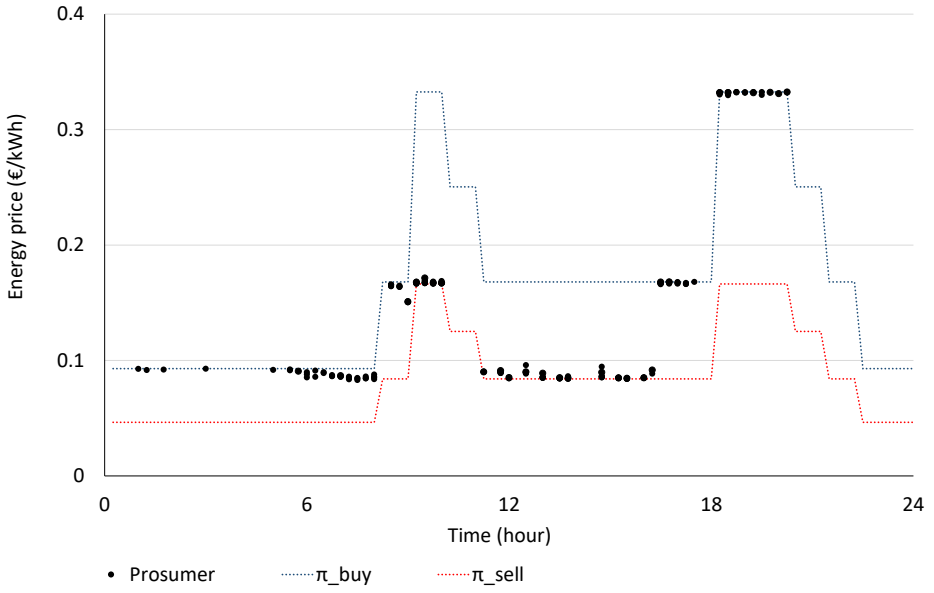

Figure 3.16 Energy prices of selling prosumers, obtained using the ADMM approach.

Table 3.5 and Table 3.6 compare the individual energy procurement costs of each participant in the community, considering: the energy exchanges with the external grid, the internal energy transactions and the prices of Figure 3.16; in addition, the tables show the corresponding values obtained by preventing the transactions between prosumers. The total energy procurement cost of the REC is around 16% less than the corresponding cost without internal transaction among the participants.

Table 3.5 Energy procurement cost in € (negative values indicate revenues) for each prosumer in feeder 1, obtained using the ADMM approach.

Prosumer	1	2	3	4	5
Cooperative – ADMM	5.24	0.08	0.96	-0.98	-0.65
Without internal exchanges	5.46	0.28	1.10	-0.82	-0.46

Table 3.6 Energy procurement cost in € (negative values indicate revenues) for each prosumer in feeder 2, obtained using the ADMM approach.

Prosumer	6	7	8	9	10
Cooperative - ADMM	-0.21	14.80	1.63	-0.47	-2.29
Without internal exchanges	-0.15	16.38	1.71	-0.30	-1.67

3.2.2 Scalability of the distributed approach

To perform an analysis of the implemented distributed approach's scalability, three different configurations have been considered for the community, namely:

- **Scenario 1**: Two feeders with five prosumers each. The characteristics of the 10 prosumers correspond to the model considered in the previous case study (i.e., PV-BES system and load characteristics) and illustrated in Figure 3.1.
- **Scenario 2**: One feeder with 10 prosumers, illustrated in Figure 3.17a. The characteristics of the prosumers are the same as in Scenario 1.
- **Scenario 3**: Two feeders with 10 prosumers each, as shown in Figure 3.17b. The 10 prosumers connected to the first feeder are the same considered in Scenario 1 and Scenario 2. The additional 10 prosumers of the second feeder are characterized by the load profiles shown in Figure 3.18, by the PV panel surfaces shown in Table 3.7 and the sizes of the BES units shown in Table 3.8.

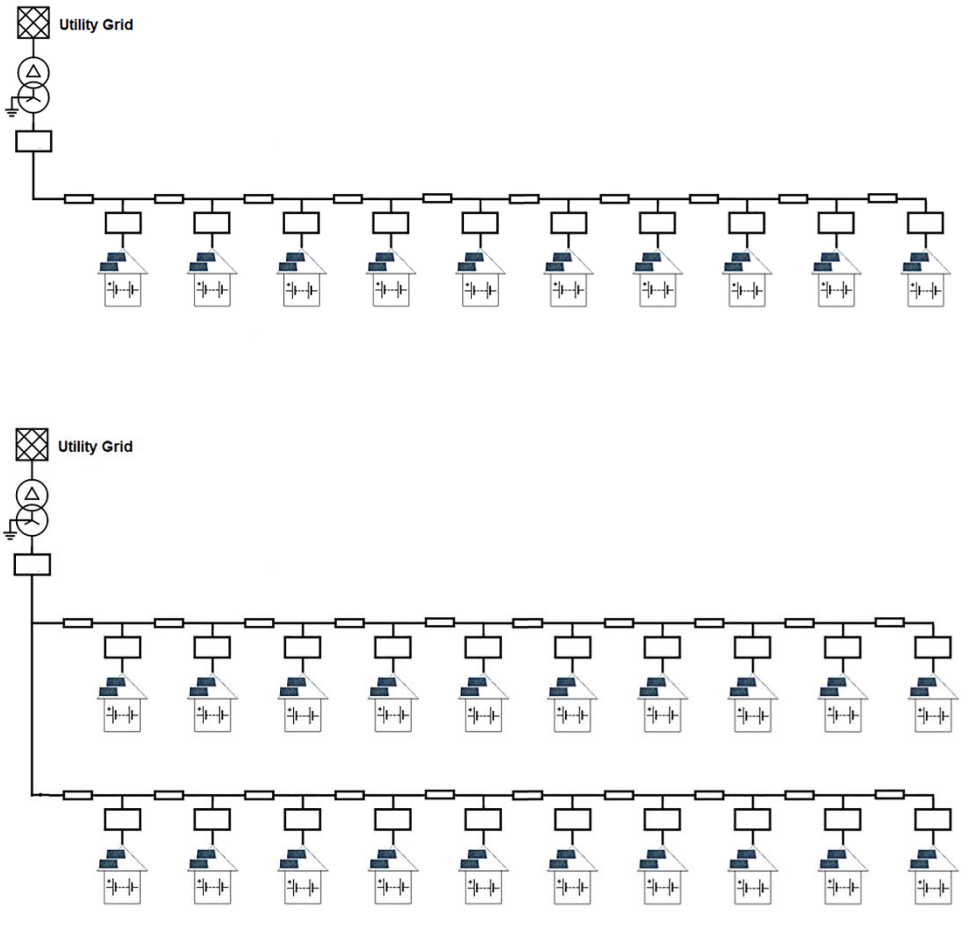

Figure 3.17 Additional configurations considered in the analysis: a) 1 feeder with 10 prosumers; b) 2 feeders with 10 prosumers each. Each prosumer is equipped with PV generation, local load and a battery storage system.

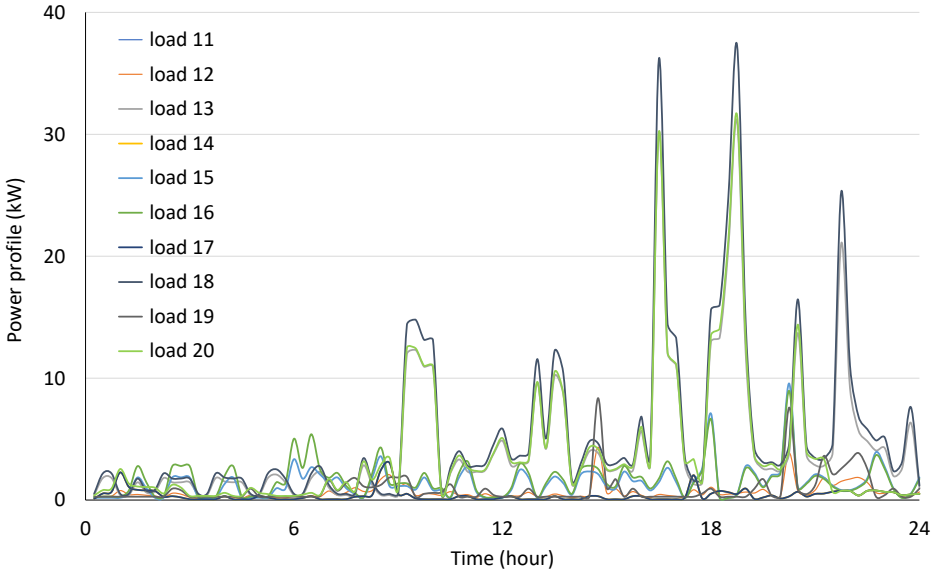

Figure 3.18 Load profiles of the 10 prosumers connected to the second feeder in Scenario 3.

For all the configurations, the profile of the ratio between power output and panel surface, and the price profile of the energy bought from the utility grid, are those shown in Figure 3.3, where π^t_{sell} is assumed to be half of π^t_{buy}.

Table 3.7 PV panel surface for each prosumer of the second feeder in Scenario 3.

Prosumer	11	12	13	14	15	16	17	18	19	20
Area (m^2)	36	20	22	25	34	35	15	13	22	33

Table 3.8 Sizes of the BES units of the second feeder in Scenario 3.

Prosumer	11	12	13	14	15	16	17	18	19	20
Size (kWh)	4	3	3	3	5	6	2	1	3	4

Energy transactions are also allowed between prosumers connected to different feeders. For each scenario, the corresponding distributed model has been solved based on the application of the ADMM procedure. Table 3.9 compares the computational effort (number of iterations and CPU time) for each scenario, where the optimization problems of the prosumers are solved in sequence, without considering delays or limitations in the communication channels.

Table 3.9 Comparison of the computational effort for the three scenarios considered in the scalability analysis.

Scenario	Total prosumers	Iterations	solution time (s)
1	10	46	600
2	10	21	900
3	20	19	3000

Furthermore, as expected, the computational effort decreases if a longer Δt is adopted. For example, if Δt=30 min, the distributed model of scenario 1 requires 350 s. If Δt=1 h, the solution of the same model requires 150 s.

To illustrate the convergence behaviour of the ADMM procedure, Figure 3.19 shows the augmented *OF* according to (3.17), the *OF* value of (3.21) and the corresponding average value of the primal residuals r_i^t (denoted by R) at each iteration, for the considered scenarios.

In Scenario 2, the solution of the centralized model needs around 300 s, whilst, for Scenario 3, which represents a particularly challenging configuration, due to the presence of 20 BES units in two different feeders, the centralized model does not reach the solution in the considered maximum time limit equal to 1.5 hours.

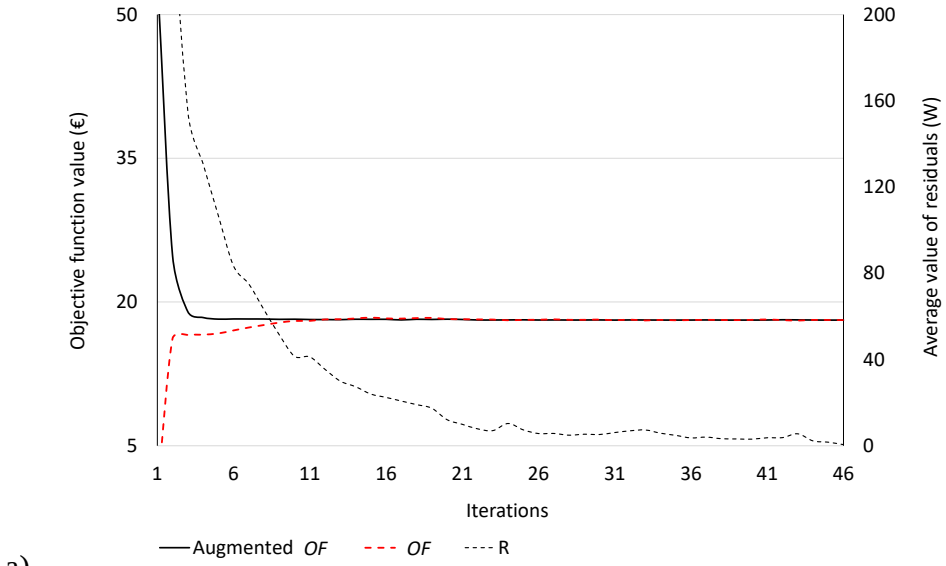

a)

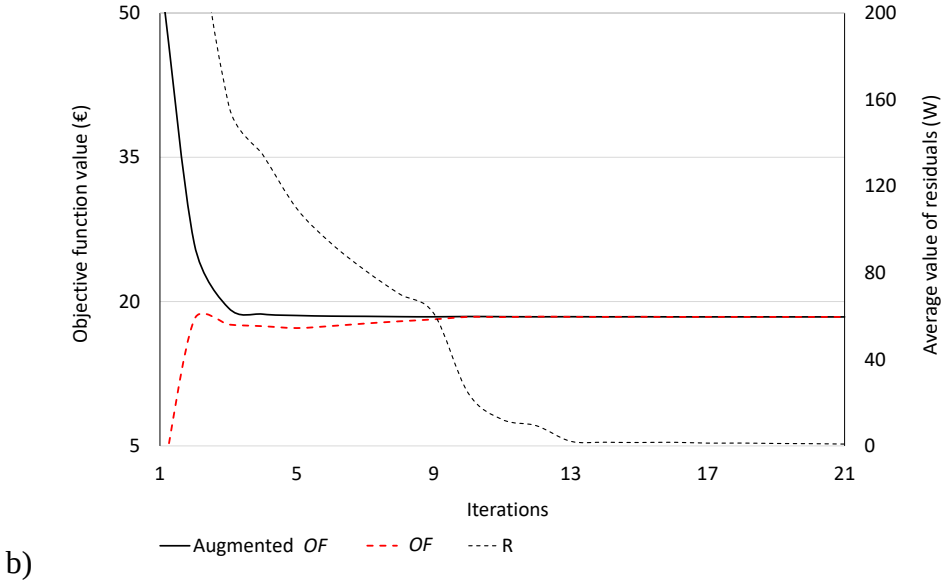

b)

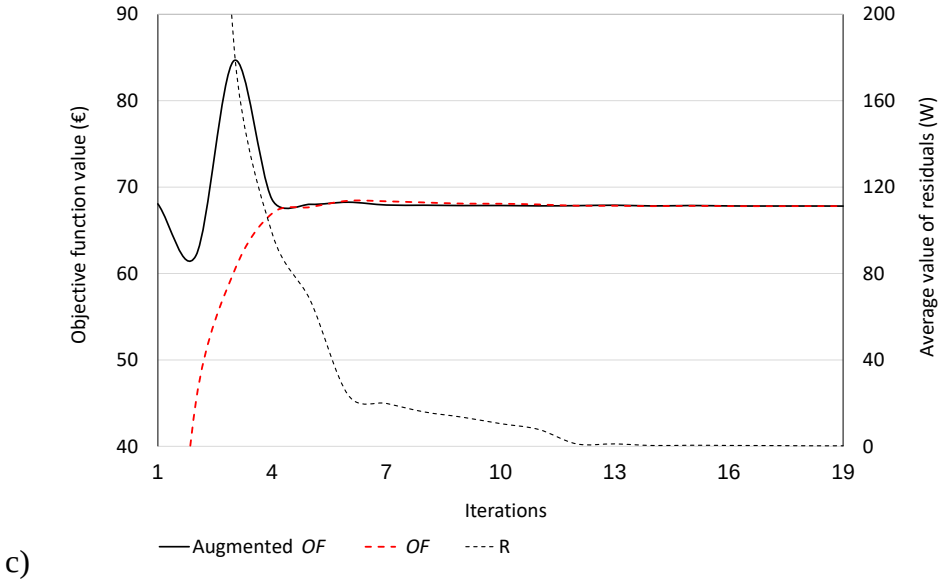

c)

Figure 3.19 ADMM convergence - Augmented *OF*; *OF* value corresponding to the exchanges with the utility grid; average value R of primal residuals at each iteration for: a) Scenario 1, b) Scenario 2, and c) Scenario 3.

3.3 Allocation of losses associated with the energy exchanges in the community

The proposed approaches considered an estimation of the internal network losses to allocate them to each energy transaction between two prosumers or between a prosumer and the utility grid. In the following, we describe an additional procedure that improves the estimation of the power loss in the internal network for both the centralized and the distributed approaches.

For both centralized and ADMM-based approaches, in the so-called first stage, the optimization is performed by using the already introduced estimation of the power loss, separately for each prosumer. Next, in the second stage, the optimization will be carried out a second time in order to refine the calculation and the corresponding allocation of the network power loss, this time due to all transactions.

3.3.1 Centralized allocation procedure

The second stage refines the estimation of the power loss in the internal network by considering the concurrent presence of the flows of all the transactions in each branch. Moreover, the second stage allocates the losses to each transaction.

By using the results of the first stage, flow F_b^t in each branch, due to all the transactions is calculated as

$$F_b^t = \sum_{i\in\Omega} A_{\text{Grid}\,b,i} P^t_{\text{buy\_Grid}\,i} - \sum_{i\in\Omega} A_{\text{Grid}\,b,i} P^t_{\text{sell\_Grid}\,i} + \sum_{i\in\Omega}\sum_{j\in\Omega} A_{b,i,j} P^t_{\text{buy}\,i,j} \qquad (3.22)$$

The total value of power loss L_b^t in branch *b* at time *t* is calculated by replacing $F_{b,i}^t$ with F_b^t in (3.12). In (Conejo et al. 2002), a typical formulation has been considered in which the losses in each branch *b* are proportionally attributed to the transactions that create flows in said branch by using coefficients $K^t_{\text{buy\_Grid}\,b,i}$, $K^t_{\text{sell\_Grid}\,b,i}$ and $K^t_{\text{buy}\,b,i,j}$ (if $F_b^t \neq 0$):

$$K^t_{\text{buy\_Grid}\,b,i} = A_{\text{Grid}\,b,i} P^t_{\text{buy\_Grid}\,i} / F_b^t \qquad (3.23)$$

$$K^t_{\text{sell\_Grid}\,b,i} = -A_{\text{Grid}\,b,i} P^t_{\text{sell\_Grid}\,i} / F_b^t \qquad (3.24)$$

$$K^t_{\text{buy}\,b,i,j} = A_{b,i,j} P^t_{\text{buy}\,i,j} / F_b^t \qquad (3.25)$$

The optimization is then repeated by using an MILP model for the second stage, in which constraints (3.3) are replaced by

$$P^t_{\text{PV}\,i} + P^t_{\text{BES\_dis}\,i} + P^t_{\text{buy\_Grid}\,i} - \sum_{b\in B} L^t_{\text{buy\_Grid}\,b,i} + \sum_{\substack{j\in\Omega \\ j\neq i}} P^t_{\text{buy}\,i,j} = P^t_{\text{Load}\,i} + P^t_{\text{BES\_ch},i} + P^t_{\text{sell\_Grid}\,i} + \sum_{b\in B} L^t_{\text{sell\_Grid}\,b,i} + \sum_{\substack{j\in\Omega \\ j\neq i}} P^t_{\text{sell}\,i,j} + \sum_{\substack{j\in\Omega \\ j\neq i}} \sum_{b\in B} L^t_{\text{buy}\,b,j,i} \tag{3.26}$$

where $L^t_{\text{buy\_Grid}\,b,i}$, $L^t_{\text{sell\_Grid}\,b,i}$ and $L^t_{\text{buy}\,b,j,i}$ are the losses in branch *b*, attributed to the power bought by *i* from the utility grid, to the power sold by *i* to the utility grid and to the power sold by *i* to *j*, respectively. The losses attributed to each transaction are obtained by the product of the corresponding coefficient, given by (3.23), (3.24), and (3.25), with the total value of power loss L^t_b in branch *b*:

$$L^t_{\text{buy\_Grid}\,b,i} = K^t_{\text{buy\_Grid}\,b,i} L^t_b \qquad i\in\Omega \tag{3.27}$$

$$L^t_{\text{sell\_Grid}\,b,i} = K^t_{\text{sell\_Grid}\,b,i} L^t_b \qquad i\in\Omega \tag{3.28}$$

$$L^t_{\text{buy}\,b,i,j} = K^t_{\text{buy}\,b,i,j} L^t_b \qquad i\in\Omega \tag{3.29}$$

According to (3.26), each prosumer *i* compensates for losses due to its transactions with the utility grid and sale transactions with other prosumers. In fact, we assume that both $P^t_{\text{buy}\,i,j}$ and $P^t_{\text{sell}\,i,j}$ (which corresponds to $P^t_{\text{buy}\,j,i}$) are measured at the buyer's connection.

Constraints (3.22) are included in the second stage model of the centralized approach for each branch *b* and time interval *t*, and the corresponding power loss, namely L^t_b, is represented by using the piecewise linear approximation of (3.12) given by (3.14)-(3.16).

In addition to the constraints of the first stage, the model of the second stage includes constraints that avoid not-present transactions in the first stage solution:

$$\begin{cases} P^t_{\text{buy\_Grid}\,i} T^t_{\text{buy\_Grid}\,i} = 0 & i\in\Omega \\ P^t_{\text{sell\_Grid}\,i} T^t_{\text{sell\_Grid}\,i} = 0 & i\in\Omega \\ P^t_{\text{buy}\,i,j} T^t_{\text{buy}\,i,j} = 0 & i \text{ and } j\in\Omega,\ i\neq j \end{cases} \tag{3.30}$$

Parameters $T^t_{\text{buy\_Grid}\,i}$, $T^t_{\text{sell\_Grid}\,i}$, and $T^t_{\text{buy}\,i,j}$ are equal to 0 if, in the first stage solution, prosumer *i* buys from the utility grid, sells to the utility grid and buys from *j*, respectively; otherwise, these

parameters are equal to 1, under the assumption that transaction decisions are not significantly affected by the losses.

3.3.2 Distributed allocation procedure

In the ADMM-based approach, we want to preserve the distributed scheme; therefore, we avoid constraint (3.22), in which all the purchase and sales decisions of all the participants in the community are coupled.

In (Lilla et al. 2020), an additional procedure, which improves the estimation of the power loss in the internal network, has been proposed for the distributed scheduling of a local energy community. Following the mentioned procedure, efficiency parameters of each transaction (between prosumer *i* and the grid, or between prosumers *i* and *j*) have been included in the energy balance of *i*, as follows:

$$P^t_{\text{PV}\,i} + P^t_{\text{dis}\,i} + \eta^t_{\text{buy\_Grid}\,i} P^t_{\text{buy\_Grid}\,i} + \sum_{\substack{j\in\Omega \\ j\neq i}} P^t_{\text{buy}\,i,j} = P^t_{\text{Load}\,i} + P^t_{\text{ch i}} + \frac{P^t_{\text{sell\_Grid}\,i}}{\eta^t_{\text{sell\_Grid}\,i}} + \sum_{\substack{j\in\Omega \\ j\neq i}} \frac{P^t_{\text{sell}\,i,j}}{\eta^t_{\text{buy}\;j,i}} \qquad i \text{ and } j \in \Omega \qquad (3.31)$$

where $\eta^t_{\text{buy\_Grid}\,i}$, $\eta^t_{\text{sell\_Grid}\,i}$, and $\eta^t_{\text{buy i},j}$ are efficiency parameters assigned to each transaction between prosumer *i* and the grid (i.e., when *i* buys from or sells to the utility grid) or between prosumer *i* and *j* (i.e., prosumer *j* sold to *i*), respectively. These efficiencies are given by:

$$\eta^t_{\text{buy\_Grid}\,i} = 1 - \frac{\sum_{b\in B} L^t_{\text{buy\_Grid}\,b,i}}{P^t_{\text{buy\_Grid}\,i}} \qquad (3.32)$$

$$\eta^t_{\text{sell\_Grid}\,i} = \frac{P^t_{\text{sell\_Grid}\,i}}{P^t_{\text{sell\_Grid}\,i} + \sum_{b\in B} L^t_{\text{sell\_Grid}\,b,i}} \qquad (3.33)$$

$$\eta^t_{\text{buy}\,i,j} = \frac{P^t_{\text{buy}\,i,j}}{P^t_{\text{buy}\,i,j} + \sum_{b\in B} L^t_{\text{buy}\,b,i,j}} \qquad j\in\Omega,\ i\neq j \qquad (3.34)$$

where $L^t_{\text{buy\_Grid}\,b,i}$, $L^t_{\text{sell\_Grid}\,b,i}$, and $L^t_{\text{buy}\,b,j,i}$, according to the same definition of the previous section (allocation for the centralized approach), correspond to the losses in branch *b* attributed to: the power bought by prosumer *i* from the utility grid, the power sold by prosumer *i* to the utility grid and the power sold by prosumer *i* to prosumer *j*, respectively.

Following the same rules as in the centralized approach, the corresponding losses are calculated at the end of a distributed optimization defined, as in section 3.2 (i.e., optimization in the first stage).

The η calculation can be carried out by a central coordinator that knows the topology and parameters of the network and collects the information regarding power exchanges of the first stage (i.e., the values $P^{t}_{\text{buy}\,i,j}$, $P^{t}_{\text{buy\_Grid}\,i}$, $P^{t}_{\text{sell\_Grid}\,i}$ from each member i of the community). In the REC, the corresponding calculation could also be done by each prosumer following a distributed scheme, to achieve this, the resistance values of the branches, matrix $A_{\text{Grid}\,b,i}$ and arrange $A_{b,i,j}$, are assumed to be known for every member of the community, and assuming that each prosumer communicates its energy transactions to the other members in the community.

Ultimately, as mentioned, the distributed optimization is repeated considering constraint (3.31) as the power balance constraint.

3.3.3 Results after the loss-allocation procedure for both centralized and distributed approaches

Now, let us consider the introduced procedures to refine the calculation and corresponding allocation of the losses to solve the scheduling problem of the community.

We will consider two different scenarios: the first one corresponds to the case described in section 3.1.2, with two feeders and 10 prosumers, each one equipped with a PV-storage system, and a second scenario, in which the participants in the same community do not have storage systems.

For both scenarios, the corresponding scheduling profiles and results obtained by the centralized and the ADMM-based approaches will be compared.

A. Case study including BES units in the community

Figure 3.20 shows the total power flow exchanged by the community with the utility grid, after the allocation of losses. Figure 3.20 includes the results for both centralized and distributed approaches.

The power profiles from each prosumer when it sells to the other participants in the community (excluding the power sold to the utility grid) have been illustrated in Figure 3.21, for both

centralized and ADMM approaches. Figure 3.22 compares the corresponding power profiles from each prosumer when it buys from the other participants in the REC (excluding the power bought from the utility grid).

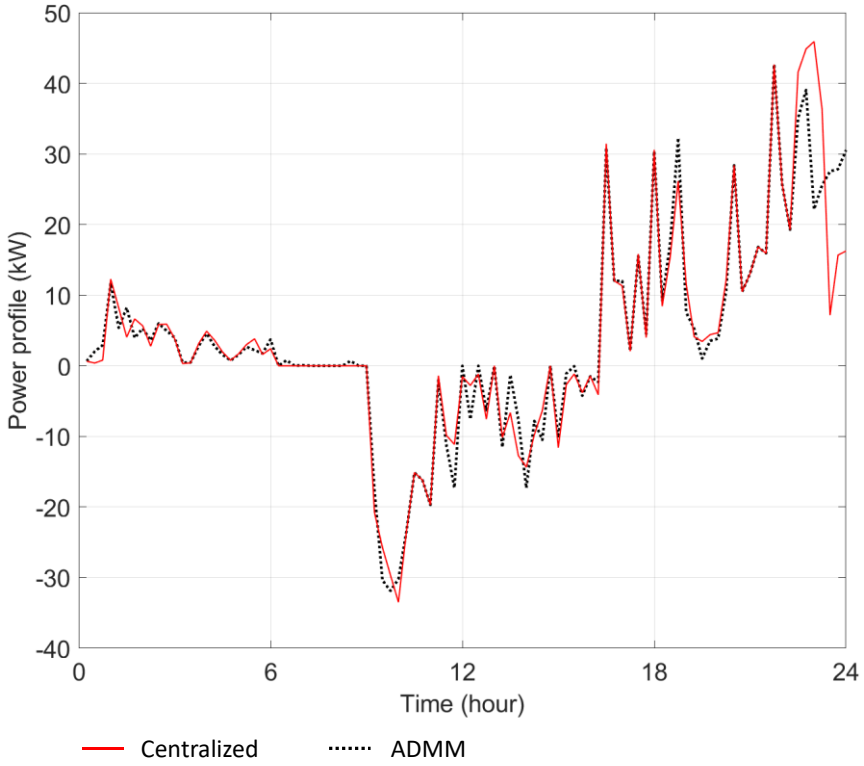

Figure 3.20 Comparison of the power flow exchanged with the utility grid (positive if consumed by the community): scenario with BES units (solid red line: centralized solution, dashed line: ADMM solution).

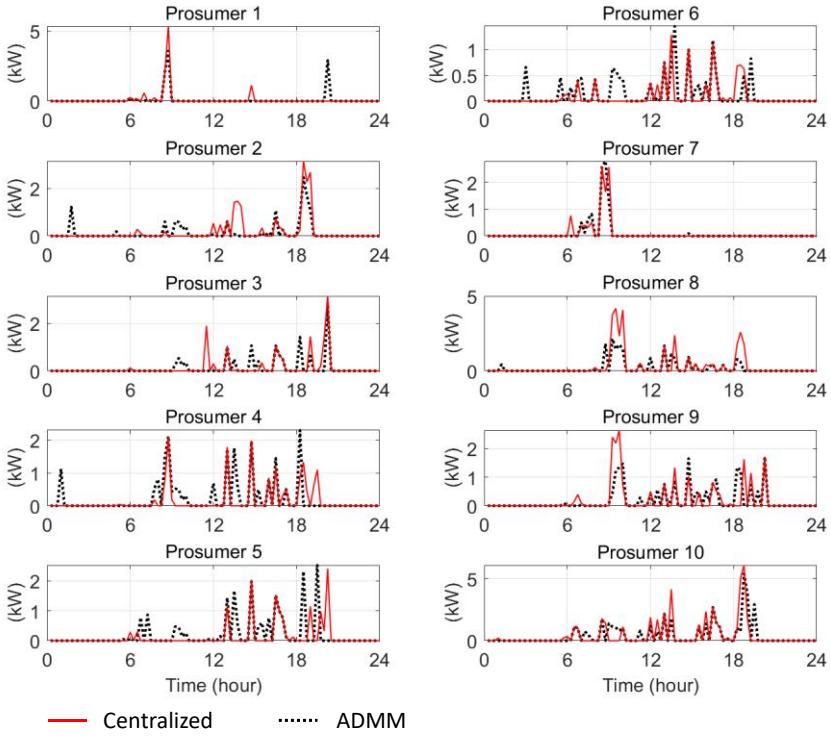

Figure 3.21 Comparison of the power flow from every prosumer when it sells to the other participants in the community: scenario with BES units (solid red line: centralized solution, dashed line: ADMM solution).

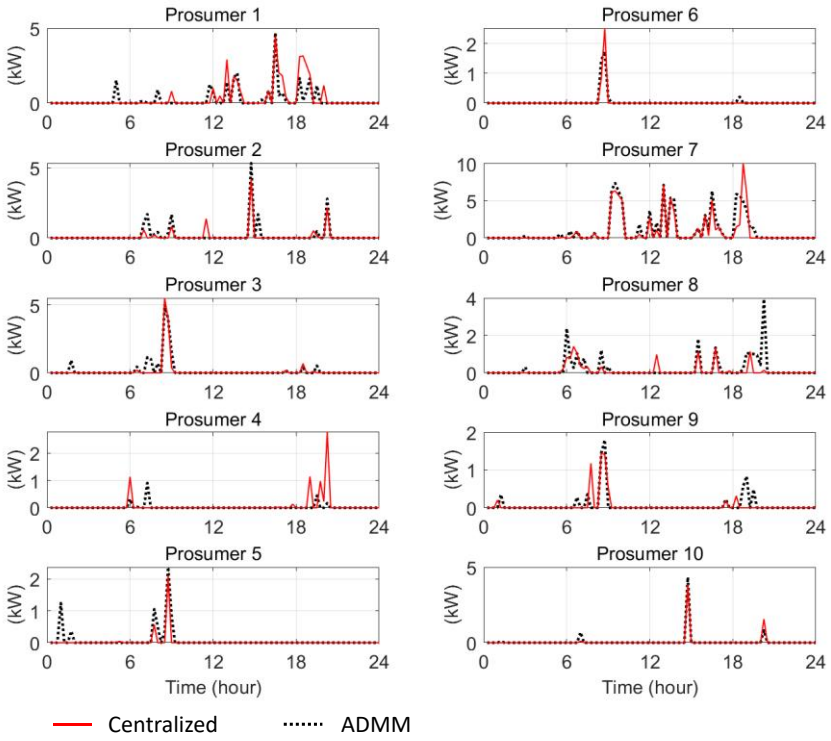

Figure 3.22 Comparison of the power flow from every prosumer when it buys from the other participants in the community: scenario with BES units (solid red line: centralized solution, dashed line: ADMM solution).

Figure 3.23 shows the profiles of the energy stored in each BES unit, whilst Figure 3.24 illustrates the total energy stored in the community's storage systems.

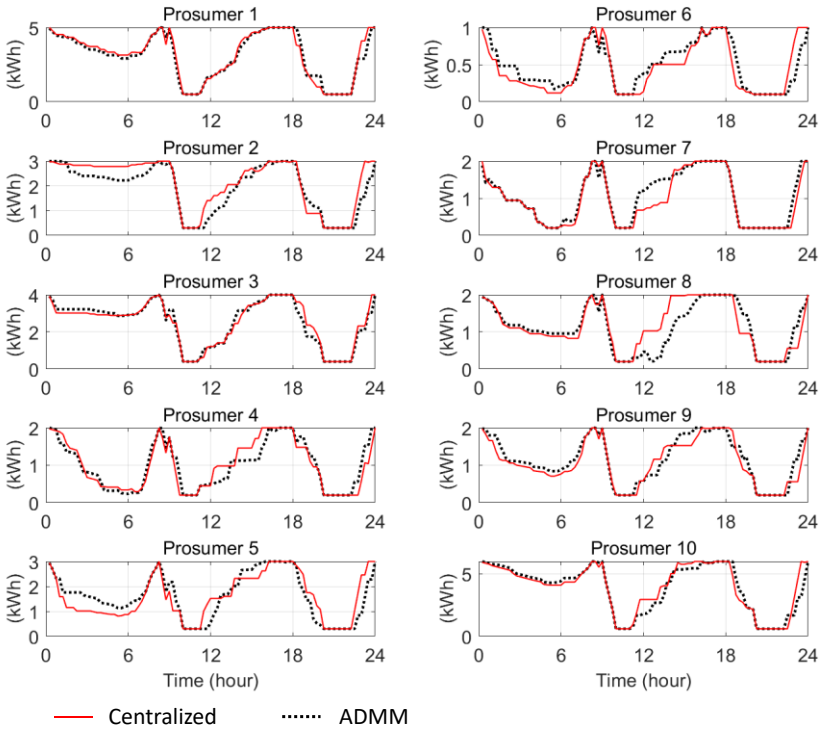

Figure 3.23 State of Energy for each BES unit in the community (solid red line: centralized solution, dashed line: ADMM solution).

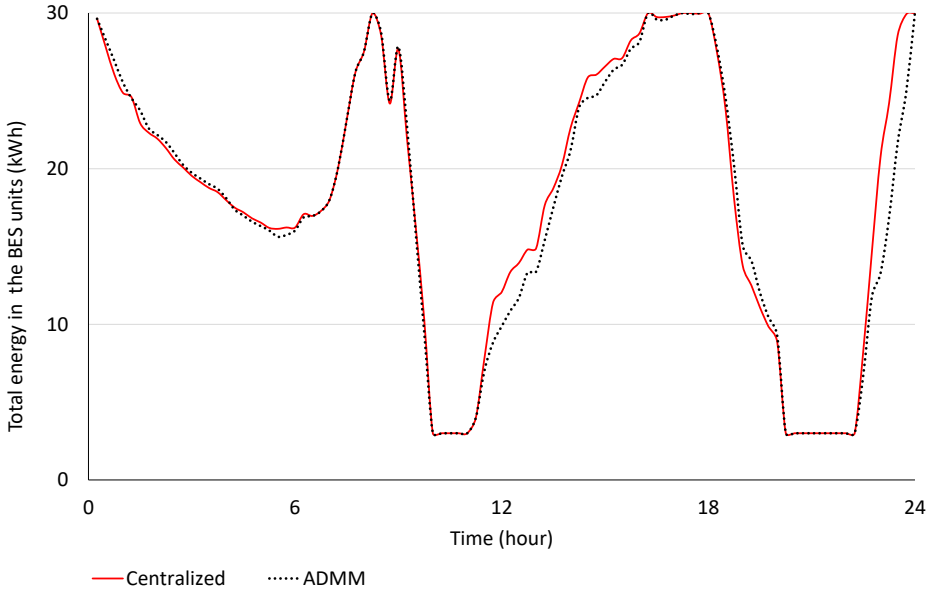

Figure 3.24 Comparison of the total energy stored in the batteries of the community obtained by the centralized and the ADMM approach.

Table 3.10 includes a comparison of the *OF* values for both stages (i.e., estimation of losses for each transaction, and calculation of total losses and allocation, respectively), and the total network losses over the 24 hours, obtained for the scenario that includes the BES units.

In this case, the distributed approach employs around 220 s / 82 iterations to solve stage two, which are added to the solution time of the first stage. The solution of the centralized model needs around 8 s for stage two. It is important to notice, that the main purpose of adopting the distributed approach instead of the centralized one is not to improve the computational performance but to better preserve the privacy and independency of the participants in the community.

In order to present a complete comparison of the proposed distributed approach and the centralized one, an additional representation of the centralized model denoted as centralized-η has been considered, in which the calculation of the second stage is carried out by the centralized model replacing (3.26) with (3.31).

Table 3.10 Comparison between centralized and ADMM approaches, including the respective total losses calculation for the day (scenario with BES units).

	OF (€)		Losses (kWh)
	Stage 1	Stage 2	Stage 2
Centralized	18.06	18.35	3.41
Centralized-η	18.06	18.34	3.35
ADMM	18.12	18.39	3.44

The reasonable accuracy of the power-loss representation in the second stage, of both the centralized and distributed optimization models, is confirmed by the maximum percentage difference of a few percent between the power loss calculated at the end of the second stage for each period and the corresponding values obtained by (3.12), with $F_{b,i}^{t}$ replaced with F_{b}^{t}.

Table 3.11 and Table 3.12 compare the energy procurement cost for each participant in the community. As already introduced in the previous sections, the cost for each one considers both the exchanges with the external grid and the internal exchanges, as well as the corresponding prices of the centralized approach in Figure 3.9 and the ADMM approach in Figure 3.16.

Table 3.11 and Table 3.12 include the procurement cost for each prosumer, assuming that energy transactions are not allowed in the community (i.e., without internal exchanges).

Table 3.11 Energy procurement cost in € (negative values indicate revenues) for each prosumer in feeder 1, obtained after the allocation of losses in the scenario with BES units.

Prosumer	1	2	3	4	5
Cooperative – Centralized	5.25	0.08	0.97	-0.96	-0.62
Cooperative – Centralized-η	5.25	0.09	0.98	-0.97	-0.63
Cooperative – ADMM	5.26	0.10	0.99	-0.96	-0.61
Without internal exchanges	5.47	0.29	1.12	-0.79	-0.43

Table 3.12 Energy procurement cost in € (negative values indicate revenues) for each prosumer in feeder 2, obtained after the allocation of losses in the scenario with BES units.

Prosumer	6	7	8	9	10
Cooperative – Centralized	-0.21	14.85	1.67	-0.45	-2.25
Cooperative – Centralized-η	-0.21	14.86	1.66	-0.45	-2.23
Cooperative – ADMM	-0.20	14.85	1.66	-0.44	-2.24
Without internal exchanges	-0.14	16.47	1.74	-0.29	-1.63

The effect of the energy transactions between prosumers is compensated in both solutions given by (3.1) and (3.21) (i.e., centralized and distributed, respectively), leading to the total value of the *OF* reported in Table 3.10.

In general, the comparison of the results given by the centralized and the distributed approaches shows a reasonable match, notwithstanding the differences in the individual profiles obtained for each prosumer, as shown in Figure 3.21, Figure 3.22 and Figure 3.23. From the results reported in Table 3.11 and Table 3.12, the total energy procurement cost of the community is around 16% less than the corresponding cost without internal transaction among the prosumers.

B. Case study without BES units

In the scenario in which BES units are not present in the community, Figure 3.25 shows the total power flow exchanged by the community with the external energy provider, obtained by both the centralized and distributed approaches.

The profiles of the power flow for each prosumer when selling and buying energy in the community are illustrated in Figure 3.26 and Figure 3.27, respectively.

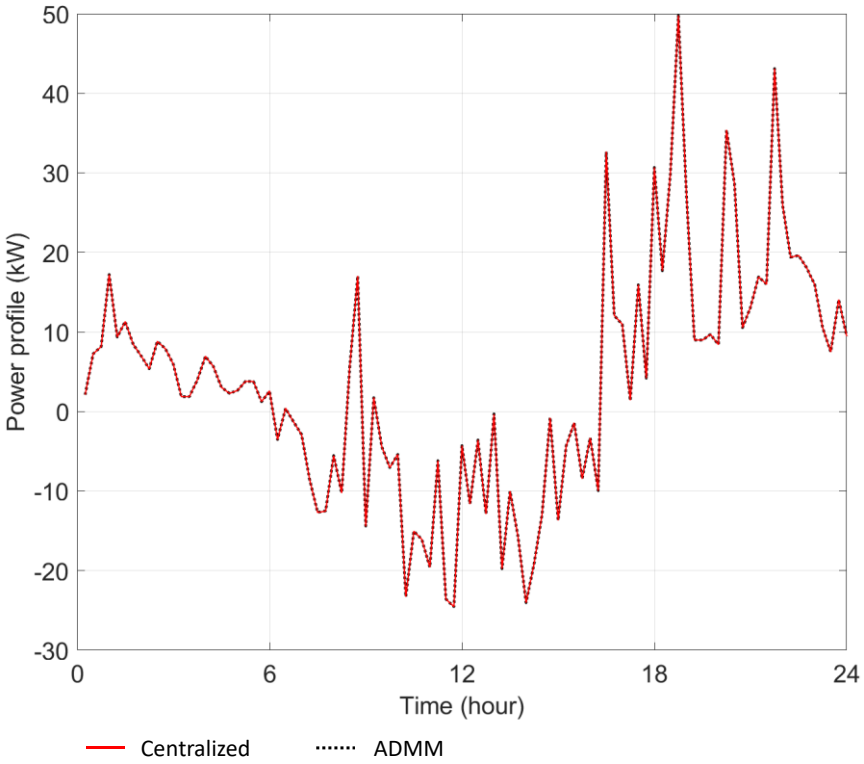

Figure 3.25 Comparison of the power flow exchanged with the utility grid (positive if consumed by the community): scenario without BES units (solid red line: centralized solution, dashed line: ADMM solution).

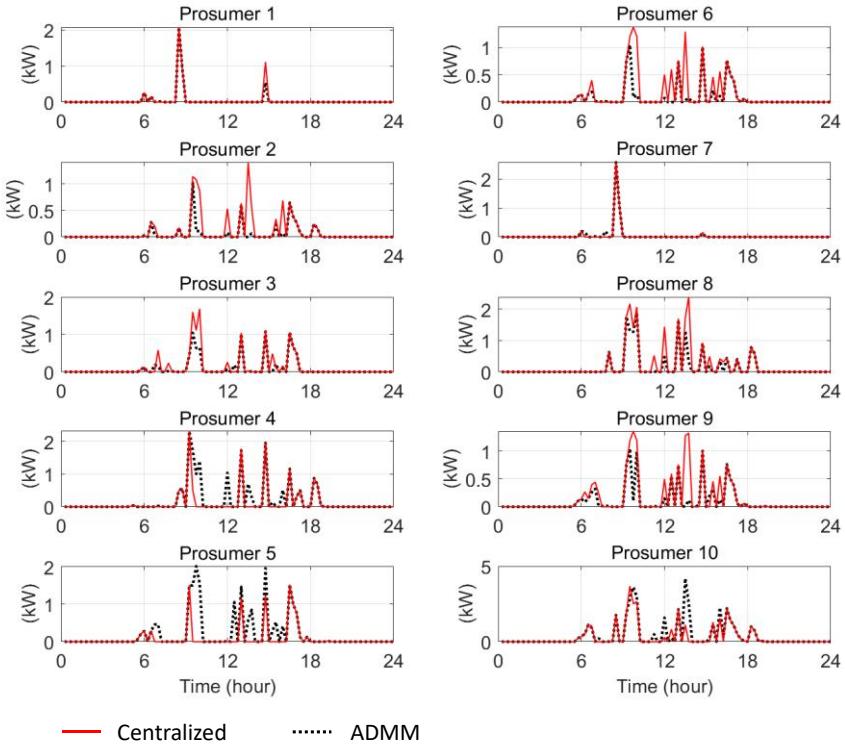

Figure 3.26 Comparison of the power flow from every prosumer when it sells to the other participants in the community: scenario without BES units (solid red line: centralized solution, dashed line: ADMM solution).

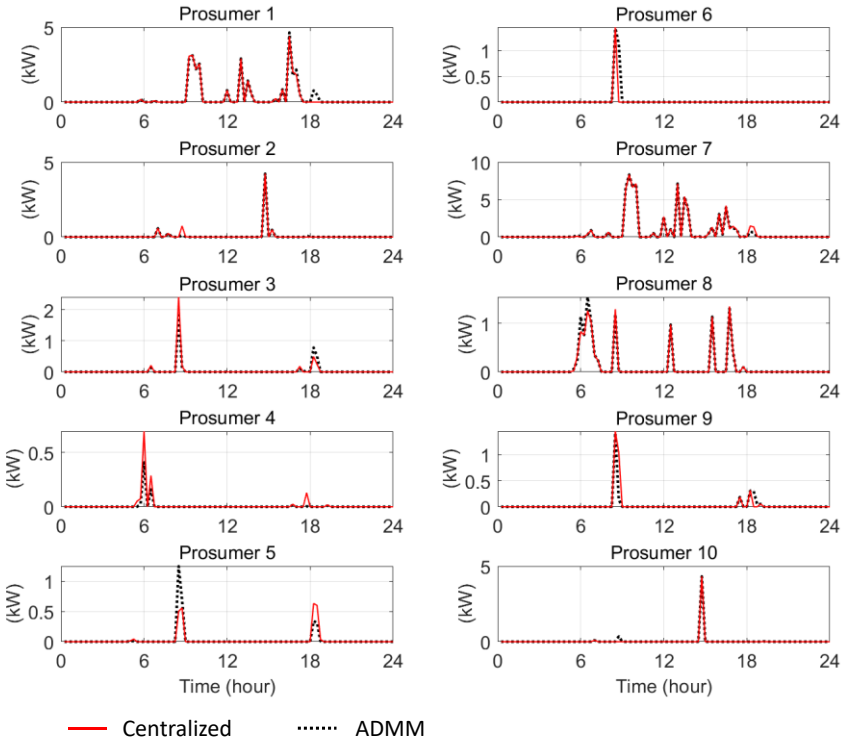

Figure 3.27 Comparison of the power flow from every prosumer when it buys from the other participants in the community: scenario without BES units (solid red line: centralized solution, dashed line: ADMM solution).

The *OF* values for both stages, and the total network losses in the 24 hours, for the centralized, the denominated centralized-η and the ADMM approaches for the community scenario without batteries are reported in Table 3.13. In the scenario without BES units, the distributed optimization problem employs around 60 s/ 13 iterations for the first stage and 80 s/ 8 iterations for the second stage. The centralized solution needs around 1s for each stage.

Table 3.13 Comparison between centralized and ADMM approaches, including the respective total losses calculation for the day (scenario without BES units).

	OF (€)		Losses (kWh)
	Stage 1	Stage 2	Stage 2
Centralized	26.85	27.19	3.65
Centralized-η	26.85	27.18	3.62
ADMM	26.87	27.18	3.63

Table 3.14 and Table 3.15 compares the individual energy procurement costs of each member of the community, taking into account the energy transactions with the utility grid and with the other participants. To achieve this, the cost calculation considers the prices obtained by the centralized and the distributed approaches for the scenario without BES units and is illustrated in Figure 3.28 and Figure 3.29, respectively.

Furthermore, the procurement costs for each prosumer obtained when preventing transactions between prosumers are also included in Table 3.14 and Table 3.15. As expected, the comparison of these values with the procurement cost obtained by both the centralized and the ADMM solutions confirms that each participant in the community has an economic benefit (e.g., increasing revenues or reducing costs). The total procurement cost of the community is reduced (by about 11%) with respect to the total cost when the energy transactions are not allowed between participants.

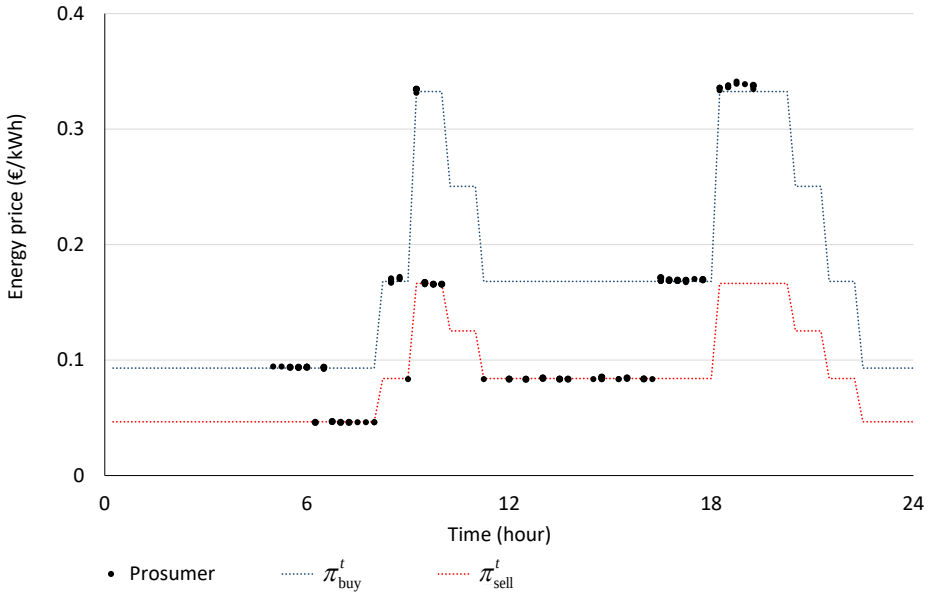

Figure 3.28 Energy prices of selling prosumers, obtained using the centralized approach (scenario without BES units).

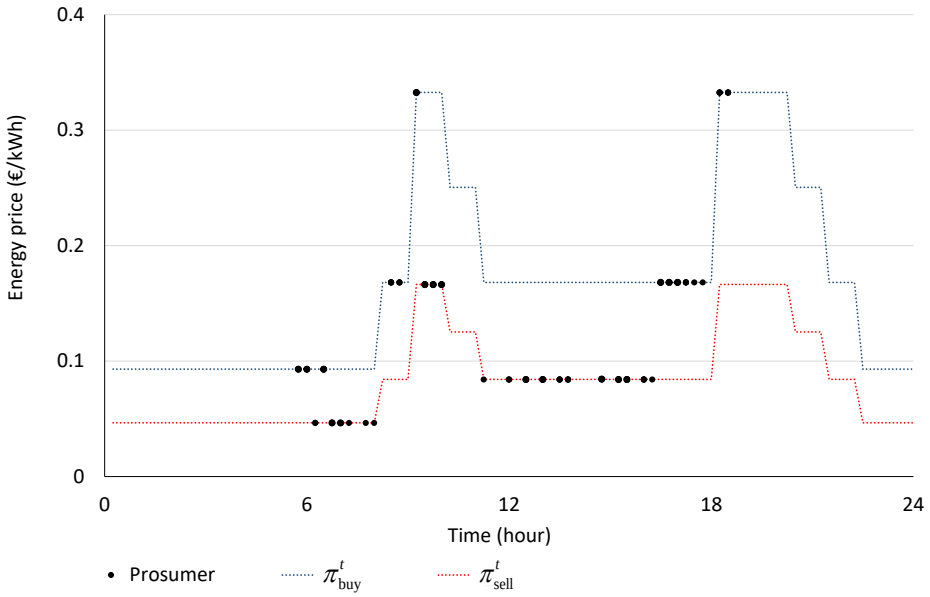

Figure 3.29 Energy prices of buying prosumers, obtained using the ADMM approach (scenario without BES units).

Table 3.14 Energy procurement cost in € (negative values indicate revenues) for each prosumer in feeder 1, obtained after the allocation of losses in the scenario without BES units.

Prosumer	1	2	3	4	5
Cooperative – Centralized	6.81	0.87	2.09	-0.43	0.23
Cooperative – Centralized-η	6.82	0.87	2.09	-0.43	0.22
Cooperative – ADMM	6.83	0.89	2.08	-0.44	0.19
Without internal exchanges	7.36	1.03	2.16	-0.20	0.37

Table 3.15 Energy procurement cost in € (negative values indicate revenues) for each prosumer in feeder 2, obtained after the allocation of losses in the scenario without BES units.

Prosumer	6	7	8	9	10
Cooperative – Centralized	0.08	15.90	2.17	0.10	-0.65
Cooperative – Centralized-η	0.08	15.90	2.17	0.10	-0.65
Cooperative – ADMM	0.08	15.95	2.17	0.09	-0.66
Without internal exchanges	0.16	17.45	2.40	0.18	-0.22

Appendix B introduces a specific representation of a prosumer-based community in a MV network. The referred model corresponds to a centralized approach, which minimizes the energy cost and is particularly oriented to reduce the power losses.

3.4 Integration of dispatchable generating units

The operation of electrical systems that integrate biogas power generation, non-dispatchable renewable generation and energy storage systems has been widely studied as in e.g., (Zhou et al. 2018; España et al. 2020; X. Zhang, Sharma, and He 2012). In (Lai et al. 2017), a techno-economic analysis of an off-grid hybrid system including PV-Storage systems and AD-biogas power plant has been presented, where the biogas consumption per kWh has been represented by the quadratic function included in (Engine and Data 2009).

The scheduling problem for electrical systems including dispatchable units can be addressed by means of centralized and distributed approaches, as in e.g., (Xu et al. 2019), where a Lagrangian dual approach has been adopted in order to solve the scheduling problem of a multicarrier energy system for interconnected microgrids.

This section is focused on the expansion of the introduced models (i.e., centralized and distributed) of the REC to consider one or more participants equipped with a dispatchable generator, specifically a biogas-powered generator.

In the following, the corresponding formulation to deal with the scheduling problem of the community that also considers the cost of energy generation from biogas will be introduced. In this context, we will study the impact of the presence of biogas power production on the prices of the energy transactions between community participants. The corresponding problem will be addressed by both a centralized and distributed approach and analysed for several case studies.

3.4.1 Biogas-powered producer formulation

One of the main characteristics of the community model in this section is that the total energy procurement cost considers those associated with the biogas-powered generation i.e., specifically with the fuel consumption.

Following (Lai et al. 2017), the cost of the biogas power generation of a *i*-th member of the community has been defined by (3.35), where the fuel consumption per kWh has been represented by the quadratic function included in (Engine and Data 2009)

$$C^t_{\text{biogas}\,i} = C_{\text{gas}i}\,\frac{P^t_{\text{biogas}\,i}[a(P^t_{\text{biogas}\,i})^2 + bP^t_{\text{biogas}\,i} + c]}{LHV} \qquad (3.35)$$

with parameters *a*, *b* and *c* equal to 0.0016 (btu/kW^{3}h), -3.935 (btu/kW^{2}h) and 10641 (btu/kWh) respectively (according to (Lai et al. 2017)).

In (3.35) , $P^t_{\text{biogas}i}$ (in kW) corresponds to the power output of the dispatchable generator owned by *i* in time interval *t* and $C_{\text{gas}\,i}$ is the AD gas cost (in €/ ft^3). The lower heating value (*LHV*) has been considered equal to 905 btu/ft^3.

In order to include (3.35) into an MILP model of the community's operation, the corresponding cost is replaced by its piece-wise linear approximation according to equations (3.36)-(3.38). For this purpose, the allowed range of the biogas power output is divided into N_{x} intervals, each one defined by breakpoints x_u, such that $U = \{1, 2, \ldots, N_{\text{x}}\}$ denotes the set of segments. At each interval of the power output, breakpoints x_u define a corresponding interval of associated costs, where α_u and β_u represent the linearization parameters of the *u-th* segment. The allowed range is defined by $P^{\max}_{\text{biogas}}$ and $P^{\min}_{\text{biogas}}$ (in kW), which are the maximum and minimum power output, respectively.

$$C^t_{\text{biogas}\,i} \geq \frac{C_{\text{gas}\,i}}{LHV}(\alpha_u P^t_{\text{biogas}\,i} + \beta_u w^t_i) \qquad u \in U \qquad (3.36)$$

$$\alpha_u = a(x_u^2 + x_{u-1}^2 + x_u x_{u-1}) + b(x_u + x_{u-1}) + c \qquad u \in U \qquad (3.37)$$

$$\beta_u = a\, x_{u-1}^3 + b\, x_{u-1}^2 + c\, x_{u-1} - \alpha_u x_{u-1} \qquad u \in U \qquad (3.38)$$

with

$$\begin{cases} x_u = P_{\text{biogas}}^{\min} & \text{if } u = 1 \\ x_u = P_{\text{biogas}}^{\min} + u\dfrac{P_{\text{biogas}}^{\max} - P_{\text{biogas}}^{\min}}{N_x} & \text{if } u > 1,\ u \in U \end{cases} \qquad (3.39)$$

Constraints (3.40)-(3.44) complete the model of the biogas power plant owned by prosumer *i*.

$$P_{\text{biogas}\,i}^{\min} \le P_{\text{biogas}\,i}^{t} \le P_{\text{biogas}\,i}^{\max} \qquad (3.40)$$

$$\sum_t \frac{P_{\text{biogas}\,i}^{t}[a(P_{\text{biogas}\,i}^{t})^2 + bP_{\text{biogas}\,i}^{t} + c]}{LHV}\Delta t \le C_{\text{fuel}\,i}^{\max\,\text{day}} \qquad (3.41)$$

$$\begin{cases} SU_i^{t=1} \ge w_i^{t=1} \\ SU_i^{t} \ge w_i^{t} - w_i^{t-1} & \text{if } t > 1 \end{cases} \qquad (3.42)$$

$$\sum_t SU_i^t \le 1 \qquad (3.43)$$

$$\begin{cases} P_{\text{biogas}\,i}^{t} = 0 & \text{if } w_i^t = 0 \\ P_{\text{biogas}\,i}^{t} \ge P_{\text{biogas}\,i}^{\min} & \text{if } w_i^t = 1 \end{cases} \qquad w_i^t \in \{1,0\},\ i \in \Omega \qquad (3.44)$$

Constraint (3.40) limits the power output of the biogas unit within its minimum and maximum value (i.e., $P_{\text{biogas}\,i}^{\min}$ and $P_{\text{biogas}\,i}^{\max}$, respectively). In (3.41), the daily amount of fuel consumption (in ft^3) is bound by maximum value $C_{\text{fuel}\,i}^{\max\,\text{day}}$. In (3.42), the non-negative variable SU_i^t is used to indicate whether the biogas power plant owned by *i* starts up at time interval *t* or not, whilst (3.43) allows each biogas power plant to be started-up only once during the following day.

Constraint (3.44) includes binary variable w_i^t, which indicates whether the biogas power plant owned by prosumer *i* is on or off during time interval *t*.

The case studies included in this chapter consider a biogas power generator with $P_{\text{biogas}\,i}^{\max}$ equal to 20kW; $P_{\text{biogas}\,i}^{\min}$ is assumed equal to 20% of $P_{\text{biogas}\,i}^{\max}$. Since the size of the considered biogas power plant is quite small, start-up and shut-down costs are neglected.

3.4.2 Centralized and distributed approaches to solve the scheduling problem

In order to consider the participation in the community of producers that own biogas-fuelled generators, the centralized and the ADMM models proposed in section 3.1 and section 3.2, respectively, are extended to include the relevant cost and operational constraints associated to such units.

A. Objective function and formulation for the centralized model

In the centralized model, the *OF* (3.1) is modified by including the piece-wise linearization of cost (3.35); thus, the total objective function minimizes the total energy cost given by

$$OF = \min \sum_{\substack{t\in T \\ i\in\Omega}} \left[\pi^t_{\text{buy}} P^t_{\text{buy\_Grid}\,i} - \pi^t_{\text{sell}} P^t_{\text{sell\_Grid}\,i} + C^t_{\text{biogas}\,i} \right] \Delta t \qquad (3.45)$$

Then, the scheduling problem is solved considering the set of constraints (3.2)-(3.16) and (3.35) -(3.44).

For the community with dispatchable generation, the power balance constraint (3.3) is replaced with (3.46), in which the power output at time period *t* of the available biogas-power generators are included

$$\begin{aligned} &P^t_{\text{PV}\,i} + P^t_{\text{BES\_dis}\,i} + P^t_{\text{buy\_Grid}\,i} + P^t_{\text{biogas}\,i} + \sum_{\substack{j\in\Omega \\ j\neq i}} P^t_{\text{buy}\,i,j} = \\ &P^t_{\text{Load}\,i} + P^t_{\text{BES\_ch}\,i} + P^t_{\text{sell\_Grid}\,i} + \sum_{\substack{j\in\Omega \\ j\neq i}} P^t_{\text{sell}\,i,j} + \frac{1}{2}\sum_{b\in B} L^t_{b,i} \end{aligned} \qquad i \in \Omega \quad (3.46)$$

The maximum power that a biogas-powered producer *i* can sell (i.e., $P^{\max}_{\text{sell}\,i}$) corresponds to $P^{\max}_{\text{biogas}\,i}$.

B. Objective function and formulation for the distributed model

The scheduling problem is suitable to be represented with a distributed optimization model based on the ADMM procedure. In this case, the *OF* (3.45) is decomposed into sub problems for each participant *i* in the community

$$OF_i = \min \sum_{t\in T} \left[\begin{array}{l} \pi^t_{\text{buy}} P^t_{\text{buy\_Grid}\,i} - \pi^t_{\text{sell}} P^t_{\text{sell\_Grid}\,i} + C^t_{\text{biogas}\,i} \\ + \sum_{\substack{j\in\Omega \\ j\neq i}} \lambda^t_j P^t_{\text{buy i},j} - \lambda^t_i \sum_{\substack{j\in\Omega \\ j\neq i}} P^t_{\text{sell}\,i,j} + \ell^t_i \end{array} \right] \Delta t \qquad (3.47)$$

where $C^t_{\text{biogas}i}$ corresponds to the piece-wise linearization of cost (3.35) for the *i*-th member of the community that owns a generator (otherwise it will be equal to zero); ℓ^t_i, defined by (3.18) , penalizes the imbalances between the intended energy transactions of *i* and the other participants.

Problem (3.47) is iteratively solved by each one of the members of the community, individually considering, for each participant *i*, constraints (3.4)-(3.16), power balance (3.46) and constraints (3.35)-(3.44) relevant to the operation of a dispatchable generator owned by *i*.

Following the implementation of the ADMM approach of section 3.2, the values of λ^t_i are iteratively updated to reduce the imbalances associated with the energy transactions that involves *i*. For this purpose, at each iteration, all the participants share with the others the resulting values of their local values, namely $\hat{P}^t_{\text{buy}\,i,j}$ and $\hat{P}^t_{\text{sell}\,i,j}$ in (3.18).

The ADMM procedure reaches the convergence when the values that reflect the imbalances are below a defined tolerance ε (assumed equal to 20 W in the case studies included in this section). The implemented approach follows the updating scheme for the penalization parameter ρ and scale factor *m* at each iteration (introduced in section 3.2) to speed up the convergence of the distributed solution.

Once the procedure converges, ℓ^t_i tends to zero, and the value of the total *OF* for the community is equal to the summations of the resulting values of every *i*-th sub problem.

3.4.3 Case studies for the integration of PV-storage systems and dispatchable generation

In the following, we describe the case studies that have been adopted to test the performance of both centralized and distributed approaches. For comparative purposes, the case studies preserve total values of the daily-energy generated by PV units, the daily-energy demand and installed storage capacity (i.e., 231 kWh, 313 kWh and 30 kWh, respectively) of the base case introduced in section 3.1.2.

- Case I – considers a REC with a biogas-powered plant owned by one of the participants (with $P^{\max}_{\text{biogas}i}$ = 20 kW, $C_{\text{gas}i}$ = 9.97 €/mcf and $C^{\max\text{day}}_{\text{fuel}i}$ =3300 ft^3), together with nine prosumers equipped with PV units, BES units and local loads each. The corresponding scheme has been illustrated in Figure 3.30a.

- Case II – same scheme as Case I, but without any BES unit.
- Case III – same scheme as Case I, but considering a more restricted fuel consumption availability in the biogas unit ($C_{\text{fuel}\,i}^{\max \text{day}}$=1000 ft^3).
- Case IV – considers a community of eight prosumers equipped with PV units and batteries (other than loads and, in addition, two biogas-powered plants, as in Figure 3.30b). The maximum power output, and the gas cost of both biogas power plants, are set equal to 20kW and 9.97 €/mcf, respectively.
- Case V – same scheme as Case IV, but with different gas costs $C_{\text{gas}i}$ for each biogas-powered generator (9.97 €/mcf for Biogas 1 and 10.97 €/mcf for Biogas 2). The maximum power output is equal to 20 kW for both generators.

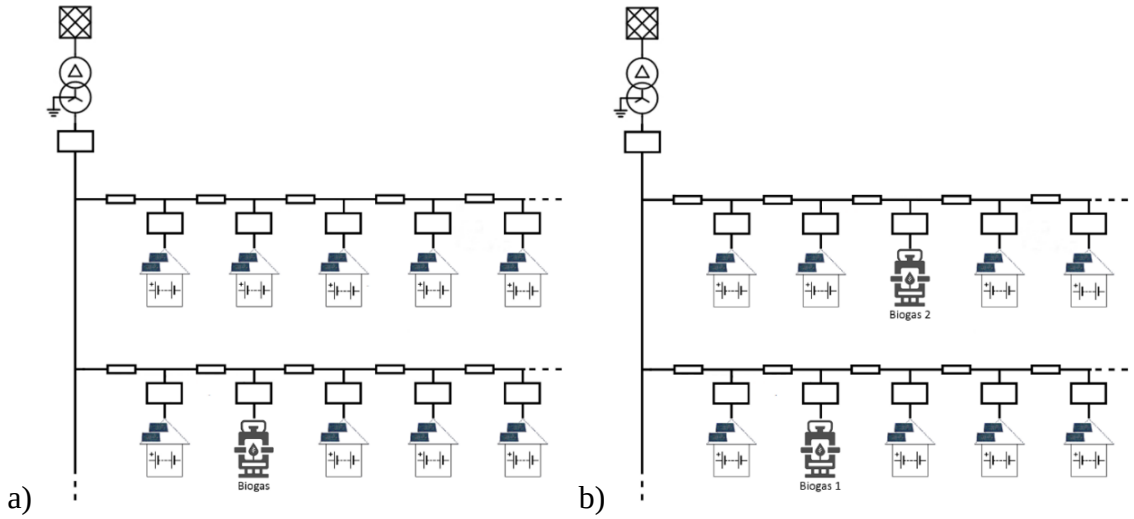

Figure 3.30 Scheme of the community that includes biogas-powered producers: a) Cases with a biogas unit; b) Cases with two biogas units.

Table 3.16 shows the *OF* value, total daily fuel consumption and percentage of the community self-consumption for each case study. The reported results have been obtained by employing both the centralized and the ADMM approaches. Moreover, Table 3.16 shows the total solution time needed from each approach and the total number of iterations of the distributed solution.

In general, the results in Table 3.16 for the centralized and the ADMM approaches are similar and confirm that the scheduling problem of the community with dispatchable units is suitable to adopt both approaches. It is important to notice that the ADMM approach is oriented to limit the information that participants share in the community and not directly oriented to improve the solution time in the case studies.

Table 3.16 Case-Studies results for the community with the presence of dispatchable generation.

	Approach	Case I	Case II	Case III	Case IV	Case V
OF (€)	Centralized	5.2	11.4	7.0	1.7	3.2
	ADMM	5.5	11.4	7.3	1.8	3.6
Total fuel consumption ($10^3 \cdot ft^3$)	Centralized	2.0	2.0	1.0	3.4	2.7
	ADMM	2.0	2.0	1.0	3.4	3.4
Self-consumption (%)	Centralized	72	70	69	73	73
	ADMM	70	70	66	73	73
Solution time (s)	Centralized	35	15	48	62	30
	ADMM	910	400	920	940	935
Iterations	ADMM	41	26	51	64	38

Some details of the solutions are illustrated by Figure 3.31-Figure 3.39 obtained by using the centralized approach. For Case I, Figure 3.31 shows the energy prices of the prosumers and the biogas-powered producers when selling energy in the community (excluding transactions with the external provider); Figure 3.32 also shows marginal cost for the Biogas unit and the energy price when buying and selling energy to the external grid. The total power flow exchanged with the external grid (assumed positive if it is consumed by the community) and the power output of the biogas unit are shown in Figure 3.32.

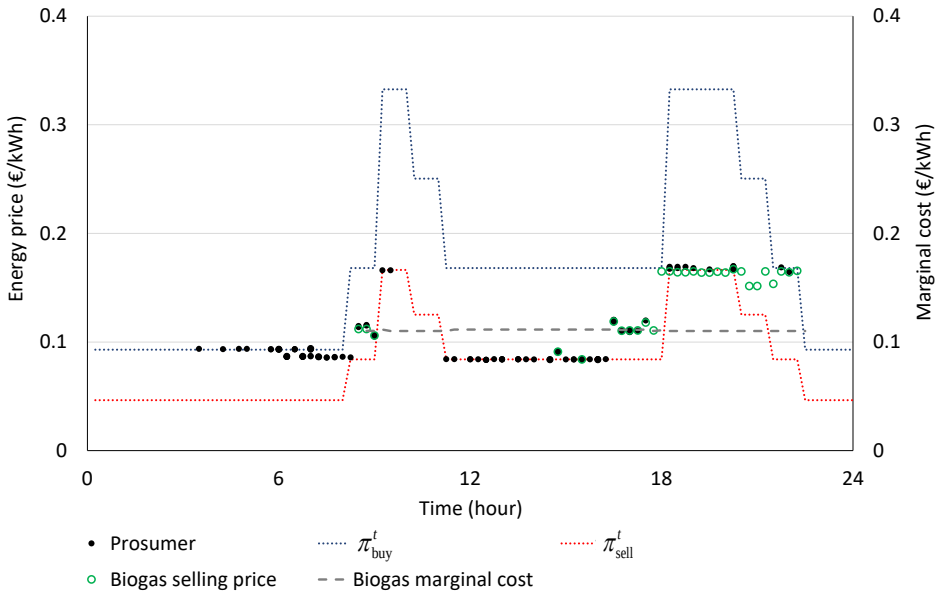

Figure 3.31 Energy prices in the community and marginal cost for the biogas unit in Case I.

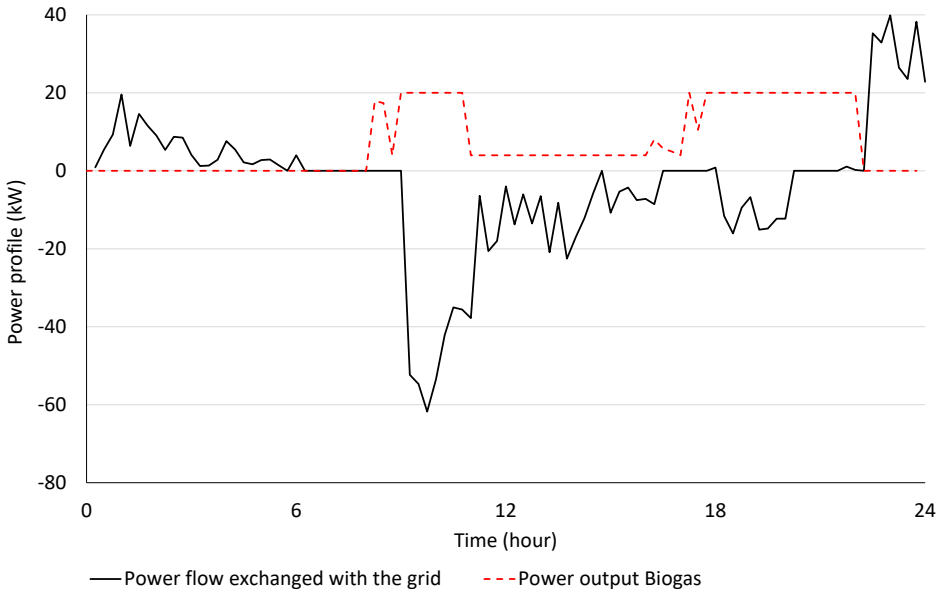

Figure 3.32 Total power flow exchanged by the community with the external grid (positive if consumed by the community) and power output of the biogas unit in Case I.

From Figure 3.31 and Figure 3.32, we can see that the prices of the energy in the community (i.e., associated with transactions between participants) are, in general, aligned with the marginal cost of the biogas unit for those moments when the REC does not exchange energy with the utility grid.

At the end of the day (around 9 pm and 10 pm), the prices in the community are higher than the marginal cost of the biogas unit, even during the period without exchange of energy with the external grid. In this period, energy production from the biogas-powered generator, as well as charging and discharging processes in the prosumers BES units, occurs simultaneously.

This effect on the prices is reasonably related to the activity of the BES units that, at the end of the day, are constrained to reach the same energy level as at the beginning of the day. To see such an effect of the BES units' operation on the prices, Figure 3.33 and Figure 3.34 show the corresponding results for Case II (without any BES unit).

In Figure 3.33, for the scenario without BES units, the prices of the energy transactions in the community are aligned; to π^t_{buy} if the community globally imports energy, to π^t_{sell} if the community is globally exporting energy and to the biogas marginal price if there are not energy exchanges with the external grid while the biogas unit is operating.

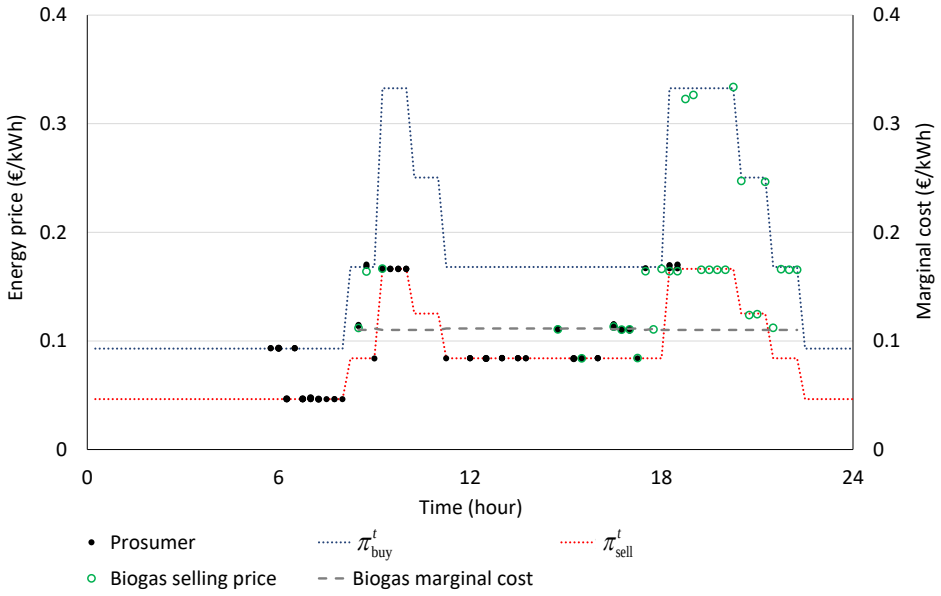

Figure 3.33 Energy prices in the community and marginal cost for the biogas unit in Case II.

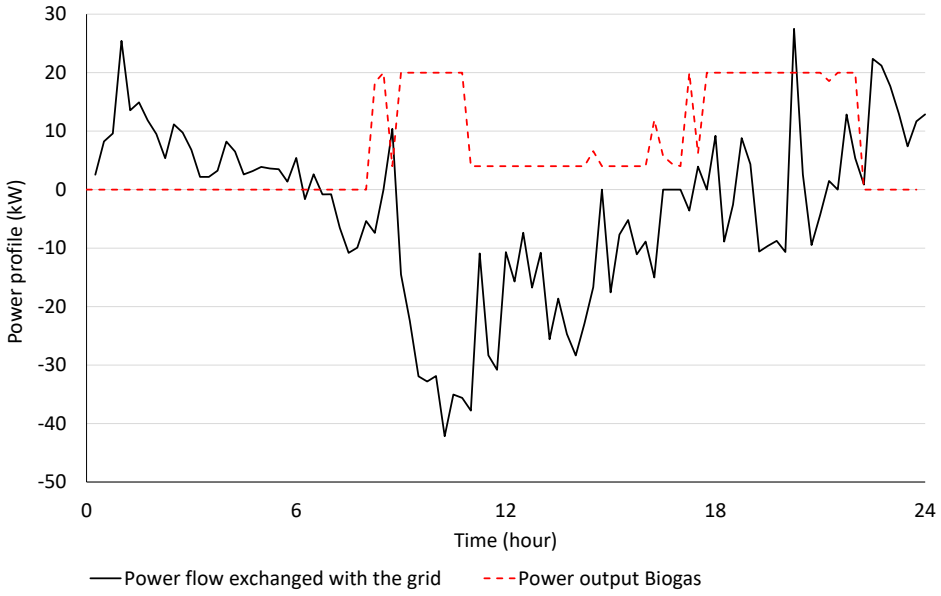

Figure 3.34 Total power flow exchanged by the community with the external grid (positive if consumed by the community) and power output of the biogas unit in Case II.

Now, let us consider the effect of $C^{\max\,\mathrm{day}}_{\mathrm{fuel}\,i}$ on the scheduling solution of the community. Figure 3.35 shows the daily profile of the fuel consumed for both Case I and Case III. When the daily fuel availability is large enough (Case I), the biogas power plant is in operation almost all day, being at minimum power during the midday hours. On the other hand, if the total fuel consumption is limited to a lower value (Case III), the biogas power plant is used for a shorter time period, concentrated, in this case, in the evening; hence, aligning the operation of the generator with a convenient period of the day in order to reduce the total procurement costs.

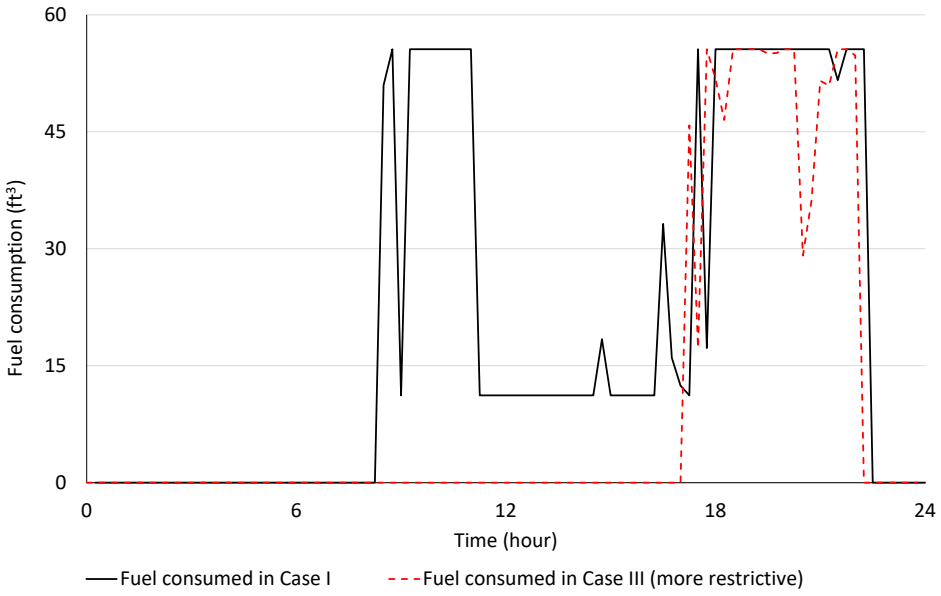

Figure 3.35 Daily profile of the fuel consumed by the Biogas unit in Case I with $C_{\text{fuel}\,i}^{\max\,\text{day}}$ =3300 ft^3 (black line) and Case III with $C_{\text{fuel}\,i}^{\max\,\text{day}}$ =1000 ft^3 (red dashed line).

In Case IV and V, with two biogas units, with equal and different gas costs, respectively, the selling prices of both biogas units are aligned with a common value. The corresponding prices for Case IV are illustrated in Figure 3.36, and in Figure 3.37 for Case V.

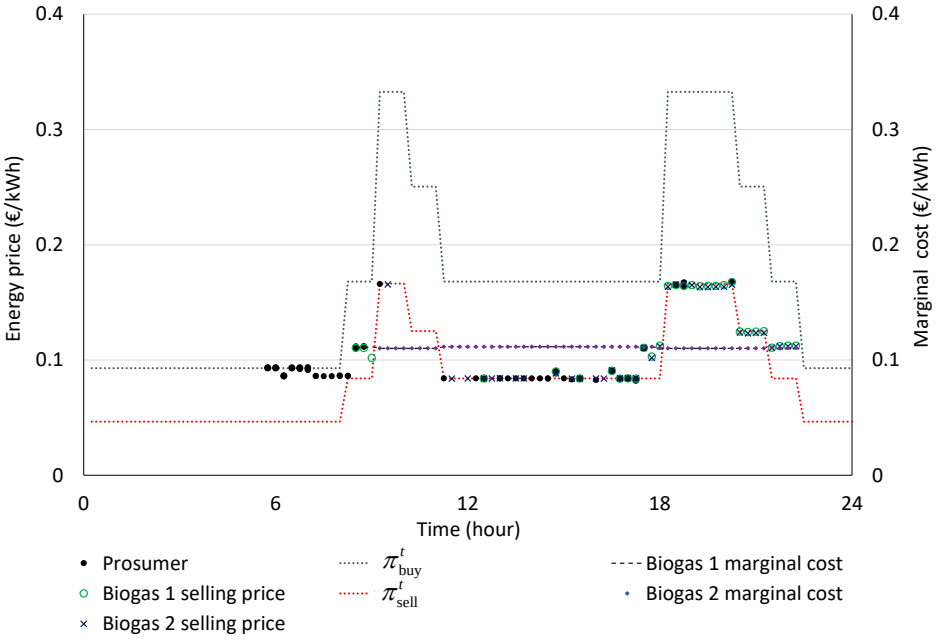

Figure 3.36 Energy prices in the community and marginal cost for the biogas units in Case IV.

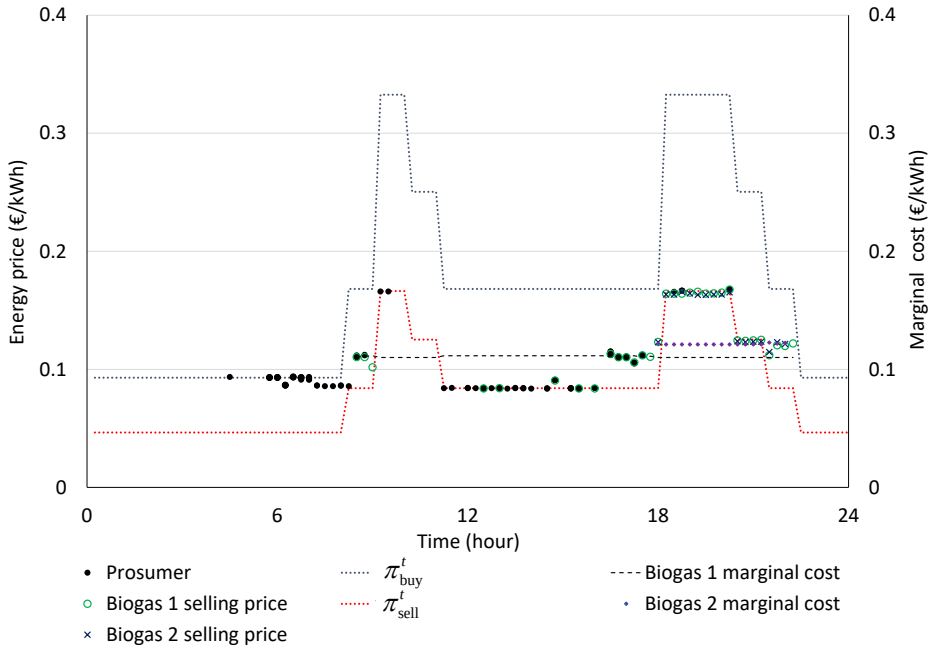

Figure 3.37 Energy prices in the community and marginal cost for the Biogas units in Case V.

Figure 3.38 shows the daily profile of fuel consumed by the two dispatchable units in Case IV, in which the same gas cost has been assumed for both generators, while Figure 3.39 shows the fuel consumption profiles for the biogas units in Case V (assuming different gas costs).

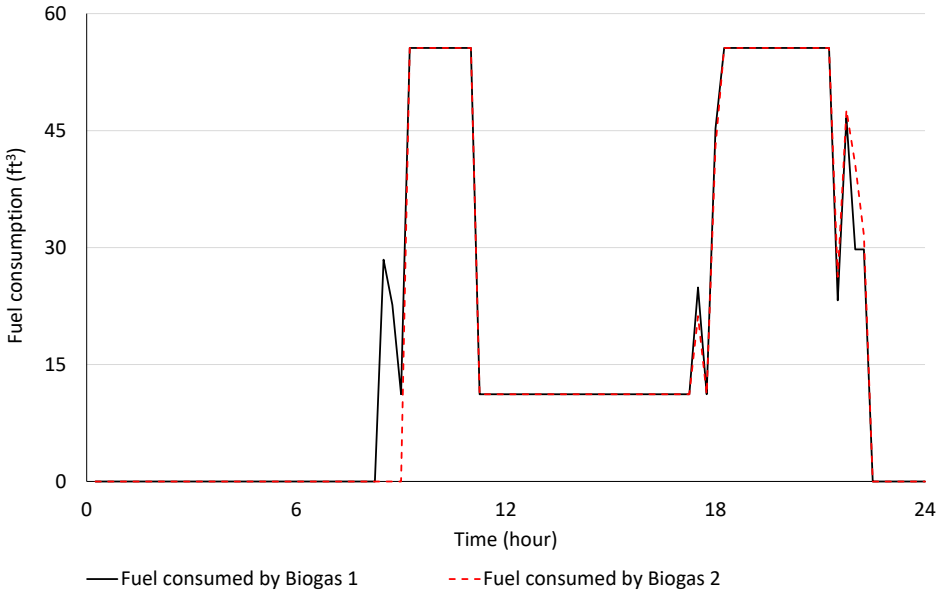

Figure 3.38 Daily profile of the fuel consumed by the biogas units in Case IV: Biogas 1 (black line) and Biogas 2 (red dashed line), both with the same $C_{\text{gas}\,i}$ = 9.97 €/mcf.

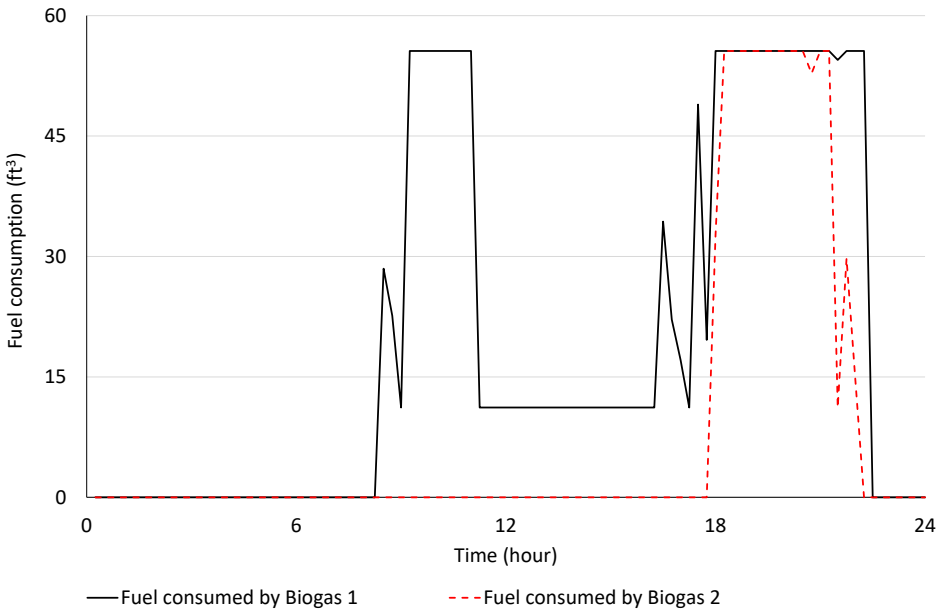

Figure 3.39 Daily profile of the fuel consumed by the biogas units in Case V: Biogas 1 with $C_{\text{gas}\,i}$ = 9.97 €/mcf (black line) and Biogas 2 with $C_{\text{gas}\,i}$ = 10.97 €/mcf (red dashed line).

The comparison between Figure 3.38 and Figure 3.39 shows that the higher cost for the Biogas unit 2 in Case V limits its use to a shorter time period than the one defined for the Biogas unit 1. Consequently, in that case, the operation of Biogas 2 is limited to a period between 6 pm and 10 pm, in which the conditions seem to be the most convenient to reduce the procurement cost, as previously discussed.

3.5 Conclusions of the chapter

This chapter has been focused on the study of the day-ahead scheduling of resources in renewable energy communities.

The grid-connected community considered in this study is characterized as being local and cooperative; that is, the participants in the community have agreed to cooperate in order to share their energy resources with the common goal of minimizing the total energy procurement costs. The participants in this REC might be equipped with generating units, ESSs and local loads.

To define a solution for this scheduling problem, which is consistent with the billing scheme and the metering units of the community, a centralized approach and then a distributed approach, based on the ADMM algorithm, have been formulated.

As already mentioned, the objective function for both approaches seeks the minimization of the energy procurement cost during the day. However, compared to a centralized approach, the distributed one, like ADMM, has been oriented to better preserve the privacy and decisional independency of the participants in the community. In fact, the information that each participant must communicate with the community is limited to those actions/decisions that compromise the other members, such as the intended transactions of energy with the other members.

For the base case included in this chapter, the results obtained by using the proposed distributed optimization have been compared with those from a centralized approach based on an MILP model.

As a result, both the centralized approach and the distributed one provide comparable results with an acceptable computational effort. Moreover, we found in detail that each prosumer in the community was able to make the cost optimal decisions, regarding optimal moments to charge and discharge the batteries, the energy transactions with other prosumers, and the exchange of energy with the external grid, leading to a match between the objective function values of both approaches.

The centralized approach couples the exchanges of energy between the members of the REC, assuring the balance between such transactions (from the point of view of the seller and the buyer); hence, the prices of the energy transactions between participants correspond to the Lagrangian multiplier of the constraint, which couples every transaction between members, obtaining a common value for everyone at each time period.

On the other hand, in the distributed procedure, the prices are updated at each iteration to reduce the mismatch between the energy sold by each participant *i* and the energy bought by the other members that bought from *i*; notwithstanding the difference with the centralized scheme, the profiles of the prices are similar.

In a detailed analysis of the procurement cost for each member of the community, we have confirmed that by means of both centralized and ADMM optimizations, it is possible to guarantee an economic benefit (increasing revenues or reducing costs according to the characteristics of the participant) for each prosumer that joins the community with respect to the case in which the individuals can exchange energy only with the external provider.

A further analysis of the scalability shows that the proposed day-ahead ADMM procedure can be applied to realistic configurations with a large number of prosumers, without compromising

the overall performance and keeping an acceptable computational effort over the corresponding situation in a centralized approach.

Moreover, in the second section of the chapter, the community picture has been extended to a REC that integrates dispatchable units, specifically biogas-powered units.

The obtained results for the considered cases confirm that the proposed formulation is suitable to adopt either a centralized or a distributed approach with similar results.

Several case studies have been considered, and the results obtained by using the proposed model formulation show that the adoption of a biogas power plant can ensure high percentages of self-consumption. Moreover, if the biogas production is somehow restricted, the optimization model schedules the biogas power plant operation according to the most convenient time period of the day.

Finally, we have seen that the introduction of a biogas power plant in the community modifies the prices of the internal energy transactions between prosumers, which, in this case, can also be aligned with the marginal cost of the biogas units.

Chapter 4. Uncertainties and Intra-Day Operation of the Renewable Energy Community

Introduction

"Adaptative operation and flexibility in front of future events"

Since the forecasts for generation from RE and energy demand are affected by significant uncertainties, the scheduling approaches of RECs are getting more oriented each time to consider such uncertainties in order to exploit the energy resources in the community in the most cost-effective and technically feasible way.

As already mentioned in a previous chapter, stochastic optimization approaches are widely used for day-ahead scheduling of electrical systems (e.g.,(Bhattacharya, Kharoufeh, and Zeng 2018) and (S. Wang et al. 2019)). In (Orozco et al. 2020), we studied the adoption of a day-ahead multistage stochastic approach for the scheduling of a small community. In this approach, the solution of the stochastic problem is employed to make decisions during day (e.g., at the end of each stage), updating the scheduling according to an intra-day procedure that finds the best fit between the actual PV and load profile and the scenarios considered in the day-ahead procedure.

To deal with the impact that uncertainties and fluctuations have on the performance of the EMS of electrical systems, and specifically of energy communities, several studies in the literature have been focused on the integration of day-ahead and intra-day scheduling approaches.

The best integration of day-ahead and intra-day scheduling of energy systems is achieved by hierarchical and online control approaches able to respond to the variations in the operational conditions as dealt with in, e.g., (De Filippo 2020) and references therein. For instance, (Fan, Ai, and Piao 2018) presents a hierarchical EMS for a microgrid, including energy storage and demand response applications, which considers a multi-time scale link between the day-ahead scheduling and the intra-day operation. In (Bao et al. 2015a) and (Bao et al. 2015b), the day-ahead scheduling model of a multi-

energy microgrid considers the uncertainty of RE generation, while a real-time dispatching model is employed to smooth out the fluctuations of generation and demand during the day. Moreover, in (Shi et al. 2017) an online EMS employs a stochastic model to solve the optimal power flow of an MG.

In (Crespo-Vazquez et al. 2020), clearing decisions for an energy community are made day-ahead by an ADMM-based two-stage approach in order to consider uncertainties in the model. Subsequently, a real time model, which has been assumed deterministic, is employed by each agent (i.e., participant in the community) to make new decisions, while keeping day-ahead commitments in the REC.

Furthermore, model predictive control (MPC) (see e.g., (Scattolini 2009)) techniques have been proposed to coordinate, in real time, the response of controllable resources of multi networked microgrids (e.g., Parisio et al. 2017).

This chapter focuses on the study of a coordinated day-ahead and intra-day multistage stochastic strategy to deal with the distributed optimal scheduling of a community.

In this case, the day-ahead scheduling of the community is defined by means of a multistage stochastic optimization. To achieve this, the uncertainties associated with the PV generation and energy consumption are represented by a scenario tree that combines the scenarios of all the participants in the REC. Next, the intra-day decision-making procedure is implemented as a recursive receding horizon optimization in order to mitigate the effect of the fluctuations in energy generation and demand.

This framework is suitable for the implementation in the automatic EMS of a REC and is characterized by some original aspects with respect to those already presented in the literature, since it allows a close coordination between day-ahead and intra-day scheduling, the use of the distributed approach in all the phases of the optimization procedure, and the definition of the fair prices of the internal transactions.

In the first part of this chapter, we present the implemented procedure for generating the corresponding scenario tree and the solution of the day-ahead multistage stochastic problem. Subsequently, the decision-making procedure, employed to adjust the operation of the REC during the day, is introduced. Finally, the performance of the coordinated approach is analysed by using a base case of prosumers in a LV network and a second case, in which a transactive scheme in an MV network has been adopted.

4.1 Day-ahead multistage approach to consider the uncertainties

In this chapter, we propose to extend the distributed scheduling approach to a coordinated day-ahead and intra-day strategy to deal with the scheduling problem of the REC considering uncertainties.

The scheme proposed has been illustrated in Figure 4.1, in which the solutions provided by the day-ahead multistage model are used as an operational framework for the intra-day decision-making procedure, which is carried out by the REC at each time *t* during the day (divided into stages).

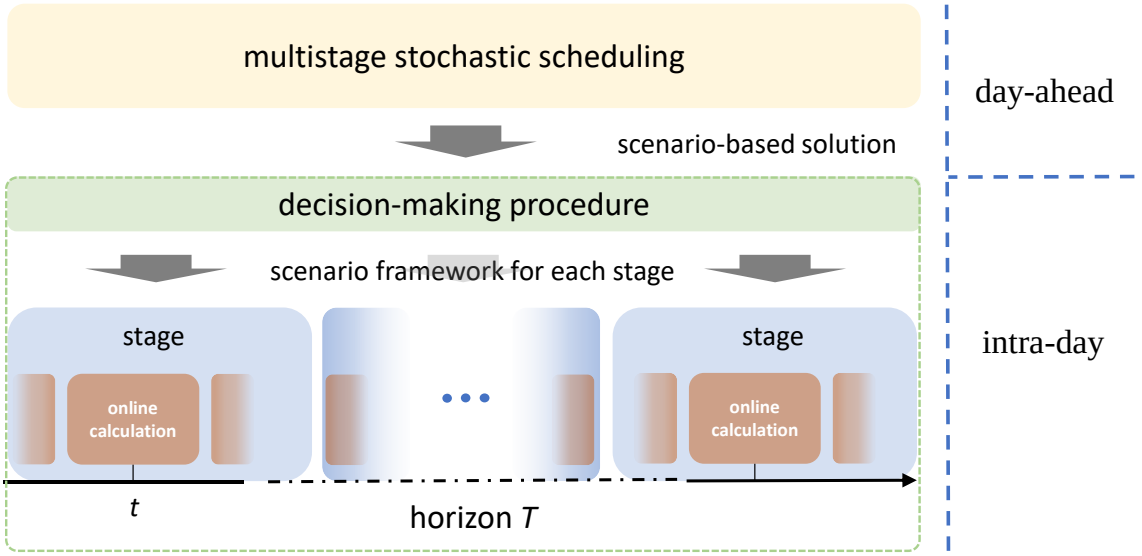

Figure 4.1 Scheme for the scheduling of the REC, employing a coordinated day-ahead and intra-day strategy.

To achieve this, first, we adopted a day-ahead scenario-based approach to determine a set of possible solutions (i.e., scheduling plans), which flexibly respond to the current operation of the community; therefore, the ADMM community model has been extended to a multistage stochastic model.

The second chapter, specifically section 2.1.3, introduced the concept of multistage stochastic optimization to deal with the uncertainties in a scheduling problem limited to a single LES equipped with a PV-Battery system. By applying the proposed multistage scheme, the LES can adjust the set values of the battery at the end of each stage during the day, choosing the most convenient option from a set of day-ahead calculated solutions.

Following the scheme presented in (Orozco et al. 2020), we can extend the ADMM scheduling of the REC, proposed in section 3.2, to take into account the uncertainties associated with the

day-ahead forecasts of the PV generation and loads consumption, adopting a multistage stochastic scheme.

Let us consider, in this section, four stages to represent the realization of the stochastic processes. In this scheme, the day-ahead multistage solution provides the corresponding set values of decision variables at the beginning of the day and, subsequently, every eight hours. In this case, the power output of the BES units in the community (i.e., $P^{t}_{\mathrm{ch}\,i}$ and $P^{t}_{\mathrm{dis}\,i}$) are assumed as the decision variables of the model; the other variables are calculated at the end of each stage for all time intervals in the stage.

As we already know, the multistage stochastic optimization needs a scenario tree, which represents the realization of the considered stochastic processes during the day (i.e., PV generation and energy consumption). In this approach, the scenario tree for the entire REC will be obtained by using a structure that considers the individual situation of each participant.

In the following, we present the procedure adopted to generate a set of initial scenarios for each prosumer *i*. Next, the routine implemented to obtain a common scenario tree for the entire community is described.

4.1.1 Scenario generation for each participant

We adopt a scenario generation technique that applies a Markov-process considering the autocorrelation between consecutive observations starting with the forecast $P^{t}_{\mathrm{PV}\,i}$ and $P^{t}_{\mathrm{Load}\,i}$ (i.e., PV generation and load, respectively), as described in (Orozco et al. 2018) and used in the case of a single LES in Chapter 2.

To achieve this, let us define a set of scenarios for each prosumer *i* denoted with Φ_i. Index φ_i denotes the scenario index corresponding to prosumer *i*. A maximum deviation has been defined so that the obtained scenario does not exceed the ±20% band with respect to both P^{t}_{Load} (for all the 24 hours) and to P^{t}_{PV} (for 75% of the periods). As we already know (from 2.1.3), the definition of these limits avoids unrealistic scenarios and guarantees that the scenarios are coherent with the day-ahead forecast profiles.

We have considered the base case of a REC composed of 10 prosumers organized in two internal feeders (i.e., five prosumers in each feeder) and connected to the same LV feeder, as the one considered e.g., in Figure 3.1.

In this case, for each one of those prosumers, equipped with a PV unit and a local load, a set of 200 scenarios has been obtained (i.e., |Φ|=200). For illustrative purposes, in the results reported for the base case (section 4.3.1), an example of the initial set of scenarios of the PV generation and load for one of the prosumers in the REC has been included (seen Figure 4.4).

From this initial set of scenarios, we denote a scenario $\xi_{\varphi_i}^t$ of prosumer *i* as the normalized difference between PV production and load for prosumer *i*, for each period *t*, namely

$$\xi_{\varphi_i}^t = \frac{P_{\text{PV}\,\varphi_i}^t - P_{\text{Load}\,\varphi_i}^t}{P_{\text{PV}\,i}^t - P_{\text{Load}\,i}^t} \tag{4.1}$$

4.1.2 Construction of the common scenario tree for the community

Since we want to achieve a coordinated response to the uncertainties in the community, a procedure that considers the stochastic information of each prosumer in a common tree has been defined.

In (Orozco et al. 2020), a routine that merges the individual scenario tree of each participant by means of a combinatorial definition of possible scenarios has been presented. However, the computational effort limits the number of stages and size of the community (i.e., the number of participants).

In this chapter, we consider that the prosumers are able to share their initial set of scenarios $\xi_{\varphi_i}^t$ with the community without comprising private information. Since $\xi_{\varphi_i}^t$ is given by (4.1), neither the value of the PV generation nor the energy demand will be directly readable.

In order to deal with the problem of scalability and computational effort, an *N*-dimensional (with *N* equal to the number of prosumers) set Γ of scenarios is conformed to generate a tree by means of a *k*-means clustering procedure. Each one of these scenarios is defined by the structure

$$\psi_{\varphi}^t = \left[\xi_{\varphi_1}^t, \xi_{\varphi_2}^t, ..., \xi_{\varphi_N}^t\right] \tag{4.2}$$

In the base case considered, *N*=10 and index φ has a value between 1 and 200.

With the introduction of this structure, the community can coordinate a response to the uncertainties associated to the operational conditions, while preserving the distributed nature of the scheduling approach.

Ultimately, the scenario tree for the community is obtained by a clustering procedure based on the *k*-means algorithm, like the one introduced in section 2.1.3, and applied to the total set of initial scenarios Γ.

The *k*-means clustering might be carried out by a coordinator unit and then communicated within the REC, or by each one of the prosumers, locally, obtaining a common scenario tree for all the participants.

The so-called elbow method and silhouette coefficient are direct methods used to determine the number of centroids (e.g., (Yuan and Yang 2019) and references therein). The first one looks for a reduction in the average distance of the aggregated data to the relevant centroid (i.e., the average value of sum of the squared errors *SSE* calculated for each scenario), and the second one reflects the relationship between the mean intra-cluster distance (i.e., distance from a sample to the other samples in the cluster) and the mean nearest-cluster distance (i.e., distance from a sample to all the samples in the nearest-cluster) of each sample.

The silhouette coefficient for each scenario ψ_φ is given by

$$s(\psi_\varphi) = \frac{b(\psi_\varphi) - a(\psi_\varphi)}{\max\left(a(\psi_\varphi), b(\psi_\varphi)\right)} \tag{4.3}$$

where $a\left(\psi_\varphi\right)$ is the mean intra-cluster and $b\left(\psi_\varphi\right)$ the mean nearest-cluster distance of each scenario. The average value of $s\left(\psi_\varphi\right)$ shows how well the scenarios have been classified. A high coefficient value is desired in order to reduce the intra-cluster dissimilarities (i.e., good cohesion) and to increase the inter-cluster dissimilarities (i.e., avoiding the presence of outliers).

Table 4.1 shows the values obtained for the average *SSE* and the average of the silhouette coefficient for the first eight hours of the day and for several number of clusters in the base case.

Table 4.1 Elbow method and silhouette coefficient for the selection of the number of centroids: Base case.

Number of centroids	3	4	5	6	7	8	9
Average *SSE*	98.91	79.14	72.15	63.95	52.54	47.10	40.41
Average $s\left(\psi_\varphi\right)$	0.54	0.53	0.52	0.50	0.53	0.50	0.51

The goal is to reduce the average distance reported by the elbow method, employing a reasonable number of centroids, and increasing the accuracy (i.e., silhouette coefficient).

However, when considering the silhouette coefficient, we can see that the accuracy of the aggregation could be undermined by a higher number of centroids, depending on the considered application. As a result, the number of centroids is influenced by the data structure (i.e., complexity and structure of the samples) and the search for reasonable solution time and computational effort. The numerical results presented in this chapter for the base case, have been obtained assuming three centroids for the *k*-means procedure. Figure 4.2 shows the scenario tree obtained by the community in the base case (starting from 200 initial scenarios).

4.1.3 Multistage stochastic solution

The solution from the scenario-based multistage scheduling provides the optimal set values of the decision variables in each node of the scenario tree.

To achieve this, an ADMM procedure, like the one introduced in section 3.2, is employed to solve the scheduling problem for each one of the final scenarios in the tree, where the values of $P^t_{\mathrm{PV}\,i}$ and $P^t_{\mathrm{Load}\,i}$ are given by the corresponding scenario in the tree ψ_φ. A tolerance ε equal to 25 W has been assumed for the day-ahead ADMM calculations of the base case, and Δt equal to 0.25 h.

In the referred ADMM procedure, the local subproblem (3.17) is solved by *i* considering set of constraints (3.3)-(3.11) and (3.14)-(3.16). The charging and discharging efficiencies limit the advantage of a simultaneous occurrence of these processes in the batteries. In this chapter, we have modified the set of constraints, excluding indicator constraint (3.9), and the binary variable associated with the operation of the BES unit $u^t_{\mathrm{BES}\,i}$. Leading to a reduction in the number of binary variables of the model, this modification has been especially oriented to speed up the solution time of the coordinated solution that also includes an online calculation.

However, at some iteration, the optimization of *i* could eventually provide a solution that charges and discharges the battery at the same time period *t*, allocating some excess of energy without generating losses associated with transactions. When this occurs, the binary variable $u^t_{\mathrm{BES}\,i}$ is activated, and the local optimization of *i* is repeated including constraint (3.9).

Once the situation has been corrected, the iterative process continues without $u^t_{\mathrm{BES}\,i}$ and (3.9). Based on the numerical tests in this chapter, this correction occurs in less than 0.1% of the total number of local optimizations performed in the implemented ADMM algorithm. Additionally, the *OF* value of the relevant prosumer is slightly corrected in the process.

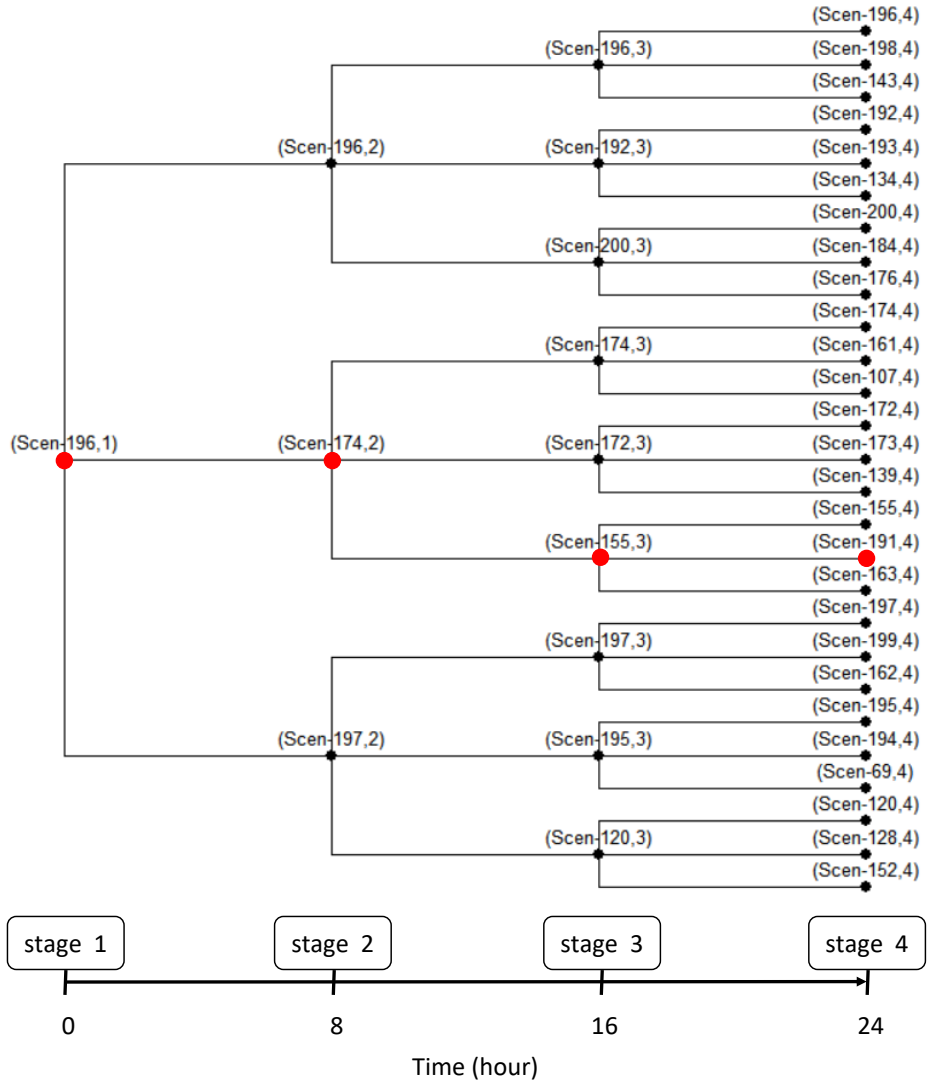

Figure 4.2 Scenario tree for the community using three centroids. In red, an example of the corresponding decision given by the intra-day decision-making procedure at the beginning of the day, and, subsequently, at the end of each stage.

In addition, as we know, a feasible multistage stochastic solution requires the implementation of non-anticipativity constraints, to assure the coherence of the stochastic variables during the day, in scenarios with common nodes in the tree. In other words, for those scenarios in the tree that share common nodes in their path from the root to the leaf, the non-anticipativity constraints, bind their decision variables to be equal at every common node (i.e., values regarding $P^t_{\mathrm{ch}i}$ and $P^t_{\mathrm{dis}i}$ for the relevant stage).

4.2 Intra-day decision-making procedure including online optimization

Until now, the implementation of a multistage decision-making procedure allows the community to more flexibly respond to the fluctuations of the PV generation and the load

throughout the day. However, for practical considerations, the definition of a finite number of stages, and the corresponding number of periods aggregated in each one of them, limits the system to more accurately follow the intra-day optimal solution considering significant deviations in a higher time resolution.

Therefore, in the proposed coordinated approach, the scenario-based solution of the day-ahead scheduling is employed to provide a framework for the intra-day operation. Next, it is exploited by using an intra-day decision making-procedure at every time period *t*, which coordinates the multistage solution with an online calculation that adjusts the operational set values also inside the stages

In general, while the decision-making procedure introduced for a LES in section 2.1.4 aims at identifying the most suitable decision at the beginning of each stage with the corresponding set values for all the periods in the stage, in this section, the decision-making occurs at every time period (i.e., every 15 minutes), adjusting the set values in the REC, based on the considered time step Δt.

By means of the Euclidean distance, the intra-day decision-making procedure is able to identify, using the common tree of the community, the scenario that best matches up to time *t*, the profile of the difference between the local generation and the energy demand from the previous observations (i.e., measurements of PV generation and energy demand). Each prosumer performs its own comparison of the local profiles and shares the corresponding distance with the others in order to make a joint decision based on the structure of the common scenario tree.

In Figure 4.2, the red dots represent an example of the decisions provided by the intra-day decision-making procedure at the end of each stage.

Since there is a common root node, the starting decision (without any previous knowledge of events) implies only one possible state of charge for the BES units at the end of the first eight hours, which depends on each prosumer. From the tree in Figure 4.2, at the beginning of the day, the REC considers, for the first eight hours, the operational framework associated with the node referred to Scen-196.

Then, based on what occurred during the first eight hours, the community updates the operational framework, in a coordinated way, to the solution of the most similar and, in a certain way, expected scenario for the following eight hours (i.e., Scen-174 in the example).

Afterward, in the example, a decision updates the operational framework again for the last eight hours, choosing the node referred to Scen-155.

Once the community has identified the corresponding operational framework from the tree, the online calculation is carried out at each time period in the relevant stage in order to adjust the set values for the operation of the REC (i.e., the power output of the BES units and the energy transactions between prosumers).

4.2.1 Online calculation: implementation and characteristics

Figure 4.3 illustrates the time scheme adopted to deal with the scheduling problem at each one of the stages.

- At first, as already described, the decision-making procedure defines the corresponding operational scenario for the stage in a coordinated action for all the prosumers. The procedure provides the expected profiles of $P^{t}_{\text{PV}\,i}$ and $P^{t}_{\text{Load}\,i}$ for the stage and the corresponding set values for the BES units, based on the day-ahead multistage solution.
- Next, the online calculation is carried out at each time period t_m by using the available measure of the energy generation and load.

  Adopting an online calculation, like receding horizon control or MPC strategies, a distributed optimization, with horizon time from the current t_m until the last period in T^s, is carried out by the REC.
- Finally, the resulting values for the first corresponding Δt are implemented. The calculation is repeated at each period until the end of the stage.

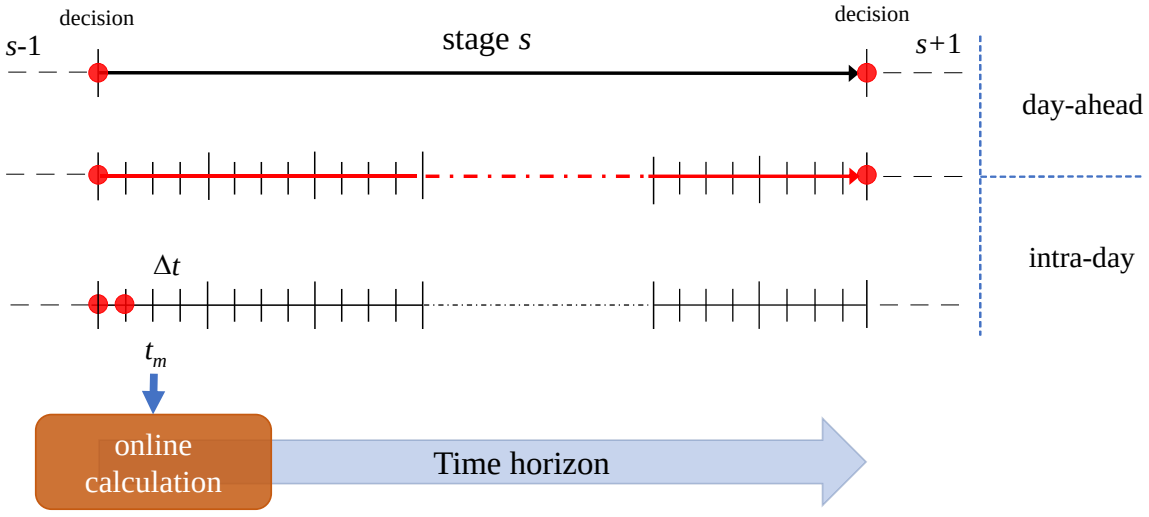

Figure 4.3 Scheme for the coordinated scheduling of the REC at each stage.

The online optimization of the REC employs a distributed procedure based on the ADMM model, like the one employed by the multistage solution, and described in detail in section 3.2, adding the following characteristics:

A. Implementation of a parallel scheme

To obtain a low time calculation in comparison with the duration of each Δt, a parallel scheme of the consensus algorithm ADMM has been adopted. In the online calculation, (3.18) is replaced by (4.4).

$$\ell_i^t = m \cdot \rho \cdot [\sum_{\substack{j \in \Omega \\ j \neq i}} (\overline{P}_{\text{exc}\, j,i}^{\,t} - P_{\text{sell}\, i,j}^{t})^2 + \sum_{\substack{j \in \Omega \\ j \neq i}} (P_{\text{buy}\, i,j}^{t} - \overline{P}_{\text{exc}\, i,j}^{\,t})^2] \tag{4.4}$$

where

$$\overline{P}_{\text{exc}\, i,j}^{\,t} = \frac{1}{2}(\hat{P}_{\text{buy}\, i,j}^{t} + \hat{P}_{\text{sell}\, j,i}^{t}) \tag{4.5}$$

B. SoE at the end of each stage as an operational condition

The SoE of the BES units at the end of the current stage (i.e., at the end of the optimization horizon of the online calculation) are fixed according to the result of the decision (i.e., chosen scenario) at the end of the previous stage. This allows us to reduce the number of variables (i.e., the associated computational effort), while keeping a good performance of the *OF*. For this purpose, (3.8) is replaced by (4.6) in the intra-day implementation.

$$\begin{cases} E_{\text{BES}\, i}^{t=t_1^s} = E_{\text{BES}\, i}^{\text{initial}^s} + (P_{\text{ch}\, i}^{t=t_1^s}\ \eta_{\text{ch}\, i} - P_{\text{dis}\, i}^{t=t_1^s} / \eta_{\text{dis}\, i})\Delta t \\ E_{\text{BES}\, i}^{t=t_{\text{end}}^s} = E_{\text{BES}\, i}^{\text{final}^s} \end{cases} \tag{4.6}$$

where t_1^s corresponds to the first time period of stage *s*; t_{end}^s represents the last period of stage *s*; $E_{\text{BES}\, i}^{\text{initial}^s}$ and $E_{\text{BES}\, i}^{\text{final}^s}$ represent the initial and final SoE of BES unit *i* in stage *s*, respectively.

C. Intra-stage update of the expected profiles of $P_{\text{PV}\, i}^t$ and $P_{\text{Load}\, i}^t$

Each local subproblem (3.17) at period t_m employs the predicted profile of power generation and load for the remaining time in the stage (i.e., $\forall t \in T^s$ such that $t > t_m$) together with the current measurements to define the optimal set values.

The scheme could be adapted to consider a new forecast profile, if any is available during the day, as an input of the online optimization; otherwise, the available stochastic information of

the scenario tree is used. In that case, the expected profiles $P^t_{\mathrm{PV}\,i}$ and $P^t_{\mathrm{Load}\,i}$ are chosen from those associated with the possible scenarios (i.e., branches in the stage) that follow the last decision node in the tree. The selection of the scenario at each period results from the decision-making (e.g., based on the Euclidean distance) occurring inside the stage at each period.

D. Warm start for the online calculation

A warm-start scheme in the online ADMM (e.g., (Boyd et al. 2010)) is adopted to initialize λ_i^t. Instead of using a default initialization of the Lagrangian multipliers for all the periods t_m, the procedure uses the prices λ_i^t obtained by the day-ahead scenario-based solution. The same principle is applied to define initial values of $\hat{P}^t_{\mathrm{buy}\,i,j}$ and $\hat{P}^t_{\mathrm{sell}\,j,i}$ to obtain a starting value for $\overline{P}^t_{\mathrm{exc}i,j}$. The mentioned initialization at each t_m depends on the result of the intra-stage evaluation of the most suitable scenario of the tree, providing a good enough approximation to determine the initial values at the first iteration and resulting in fewer iterations.

As a result, considering the mentioned characteristics, each prosumer in the REC updates, in a coordinated, cost-effective way, at each period *t*, the scheduling of the BES unit, the exchange of energy with other prosumers and the corresponding transactions with the external provider.

4.3 Case studies and numerical results

The procedures have been implemented and tested in an AIMMS Developer environment and tested by using the solver Cplex V12.9. The numerical results have been obtained on a 2.60-GHz Intel Xeon two-processor computer with 64 GB of RAM, running 64-bit Windows 10. We have considered two different case studies.

4.3.1 Base case study: prosumers in the same LV network

As already mentioned, the base case study corresponds to a set of 10 prosumers distributed in two feeders connected to the same LV distribution network. The characteristics of these prosumers, regarding the area of the installed PV unit and size of the BES unit, are equal to those in section 3.1.2. and reported in Table 3.1 and Table 3.2, respectively. Furthermore, the profiles of the ratio between power output and the panel surface (assumed equal for all the PV units) and the prices of the energy bought from the utility grid π^t_{buy} correspond to those

illustrated in Figure 3.3 (for the numerical tests $\pi^t_{sell} = 0.5\pi^t_{\text{buy}}$). Figure 3.2 shows the corresponding load profile for each prosumer. The considered optimization horizon corresponds to one day, which is divided into 96 periods of 15 minutes each.

Figure 4.4 shows an example of the initial set of scenarios obtained by prosumer 1. From these profiles, the corresponding scenarios $\xi^t_{\varphi_1}$ have been defined, which, subsequently, have been communicated to the community, and have been employed together with the corresponding scenarios of the other prosumers in order to apply the *k*-means routine that constructs the scenario tree in Figure 4.2.

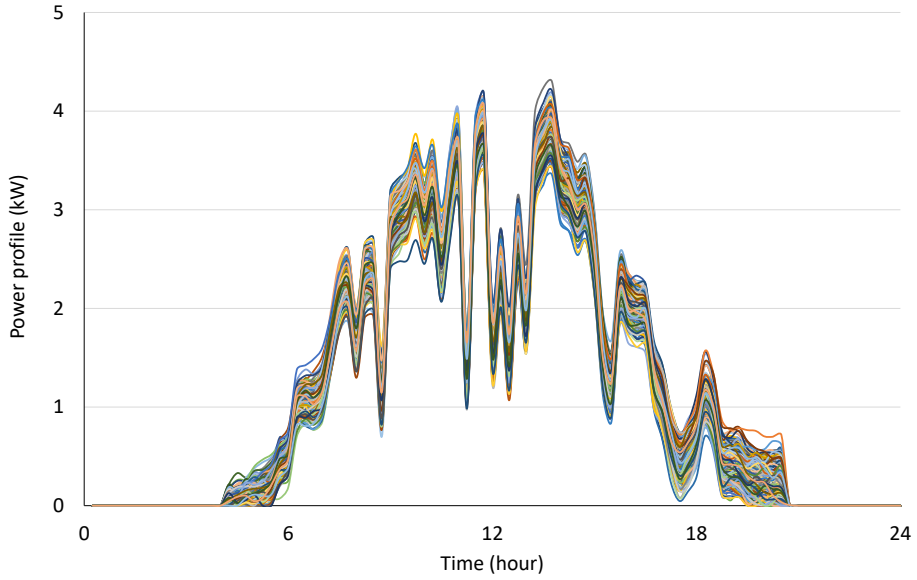

a)

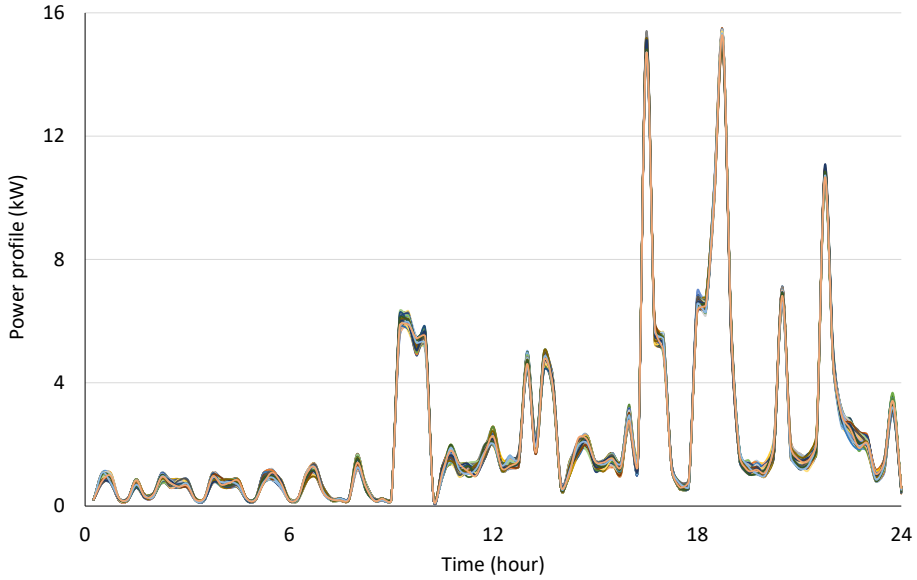

b)

Figure 4.4 Initial set of 200 scenarios obtained by prosumer 1: a) PV production; b) load.

To test the intra-day operation of the community, an MILP solver has also been implemented to perform the calculations, where the variables are fixed to a certain value. In that case, each prosumer implements the corresponding $P^t_{\text{ch}\,i}$, $P^t_{\text{dis}\,i}$, $P^t_{\text{sell}\,i,j}$ and $P^t_{\text{buy}\,i,j}$, and then solves the problem (3.17) with $\ell^t_i = 0$ and the corresponding set of constraints (3.3)-(3.13) for the operation of each prosumer and the community. The differences are compensated by the exchange of energy with the external utility grid ($P^t_{\text{buy\_Grid}\,i}$ and $P^t_{\text{sell\_Grid}\,i}$) in order to satisfy the local power balance given by (3.3).

As already introduced in Chapter 2, the value of stochastic solution (*VSS*) and the expected value of perfect information (*EVPI*) are typical performance metrics used to study the effectiveness of a stochastic solution. Table 4.2 shows the *VSS* and *EVPI* metrics calculated for the base case and the scenario tree in Figure 4.2.

Table 4.2 Stochastic metrics *VSS* and *EVPI* for the base case.

Solution	*OF* Value (€)	*VVS* (€)	*EVPI* (€)
EEV	17.07		
RP	16.55	0.52	0.09
WS	16.46		

The resulting *VSS* shows the potential advantage of using the multistage solution over the implementation of the day-ahead forecast-based solution (i.e., *EEV*). A small *EVPI* gives an idea of how close the implementation of the stochastic solution, and a solution assuming perfect forecast (e.g., *WS*), could be.

For each scenario of the tree in Figure 4.2, Figure 4.5 shows the comparison between the *OF* values calculated by using a decision-making procedure that defines the set values at the beginning of the stage for all the periods associated with that stage (i.e., based on the day-ahead multistage solution) and those given by the day-ahead scheduling that takes into account only the forecast profiles (forecast-based). As expected, the multistage scheduling provides better results with respect to a forecast-based solution. Figure 4.5 also shows the *OF* values of the solution of (3.17) assuming a perfect forecast.

Furthermore, Figure 4.5 includes the *OF* values of the operational situation in which the prosumers are only allowed to exchange energy with the external energy provider (i.e., energy

exchanges inside of the community are prohibited). As expected, the obtained costs confirm the advantage of exploiting the cost-optimization of the REC.

In order to test the *OF* performance of such a decision-making procedure, the values of the BES charges and discharges ($P^{t}_{\text{ch}\,i}$ and $P^{t}_{\text{dis}\,i}$) and the energy exchanges among the prosumers ($P^{t}_{\text{sell}\,i,j}$ and $P^{t}_{\text{buy}\,i,j}$) have been fixed to the resulting values of the procedure (i.e., set values associated with the most similar node of the scenario tree). Then, the MILP model has been employed to find the total *OF*.

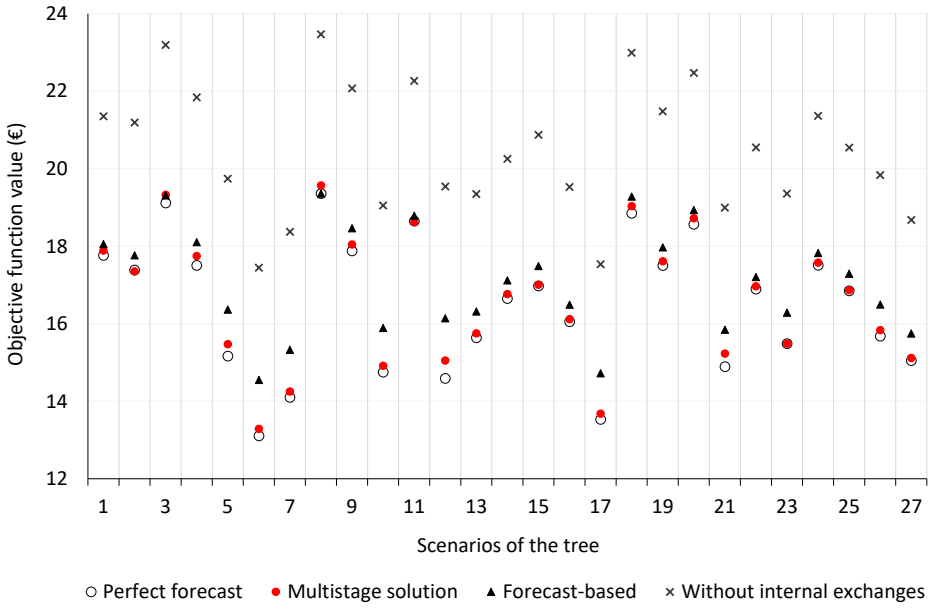

Figure 4.5 Comparison of the community's total *OF* values for each scenario of the tree: Base case.

To test the coordinated strategy proposed in this section, a set with 20 new intra-day scenarios (i.e., operational conditions during the day different from those included in the scenario tree) has been generated following the technique employed in section 2.1.3A (based on a Markov-process). These scenarios represent measurement values at each period for $P^{t}_{\text{PV}\,i}$ and $P^{t}_{\text{Load}\,i}$.

For this set of new scenarios, the implementation of the day-ahead ADMM scheduling described in section 3.2, and based only on the forecast profiles, is, on average, 4.25% higher than the deterministic *OF* (i.e., calculated assuming perfect forecast), while the implementation of a multistage solution based only on the day-ahead scenario-based solution and with decisions only at the end of each stage, gives, on average, an increase of 3.69% over the same deterministic solution.

In addition to the advantage of the multistage solution over the so-called forecast-based solution, the coordinated approach more accurately reacts to the fluctuations in each period during the day, and not only to the cumulative deviations in each stage. Figure 4.6 shows the total energy in the BES units of the community by implementing the solution of the decision making-procedure (based only on the day-ahead multistage solution), and then by adding the online calculation scheme (Figure 4.6a and Figure 4.6b, respectively) for each one of the 20 new scenarios. Figure 4.6 makes evident the advantage of adopting the coordinated strategy.

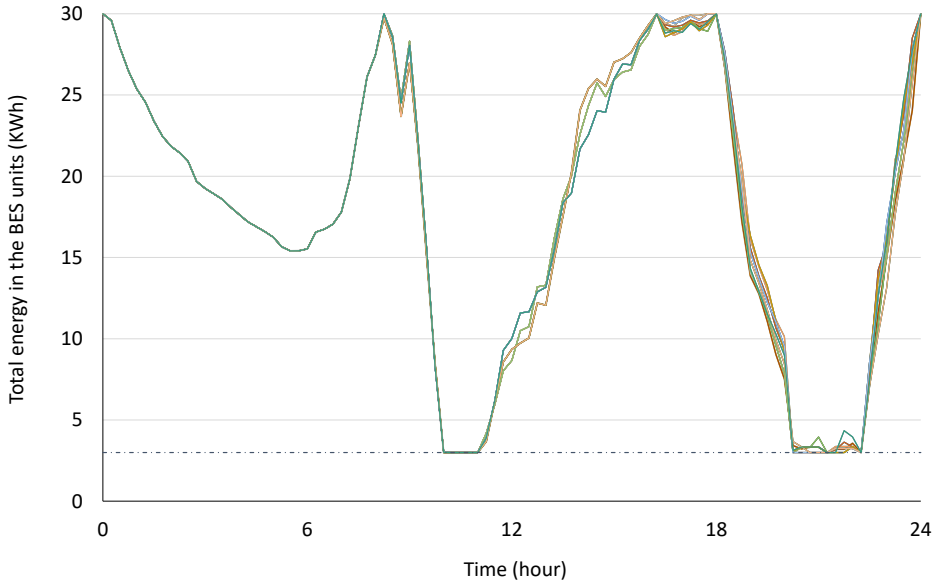

a)

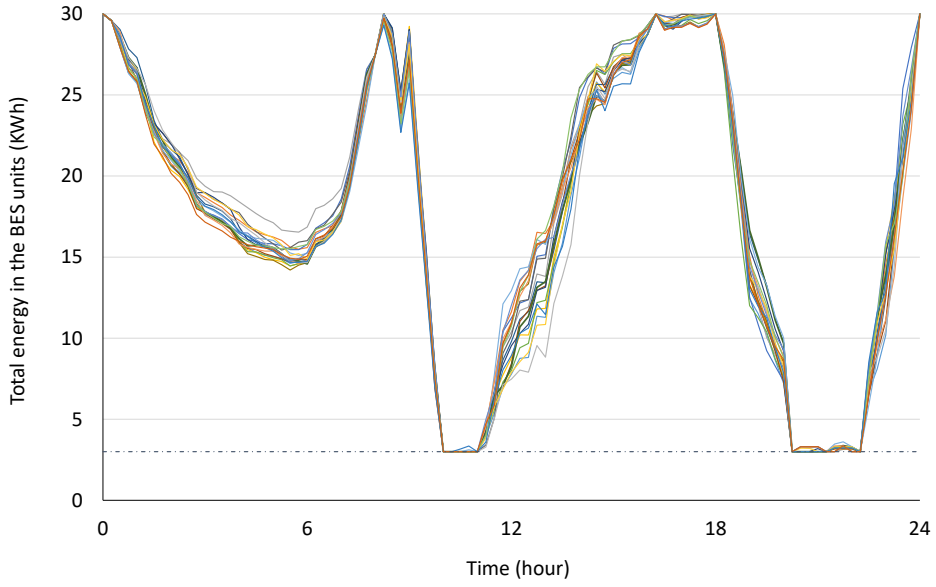

b)

Figure 4.6 Total energy stored in the community during the day for the base case: a) possible solutions according to the day-ahead scenario-based solution; b) profiles obtained using the coordinated strategy that includes online optimization.

Figure 4.6a shows that the decision making-procedure based only on the day-ahead multistage solution gives some flexibility for reacting to the fluctuations during the day, but it is limited by the structure of the scenario tree, whilst Figure 4.6b shows that the online calculation is able to react more flexibly at each perturbation in *t* even in the first part of the day.

For the set of 20 new scenarios, Figure 4.7 shows the *OF* values obtained using: the deterministic model (assuming a perfect forecast), the multistage solution and the coordinated day-ahead and intra-day strategy. In general, the results of Figure 4.7 confirm the improved performance of the coordinated scheduling strategy with respect to the multistage solution. Additionally, the *OF* performance illustrated in Figure 4.7 confirms that the coordinated strategy effectively tackles the problem associated with uncertainties in the community, while maintaining a cost-effective result (i.e., considering, as a reference, the deterministic solution).

Moreover, Figure 4.7 also includes, for the 20 new intra-day scenarios, the *OF* value obtained without the optimization of the REC (i.e., without internal exchanges). The results confirm the economic advantage for the intra-day scenarios as well.

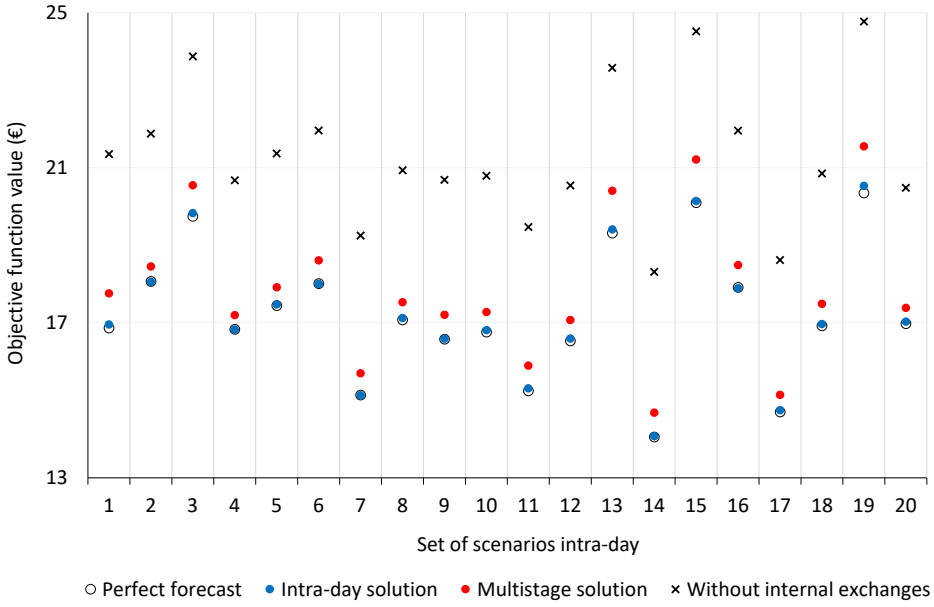

Figure 4.7 Comparison of the community's total *OF* values for 20 intra-day scenarios: Base case.

Since the number of variables and time horizon decrease constantly until the end of each stage (from the characteristics of the online calculation), the time employed by the online optimization at each time period varies, on average, from around 20 seconds to around a second depending on the corresponding time at which it occurs.

With respect to the day-ahead tolerance of the ADMM procedure, a lower value of tolerance ε might be implemented in the intra-day optimization. For the online calculations of the base case a tolerance ε equal to 10W has been used.

4.3.2 Second case: scheduling of prosumers in MV network

The second test system considers the 14-bus network illustrated in Figure 4.8, in which three feeders are connected to the same substation bus. The MV side of the substation has constant rated voltage equal to 23 kV. Each prosumer might be equipped with a PV system, a load, and a BES unit. All the calculations refer to a time window of one day, divided into 24 periods of one hour each. In this case, the tolerance ε has been defined equal to 1 kW for both the day-ahead and intra-day calculations.

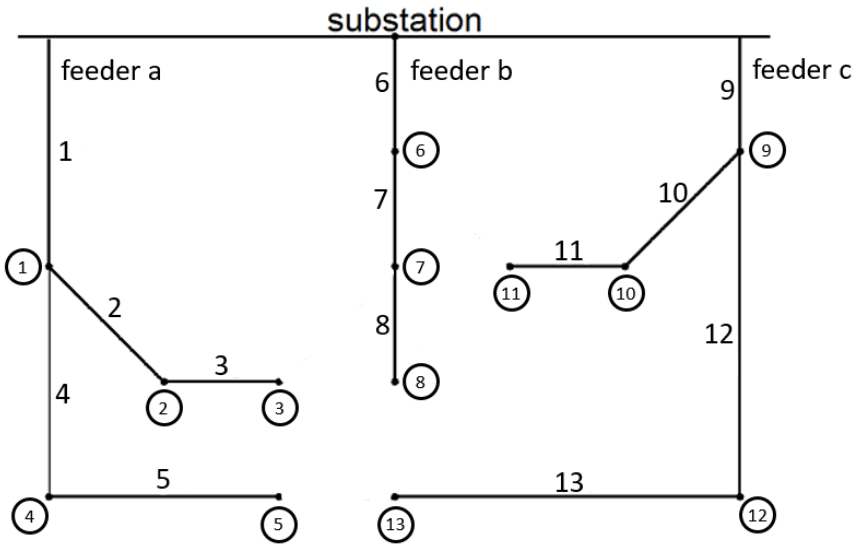

Figure 4.8 Second case configuration. Circles indicate the location of the prosumers. Adapted from (Cinvalar et al. 1988).

Figure 4.9 shows the profile of the ratio between power output and the panel surface (reported in Table 4.3), which is assumed equal for all the PV units in the community. Figure 4.9 also shows the price profile of the energy bought from the utility grid π^t_{buy} (for the numerical test $\pi^t_{sell} = 0.5\pi^t_{\text{buy}}$). Table 4.3 also shows the value of sizes $E^{\max}_{\text{BES}}$ of the BES units, with energy to power ratio equal to 1 h. Additionally, the resistance values associated with each branch in Figure 4.8 are reported in Table 4.3. The load profiles adopted for each prosumer are shown in Figure 4.10.

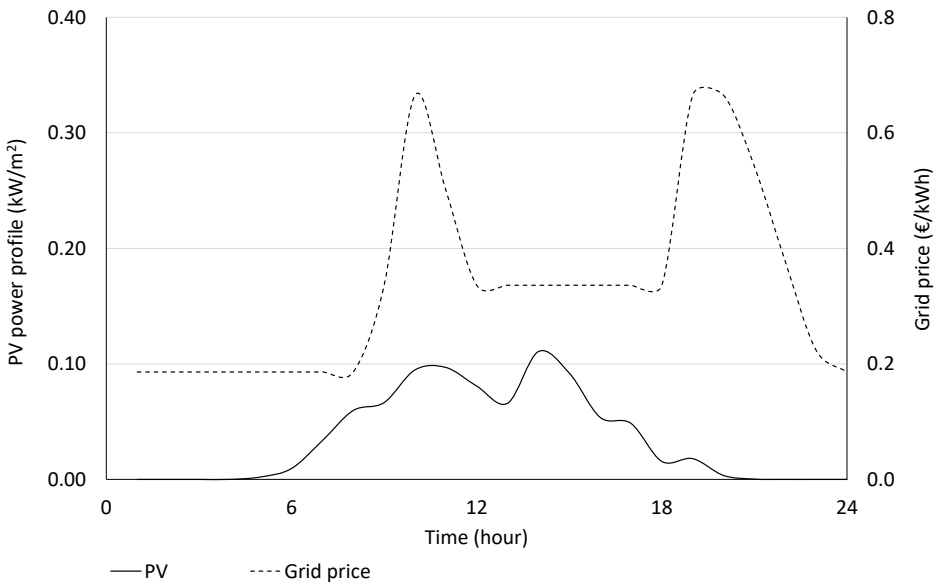

Figure 4.9 Profile of the PV production and grid purchase price π_{buy}^{t} for the second case.

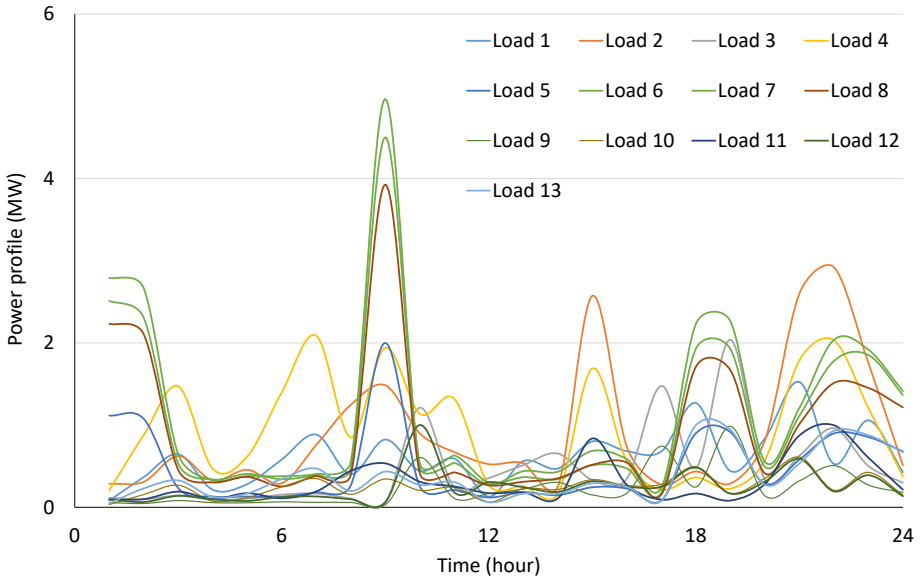

Figure 4.10 Load profile for each prosumer in the second case.

Table 4.3 Characteristics of the community in the second case.

Prosumer	PV area ($10^3 \cdot m^2$)	BES Size (MWh)	Branch	Resistance (mΩ)
1	1.12	0.5	1	0.397
2	2.56	0.3	2	0.423
3	11.2	0.4	3	0.212
4	25.6	0.2	4	0.476
5	2.24	0.3	5	0.212
6	0	1	6	0.582
7	0	0.5	7	0.423
8	0	1	8	0.423
9	6.72	0.2	9	0.582
10	5.12	0.6	10	0.476
11	4.48	0.1	11	0.212
12	3.36	0.2	12	0.423
13	3.36	0.2	13	0.212

Table 4.4 shows the resulting values of the elbow method and the silhouette coefficient calculations. The reported values have been calculated for the first eight hours of the day and for several number of centroids. As a result, a number of three centroids has been selected to generate the scenario tree. The structure of the obtained three is similar to the one illustrated in Figure 4.2 (i.e., with 27 final scenarios).

Table 4.4 Elbow method and silhouette coefficient for the selection of the number of centroids: Second case.

Number of centroids	3	4	5	6	7	8	9
Average *SSE*	1.82	1.74	1.65	1.63	1.58	1.54	1.52
Average $s\left(\psi_{\varphi}\right)$	0.43	0.40	0.38	0.39	0.36	0.37	0.38

Table 4.5 shows the *VSS* and *EVPI* values calculated for the second case and a scenario tree obtained with three centroids, confirming the advantage of the stochastic solution over the forecast-based solution.

Table 4.5 Stochastic metrics *VSS* and *EVPI* for the second case.

Solution	*OF* Value (k€)	*VVS* (k€)	*EVPI* (k€)
EEV	45.29		
RP	45.16	0.13	0.02
WS	45.14		

Figure 4.11 shows for each one of the scenarios in the tree, the comparison of the total *OF* values calculated by using the intra-day decision-making procedure (based on the multistage solution) and those given by the forecast-based solution. As expected, the multistage scheduling provides better results with respect to the forecast-based solution. Figure 4.11 also shows the *OF* value of (3.17) (distributed problem that minimizes the energy procurement cost) assuming a perfect forecast.

Furthermore, Figure 4.11 includes the *OF* values obtained for each scenario in the tree, when the prosumers are not allowed to exchange energy inside of the REC. For the second case, the obtained costs also confirm the advantage of implementing the REC and the associated cost-optimization.

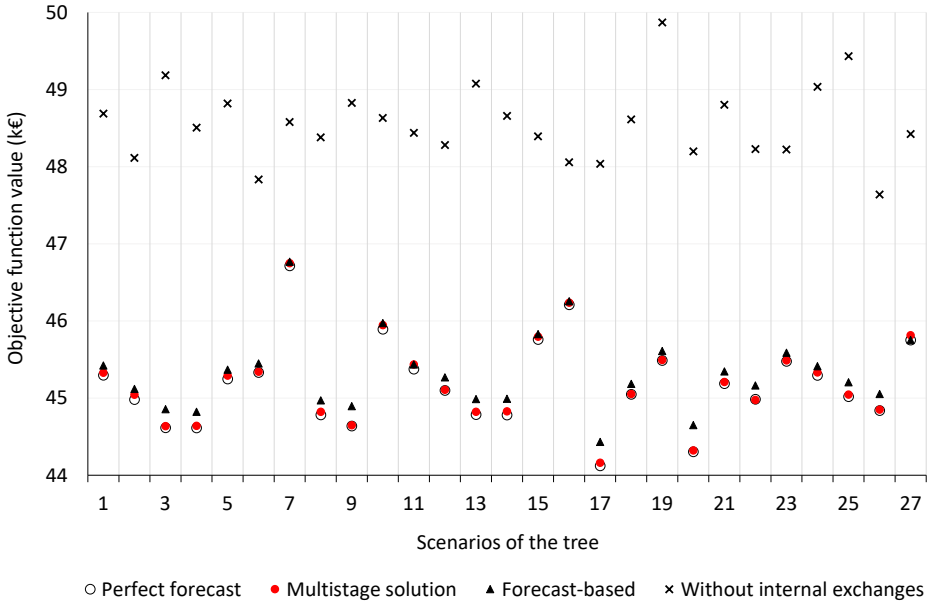

Figure 4.11 Comparison of the community's total *OF* values for each scenario of the tree: Second case

For a set of 20 new scenarios different from those in the tree, the implementation of the day-ahead scheduling described in section 3.2, and based only on the forecast profiles, is, on average, 0.73% higher than the deterministic *OF*, while the implementation of the decision making-procedure (based on the multistage solution) gives, on average, an increase of 0.62% over the same deterministic solution.

Figure 4.12 shows the total energy in the BES units obtained when applying the coordinated strategy for each test scenario (i.e., for each one of the 20 new scenarios). Like for the base case, the proposed strategy is suitable to implement an adaptable scheduling for a REC even when considering different topologies and size of the installed equipment.

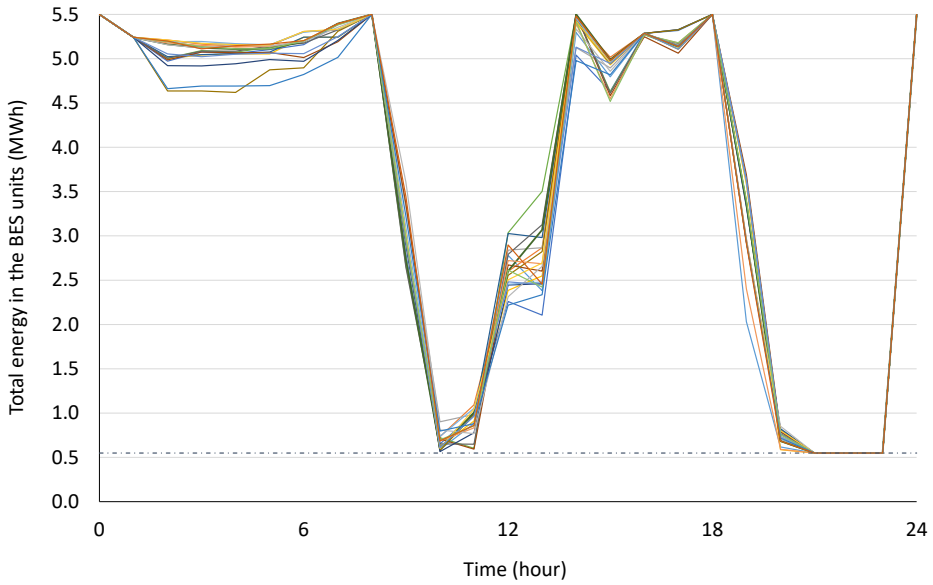

Figure 4.12 Total energy stored in the community during the day for the second case: profiles obtained using the coordinated strategy that includes online optimization.

In Figure 4.13, the obtained *OF* values, using: a deterministic solution (i.e., assuming a perfect forecast), intra-day solution (i.e., coordinated strategy) and multistage solution (based only on day-ahead calculations and decisions only at the end of each stage), are compared.

As expected, the results of Figure 4.13 show the advantages of the coordinated day-ahead and intra-day approach over the multistage solution. In comparison with the deterministic solution for several scenarios, the proposed strategy effectively adapts the scheduling of the community to deal with the uncertainties while minimizing the energy procurement cost.

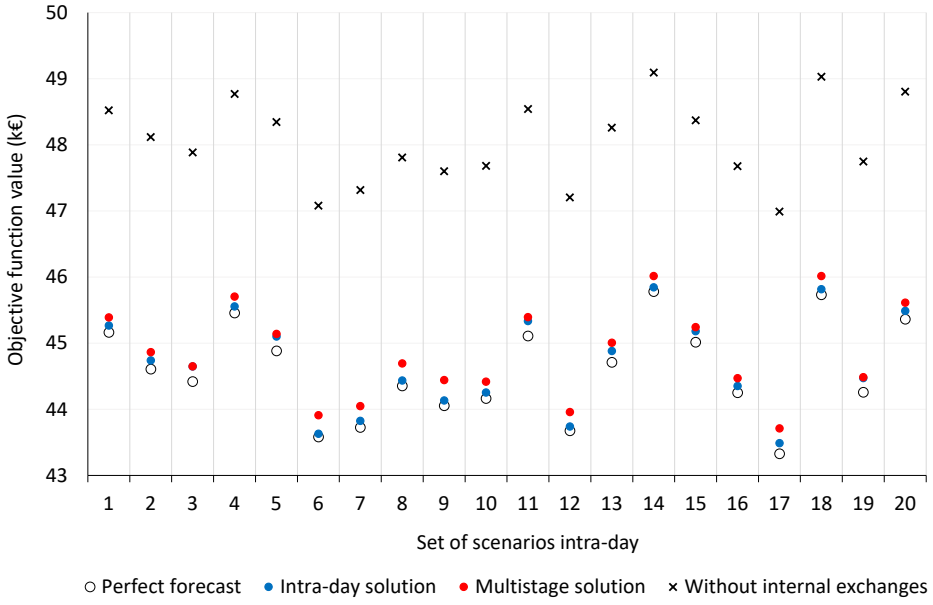

Figure 4.13 Comparison of the community's total *OF* values for 20 new intra-day scenarios: Second case.

Moreover, Figure 4.13 also includes the *OF* value obtained without the optimization of the REC (i.e., without internal exchanges). As expected, the results once again confirm the economic benefit of allowing the cooperative operation of the REC.

In the second case, with a time step equal to 1h, the time employed by the online optimization at each time period varies, on average, from around eight seconds to less than a second depending on the corresponding time at which it occurs.

4.4 Conclusions of the chapter

A significant issue in the operation of the community concerns the uncertainties associated with the distributed generation and loads consumption.

In this chapter, we have presented a coordinated day-ahead and intra-day strategy to define a cost-oriented scheduling of a REC. The scheduling of the energy resources is implemented by means of a distributed scheme based on the ADMM algorithm. The proposed strategy has been suitably conceived to consider the uncertainties of the PV generation and energy consumption.

In the first part of this chapter, we have adapted the day-ahead ADMM-based scheduling procedure defined for a REC in order to consider the uncertainties of local generation (PV in this case) and energy consumption. To achieve this, a multistage stochastic approach has been adopted to define a scenario-based solution for the resources in the community. The implementation of such a scheme demands the representation of the stochastic processes (i.e., PV generation and load) with the corresponding scenario tree. In this approach, a tree generation method based on the *k*-means algorithm has been employed to deal with the problem of merging the stochastic information of the several prosumers in a common tree for the community.

The obtained tree is employed to define the day-ahead multistage stochastic solution that provides the set values for the batteries of the community corresponding to each stage of the day and at each node of the tree.

From the presented numerical results, we have confirmed that the proposed multistage scheduling provides, in general, improved results with respect to the corresponding forecast-based solution of the community, owing to the chance to adapt the set values of the BES units and the energy transactions among the prosumers according to the current operational conditions of the day.

Furthermore, the proposed multistage day-ahead scheduling has been employed to provide an operational framework for an intra-day decision-making procedure, in which an online optimization calculates new set values for the operation of the community. The online decisions concern the power output of the BES units, energy transactions between prosumers, and energy transactions with the external energy provider.

To achieve this, the decisions made at the end of each stage bring an operational framework to the online intra-day scheduling, in which several characteristics have been implemented to speed up the solution time, while maintaining good accuracy.

This coordinated approach accurately reacts to the fluctuations of energy generation and local load during the day, not only to the cumulative deviations of each stage. Furthermore, a reduced tolerance value for the ADMM procedure can be used in the online calculations with an acceptable solution time.

As a result, the coordinated approach effectively minimizes the total energy procurement cost for the community, considering the current operational conditions of the participants and adjusting the scheduling of the set values in a distributed and coordinated way.

Chapter 5. Concluding remarks

This thesis presents a detailed study of resources scheduling in renewable energy communities. The analysis has considered quite a few technical problems, from the operation of the basic unit of the community, i.e., the prosumer, to the mathematical formulation, scheduling and expansion, for several scenarios, of the energy community concept. This has been achieved through the implementation of both a centralized and a distributed approach. Moreover, the thesis presents an integration of day-ahead and intra-day optimization.

The second chapter of this thesis has been dedicated to the scheduling problem of local energy systems acting as prosumers, with the possibility of exploiting their installed renewable resources (e.g., PV-Storage systems) by covering the local energy demand and enabling the energy exchange with the provider (i.e., buying and selling). The operation of such a system requires the implementation of an energy management system to exploit the economic potential of the resources, while also considering the technical constraints relevant to the operation of the equipment.

The considered formulation deals with day-ahead scheduling decisions. The problem has been extended to consider uncertainties associated with energy generation and demand by adopting a multistage stochastic scheme. Several comparisons between the two approaches (i.e., without and with uncertainties) have been presented. Within this framework, the multistage stochastic approach represents an attractive method for the day-ahead scheduling and provided improved results in comparison to other stochastic-based method, such as e.g., Monte Carlo simulations.

One of the key-steps in defining the multistage stochastic solution is the adequate representation of the stochastic behaviour of the variables in the problem by means of a scenario tree. For the study, a tree-generation technique based on the *k*-means clustering algorithm, which provides appropriate results even with a limited number of centroids, has been implemented. The time employed by the multistage solution is reasonable for several cases with different number of clusters.

The approach presented in the second chapter can be coupled with an intra-day decision-making procedure that adjust the operation of the energy system according to the current conditions of energy generation and consumption. Furthermore, the stochastic approach is also suitable for

application in models that include a detailed representation of the battery (e.g., KiBaM), assuming that the MILP characteristics of the model are preserved.

In the second chapter, we have also considered an additional scenario where a microgrid integrates bidirectional EV charging stations in a parking lot and PV units. The operation model of the microgrid has been adapted to a multistage stochastic approach, obtaining an adaptative response to the uncertainties. In this case, which is particularly oriented to exploiting the benefits of V2G services, additional uncertainties associated with the behaviour of the EVs in the parking lot (e.g., time of entrance, leaving time, number of vehicles) have been included in the formulation proposed. In general, the solution confirms the characteristics and advantages of adopting a multistage stochastic scheme to deal with uncertainties.

Next, in the third chapter, we have extended the prosumer concept within a so-called renewable energy community. To achieve this, we considered a set of prosumers that agreed to cooperate in order to minimize the total energy procurement costs. This collective entity is characterized by being local and having a common objective for all their members, which is different than other approaches in which each participant might define a self-interest strategy to exploit their own available resources.

The potential of the energy community has been gaining special interest in the last years, since the regulation framework in several countries is opening the door to allowing direct energy transactions between neighbours (e.g., residential units, industrial/commercial sites). Apart from the relevant legal and socio-economic aspects, the establishment of these communities represents an important challenge from a technical point of view.

In this context, one of the main aspects to be considered is the adequate coordination of the decisions in the community to cost-effectively share the energy resources while guaranteeing fairness for all the participants. To achieve this, the concept of REC requires the implementation of an automatic energy management system that provides the optimal scheduling of the energy resources.

In this thesis, the definition of such a scheduling approach for the REC has been studied, first, by formulating the mathematical model that represents the components and interactions of the prosumers within the community and with the external energy provider, and then by analysing the day-ahead scheduling under the assumption of both a centralized and a distributed approach.

In the centralized approach the prosumers communicate all the details of the equipment features as well as the load and production forecasts. In the distributed version of the EMS, based on the use of the ADMM algorithm, the prosumers are autonomous in identifying the cost optimal decisions based on the forecasts of energy generation and consumption. Only the actions that affect the other members, such as the internal exchanges of energy, must be mutually agreed on. In this case, the information that each prosumer must share within the community is limited, preserving the autonomy and privacy of each member.

The so-called ADMM-based approach has been characterized as follows:

- it aims at minimizing the energy procurement cost of the community, considering the power loss in the internal network
- a loss-allocation procedure has been adopted in order to assign the corresponding losses to each energy transaction between two prosumers or between a prosumer and the external energy provider
- the structure of the proposed scheduling procedure is consistent with the billing procedure and the metering systems typically installed in an energy community.

The comparison of the results obtained by the centralized and the ADMM approach confirm that the scheduling problem of the community is suitable for adopting either a centralized or a distributed scheme. However, as already mentioned, the distributed approach is oriented to better preserve the privacy of the participants in the community and allows the scalability of the scheduling approach to communities of many prosumers.

As a result, it has been confirmed that the proposed approaches effectively minimize the energy procurement cost for the community, and with an economic benefit for each one of its members.

The definition of energy prices in the community is an important aspect of the procedure, since one of the main objectives of the community is to assure the definition of fair prices that align the economic-benefit goals with the non-competitive nature assumed by the participants.

The additional scenario in which dispatchable generating units are integrated as participants in the community shows the extent up to which the presence of dispatchable power plants can ensure high percentages of self-consumption in different operational scenarios. In this scenario, the marginal prices associated with the operation of the biogas influence the price definition in the community.

The last chapter of this thesis presents a coordinated day-ahead and intra-day strategy in order to define a cost-oriented scheduling of the community. The scheduling of the energy resources is implemented by means of a distributed scheme based on the ADMM algorithm. The proposed strategy has been suitably conceived to consider the uncertainties associated with the energy generation (PV generation in the considered case studies) and energy consumption.

In the day-ahead stage, a scenario-based scheduling solution is provided for the operation of the community during the next day. To achieve that, the scheduling approach based on the ADMM algorithm has been adapted to a multistage stochastic scheme, with decisions associated with each stage during the optimization horizon (i.e., a day). The adoption of such an approach requires the implementation of a scenario-generation technique for each prosumer, and subsequently, the construction of a scenario tree for the entire community. In this case, the tree-generation procedure, which is based on the *k*-means algorithm, combines the situation of each participant in the community to obtain a common tree that allows a coordinated response of all the prosumers at each scenario.

During the day, a decision-making procedure is implemented as an online optimization at each time period and following the basic scheme of a receding horizon approach. The goal is to adjust the set values in the community according to the current operation conditions (i.e., fluctuations of the PV generation and energy demand), while exploiting the available day-ahead calculations by using them as an operational framework for the optimization during the day.

As expected, the multistage day-ahead scheduling generally provides improved results with respect to the corresponding forecast-based solution of the community (in terms of energy procurement costs), exploiting the possibility of adapting the set values of the BES units and the energy transactions among the prosumers according to the current operational conditions of the day.

During the day, the decisions made at the end of each stage bring an operational framework to the online intra-day scheduling, in which several techniques have been implemented to speed up the solution time while keeping a good accuracy. This proposed approach accurately reacts to the fluctuations of generation and local load during the day and not only to the cumulative deviations of each stage. Furthermore, a reduced tolerance value for the ADMM procedure can be used in the online calculations, with an acceptable solution time.

As a result, the coordinated day-ahead and intra-day strategy effectively minimizes the total energy procurement cost for the community, considering the current operational conditions during the day and adjusting the scheduling of the set values in a distributed and coordinated way.

On the basis of the work carried out in this thesis, some topics have been identified as particularly interesting for the further development and implementation of RECs.

A relevant concern in the field of scheduling and operation of BES units is associated with degradation and aging conditions. Thus, considering the crucial role that the storage systems play in the successful achievement of the community goals, it will be worthwhile to incorporate the consideration of battery-aging conditions in the modelling and scheduling of the REC's resources.

In addition, in a future project, we plan to address a refined representation of the REC's network into the ADMM-based approach in which voltage, current and technical constraints of the network will be incorporated. The development of such a model will allow us to study additional state-of-the-art questions, such as voltage issues and violation of capacity-constraints in the network due to the energy transacted by the prosumers.

Moreover, as a further extension, we would like to develop a specific procedure to adapt the operation of the REC in case of operational failures, such as the temporary or permanent non-availability of a given resource or a communication link during the optimization horizon.

Appendix A. Alternative Representation of the Battery: Kinetic Battery Model

The representation of the batteries employed in Chapter 2-Chapter 4 correspond to a simple energy balance, which is widely employed to study the operation of energy systems while providing a good enough approximation corresponding to the operation of the storage units; however, it is important to notice that the formulation of the considered systems is suitable for considering more detailed, or refined, MILP models of the battery.

For instance in (Sakti et al. 2017), several models have been presented to represent the battery model and enhance their use in MILP. In several studies e.g., (Manwell and McGowan 1993; Daniil, Drury, and Mellor 2015; Bordin et al. 2017) the so-called kinetic battery model (KiBaM) has been considered, in order to provide a more detailed representation.

According to (Daniil, Drury, and Mellor 2015), in the KiBaM representation, the total charge in the battery is modelled with two tanks separated by a conductance, distinguishing between available energy and chemically bound energy (not immediately available), illustrated in Figure A.1

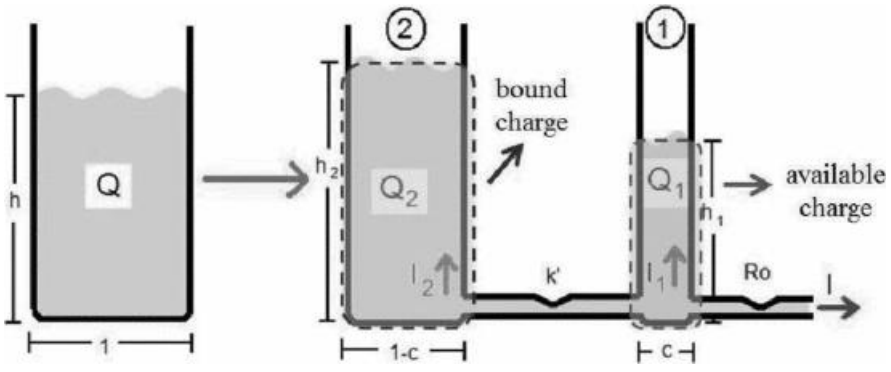

Figure A.1 Hydraulic scheme for the kinetic battery model; adapted from (Daniil, Drury, and Mellor 2015).

For illustrative purposes, some of the base-case calculations corresponding to the optimization of the LES in Chapter 2 have been repeated by using a KiBaM representation of the BES unit.

To achieve this, constraint (2.12), which corresponds to the simple energy balance at time period *t* in the battery, is replaced with the following constraints:

Appendix A. Alternative Representation of the Battery: Kinetic Battery Model

$$E_{\mathrm{BES}}^{t} = q1^{t} + q2^{t} \tag{A.1}$$

$$q1^{t} = q1^{t-1} e^{-k\cdot\Delta t} + \frac{(k\, c\, E_{\mathrm{BES}}^{t-1} + P_{\mathrm{BES}}^{t})(1-e^{-k\cdot\Delta t})}{k} + \frac{k_{q1}\, P_{\mathrm{BES}}^{t}}{k} \tag{A.2}$$

$$q1^{t=0} = c\, SOC^{0} E_{\mathrm{BES}}^{\max} \tag{A.3}$$

$$q2^{t} = q2^{t-1} e^{-k\cdot\Delta t} + E_{\mathrm{BES}}^{t-1}(1-c)(1-e^{-k\Delta t}) + \frac{k_{q2}\, P_{\mathrm{BES}}^{t}}{k} \tag{A.4}$$

$$P_{\mathrm{ch}}^{t} \le \frac{1}{\eta_{\mathrm{BES}}} \frac{k\, c\, E_{\mathrm{BES}}^{\max} - k\, q1^{t}\, e^{-k\Delta t} - E_{\mathrm{BES}}^{t}\, k\, c\,(1-e^{-k\Delta t})}{1-e^{-k\Delta t} + k_{q1}} \tag{A.5}$$

$$P_{\mathrm{ch}}^{t} \le \frac{1}{\eta_{\mathrm{BES}}} \frac{(1-e^{-a\cdot\Delta t})(E_{\mathrm{BES}}^{\max} - E_{\mathrm{BES}}^{t})}{\Delta t} \tag{A.6}$$

$$P_{\mathrm{dis}}^{t} \le \eta_{\mathrm{BES}} \frac{q1^{t}\, k\, e^{-k\Delta t} + E_{\mathrm{BES}}^{t}\, k\, c\,(1-e^{-k\Delta t})}{1-e^{-k\Delta t} + k_{q1}} \tag{A.7}$$

where $k_{q1} = c(k\cdot\Delta t - 1 + e^{-k\Delta t})$ and $k_{q2} = (1-c)(k\Delta t - 1 + e^{-k\Delta t})$.

The constraints (A.1)-(A.4) consider the definitions of readily available charge $q1^{t}$ and bound charge $q2^{t}$ at each time interval *t*. The battery power outputs during charging and discharging phases are limited by constraints (A.5)-(A.7); η_{BES} is the battery's efficiency factor for charging and discharging, *k* is the battery rate constant, *c* is the battery's capacity ratio and *a* is the battery's maximum charge rate. Table A.1 shows the corresponding parameters value indicated in (Bordin et al. 2017).

Table A.1 Parameters for the kinetic battery model (KiBaM) adapted from (Bordin et al. 2017).

Parameter	Value
η_{BES}	0.9 pu
k	9.51 h^{-1}
a	0.61
c	2 A/Ah

The obtained deterministic *OF* value (2.1), by using the KiBaM representation of the 630-kWh battery is equal to €61.21. Figure A.2 shows the comparison of the stage of charge by using the simple model and the KiBaM.

Appendix A. Alternative Representation of the Battery: Kinetic Battery Model

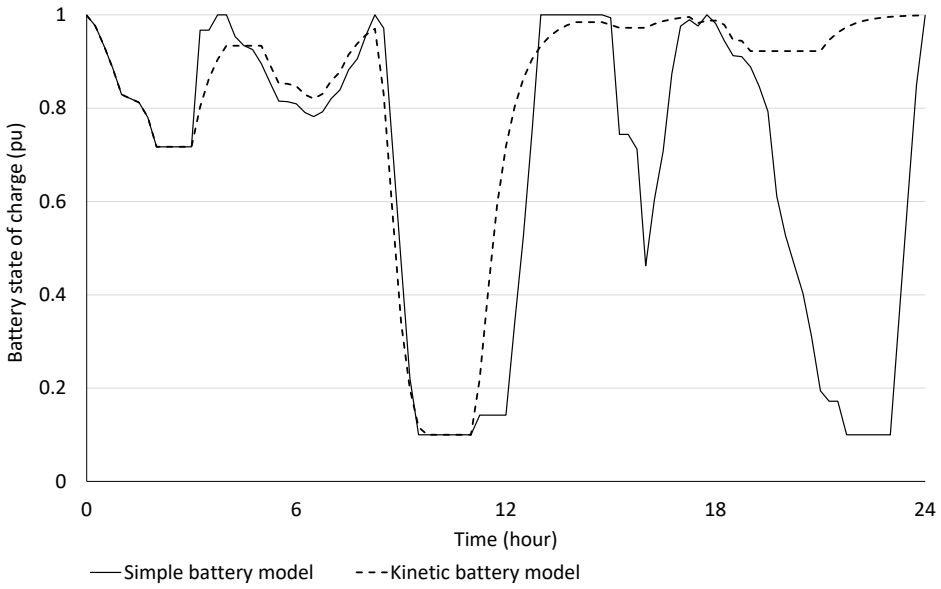

Figure A.2 Comparison of the stage of charge by the simple model and the KiBaM.

Table A.2 shows the *OF* values of the stochastic solution and metrics for the base case in section 2.1.2 by using the KiBaM representation. The solutions reported in Table A.2 correspond to the case with a 630-kWh battery, as well as to the case with a 315-kWh battery. Moreover, two different scenarios trees have been considered (with K=3 as the one in Figure 2.6 and one additional tree with K=4 centroids).

Table A.2 Stochastic solution, *VVS* and *EVPI* metrics by using the KiBaM representation for a case with a 630-kWh battery and a case with a 315-kWh battery.

Size of the BES unit (kWh)	630		315	
Number of centroids	3	4	3	4
OF (€)	61.67	61.80	80.69	80.80
VSS (€)	1.11	1.12	0.98	0.98
EVPI (€)	0.47	0.56	0.43	0.52
Number of scenarios in the tree	64	139	64	139
Solution time (s)	3.47	8.26	2.97	7.39

The comparison of Table 2.2 (results obtained by the simple model) and Table A.2 shows that the use of the more refined battery model increases both the *OF* values and the computation time, as expected.

We have repeated the comparison showed in Table 2.3 (i.e., *SP-MC* and *SP-WS*) by using the KiBaM representation. The results in Table A.3 confirm, as expected, the advantage of using

the SP approach and the benefit of a more accurate clustering procedure, especially in the case of a smaller battery, even for a more detailed representation of the battery.

Table A.3 Comparison between SP and Monte Carlo simulations and between SP and deterministic solutions (630-kWh battery) by using the KiBaM representation.

Size of the BES unit (kWh)		630		315	
Number of centroids		3	4	3	4
Scenarios of the tree	*SP – MC*	-0.71	-0.69	-0.60	-1.58
	SP – WS	0.55	0.60	0.49	0.55
Set of initial scenarios	*SP – MC*	-0.23	-0.34	-0.26	-0.35
	SP – WS	1.81	1.70	1.60	1.50
Set of new scenarios	*SP – MC*	-0.26	-0.24	-0.30	-1.14
	SP – WS	1.91	1.92	1.67	2.79

Appendix B. Exchange of Energy for Prosumers in Medium Voltage Network

The optimization problem that minimizes the procurement costs in a community, like the one in (3.1), gets harder to solve if power loss and typical operational constraints (such as bus voltage and branch current limits) are considered, e.g., (Madani, Ashraphijuo, and Lavaei 2014) and references therein. This appendix describes an alternative for dealing with such a minimization, which follows the approach introduced in (Gambini et al. 2020).

The procedure is characterized by being based on the classical second order cone programming (SOCP) formulation for the distribution optimal power flow in radial networks described in, e.g., (Gan et al. 2015) and (Wei et al. 2017). In (Low 2014b, 2014a), the conditions for achieving relaxation exactness have been presented, whilst (Molzahn and Hiskens 2016) presents an analysis of topologies for which it is not possible to guarantee the conditions for exactness.

Furthermore, the procedure distinguishes between the power exchanged with the external grid and the power exchanges between the prosumers, in order to prioritize the use of local energy resources.

The approach introduced in (Gambini et al. 2020) corresponds to a centralized approach and has been conceived as suitable for adaptation to a distributed optimization procedure, like the one considered in Chapter 3. The considered case corresponds to a community composed of a set of MV prosumers connected to the same, or different, feeders of the same primary substation, like the case described in section 4.3.2.

Figure B.1 illustrates the model of the community, in which the internal network, connected to the utility grid, is divided into elements corresponding to the prosumers. Each prosumer is characterized by a single connection point to the network. The prosumer element imports and exports power; additionally, it incorporates the losses of the branch that connects its coupling bus with the coupling bus of the previous prosumer closest to the substation.

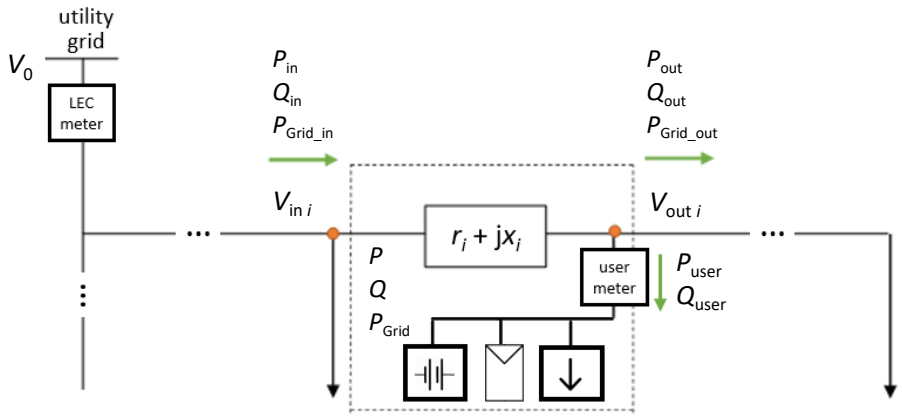

Figure B.1 Model of the community (the arrows indicate the positive directions assumed in the equations); adapted from (Gambini et al. 2020).

The attribution of the entire losses in each branch to the prosumer at the end of the branch is used only in the scheduling optimization procedure, whilst the billing procedure is aligned with a fair repartition of the branch losses to all the prosumers in the feeder, like the one introduced in (Lilla et al. 2020) and described in Chapter 3. This procedure is justified by the cooperative nature of the REC, in which the participants collaborate to minimize the community procurement costs.

As in (3.1), the objective minimizes the total energy procurement costs of the community, considering the exchange of energy with the external grid (i.e., $P^t_{\text{buy\_Grid}\,i}$ and $P^t_{\text{sell\_Grid}\,i}$) and the associated prices (i.e., π^t_{buy} and π^t_{sell}, respectively). The mathematical formulation corresponds to a day-ahead scheduling with an optimization horizon equal to one day dived into one-hour periods.

Figure B.1 illustrates the connection constraints between each branch (and the relevant prosumer) and the next one in the feeder. According to the usual convention of the Distflow or branch flow model (Baran and Wu 1989):

- the values of v_{out}, P_{out}, Q_{out}, and $P_{\text{Grid\_out}}$ of i are constrained to be equal to the values of v_{in}, P_{in}, Q_{in}, and $P_{\text{Grid\_in}}$ of prosumer i+1
- for the prosumers located at one of the feeder's ends, P_{out}, Q_{out}, and $P_{\text{Grid\_out}}$ are constrained to be equal to 0
- in case of branching, for active and reactive power, the equality is replaced by the balancing constraints at the branching node, as in (Baran and Wu 1989).

- values v_{in} of the branches connected to the substation (assumed to be the slack bus) are constrained to be the square of the known value of the slack bus voltage (V_0^2).

For each prosumer i at time t, the links between v_{in} and v_{out}, P_{in} and P_{out} and Q_{in} and Q_{out} are represented by:

$$P_{\text{in}i}^t + P_{\text{out}i}^t = P_i^t \tag{B.1}$$

$$Q_{\text{in}i}^t - Q_{\text{out}i}^t = Q_i^t \tag{B.2}$$

$$v_{\text{in}i}^t - v_{\text{out}i}^t = 2r_i \cdot P_{\text{in}i}^t + 2x_i \cdot Q_{\text{in}i}^t - \left(r_i^2 + x_i^2\right) \cdot u_i^t \tag{B.3}$$

$$\left(P_{\text{in}i}^t\right)^2 + \left(Q_{\text{in}i}^t\right)^2 = v_{\text{in}i}^t \cdot u_i^t \tag{B.4}$$

The square of the branch current's rms value, u, is constrained to be lower than the square of the maximum current limit, and $P=P_{\text{user}}+r\cdot u$ and $Q= Q_{\text{user}}+x\cdot u$ also include the branch active and reactive power losses (shunt capacitances of the branches are neglected). Constraint (B.4) corresponds to the usual rotated second order cone convex relaxation of the branch flow model.

Considering that each participant in the community might be equipped with a generating unit (PV panels in this case) and a storage unit, in addition to its load, net powers at the coupling bus are given by

$$P_{\text{user}i}^t = P_{\text{Load}i}^t - P_{\text{PV}i}^t - P_{\text{BES}i}^t \tag{B.5}$$

$$Q_{\text{user}i}^t = Q_{\text{Load}i}^t - Q_{\text{PV}i}^t \tag{B.6}$$

where P_{BES} represents the power output of the storage unit and is considered positive if supplied by the battery. The PV units are assumed to operate at the unity power factor (Q_{PV}=0). P_{BES} is the main control variable together with the trade decisions in the community (i.e., energy exchanges between participants).

The operation of the BES unit is represented by the following constraints, which correspond to a simple model considering charging and discharging efficiencies (η_{ch} and $\eta_{\text{dis,}}$ respectively)

$$P_{\text{BES}i}^t = P_{\text{dis}i}^t - P_{\text{ch}i}^t \tag{B.7}$$

$$L_{\text{ch}i}^t = \left(1-\eta_{\text{ch}i}\right) P_{\text{ch}i}^t \tag{B.8}$$

$$L_{\text{dis}i}^t = \left(1 \big/ \eta_{\text{dis}i} - 1 \right) P_{\text{dis}i}^t \tag{B.9}$$

Nonnegative variables $P^t_{\mathrm{ch}i}$ and $P^t_{\mathrm{dis}i}$ are constrained by the maximum power limit of the battery. The energy level E_{BES} inside each battery is constrained to be between 10% and 100% of the battery rating and is calculated by

$$E^t_{\mathrm{BES}i} = E^{t-1}_{\mathrm{BES}i} - \left(P^t_{\mathrm{BES}i} + L^t_{\mathrm{ch}i} + L^t_{\mathrm{dis}i}\right)\Delta t \tag{B.10}$$

The BES units have been assumed fully charged at the beginning and at the end of the day.

The direct exchanges with the utility grid are described by variable P_{Grid} (and the corresponding variables at the boundaries, namely $P_{\mathrm{Grid\_in}}$, and $P_{\mathrm{Grid\_out}}$):

$$P^t_{\mathrm{Grid}i} = P^t_{\mathrm{buy\_Grid}i} - P^t_{\mathrm{sell\_Grid}i} \tag{B.11}$$

$$P^t_{\mathrm{Grid\_in}i} - P^t_{\mathrm{Grid\_out}i} = P^t_{\mathrm{Grid}i} \tag{B.12}$$

$$P^t_i = P^t_{i+} - P^t_{i-} \tag{B.13}$$

$$\left|P^t_i\right| = P^t_{i+} + P^t_{i-} \tag{B.14}$$

where nonnegative variables P^t_{i+} and P^t_{i-}, defined by (B.13) and (B.14), are used to constrain nonnegative variables $P_{\mathrm{buy\_Grid}}$ and $P_{\mathrm{sell\_Grid}}$, respectively; $P_{\mathrm{buy\_Grid}} \le P^t_{i+}$ and $P_{\mathrm{sell\_Grid}} \le P^t_{i-}$.

For each prosumer *i* and time interval *t*, the transactions inside the community are calculated by the difference between *P* and $P^t_{\mathrm{Grid}i}$; P^t_{i+} - $P_{\mathrm{buy\_Grid}}$ is the power bought from other prosumers and P^t_{i-} - $P_{\mathrm{sell\_Grid}}$ is the power sold to other prosumers. The modulus of the dual values associated to constraints (B.12) are used as the prices for the transactions between prosumers in the community.

The following constraint allows exchanges between different feeders connected to the same substation:

$$\sum_{k\in\Omega_0} P^t_{Grid\_\mathrm{in}k} = \sum_{k\in\Omega_0} P^t_{\mathrm{in}k} \tag{B.15}$$

where Ω_0 is the set of branches connected to the slack bus.

In a feasible solution, (B.4) is verified as equality, and powers P_{ch} and P_{dis} of (B.7) can never be simultaneously different from zero for the same prosumer. Specific checks are included in the implementation of the model, and additional penalization terms are added to the total energy procurement costs (3.1), with increasing weights if needed. For each *i* and *t*, the penalization

term relevant to (B.4) is $r \cdot u$ (branch power loss), and the penalization term for the battery model is $L_{\text{ch}} + L_{\text{dis}}$ (losses in the storage unit). In the case study, the penalization terms are negligible with respect to the cost terms considered in (3.1).

Ultimately, the optimization problem is composed of the augmented objective function (3.1), constraints (B.1)-(B.15) and the limits of each variable (i.e., upper and lower values).

As already mentioned, the case study corresponds to the case described in section 4.3.2, in which a transactive scheme between a set of prosumers in a MV network has been considered. Figure 4.9 shows the profile of the ratio between power output and panel surface, which has been assumed equal for all the prosumers. Figure 4.9 also shows the price profile of the energy bought from the utility grid π^t_{buy} (π^t_{sell} is assumed to be half of π^t_{buy}). Table 4.3 shows additional characteristics of the community, such as e.g., PV area for each prosumer, size of the BES units and branch resistances. The load profiles correspond to those illustrated in Figure 4.10.

The introduced model has been implemented in Matlab and tested by using the Gurobi 9.0 solver (MIQCP model) on an Intel-i7 computer with 8 GB of RAM, running 64-bit Windows 10.

Figure B.2 shows the prices associated with the energy transactions in the community (black solid marks). Since the model contains integer variables due to the modulus in constraint (B.15) and Gurobi provides the dual values only for continuous models, the solution is repeated without constraint (B.15) and by fixing P^t_{i+} or P^t_{i-} to zero, according to the first solution. As expected, the solutions of the continuous and mixed integer models are the same.

Moreover, price profiles π^t_{buy} and π^t_{sell} are also represented in Figure B.2 by the dotted blue and red line, respectively.

Appendix B. Exchange of Energy for Prosumers in Medium Voltage Network

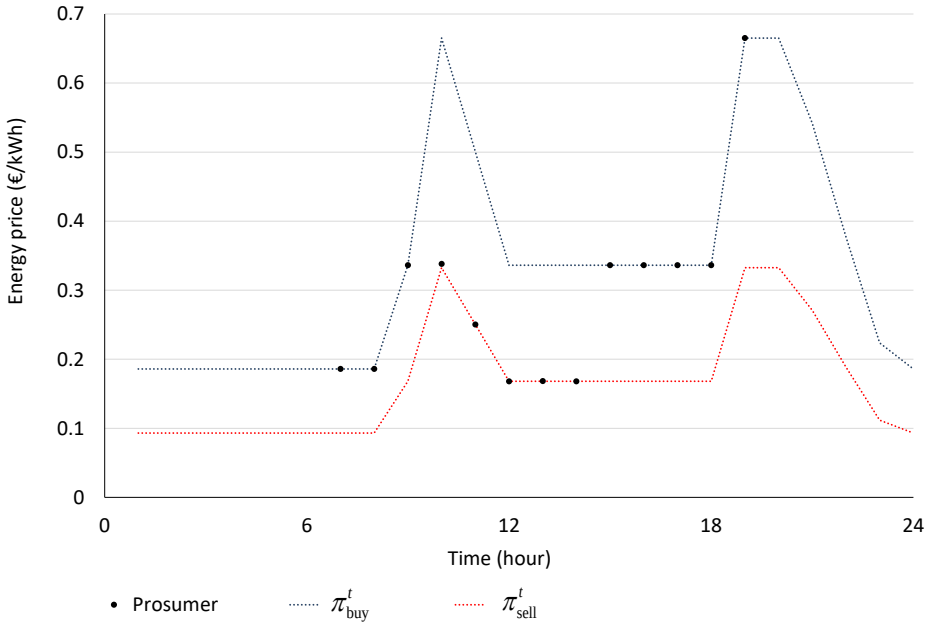

Figure B.2 Prices associated to the energy exchanges in the community

The optimization problem considered in the case study, has been solved assuming three different operational models for the community, namely:

- **Community**: in which transactions between all the participants are allowed
- **Without internal exchanges**: the model in which internal transactions are forbidden, i.e., $P_{\text{Grid}} = P$ for each i and t
- **Community with separated feeders**: a community in which energy transactions between prosumers connected to different feeders (separated feeders) are not allowed, i.e., constraint (B.15) is replaced by

$$P^t_{\text{Grid\_in}k} = P^t_{\text{in}k} \tag{B.16}$$

for each branch k connected to the substation.

Table B.1 shows the comparison of: the obtained *OF* value (3.1), the *OF* augmented with the weighted penalization of network and battery losses, the value of power loss in the network inside the community and the computational time, considering the three different models. The community model allows for a reduction in the total procurement costs and reduces the power loss in the internal network. The community model that couples all the feeders achieves the lowest total costs. Furthermore, in all the considered models, the computational time is low. The solutions have been obtained by using the default values of Gurobi parameters.

Appendix B. Exchange of Energy for Prosumers in Medium Voltage Network

Table B.1 Comparison of the solutions for the case study.

	OF (k€)	Augmented *OF*	Losses (MWh)	CPU time (s)
Community	45.7	$45.7 \cdot 10^3$	3.19	9.9
Without internal exchanges	49.2	$49.2 \cdot 10^3$	3.48	4.9
Community with separated feeders	47.1	$47.1 \cdot 10^3$	3.34	6.51

Figure B.3 shows the profiles of the power flow exchanged with the utility grid (positive if consumed by the community) given by the three different models, whilst Figure B.4 shows the comparison of the total energy stored in the BES units.

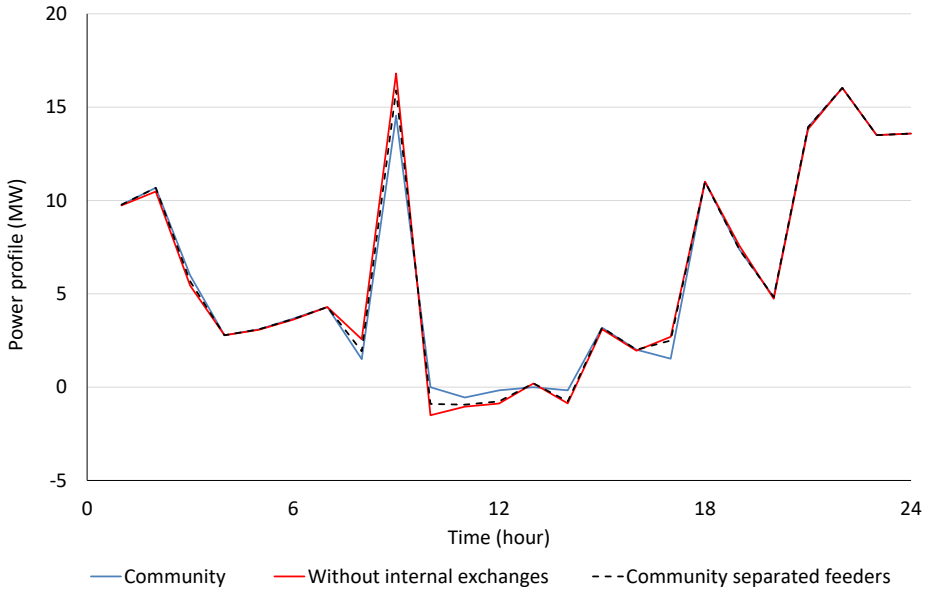

Figure B.3 Power flow exchanged with utility grid (positive if consumed by the community).

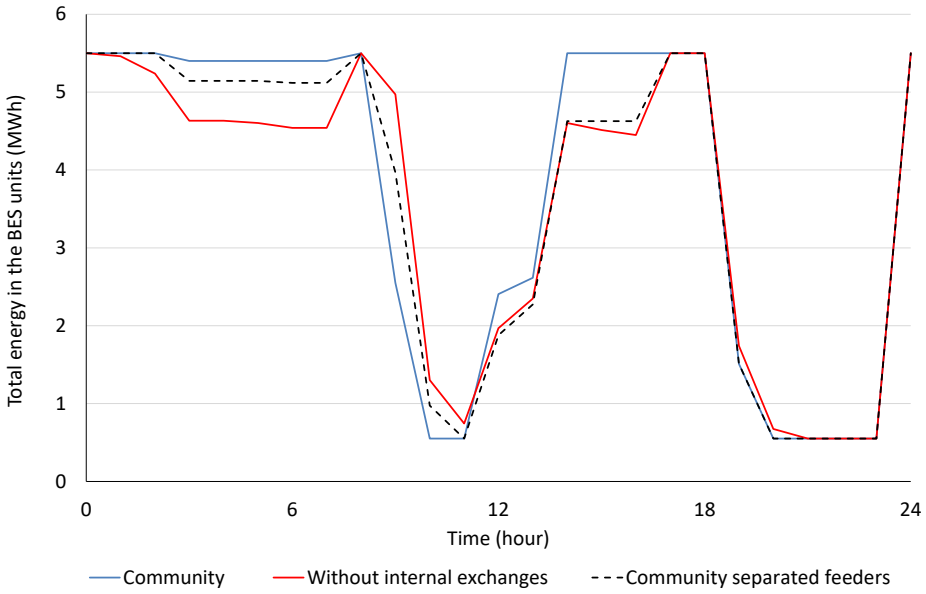

Figure B.4 Profile of the total energy in the community's batteries given by the three considered models.

Figure B.5 shows the profiles of the total energy injected into the community network by the producers. Moreover, Figure B.5 shows the profile of the energy directly sold by the producers to other participants in the community. The total energy absorbed by the consumers at each time *t* has been illustrated in Figure B.6.

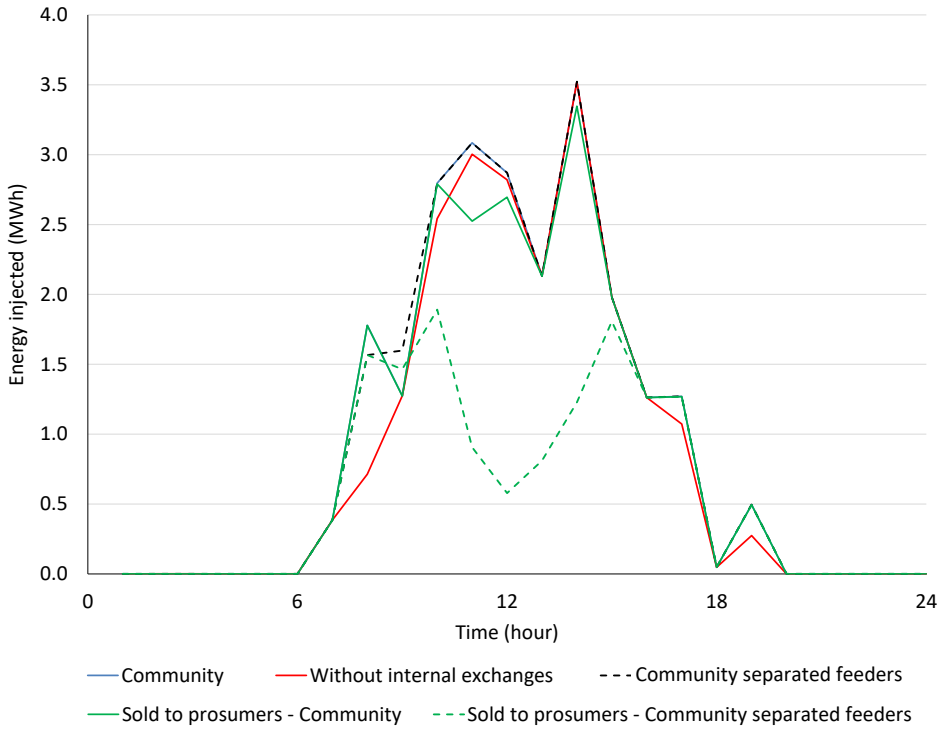

Figure B.5 Total energy injected in the community network by the producers and the energy sold directly to other participants in the community.

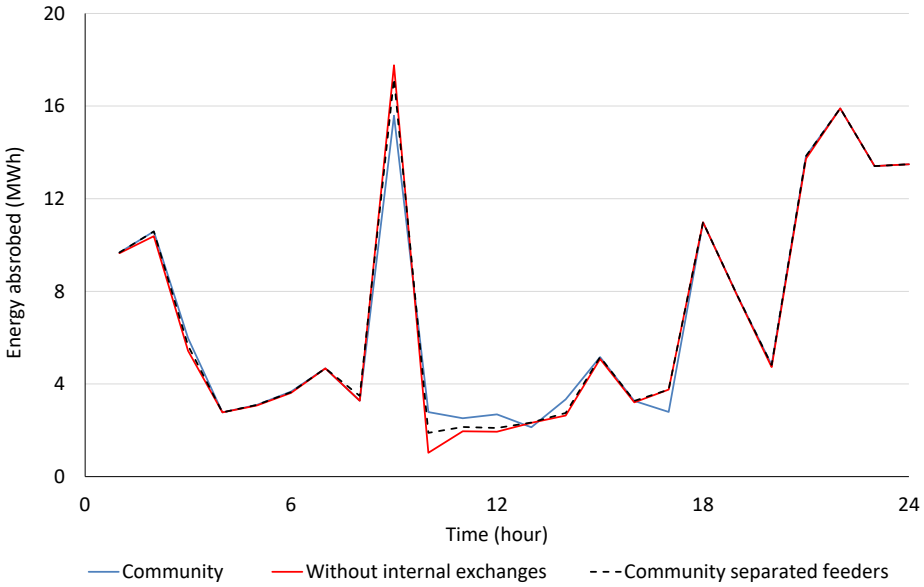

Figure B.6 Profiles of the total energy consumed by the users in the community.

Table B.2 shows the total cost for each participant in the community. The results confirm the economic benefit for each one of the participants in the community model over the case without direct energy transactions. The results are obtained by allocating the losses in each feeder to the prosumers connected to the same feeder proportionally to the power injection or consumption.

Table B.2 Energy procurement costs in the thousands of euros for each prosumer.

Prosumer	Feeder	Community	Without internal exchanges	Community separated feeders
1	a	4.20	4.56	4.20
2	a	6.54	6.91	6.54
3	a	1.47	1.80	1.47
4	a	0.77	1.34	0.78
5	a	3.05	3.07	3.05
6	b	8.82	9.30	9.30
7	b	8.12	8.56	8.54
8	b	6.96	7.36	7.36
9	c	0.48	0.69	0.64
10	c	0.44	0.49	0.47
11	c	1.36	1.37	1.24
12	c	1.16	1.37	1.18
13	c	2.33	2.34	2.30

Comparing the results from the community model with separated feeders with those of the community model that allows transactions between different feeders, some of the prosumers have reduced costs and some increased costs. The prosumers connected to feeder *b* obtain increased costs in the model with three separate feeders since none of them is equipped with PV units, although some advantages in the community's participation could be achieved due to a presence of the batteries.

The model provides an indication of the optimal prices of the transactions between prosumers of the community. The comparison between the results obtained with the same model with and without the possibility of direct transactions among the prosumers shows that each prosumer has an advantage by the participating in the community without cross-subsidization between active and non-active customers.

Appendix C. Publications

"Comparison Between Multistage Stochastic Optimization Programming and Monte Carlo Simulations for the Operation of Local Energy Systems"

IEEE International Conference on Environment and Electrical Engineering (EEEIC), Palermo, Italy, 2008 (Conference paper).

Authors: C. Orozco, A.Borghetti, S. Lilla, G. Pulazza, F. Tossani.

"An ADMM Approach for Day-Ahead Scheduling of a Local Energy Community"

IEEE Milan PowerTech, Milan, Italy, 2019. (Conference paper).

Authors: C. Orozco, S. Lilla, A. Borghetti, F. Napolitano, F. Tossani.

"Day-ahead Scheduling of a Local Energy Community: An Alternating Direction Method of Multipliers Approach"

IEEE Transactions on Power Systems, 2020 (Journal paper).

Authors: S. Lilla, C. Orozco, A. Borghetti, F. Napolitano, F. Tossani.

"Multistage day-ahead scheduling of the distributed energy sources in a local energy community"

IEEE International Conference on Environment and Electrical Engineering (EEEIC), Madrid, Spain, 2020 (Conference paper).

Authors: C. Orozco, A. Borghetti, F. Napolitano, F. Tossani.

"Power Loss Reduction in the Energy Resource Scheduling of a Local Energy Community"

International Conference on Smart Energy Systems and Technologies (SEST), Istanbul, Turkey, 2020 (Conference paper).

Authors: M.M. Gambini, C. Orozco, A. Borghetti, F. Tossani.

"Coordinated Operation of EV Charging Stations and Power Generation Integrated in A Microgrid"

(Accepted book chapter, in print)

Authors: A. Borghetti, F. Napolitano, C. Orozco, F. Tossani.

"Impact of Neighbourhood Energy Trading and Renewable Energy Communities on the Operation and Planning of Distribution Networks"

Chapter 5 of the book *Distributed energy resources in local integrated energy systems*, edited by G. Graditi and M. Di Somma, Elsevier, 2021.

Authors: A. Borghetti, C. Orozco, C. A. Nucci, A. Arefi, J. Delarestaghi, M. Di Somma, G. Graditi.

"Procurement Cost Minimization of an Energy Community with Biogas, Photovoltaic, and Storage Units"

2021 IEEE Power Tech Conference (accepted paper).

Authors: G. Pulazza, C. Orozco, A.Borghetti, F. Tossani, F. Napolitano.

"Coordinated Day-Ahead and Intra-Day Scheduling of a Local Energy Community"

(Journal paper in review process)

Authors: C. Orozco, A. Borghetti, B. De Schutter, F. Napolitano, G. Pulazza, F. Tossani.

Bibliography

Bao, Zhejing, Qin Zhou, Zhihui Yang, Qiang Yang, Lizhong Xu, and Ting Wu. 2015a. "A Multi Time-Scale and Multi Energy-Type Coordinated Microgrid Scheduling Solution - Part I: Model and Methodology." *IEEE Transactions on Power Systems* 30 (5): 2257–66. https://doi.org/10.1109/TPWRS.2014.2367127.

———. 2015b. "A Multi Time-Scale and Multi Energy-Type Coordinated Microgrid Scheduling Solution—Part II: Optimization Algorithm and Case Studies." *IEEE Transactions on Power Systems* 30 (5): 2267–77. https://doi.org/10.1109/TPWRS.2014.2367124.

Baran, Mesut E., and Felix F. Wu. 1989. "Optimal Sizing of Capacitors Placed on a Radial Distribution System." *IEEE Transactions on Power Delivery* 4 (1): 735–43. https://doi.org/10.1109/61.19266.

Battistelli, Claudia., Luis. Baringo, and Antonio J. Conejo. 2012. "Optimal Energy Management of Small Electric Energy Systems Including V2G Facilities and Renewable Energy Sources." *Electric Power Systems Research* 92: 50–59. https://doi.org/10.1016/j.epsr.2012.06.002.

Belli, Grazia., Giovanni. Brusco, Alessandro. Burgio, Michele. Motta, Daniele. Menniti, Anna. Pinnarelli, and Nicola. Sorrentino. 2017. "An Energy Management Model for Energetic Communities of Smart Homes: The Power Cloud." In *Proceedings of the 2017 IEEE 14th International Conference on Networking, Sensing and Control, ICNSC 2017*, 158–62. https://doi.org/10.1109/ICNSC.2017.8000084.

Bhattacharya, Arnab, Jeffrey P. Kharoufeh, and Bo Zeng. 2018. "Managing Energy Storage in Microgrids: A Multistage Stochastic Programming Approach." *IEEE Transactions on Smart Grid* 9 (1): 483–96. https://doi.org/10.1109/TSG.2016.2618621.

Bordin, Chiara, Harold Oghenetejiri Anuta, Andrew Crossland, Isabel Lascurain Gutierrez, Chris J. Dent, and Daniele Vigo. 2017. "A Linear Programming Approach for Battery Degradation Analysis and Optimization in Offgrid Power Systems with Solar Energy Integration." *Renewable Energy* 101: 417–30. https://doi.org/10.1016/j.renene.2016.08.066.

Borghetti, Alberto., Fabio. Napolitano, Saeed. Rahmani-Dabbagh, and Fabio. Tossani. 2017. "Scenario Tree Generation for the Optimization Model of a Parking Lot for Electric Vehicles." In *2017 AEIT International Annual Conference*. Cagliari, Italy. https://doi.org/10.23919/AEIT.2017.8240519.

Boyd, Stephen, Neal Parikh, Eric Chu, Borja Peleato, and Jonathan Eckstein. 2010. *Distributed Optimization and Statistical Learning via the Alternating Direction Method of Multipliers*. *Foundations and Trends in Machine Learning*. Vol. 3. Foundations and Trends in Machine Learning. https://doi.org/10.1561/2200000016.

Cinvalar, S., J. J. Grainger, H. Yin, and S. S. H. Lee. 1988. "Distribution Feeder Reconfiguration for Loss Reduction." *IEEE Transactions on Power Delivery* 3 (3): 1217–23. https://doi.org/10.1109/61.193906.

Conejo, Antonio. J., Jose. M. Arroyo, Natalia. Alguacil, and A. L. Guijarro. 2002. "Transmission Loss Allocation: A Comparison of Different Practical Algorithms." *IEEE Power Engineering Review* 22 (5): 66. https://doi.org/10.1109/MPER.2002.4312201.

Conte, Francesco, Fabio D'Agostino, Paola Pongiglione, Matteo Saviozzi, and Federico Silvestro. 2019. "Mixed-Integer Algorithm for Optimal Dispatch of Integrated PV-Storage Systems." *IEEE Transactions on Industry Applications* 55 (1): 238–47. https://doi.org/10.1109/TIA.2018.2870072.

Crespo-Vazquez, Jose L., Tarek Al Skaif, Angel M. Gonzalez-Rueda, and Madeleine Gibescu. 2020. "A Community-Based Energy Market Design Using Decentralized Decision-Making under Uncertainty." *IEEE Transactions on Smart Grid*, 1–11. https://doi.org/10.1109/TSG.2020.3036915.

Dabbagh, Saeed Rahmani, Mohammad Kazem Sheikh-El-Eslami, and Alberto Borghetti. 2016. "Optimal Operation of Vehicle-to-Grid and Grid-to-Vehicle Systems Integrated with Renewables." *19th Power Systems Computation Conference, PSCC 2016*, 1–7. https://doi.org/10.1109/PSCC.2016.7540933.

Daniil, Nikolaos, David Drury, and Phil H. Mellor. 2015. "Performance Comparison of Diffusion, Circuit-Based and Kinetic Battery Models." *2015 IEEE Energy Conversion Congress and Exposition, ECCE 2015*, 1382–89. https://doi.org/10.1109/ECCE.2015.7309854.

De Filippo, Allegra. 2020. "Hybrid Offline / Online Methods for Optimization under Uncertainty." PhD thesis - University of Bologna. http://amsdottorato.unibo.it/9425/1/DeFilippo_Allegra_tesi.pdf.

Delnooz, A, J Vanschoenwinkel, and Y Mou. 2020. "Possibilities of Collective Activities in Flanders." https://www.energyville.be/sites/energyville/files/downloads/2020/infographic_energycommunities_engels.pdf

Derakhshandeh, S. Y., Amir S. Masoum, Sara Deilami, Mohammad A. S. Masoum, and M. E. Hamedani Golshan. 2013. "Coordination of Generation Scheduling with PEVs Charging in Industrial Microgrids." IEEE Transactions on Power Systems 28 (3): 3451–61. https://doi.org/10.1109/TPWRS.2013.2257184.

Develder, Chris, Matthias Strobbe, Klaas De Craemer, and Geert Deconinck. 2016. "Charging Electric Vehicles in the Smart Grid." In *Smart Grids from a Global Perspective: Bridging Old and New Energy Systems*, edited by Anne Beaulieu, Jaap de Wilde, and Jacquelien M A Scherpen, 147–61. Cham: Springer International Publishing. https://doi.org/10.1007/978-3-319-28077-6_10.

Di Silvestre, Maria Luisa, Pierluigi Gallo, Mariano Giuseppe Ippolito, Eleonora Riva Sanseverino, and Gaetano Zizzo. 2018. "A Technical Approach to the Energy Blockchain in Microgrids." *IEEE Transactions on Industrial Informatics* 14 (11): 4792–4803. https://doi.org/10.1109/TII.2018.2806357.

Dvorkin, Vladimir, Jalal Kazempour, Luis Baringo, and Pierre Pinson. 2018. "A Consensus-ADMM Approach for Strategic Generation Investment in Electricity Markets." In *Proceedings of the IEEE Conference on Decision and Control (CDC)* 2018 Miami, FL, USA, 780–85. https://doi.org/10.1109/CDC.2018.8619240.

Engine, G A S, and Technical Data. 2009. "Gas Engine Technical Data" 02: 8–11.

Escudero, Laureano F., Araceli Garín, María Merino, and Gloria Pérez. 2007. "The Value of the Stochastic Solution in Multistage Problems." *Top* 15 (1): 48–64. https://doi.org/10.1007/s11750-007-0005-4.

España, Nohora, John Barco-Jiménez, Andrés Pantoja, and Nicanor Quijano. 2020. "Distributed Population Dynamics for Active and Reactive Power Dispatch in Islanded Microgrids." *International Journal of Electrical Power and Energy Systems* 125 (March 2020): 106407. https://doi.org/10.1016/j.ijepes.2020.106407.

EU2018/2001. 2018. *Directive (EU) 2018/2001 of the European Parliament and of the Council on the Promotion of the Use of Energy from Renewable Sources*. *Official Journal of the European Union*. Vol. 2018.

EU2019/944. 2019. *Directive (EU) 2019/944 on Common Rules for the Internal Market for Electricity*. *Official Journal of the European Union*.

Fan, Songli, Qian Ai, and Longjian Piao. 2018. "Hierarchical Energy Management of Microgrids Including Storage and Demand Response." *Energies* 11 (5). https://doi.org/10.3390/en11051111.

Frieden, Dorian, Josh Roberts, and Andrej F. Gubina. 2019. "Overview of Emerging Regulatory Frameworks on Collective Self-Consumption and Energy Communities in Europe." *International Conference on the European Energy Market, EEM* 2019-Septe. https://doi.org/10.1109/EEM.2019.8916222.

Gambini, Maria Maddalena, Camilo Orozco, Alberto Borghetti, and Fabio Tossani. 2020. "Power Loss Reduction in the Energy Resource Scheduling of a Local Energy Community." In *SEST 2020 - 3rd International Conference on Smart Energy Systems and Technologies*, 1–6. https://doi.org/10.1109/SEST48500.2020.9203444.

Gan, Lingwen, Na Li, Ufuk Topcu, and Steven H. Low. 2015. "Exact Convex Relaxation of Optimal Power Flow in Radial Networks." *IEEE Transactions on Automatic Control* 60 (1): 72–87. https://doi.org/10.1109/TAC.2014.2332712.

García-Villalobos, J., I. Zamora, J. I. San Martín, F. J. Asensio, and V. Aperribay. 2014. "Plug-in Electric Vehicles in Electric Distribution Networks: A Review of Smart Charging Approaches." *Renewable and Sustainable Energy Reviews* 38: 717–31. https://doi.org/10.1016/j.rser.2014.07.040.

Gerossier, Alexis, Robin Girard, Alexis Bocquet, and George Kariniotakis. 2018. "Robust Day-Ahead Forecasting of Household Electricity Demand and Operational Challenges." *Energies* 11 (12). https://doi.org/10.3390/en11123503.

Guerrero, Jaysson, Archie C. Chapman, and Gregor Verbic. 2018. "Decentralized P2P Energy Trading under Network Constraints in a Low-Voltage Network." *IEEE Transactions on Smart Grid* 10 (5): 5163–73. https://doi.org/10.1109/TSG.2018.2878445.

Guerrero, Jaysson, Archie C. Chapman, and Gregor Verbič. 2019. "Local Energy Markets in LV Networks: Community Based and Decentralized P2P Approaches." *2019 IEEE Milan PowerTech, PowerTech 2019*. https://doi.org/10.1109/PTC.2019.8810588.

Honarmand, Masoud, Alireza Zakariazadeh, and Shahram Jadid. 2014. "Integrated Scheduling of Renewable Generation and Electric Vehicles Parking Lot in a Smart Microgrid." *Energy Conversion and Management* 86: 745–55. https://doi.org/10.1016/j.enconman.2014.06.044.

Inês, Campos, Pontes Luz Guilherme, Marín González Esther, Gährs Swantje, Hall Stephen, and Holstenkamp Lars. 2020. "Regulatory Challenges and Opportunities for Collective Renewable Energy Prosumers in the EU." *Energy Policy* 138. https://doi.org/10.1016/j.enpol.2019.111212.

IRENA. 2019. Future of Solar Photovoltaic: Deployment, investment, technology, grid integration and socio-economic aspects (A Global Energy Transformation: paper), International Renewable Energy Agency, Abu Dhabi.

———. 2020a. Global Renewables Outlook: Energy transformation 2050.

———. 2020b. Innovation landscape brief: Community-ownership models, International Renewable Energy Agency, Abu Dhabi.

Kargarian, Amin, Javad Mohammadi, Junyao Guo, Sambuddha Chakrabarti, Masoud Barati, Gabriela Hug, Soummya Kar, and Ross Baldick. 2018. "Toward Distributed/Decentralized DC Optimal Power Flow Implementation in Future Electric Power Systems." *IEEE Transactions on Smart Grid* 9 (4): 2574–94. https://doi.org/10.1109/TSG.2016.2614904.

Khodayar, Mohammad E., Lei Wu, and Mohammad Shahidehpour. 2012. "Hourly Coordination of Electric Vehicle Operation and Volatile Wind Power Generation in SCUC." *IEEE Transactions on Smart Grid* 3 (3): 1271–79. https://doi.org/10.1109/TSG.2012.2186642.

Koirala, Binod Prasad, Elta Koliou, Jonas Friege, Rudi A. Hakvoort, and Paulien M. Herder. 2016. "Energetic Communities for Community Energy: A Review of Key Issues and Trends Shaping Integrated Community Energy Systems." *Renewable and Sustainable Energy Reviews* 56: 722–44. https://doi.org/10.1016/j.rser.2015.11.080.

Lai, Chun Sing, Youwei Jia, Zhao Xu, Loi Lei Lai, Xuecong Li, Jun Cao, and Malcolm D. McCulloch. 2017. "Levelized Cost of Electricity for Photovoltaic/Biogas Power Plant Hybrid System with Electrical Energy Storage Degradation Costs." *Energy Conversion and Management* 153 (May): 34–47. https://doi.org/10.1016/j.enconman.2017.09.076.

Lavrijssen, Saskia, and Arturo Carrillo Parra. 2017. "Radical Prosumer Innovations in the Electricity Sector and the Impact on Prosumer Regulation." *Sustainability (Switzerland)* 9 (7): 1–21. https://doi.org/10.3390/su9071207.

Lazaroiu, George Cristian, Virgil Dumbrava, Georgiana Balaban, Michela Longo, and Dario Zaninelli. 2016. "Stochastic Optimization of Microgrids with Renewable and Storage Energy Systems." *EEEIC 2016 - International Conference on Environment and Electrical Engineering*. https://doi.org/10.1109/EEEIC.2016.7555486.

Le Cadre, Hélène, and Jean Sébastien Bedo. 2020. "Consensus Reaching with Heterogeneous User Preferences, Private Input and Privacy-Preservation Output." *Operations Research Perspectives* 7 (December 2019): 100138. https://doi.org/10.1016/j.orp.2019.100138.

Le Cadre, Hélène, Paulin Jacquot, Cheng Wan, and Clémence Alasseur. 2020. "Peer-to-Peer Electricity Market Analysis: From Variational to Generalized Nash Equilibrium." *European Journal of Operational Research* 282 (2): 753–71. https://doi.org/10.1016/j.ejor.2019.09.035.

Lee, Joohyung, Jun Guo, Jun Kyun Choi, and Moshe Zukerman. 2015. "Distributed Energy Trading in Microgrids: A Game-Theoretic Model and Its Equilibrium Analysis." *IEEE Transactions on Industrial Electronics* 62 (6): 3524–33. https://doi.org/10.1109/TIE.2014.2387340.

Leeuwen, Gijs van, Tarek AlSkaif, Madeleine Gibescu, and Wilfried van Sark. 2020. "An Integrated Blockchain-Based Energy Management Platform with Bilateral Trading for Microgrid Communities." *Applied Energy* 263. https://doi.org/10.1016/j.apenergy.2020.114613.

Lilla, Stefano., Alberto. Borghetti, Fabio. Napolitano, Fabio. Tossani, Davide. Pavanello, Dominique. Gabioud, Y. Maret, and Carlo Alberto. Nucci. 2017. "Mixed Integer Programming Model for the Operation of an Experimental Low-Voltage Network." *2017 IEEE Manchester PowerTech, Powertech 2017*, 1–6. https://doi.org/10.1109/PTC.2017.7981175.

Lilla, Stefano, Camilo Orozco, Alberto Borghetti, Fabio Napolitano, and Fabio Tossani. 2020. "Day-Ahead Scheduling of a Local Energy Community: An Alternating Direction Method of Multipliers Approach." *IEEE Transactions on Power Systems* 35 (2): 1132–42. https://doi.org/10.1109/TPWRS.2019.2944541.

Liu, Yun, Yuanzheng Li, Hoay Beng Gooi, Ye Jian, Huanhai Xin, Xichen Jiang, and Jianfei Pan. 2019. "Distributed Robust Energy Management of a Multimicrogrid System in the Real-Time Energy Market." *IEEE Transactions on Sustainable Energy* 10 (1): 396–406. https://doi.org/10.1109/TSTE.2017.2779827.

Low, Steven H. 2014a. "Convex Relaxation of Optimal Power Flow-Part II: Exactness." *IEEE Transactions on Control of Network Systems* 1 (2): 177–89. https://doi.org/10.1109/TCNS.2014.2323634.

———. 2014b. "Convex Relaxation of Optimal Power Flow - Part I: Formulations and Equivalence." *IEEE Transactions on Control of Network Systems* 1 (1): 15–27. https://doi.org/10.1109/TCNS.2014.2309732.

Madani, Ramtin, Morteza Ashraphijuo, and Javad Lavaei. 2014. "Promises of Conic Relaxation for Contingency-Constrained Optimal Power Flow Problem." *2014 52nd Annual Allerton Conference on Communication, Control, and Computing, Allerton 2014* 31 (2): 1064–71. https://doi.org/10.1109/ALLERTON.2014.7028573.

Manwell, James F., and Jon G. McGowan. 1993. "Lead Acid Battery Storage Model for Hybrid Energy Systems." *Solar Energy* 50 (5): 399–405. https://doi.org/10.1016/0038-092X(93)90060-2.

Masson, Gaëtan, Jose Ignacio Briano, and Maria Jesus Baez. 2016. "Review and Analysis of Self-Consumption Policies." *Report IEA-PVPS T1-28:2016*. http://iea-pvps.org/index.php?id=353&eID=dam_frontend_push&docID=3066.

Mengelkamp, Esther, Johannes Gärttner, Kerstin Rock, Scott Kessler, Lawrence Orsini, and Christof Weinhardt. 2018. "Designing Microgrid Energy Markets: A Case Study: The Brooklyn Microgrid." *Applied Energy* 210: 870–80. https://doi.org/10.1016/j.apenergy.2017.06.054.

Molzahn, Daniel K., and Ian A. Hiskens. 2016. "Convex Relaxations of Optimal Power Flow Problems: An Illustrative Example." *IEEE Transactions on Circuits and Systems I: Regular Papers* 63 (5): 650–60. https://doi.org/10.1109/TCSI.2016.2529281.

Moret, Fabio, and Pierre Pinson. 2019. "Energy Collectives: A Community and Fairness Based Approach to Future Electricity Markets." *IEEE Transactions on Power Systems* 34 (5): 3994–4004. https://doi.org/10.1109/TPWRS.2018.2808961.

Munsing, Eric, Jonathan Mather, and Scott Moura. 2017. "Blockchains for Decentralized Optimization of Energy Resources in Microgrid Networks," *2017 IEEE Conference on Control Technology and Applications (CCTA)*, Maui, HI, USA, 2017, pp. 2164-2171. https://doi.org/10.1109/CCTA.2017.8062773.

Mwasilu, Francis, Jackson John Justo, Eun-Kyung Kim, Ton Duc Do, and Jin-Woo Jung. 2014. "Electric Vehicles and Smart Grid Interaction: A Review on Vehicle to Grid and Renewable Energy Sources Integration." *Renewable and Sustainable Energy Reviews* 34 (June): 501–16. https://doi.org/10.1016/j.rser.2014.03.031.

Nespoli, Alfredo, Emanuele Ogliari, Sonia Leva, Alessandro Massi Pavan, Adel Mellit, Vanni Lughi, and Alberto Dolara. 2019. "Day-Ahead Photovoltaic Forecasting: A Comparison of the Most Effective Techniques." *Energies* 12 (9): 1–15. https://doi.org/10.3390/en12091621.

Orozco, Camilo., Alberto. Borghetti, Stefano. Lilla, Giorgia. Pulazza, and Fabio. Tossani. 2018. "Comparison between Multistage Stochastic Optimization Programming and Monte Carlo Simulations for the Operation of Local Energy Systems." In *Proceedings - 2018 IEEE International Conference on Environment and Electrical Engineering and 2018 IEEE Industrial and Commercial Power Systems Europe, EEEIC/I and CPS Europe 2018*. Palermo. https://doi.org/10.1109/EEEIC.2018.8494563.

Orozco, Camilo., Stefano. Lilla, Alberto. Borghetti, Fabio. Napolitano, and Fabio. Tossani. 2019. "An ADMM Approach for Day-Ahead Scheduling of a Local Energy Community." *2019 IEEE Milan PowerTech, PowerTech 2019,* 737434: 1–6. https://doi.org/10.1109/PTC.2019.8810578.

Orozco, Camilo, Alberto Borghetti, Fabio Napolitano, and Fabio Tossani. 2020. "Multistage Day-Ahead Scheduling of the Distributed Energy Sources in a Local Energy Community." In *2020 IEEE International Conference on Environment and Electrical Engineering Europe, EEEIC Europe 2020*, 1–7. https://doi.org/10.1109/EEEIC/ICPSEurope49358.2020.9160579.

Osório, Gerardo. J., J. M. Lujano-Rojas, Joao. C.O. Matias, and Joao. P.S. Catalão. 2015. "A New Scenario Generation-Based Method to Solve the Unit Commitment Problem with High Penetration of Renewable Energies." *International Journal of Electrical Power and Energy Systems* 64: 1063–72. https://doi.org/10.1016/j.ijepes.2014.09.010.

Parisio, Alessandra, Christian Wiezorek, Timo Kyntäjä, Joonas Elo, Kai Strunz, and Karl Henrik Johansson. 2017. "Cooperative MPC-Based Energy Management for Networked Microgrids." *IEEE Transactions on Smart Grid* 8 (6): 3066–74. https://doi.org/10.1109/TSG.2017.2726941.

Paudel, Amrit, Kalpesh Chaudhari, Chao Long, and Hoay Beng Gooi. 2019. "Peer-to-Peer Energy Trading in a Prosumer-Based Community Microgrid: A Game-Theoretic Model." *IEEE Transactions on Industrial Electronics* 66 (8): 6087–97. https://doi.org/10.1109/TIE.2018.2874578.

Pranevicius, H, and K Šutiene. 2007. "Scenario Tree Generation by Clustering the Simulated Data Paths," In *Proceedings 21st European Conference on Modelling and Simulation ECMS 2007*, 2007, pp. 203–208.

Reddy, S. Surender, Vuddanti Sandeep, and Chan Mook Jung. 2017. "Review of Stochastic Optimization Methods for Smart Grid." *Frontiers in Energy* 11 (2): 197–209. https://doi.org/10.1007/s11708-017-0457-7.

Richardson, David B. 2013. "Encouraging Vehicle-to-Grid (V2G) Participation through Premium Tariff Rates." *Journal of Power Sources* 243: 219–24. https://doi.org/10.1016/j.jpowsour.2013.06.024.

Rodríguez-Molina, Jesús, Margarita Martínez-Núñez, José Fernán Martínez, and Waldo Pérez-Aguiar. 2014. “Business Models in the Smart Grid: Challenges, Opportunities and Proposals for Prosumer Profitability.” *Energies* 7 (9): 6142–71. https://doi.org/10.3390/en7096142.

Roelofs, Marcel;, and Johannes Bisschop. 2013. *AIMMS Language Reference. Technology*.

Sakti, Apurba, Kevin G. Gallagher, Nestor Sepulveda, Canan Uckun, Claudio Vergara, Fernando J. de Sisternes, Dennis W. Dees, and Audun Botterud. 2017. “Enhanced Representations of Lithium-Ion Batteries in Power Systems Models and Their Effect on the Valuation of Energy Arbitrage Applications.” *Journal of Power Sources* 342: 279–91. https://doi.org/10.1016/j.jpowsour.2016.12.063.

Sangrody, Hossein, Morteza Sarailoo, Ning Zhou, Nhu Tran, Mahdi Motalleb, and Elham Foruzan. 2017. “Weather Forecasting Error in Solar Energy Forecasting.” *IET Renewable Power Generation* 11 (10): 1274–80. https://doi.org/10.1049/iet-rpg.2016.1043.

Sbordone, D., I. Bertini, B. Di Pietra, M. C. Falvo, A. Genovese, and L. Martirano. 2015. “EV Fast Charging Stations and Energy Storage Technologies: A Real Implementation in the Smart Micro Grid Paradigm.” *Electric Power Systems Research* 120: 96–108. https://doi.org/10.1016/j.epsr.2014.07.033.

Scattolini, Riccardo. 2009. “Architectures for Distributed and Hierarchical Model Predictive Control - A Review.” *Journal of Process Control* 19 (5): 723–31. https://doi.org/10.1016/j.jprocont.2009.02.003.

Shafie-Khah, Miadreza, Ehsan Heydarian-Forushani, Gerardo J. Osorio, Fabio A.S. Gil, Jamshid Aghaei, Mostafa Barani, and Joao P.S. Catalao. 2016. “Optimal Behavior of Electric Vehicle Parking Lots as Demand Response Aggregation Agents.” *IEEE Transactions on Smart Grid* 7 (6): 2654–65. https://doi.org/10.1109/TSG.2015.2496796.

Shi, Wenbo, Na Li, Chi Cheng Chu, and Rajit Gadh. 2017. “Real-Time Energy Management in Microgrids.” *IEEE Transactions on Smart Grid* 8 (1): 228–38. https://doi.org/10.1109/TSG.2015.2462294.

Sokoøowski, Maciej M. 2018. “European Law on the Energy Communities: A Long Way to a Direct Legal Framework.” *European Energy and Environmental Law Review* 27 (2): 60–70.

Thimsen, D. 2004. “Assessment of Biogas-Fueled Electric Power Systems.”

Traube, Joshua, Fenglong Lu, Dragan Maksimovic, Joseph Mossoba, Matthew Kromer, Peter Faill, Stan Katz, Bogdan Borowy, Steve Nichols, and Leo Casey. 2013. “Mitigation of Solar Irradiance Intermittency in Photovoltaic Power Systems with Integrated Electric-Vehicle Charging Functionality.” *IEEE Transactions on Power Electronics* 28 (6): 3058–67. https://doi.org/10.1109/TPEL.2012.2217354.

Van der Meer, D. W., J. Widén, and J. Munkhammar. 2018. "Review on Probabilistic Forecasting of Photovoltaic Power Production and Electricity Consumption." *Renewable and Sustainable Energy Reviews* 81 (June 2017): 1484–1512. https://doi.org/10.1016/j.rser.2017.05.212.

Vangulick, David, Bertrand Cornelusse, and Damien Ernst. 2018. "Blockchain for Peer-to-Peer Energy Exchanges: Design and Recommendations." *20th Power Systems Computation Conference, PSCC 2018*, 1–7. https://doi.org/10.23919/PSCC.2018.8443042.

Wang, Hao, and Jianwei Huang. 2018. "Incentivizing Energy Trading for Interconnected Microgrids." *IEEE Transactions on Smart Grid* 9 (4): 2647–57. https://doi.org/10.1109/TSG.2016.2614988.

Wang, Shasha, Harsha Gangammanavar, Sandra D. Eksioglu, and Scott J. Mason. 2019. "Stochastic Optimization for Energy Management in Power Systems with Multiple Microgrids." *IEEE Transactions on Smart Grid* 10 (1): 1068–79. https://doi.org/10.1109/TSG.2017.2759159.

Wei, Wei, Jianhui Wang, Na Li, and Shengwei Mei. 2017. "Optimal Power Flow of Radial Networks and Its Variations: A Sequential Convex Optimization Approach." *IEEE Transactions on Smart Grid* 8 (6): 2974–87. https://doi.org/10.1109/TSG.2017.2684183.

Williams, H. Paul. 2013. *Model Building in Mathematical Programming*. 5th ed. John Wiley & Sons, Chichester, 2013.

Xiang, Yue, Shuai Hu, Youbo Liu, Xin Zhang, and Junyong Liu. 2019. "Electric Vehicles in Smart Grid: A Survey on Charging Load Modelling." *IET Smart Grid* 2 (1): 25–33. https://doi.org/10.1049/iet-stg.2018.0053.

Xu, Da, Bin Zhou, Ka Wing Chan, Canbing Li, Qiuwei Wu, Biyu Chen, and Shiwei Xia. 2019. "Distributed Multienergy Coordination of Multimicrogrids with Biogas-Solar-Wind Renewables." *IEEE Transactions on Industrial Informatics* 15 (6): 3254–66. https://doi.org/10.1109/TII.2018.2877143.

Yan, Bing, Marialaura Di Somma, Peter B. Luh, and Giorgio Graditi. 2018. "Operation Optimization of Multiple Distributed Energy Systems in an Energy Community." *Proceedings - 2018 IEEE International Conference on Environment and Electrical Engineering and 2018 IEEE Industrial and Commercial Power Systems Europe, EEEIC/I and CPS Europe 2018*. https://doi.org/10.1109/EEEIC.2018.8494476.

Yuan, Chunhui, and Haitao Yang. 2019. "Research on K-Value Selection Method of K-Means Clustering Algorithm." *J MDPI* 2 (2): 226–35. https://doi.org/10.3390/j2020016.

Zakariazadeh, Alireza, Shahram Jadid, and Pierluigi Siano. 2015. "Integrated Operation of Electric Vehicles and Renewable Generation in a Smart Distribution System." *Energy Conversion and Management* 89: 99–110. https://doi.org/10.1016/j.enconman.2014.09.062.

Zhang, Chenghua, Jianzhong Wu, Chao Long, and Meng Cheng. 2017. “Review of Existing Peer-to-Peer Energy Trading Projects.” *Energy Procedia* 105: 2563–68. https://doi.org/10.1016/j.egypro.2017.03.737.

Zhang, Tian, Wei Chen, Zhu Han, and Zhigang Cao. 2014. “Charging Scheduling of Electric Vehicles with Local Renewable Energy under Uncertain Electric Vehicle Arrival and Grid Power Price.” *IEEE Transactions on Vehicular Technology* 63 (6): 2600–2612. https://doi.org/10.1109/TVT.2013.2295591.

Zhang, Xianjun, Ratnesh Sharma, and Yanyi He. 2012. “Optimal Energy Management of a Rural Microgrid System Using Multi-Objective Optimization.” *2012 IEEE PES Innovative Smart Grid Technologies, ISGT 2012*, 1–8. https://doi.org/10.1109/ISGT.2012.6175655.

Zhao, Yi, Jilai Yu, Mingfei Ban, Yiqi Liu, and Zhiyi Li. 2018. “Privacy-Preserving Economic Dispatch for an Active Distribution Network with Multiple Networked Microgrids.” *IEEE Access* 6: 38802–19. https://doi.org/10.1109/ACCESS.2018.2854280.

Zheng, Yu, Yue Song, David J. Hill, and Yongxi Zhang. 2018. “Multiagent System Based Microgrid Energy Management via Asynchronous Consensus ADMM.” *IEEE Transactions on Energy Conversion* 33 (2): 886–88. https://doi.org/10.1109/TEC.2018.2799482.

Zhou, Bin, Da Xu, Canbing Li, Chi Yung Chung, Yijia Cao, Ka Wing Chan, and Qiuwei Wu. 2018. “Optimal Scheduling of Biogas-Solar-Wind Renewable Portfolio for Multicarrier Energy Supplies.” *IEEE Transactions on Power Systems* 33 (6): 6229–39. https://doi.org/10.1109/TPWRS.2018.2833496.